1030
Dt. 23/11/89

Indian J. Chem. Vol. 27A No. 10 pp. 829-922
October 1988
CODEN : IJOCAP ISSN : 0019-5103
27A(10) 829-922 (1988)

Indian Journal of
CHEMISTRY

SECTION A
(Inorganic, Physical, Theoretical & Analytical)

Published by
PUBLICATIONS & INFORMATION DIRECTORATE, CSIR, NEW DELHI
in association with
THE INDIAN NATIONAL SCIENCE ACADEMY, NEW DELHI

A RANGE OF HIGH PRECISION, HIGH QUALITY RECORDING INSTRUMENTS FOR THE DISCRIMINATING RESEARCH SCIENTIST

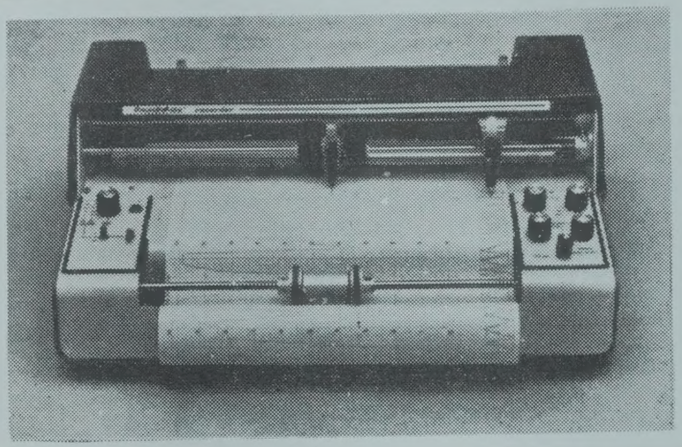

Series 5000 Strip Chart Recorder

The series 5000 Strip Chart Recorder and the series 2000 XY Recorder are well proven instruments incorporating State of the Art Circuitry. A wide range of models offer tremendous flexibility to the user. With over 5000 installations, these instruments are the preferred choice of discriminating users all over India.

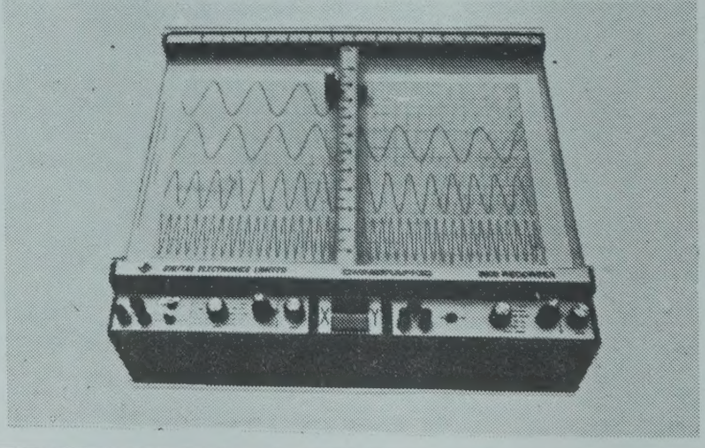

Series 2000 XY Recorder

Another quality product from

DIGITAL ELECTRONICS LIMITED

Reliability in Recording Instruments.

Digilog House 74/II, Marol Industrial Area MIDC, Andheri (East), Bombay- 400 093 Tel: 634 09 01, 632 86 76 Grams: 'DIGILOG'

A Company in collaboration with houston instrument

Special Effects/DE/25/86

RENEWAL NOTICE

Your subscription which expires with the despatch of December 1988 issue of the journal, stands for renewal. We request you to be so good as to return the enclosed order form duly filled early, so as to ensure continuity in despatch.

Sales & Distribution Officer

DATED:

The Sales & Distribution Officer
PUBLICATIONS & INFORMATION DIRECTORATE
HILLSIDE ROAD, NEW DELHI-110012 (INDIA)

Dear Sir,

Please renew my subscription/enrol me as subscriber to:

			Rs.	$	£
1	Journal of Scientific & Industrial Research	(Monthly)	200.00	70.00	45.00
2	Indian Journal of Chemistry, Section A	(Monthly)	300.00	100.00	70.00
3	Indian Journal of Chemistry, Section B	(Monthly)	300.00	100.00	70.00
4	Indian Journal of Experimental Biology	(Monthly)	250.00	85.00	55.00
5	Indian Journal of Technology	(Monthly)	250.00	85.00	55.00
6	Indian Journal of Pure & Applied Physics	(Monthly)	250.00	85.00	55.00
7	Indian Journal of Biochemistry & Biophysics	(Bimonthly)	125.00	42.00	28.00
8	Indian Journal of Radio & Space Physics	(Bimonthly)	125.00	42.00	28.00
9	Indian Journal of Marine Sciences	(Quarterly)	125.00	42.00	28.00
10	Indian Journal of Textile Research	(Quarterly)	125.00	42.00	28.00
11	Research & Industry	(Quarterly)	125.00	42.00	28.00
12	Current Literature on Science of Science	(Monthly)	100.00	30.00	12.00
13	Medicinal & Aromatic Plants Abstracts	(Bimonthly)	225.00	75.00	50.00

(Please tick off the periodicals you would like to subscribe).

for one year from January 1989 for which I/we have remitted to you a sum of Rs .....£ ..... $ ..... by Cheque/Demand Draft No. ..... dated ..... in favour of PUBLICATIONS & INFORMATION DIRECTORATE, NEW DELHI.

COMPLETE MAILING ADDRESS

Name .....

Address .....

Country/State .....

(Signature)

Note:

1. Subscribers at annual rates for all the periodicals are enlisted for the full volumes, i.e. for the period from January to December only.
2. The Cheque Demand Draft may plese be drawn in favour of "PUBLICATIONS & INFORMATION DIRECTORATE, NEW DELHI". Banking charges shall be borne by the subscriber. For inland outstation cheques please add Rs. 3.50. For foreign cheques please add $ 1.00 or £ 0.45.
3. The supply will commence on receipt of subscription in advance.

INDIAN JOURNAL OF CHEMISTRY

Section A: Inorganic, Physical, Theoretical & Analytical Chemistry

Editorial Board

Prof. C.N.R. Rao
Director
Indian Institute of Science
Bangalore 560 012

Prof. R.P. Rastogi
Vice-Chancellor
Banaras Hindu University
Varanasi 221 005

Prof. A.R. Vasudeva Murthy
Department of Inorganic &
Physical Chemistry
Indian Institute of Science
Bangalore 560 012

Prof. J.C. Kuriacose
Department of Chemistry
Indian Institute of Technology
Madras 600 036

Prof. D.V.S. Jain
Department of Chemistry
Panjab University
Chandigarh 160 014

Prof. P. Natarajan
Department of Inorganic Chemistry
University of Madras
Madras 600 025

Prof. N.K. Ray
Department of Chemistry
University of Delhi
Delhi 110 007

Prof. A. Chakravorty
Department of Inorganic Chemistry
Indian Association for the
Cultivation of Science
Calcutta 700 032

Prof. S. Mitra
Tata Institute of Fundamental Research
Bombay 400 005

Dr K.N. Rao
Chemistry Division
Bhabha Atomic Research Centre
Trombay, Bombay 400 085

Prof. S.M. Khopkar
Department of Chemistry
Indian Institute of Technology
Powai, Bombay 400 076

Prof. P.T. Manoharan
Department of Chemistry
Indian Institute of Technology
Madras 600 036

Dr A.C. Dash
Department of Chemistry
Utkal University
Bhubaneswar 751 004

Shri S.P. Ambasta, Editor-in-Chief
(*Ex-officio*)

Editors

S.S. Saksena — B.C. Sharma — S. Sivakamasundari

Assistant Editor

S.K. Bhasin

Published by the Publications & Information Directorate (CSIR), Hillside Road, New Delhi 110 012

Editor-in-Chief: S.P. Ambasta

Copyright, 1988, by the Council of Scientific & Industrial Research, New Delhi 110 012

The Indian Journal of Chemistry is issued monthly in two sections: A and B. Communications regarding contributions for publication in the journal should be addressed to the Editor, Indian Journal of Chemistry, Publications & Information Directorate, Hillside Road, New Delhi 110 012.

Correspondence regarding subscriptions and advertisements should be addressed to the Sales & Distribution Officer, Publications & Information Directorate, hillside Road, New Delhi 110 012.

The Publications & Information Directorate (CSIR) assumes no responsibility for the statements and opinions advanced by contributors. The Editorial Board in its work of examining papers received for publication is assisted, in an honorary capacity by a large number of distinguished scientists, working in various parts of India.

Annual Subscription: Rs. 300.00 £ 70.00 $ 100.00; 50% discount admissible to research workers and students and 25% discount to non-research individuals on annual subscription.

Single Copy: Rs. 30.00 £ 7.00 $ 10.00

Payments in respect of subscriptions and advertisements may be sent by cheque, bank draft, money order or postal order marked payable to Publications & Information Directorate, Hillside Road, New Delhi 110 012.

Claims for missing numbers will be allowed only if received within 3 months of the date of issue of the journal plus the time normally required for postal delivery of the journal and the claim.

AUTHOR INDEX

Arur P V 918
Bal Reddy K 876
Balgi V D 918
Behera G B 889
Biermann Christopher J 855

Caroling G 873
Chattopadhyay T K 912
Chaudhry Subash C 914

Das Susanta 898
Dash Anadi C 862, 905
Dogra Sneh K 851
Dongare M K 902

Goyal R N 858
Gupta Jatindra 914
Gupta Raj K 829
Gutman I 847

Hazra Dilip Kumar 898

Jadhav P K 918
Jagannadham V 907
Jayakumar N 916
Jelicks Linda A 829

Kamat Usha P 918
Kampli S 883
Katgeri S N 880
Kumar A K 912
Kuriacose J C 873

Mahadevappa D S 880
Mathai I M 909
Mishra Ashok K 851
Mishra B K 889
Mishra P K 889
Mukherjee A K 847
Mulla I S 902

Nagarjun Rao Ch 893
Naidu H M K 880
Nanda R K 905
Nandibewoor S T 883
Natarajan K 916
Navaneeth Rao T 876
Nayak Ramesh C 862

Pradhan G C 905

Rai H C 886
Rajanna K C 893
Rajaram J 873
Raju J R 883
Ramesh Kumar 886
Rivarola E 912

Saiprakash P K 893
Sankaran K R 868
Sethuram B 876
Shinde V M 921
Singh Balmiki 886
Sinha A P B 902
Srinivasan Vangalur S 868
Steenken S 907
Subramani K 868
Subramanian K 909

Uma Devi Y 893

Veera Somaiah P 876
Vidyarthi S N 886

Indian Journal of Chemistry

Sect. A: Inorganic, Physical, Theoretical & Analytical

VOLUME 27A NUMBER 10 OCTOBER 1988

CONTENTS

Advances in Contemporary Research

NMR Spectroscopy of Sodium Cations in Intact Cells 829
Raj K Gupta* & Linda A Jelicks

Papers

Hückel Rule in Annulenes with One Heteroatom 847
I Gutman* & A K Mukherjee

Semiempirical CNDO/S & PPP Calculations on Benzimidazole-2(3H)-one & Its Different Prototropic Species 851
Ashok K Mishra & Sneh K Dogra*

Dimerization in Binary Gaseous Mixtures: Nonadditive Effects & Argon-Krypton Example 855
Christopher J Biermann

Electrochemical Behaviour of *cis- &trans*-2,2′-Azopyridines at Solid Electrodes . . 858
R N Goyal

Effect of Sodium Dodecyl Sulphate on Protonation Equilibrium of (Salicylato)bis(ethylenediamine)cobalt (III): Test of Validity of Pseudo-phase Ion-Exchange Model for SDS Micelles 862
Anadi C Dash* & Ramesh C Nayak

Cerium(IV) & Manganese (III) Oxidation of Pentaamminecobalt(III) Complexes of Malonic & Methylmalonic Acids 868
K Subramani, K R Sankaran & Vangalur S Srinivasan*

Kinetics & Mechanism of Ru (III) Catalyzed Oxidation of Olefins by N-Methylmorpholine N-Oxide. 873
G Caroling, J Rajaram & J C Kuriacose*

Kinetics of Oxidation of Alcohols, Diols & α-Hydroxy Acids by Os(VIII) in Aqueous Alkaline Medium: Evidence in Support of Hydride Ion Abstraction Mechanism . 876
P Veera Somaiah, K Bal Reddy, B Sethuram & T Navaneeth Rao*

Kinetics & Mechanism of Oxidation of Unsaturated Alcohols by Chloramine-T in Sulphuric Acid Medium 880
H M K Naidu, S N Katgeri & D S Mahadevappa*

Kinetics of Chromium (VI) Oxidation of DMSO in Aqueous Acetic Acid . . . 883
(Miss) S Kampli, S T Nandibewoor & J R Raju*

Continued overleaf

Complexes of Copper(II) & Cobalt(II) with Ligands Derived from the Reactions of 1,2-Diphenyl-1-hydroxyiminoethane-2-one with 1,2-Diaminoethane & 1,3-Diaminopropane 886
H C Rai*, Ramesh Kumar, S N Vidyarathi & Balmiki Singh

Determination of Dissociation Constants of Salicylidene-2-aminobenzothiazole & *p*-Hydroxybenzylidene-2-aminobenzothiazole in Different Surfactant Systems . . 889
(Miss) P K Mishra, B K Mishra & G B Behera*

Synthesis, Characterisation & Dissociation Constants of 1-(3-Aryl-5-hydroxy-4-isoxazolylazo)-4-sulphonic Acid & Its Derivatives 893
Ch Nagarjun Rao, K C Rajanna, Y Uma Devi & P K Saiprakash*

Notes

Viscosity B-Coefficients of Tetraalkylammonium Bromides in Dimethyl Sulphoxide-Water Mixtures 898
Susanta Das & Dilip Kumar Hazra*

Suppression of Formation of Silicon Tetrachloride during Preparation of Silicon from Trichlorosilane 902
M K Dongare*, I S Mulla & A P B Sinha

Kinetics of Acid & Base Hydrolyses of *cis*-(Formato/Acetato)-(methylamine) bis(ethylenediamine)cobalt (III) Ions 905
G C Pradhan, R K Nanda* & A C Dash

Heterolysis of *o*-(α-Hydroxyalkyl)-4-cyanophenyl Nitrite: Simultaneous Polar & Steric Effects 907
V Jagannadham* & S Steenken

Iodide-induced Debromination of Cinnamic Acid & Substituted Cinnamic Acid Dibromides in 2-Methoxyethanol 909
K Subramanian & I M Mathai*

Organotin(IV) Complexes of Arylazopyridines 912
A K Kumar, T K Chattopadhyay*, & E Rivarola

Chelated Complexes of Chlorophenoxides of Titanium(IV) with Acetoacetanilide . 914
Subash C Chaudhry* & (Ms) Jatindra Gupta

New Mixed Ligand Complexes of Ruthenium(II) with β-diketones & Triphenylphosphine 916
N Jayakumar & K Natarajan*

Protolysis Constants (pK_a) of Some Antitubercular Compounds Containing Diaryl Sulphide & Diaryl Sulphone Moieties 918
P K Jadhav*, P V Arur, V D Balgi & (Mrs) Usha P Kamat

Extraction of Copper from Sodium Salicylate & Its Spectrophotometric Determination with 4-(2-Pyridylazo)resorcinol 921
V M Shinde

Indian Journal of Chemistry
Vol. 27A, October 1988, pp. 829-846

NMR Spectroscopy of Sodium Cations in Intact Cells

RAJ GUPTA* & LINDA A JELICKS
Departments of Physiology & Biophysics, and Biochemistry, Albert Einstein College of Medicine, Bronx, New York 10461

Introduction

The unequal distribution of Na^+ and K^+ aquo cations across cell membranes is essential for sustaining chemistry in all living cells. The concentrations, electrochemical gradients, and transmembrane fluxes of Na^+ are of fundamental importance in cell physiology and play an important role in a variety of vital cell functions, such as nerve transmission and generation of action potentials. The energy stored in the Na^+ gradient across the plasma membrane is utilized for the transport of other cations and essential nutrients into the cell. Intracellular Na^+ concentrations are regulated by the coordinate action of a number of membrane pumps and exchange systems. These include the Na^+/K^+-ATPase (Na^+-pump), $Na^+:Ca^{2+}$ exchange, $Na^+:H^+$ exchange, Na^+/K^+-co-transport and Na^+ selective channels in the plasma membrane. Each tissue is characterized by a well-defined intracellular Na^+ level, which is often dependent on its physiological state and the maintenance of which appears crucial for its viability. Changes in the intracellular concentration of this cation are often an indication of tissue disease or malfunction. Thus, alterations in intracellular Na^+ concentration have been variously associated with cancer, hypertension, and diabetic states, as well as with sickle cell disease[1-9].

From the point of view of magnetic properties, the ^{23}Na nucleus is especially attractive, with an isotopic abundance of 100% and a resonance frequency close to that of the widely studied ^{13}C nucleus. The ^{23}Na cation can be observed directly through its own NMR absorption. The magnetic properties of the ^{23}Na nucleus and other alkali metal cations are compared in Table 1. While the signal produced by the ^{23}Na nucleus following a single NMR pulse is an order of magnitude smaller than that generated by protons, its relaxation times are often two orders of magnitude shorter than those of protons in a similar environment. Therefore, in time-averaging experiments, the ^{23}Na NMR signal acquired per unit time is comparable to that resulting from a similar population of protons. Because of its 3/2 nuclear spin, the ^{23}Na nucleus exhibits three single-quantum NMR transitions: a central $I_z = -1/2 \rightarrow +1/2$ transition; and two equivalent outer transitions, $-3/2 \rightarrow -1/2$ and $+1/2 \rightarrow +3/2$. The relaxation behaviour of quadrupolar nuclei with $I > 1$ is simple (i.e, a single exponential curve) only within a certain range of correlation times called the "region of extreme narrowing" ($\tau_c \ll 1/\omega_0$). When molecular tumbling becomes relatively slow as is often the case with ions interacting with biomolecules, τ_c will be greater than $1/\omega_0$ and these nuclei will exhibit significantly nonexponential relaxation. The situation is complicated by the fact that these ions are usually exchanging between several sites which may vary markedly in their correlation times (i.e., free ions and ions bound to macromolecules). The equations are quite complex for nuclei possessing spin greater than 3/2 (e.g., ^{25}Mg and ^{43}Ca). However, for the ^{23}Na nucleus under typical biological conditions, the transverse relaxation reduces to a sum of two exponentials which can be expressed by the relation (1),

$$M_Z(t) = M_0\{0.6\ e^{-t/T_{2f}} + 0.4\ e^{-t/T_{2s}} \quad \ldots (1)$$

Table 1—Magnetic Properties of ^{23}Na Nucleus and Other Alkali Metal Cations

Nucleus	I	Larmor Freq. at 4.7 Tesla (MHz)	Natural isotopic abundance (%)	Rel sensitivity for equal number of nuclei	Electric quadrupole moment
^6Li	1	29.4	7.4	0.092	0.0007
^7Li	3/2	77.7	92.6	3.17	−0.03
^{23}Na	3/2	52.9	100	1.00	0.145
^{39}K	3/2	9.3	93.1	0.0055	0.11
^{87}Rb	3/2	65.4	27.8	1.89	0.13
^{133}Cs	7/2	26.2	100	0.51	−0.003

†Dedicated to Prof P.T. Narasimhan, IIT, Kanpur on his sixtieth birthday

where $1/T_{2f}$ and $1/T_{2s}$ are determined by the relative amounts, the exchange rates, and the relaxation rates of free and bound ions. This effect becomes apparent in the shape of the resonance lines of these nuclei which are "non-lorentzian" and appear to have relative areas of 6:4, 60% of the intensity corresponding to the two outer transitions and 40% to the inner transition. The widths of these two types of transitions may be very different and under certain conditions it is possible to have outer transitions broadened beyond detectability while the central transition stays narrow, leaving only 40% of the signal observable. This presents a complication in that observed NMR intensities may not be proportional to concentrations and the possibility of invisible transitions affecting the NMR intensities should therefore be kept in mind in calculating concentrations.

Localization of Sodium Cations in Intra- and Extracellular Compartments by NMR

It is of considerable interest to study sodium ions in the intracellular compartment and their transport across membranes in intact cells and tissues. Measurement of intracellular Na^+ is generally hampered by the large difference in its concentration across the plasma membrane. Even a slight contamination by occluded extracellular fluid, because of its high Na^+ content, significantly distorts the measurement of the intracellular Na^+ levels by techniques which are not specific to the intracellular compartments. Several methods are available for the determination of intracellular sodium cation content. These include straightforward chemical analysis, electron microprobe X-ray analysis, and ion-selective microelectrodes. Chemical analysis involves rigorous separation of cells from the extracellular fluid, tissue homogenization and measurement of metal cation content using flame emission photometry or atomic absorption techniques. The electron microprobe technique is based on an analysis of element-specific X-rays emitted when a high energy electron beam impinges on a very small region of a specimen in an electron microscope. The advantages of this technique are its high sensitivity, its ability to study subcellular organelles and its detection of virtually any element. However, the technique is destructive as it requires very rapid freezing of the sample followed by dehydration and ultrathin sectioning. Cation-selective microelectrodes have also been used to study intracellular sodium activity but require impalement of cells and tissues, and suffer, even when successful impalement can be achieved, from electrode calibration problems. The potential measured is affected by transmembrane electrical potential. In addition, the electrodes often produce cell injury, are limited in use to large cells, and sample only that region of the cell at the electrode tip. A noninvasive technique for measurement of intracellular Na^+ concentration is most advantageous and NMR spectroscopy offers such a technique. NMR can be used to detect cations within intact cells and because it is nondestructive and allows the observation of ionic changes in the cellular environment as they take place within an essentially unperturbed living system it is preferred over other methods, such as atomic absorption or electron X-ray microanalysis. In addition to providing a measurement of concentrations, NMR can provide information about the physical state of the cations.

The noninvasive spectroscopic technique of ^{23}Na NMR has enjoyed a growing enthusiasm within the scientific community since the first study of the continuous wave NMR spectra of $^{23}Na^+$ in muscle, kidney and brain by Cope[10-12]. Earlier ^{23}Na NMR studies of cells and tissues were carried out in a number of laboratories[10-16].

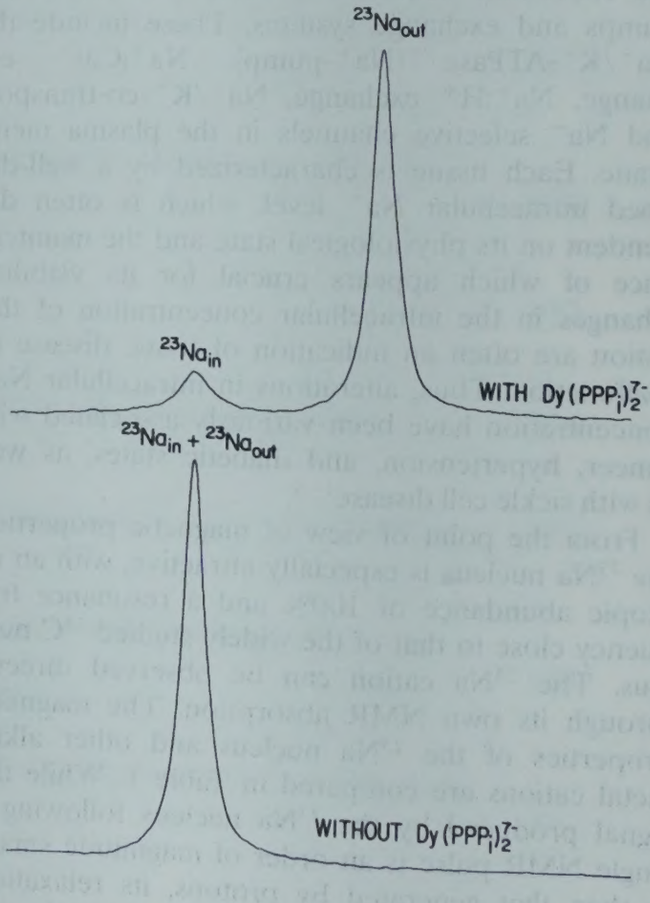

Fig. 1 — ^{23}Na NMR spectra of red cells in heparinized whole human blood with (top) and without (bottom) 3 m*M* $Dy(PPP_i)_2^{7-}$ showing spectral resolution of intra- and extracellular Na^+ ions by the paramagnetic shift reagent [The resonances of intra- and extracellular Na^+ ions are labeled as $^{23}Na_{in}$ and $^{23}Na_{out}$, respectively]

It became clear from these studies that the ^{23}Na signals from the extra- and intracellular compartments occur precisely at the same chemical shift. This is presumably because Na^+ is present mostly as hydrated cation and therefore the chemical environment or chemical shift of the ^{23}Na nucleus which is dependent on its immediate electronic environment remains unaltered in different compartments. The interesting small ^{23}Na resonance of intracellular ions is masked by the uninteresting but much larger resonance of extracellular ions. Until 1982, this lack of spectral discrimination between intra- and extracellular ^{23}Na resonances precluded the use of NMR in the study of intracellular Na^+ ions. The discovery in 1982 of a highly anionic paramagnetic shift reagent dysprosium bis(tripolyphosphate), $Dy(PPP_i)_2^{7-}$, effectively circumvented this problem[17,18] and for the first time allowed direct observation of well-resolved ^{23}Na resonances from intra- and extracellular Na^+ ions in intact cells at non-perturbing, low reagent concentrations (Fig. 1). This permitted a study of the intracellular Na^+ without interference from the extracellular ions and paved the way for future noninvasive NMR studies of monovalent cations in cells, tissues, organs and organisms[3,4,6,7,18–49]. The detection of resolved resonances from intra- and extracellular Na^+ ions exploits the fact that the anionic paramagnetic reagents cause a hyperfine shift in the frequency, without significant broadening, of the resonance of Na^+ ions in their environment. $Dy(PPP_i)_2^{7-}$, because of its highly anionic character, can not permeate through the cell membrane over the time scale of NMR measurements, and remains localized only in the extracellular compartments so that the NMR resonance of extracellular Na^+ is shifted away from the resonance of intracellular Na^+. Because the technique is noninvasive, consecutive steps in a protocol can be carried out on the same cell sample.

Other anionic reagents were independently introduced by Pike and Springer[50] and Bryden *et al.*[51], but required the use of over an order of magnitude higher reagent concentration to achieve the same spectral discrimination[23,52]. Balschi *et al.*[53] used such a reagent to obtain intracellular Na^+ in yeast cells at very low (15 mM) extracellular Na^+ concentrations. Two years later Chu, *et al.*[52] suggested $Dy(TTHA)^{3-}$ which, although again causing much smaller hyperfine shifts of extracellular Na^+ than those by $Dy(PPP_i)_2^{7-}$, possesses certain other advantages[42].

$Dy(PPP_i)_2^{7-}$ causes especially large hyperfine shifts in the NMR absorption of ^{23}Na. This is ascribed to its highly anionic nature and its ability to bind Na^+ in close spatial proximity of dysprosium. In order to obtain information on the structure of the complex of Na^+ with $Dy(PPP_i)_2^{7-}$, we studied the interaction of Na^+ with the corresponding relaxation reagent $Gd(PPP_i)_2^{7-}$. The magnitude of the paramagnetic effect of Gd^{3+} on the longitudinal nuclear relaxation rate of ^{23}Na in the complex of Na^+ with $Gd(PPP_i)_2^{7-}$ was measured. From the magnitude of this paramagnetic effect (10,000/s) and the rotational correlation time derived from Stokes' law, and assuming that only one ^{23}Na cation interacts with a Gd^{3+} to ^{23}Na distance of 4 Å was obtained using Eq. (2) for distance-dependent paramagnetic dipolar interactions[54,55].

$$\frac{1}{T_{1p}} = \frac{2fqS(S+1)g^2\beta^2\gamma_I^2}{15r^6}\left(\frac{3\tau_{c_1}}{1+\omega_I^2\tau_{c_1}^2} + \frac{7\tau_{c2}}{1+\omega_S^2\tau_{c_2}^2}\right) \quad \ldots(2)$$

where f is the ratio of concentrations of the paramagnet and the relaxing ligand, q is the relative stoichiometry of the bound ligand and bound paramagnet (i.e., the coordination number), S is the electron spin, γ_I is the nuclear gyromagnetic ratio, g is the electron's g-factor, β is the Bohr magneton, r is the metal-nucleus distance, ω_I and ω_S are the nuclear and electron angular precession frequencies, and τ_{c1} and τ_{c2} are the correlation times for the dipolar interaction, which in our case are equal to τ_R, the rotational correlation time. Interaction of 7 equidistant Na^+ cations at a distance of 5.5 Å would also be consistent with the measured paramagnetic relaxation effect.

$Dy(PPP_i)_2^{7-}$ causes an upfield paramagnetic shift in the frequency of the extracellular ^{23}Na resonance and only minimal line-broadening. In contrast, a complex of the same ligand with thulium, $Tm(PPP_i)_2^{7-}$, causes a downfield paramagnetic shift but is only half as effective as $Dy(PPP_i)_2^{7-}$, as judged by the magnitudes of the observed shifts[23,52]. The opposite directions of the observed paramagnetic shifts with Tm^{3+} and Dy^{3+} complexes indicate their dipolar origin and presumably reflect differences in orientation of the principal axes of the electron's g-tensor in the two cases.

Quantitation of Intracellular Sodium Concentration

Once the separation of intra- and extracellular ^{23}Na resonances by the shift reagent has been achieved, a comparison of the intensity of the resonance of extracellular ions (A_{out}) in the cell sam-

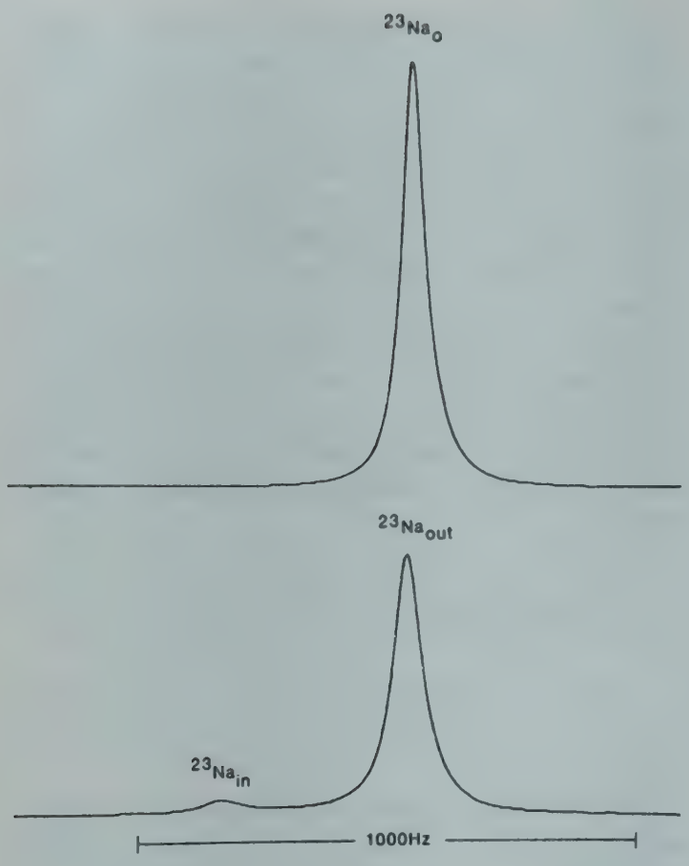

Fig. 2—Comparison of ^{23}Na NMR spectrum of red cells suspended in serum containing 3 m*M* $Dy(PPP_i)_2$ (lower trace) with that of the suspension medium alone (upper trace) [The ratio of intensities of the $^{23}Na_{out}$ and $^{23}Na_0$ signals directly gives the fractional extracellular space]

ple with the intensity of ^{23}Na resonance from a cell-free control (A_0) containing only the suspension medium [Na_{out}] (Fig. 2) directly yields the fractional space in the NMR-sensitive volume that is extracellular (S_{out}). It should be noted that the extracellular space defined in this way is the space seen by the ^{23}Na ions themselves and includes the space occupied by the medium as well as any vascular and interstitial spaces. The ratio of intensities of the ^{23}Na resonances of intracellular (A_{in}) and extracellular ions (A_{out}) together with a knowledge of the fractional space that is extracellular then directly yield the concentration of intracellular Na^+ ions [Na_{in}] that contribute to the observed resonance signal. Equations (3) and (4) provide the relationship between the observed resonance intensities and the "NMR-visible" intracellular Na^+ concentration[18,23].

$$S_{out} = \frac{A_{out}}{A_0} \quad \ldots (3)$$

$$[Na_{in}] = \left\{ \frac{A_{in}}{A_{out}} \frac{S_{out}}{(1 - S_{out})} \right\} [Na_{out}] \quad \ldots (4)$$

When [Na_{out}] is expressed in m*M*, the units of [Na_{in}] are mmols/litre cells. A knowledge of tissue water content enables calculation of [Na_{in}] on the basis of kilogram cell water.

Measurement of Intracellular Water Content

Knowledge of intracellular water volume is required for expressing the NMR-measured concentrations of intracellular ions and metabolites on the cell-water basis. Intracellular water volume can be measured gravimetrically, by comparing dry weight of cells with their wet weight, or by using ^3H_2O to determine the total water space. In both methods [^{14}C]-*inulin* is generally used as a membrane impermeant marker for the estimation of extracellular space. However, it has been shown (see e.g., ref. 22, 29) that cells can take up inulin by fluid-phase endocytosis. This results in inaccurate estimation of the amount of extracellular water, which may introduce sizeable errors in the calculation of intracellular water content. An additional source of error in the gravimetric method is partial decomposition of solid cell components to volatile compounds during drying of cells to a constant weight.

Hoffman and Gupta have described[56] an NMR method which is based on the use of ^{35}Cl and ^{2}H nuclei (Fig. 3). Measurements may be carried out without changing the NMR probe-configuration and they do not require the perturbation of the cell system by a shift reagent. The method is equally applicable to situations of slow and fast transmembrane water exchange and is based on the observation[31] that the resonance of intracellular $^{35}Cl^-$ ions in most cells is so broad as to become NMR-invisible. Therefore, the intensity of the $^{35}Cl^-$ NMR signal of a cell-suspension is proportional to the extracellular water volume within the NMR receiver coil. The intensity of the $^{35}Cl^-$ NMR signal of the cell-free medium in an identical sample-geometry is proportional to the total volume sampled by the NMR coil. The ratio of the two intensities (f_{Cl}) yields the extracellular water volume as a fraction of the total suspension volume. The ratio of the intensities of the water ^{2}H NMR signals of the cell-suspension and the cell-free medium (f_D) gives the water volume as a fraction of the total suspension volume. The intracellular water content (f_w), i.e., the volume of the intracellular water as a fraction of the total cell-volume, is given by Eq. (5)

$$f_w = \frac{f_D - f_{Cl}}{1 - f_{Cl}} \quad \ldots (5)$$

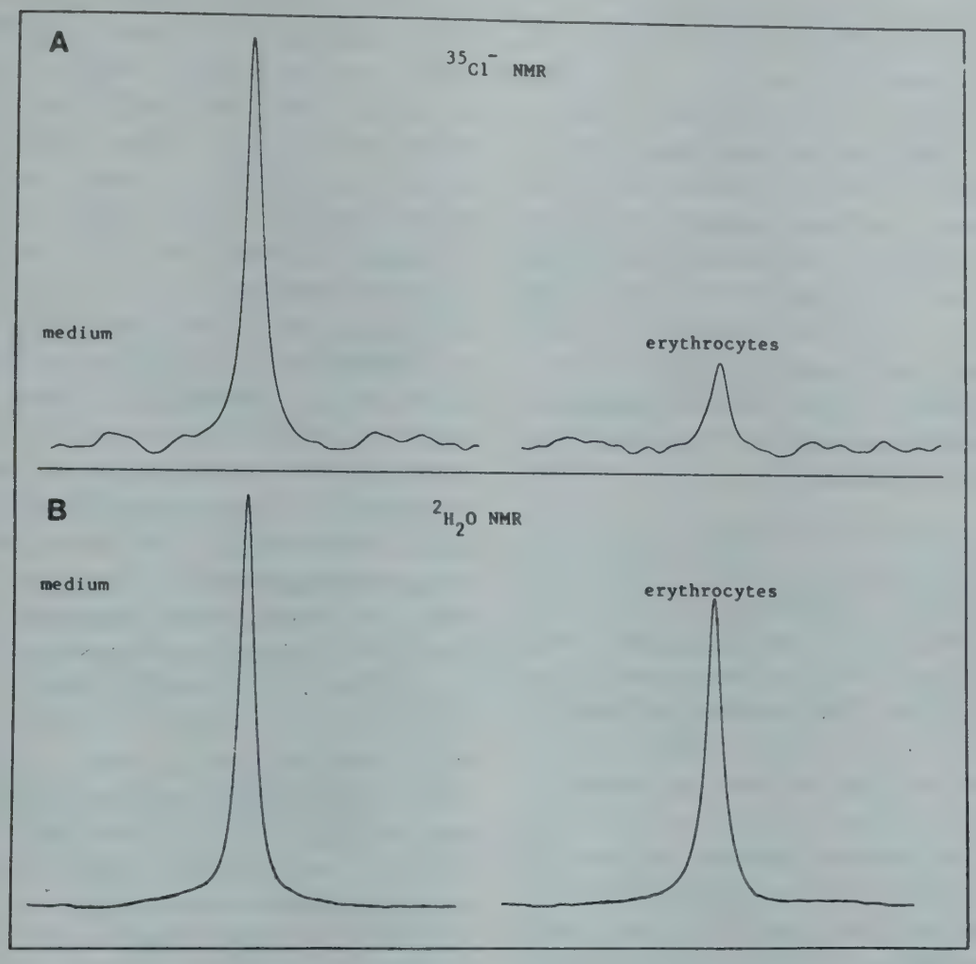

Fig. 3—Representative pairs of $^{35}Cl^-$ (A) and ^{2}H (B) NMR spectra [The left traces correspond to the cell-free medium and the right traces to the red cell suspension. Measurements may be carried out without changing the NMR probe configuration and they do not require perturbation of the cell system by addition of membrane impermeable reagents. The method is equally applicable to situation of slow and fast water exchange]

The water content values obtained by this method are expressed in units of intracellular water volume/total cell volume. This has the advantage that the values can be used directly to calculate the concentrations of intracellular constituents. No further assumptions concerning cell density are needed. For red blood cells, this method yields a value of 73.4 ± 2.4 ml water/100 ml cells[56], in good agreement with the gravimetric method, which yields 71.1 ml of water/100 ml cells. Ovarian oocytes from the frog *Rana pipiens* are much more anhydrous and yield an average intracellular water content of only $42.6 \pm 0.8\%$ (ref. 57). Previous gravimetric measurements indicated a significantly higher water content of $49.8 \pm 0.4\%$ (vol/weight). The gravimetric values may therefore include contributions from interstitial spaces and reflect difficulty in correcting for the density of the non-aqueous phase of the oocyte. Thus, NMR may well provide a useful nondestructive approach to the measurement of intracellular water content.

Applications of ^{23}Na NMR to Cells and Tissues

(a) Sodium Ions In Amphibian Oocytes And Eggs

Sodium ions appear to play an important role in the regulation of early embryonic development. *Rana* frog oocytes constitute a particularly favourable cell system for ^{23}Na NMR studies. A *Rana* female contains up to 2000-3000 large (1.8 mm diameter) oocytes arrested in first meiotic prophase. They can be readily superfused in the NMR tube and induced to undergo nearly synchronous meiotic and early mitotic divisions. Changes in ion-transport and electrical properties of the plasma membrane occur following hormonal stimulation and the effects on intracellular Na^+ have been investigated by NMR[22,28,29,33,34]. In particular, progesterone is thought to provide the physiological stimulus for reinitiation of meiotic division, and the mechanism of action, which is not well understood, is accompanied by changes in intracellular Na^+.

$Dy(PPP_i)_2$ was used to separate the resonances of intra- and extracellular Na^+ ions in *Rana* oo-

cytes, ovulated eggs, and early embryos[33]. A 4 m*M* concentration of $Dy(PPP_i)_2$ had no adverse effects on oocyte membrane potential, membrane conductance, or on the phosphocreatine level as observed by ^{31}P NMR for periods of at least 2 hr[29,33] and the reagent did not inhibit insulin or progesterone-induced nuclear breakdown. Thus, the shift reagent appears to be non-toxic to *Rana* oocytes and enabled a noninvasive analysis of intracellular Na^+ *in situ* and the detection of small changes in cell Na^+. An accurate analysis of Na^+ levels in the amphibian egg in meiotic prophase arrest, second meiotic metaphase arrest, and during early cleavage was possible[33].

The NMR data indicated that only $17 \pm 3\%$ of the total intact follicle Na^+ is detectable[22,23]. In contrast, about 40% of the total Na^+ of "denuded" oocytes (obtained by removing surrounding follicular epithelial cell layers) was found to be NMR-visible. The higher Na^+ content of denuded oocytes compared to that of follicles reflects an increase in intracellular Na^+ (about 10 mmols/kg cells) caused by exposure (30 min) to Ca^{2+}-free Ringer's solution during the denuding process. In progesterone-treated denuded oocytes NMR visible Na^+ decreased to about one-half prior to onset of nuclear breakdown (7-9 hr) and increased about 2-fold in progesterone-treated follicles following nuclear breakdown without a change in total oocyte Na^+. By ovulation (second metaphase arrest) the total intracellular Na^+ also increased and NMR-visible Na^+ now accounted for about 25% of the total egg Na^+. During early cleavage in hypotonic ($< 0.5 \times$ normal ionic strength) Ringer's solution, there was a small (6%) decrease in total Na^+, but a further increase in the NMR-visible fraction. By the 2-16 cell stage, 66-70% of the total intracellular Na^+ became NMR-visible. Thus, NMR-visible Na^+ increases markedly during early development[33].

It is quite apparent that the NMR-visible Na^+ concentration in *Rana* oocytes is significantly lower than the total concentration estimated by atomic absorption. This suggests either that all of the intracellular Na^+ is not contributing to the observed resonance, or that the observed resonance does not represent the full absorption associated with all of the magnetic transitions of the ^{23}Na nucleus. The loss of signal intensity may be due to a broadening beyond detectability of the two outer nuclear transitions by first order nuclear quadrupolar interactions involving the entire pool of cell Na^+ and is expected to be either 60% or none[14-16]. Since only about 17% of the total Na^+ is NMR-visible in prophase-arrested, follicle-enclosed oocytes and as much as 70% is visible in early cleavage stages, it does not appear possible to explain the ^{23}Na NMR data in terms of this simple picture. The observation of an intensity loss of only 30% or as much as 83%, depending upon the physiological state, in comparison to the expected full signal, must be interpreted in terms of compartmentation and selective quadrupolar broadening of the NMR-invisible Na^+. Quadrupolar interactions could cause sufficient broadening of all nuclear transitions resulting in total disappearance of the ^{23}Na resonance of a given compartment. The broadening effect may be enhanced by increases in asymmetric electric field gradients and/or immobilization of Na^+ ions. However, the compartmentalized Na^+ pool undergoing quadrupolar broadening must exchange with the NMR-visible Na^+ slowly in comparison to the magnitude of quadrupolar interaction; otherwise the observed ^{23}Na resonance would be expected to reflect the entire concentration of intracellular Na^+ ions. In the *in situ* prophase-arrested oocyte, invisible Na^+ may be only 57% if the first order quadrupolar interactions were actually causing a 60% decrease in the amplitude of NMR-visible Na^+, but as high as 83% if such interactions were not affecting the "free" Na^+ pool.

The evidence for the existence of some NMR-invisible Na^+ in the follicular oocyte and its release during early development are consistent with other studies. For example, Morrill *et al.*[58] found that a sizeable fraction of the intracellular Na^+ in prophase-arrested, follicle-enclosed oocytes could be recovered with the yolk platelet fraction and was released inpart into the cytosol by ovulation. Palmer *et al.*[59] reported that only 8% of the total Na^+ in the *Rana* follicle could be detected with Na^+-sensitive microelectrodes, although the small tip of an impaling microelectrode can sense the properties of only a small volume of the intracellular fluid and the composition of this fluid may not be representative of the total intracellular fluid when subcellular compartmentalization is present. The identity of intracellular organelles responsible for compartmentation of ions within mature oocytes is unknown. The yolk platelets, occupying a sizeable part of the oocyte, appear to be a possible site of Na^+ compartmentalization although the nucleus itself may also play a significant role. Yolk platelets, isolated in isotonic, Na^+-free, sucrose medium at room temperature did not yield a detectable NMR signal, although atomic absorption studies indicated appreciable Na^+-content (about 30% of the total oocyte Na^+). Thus, while yolk

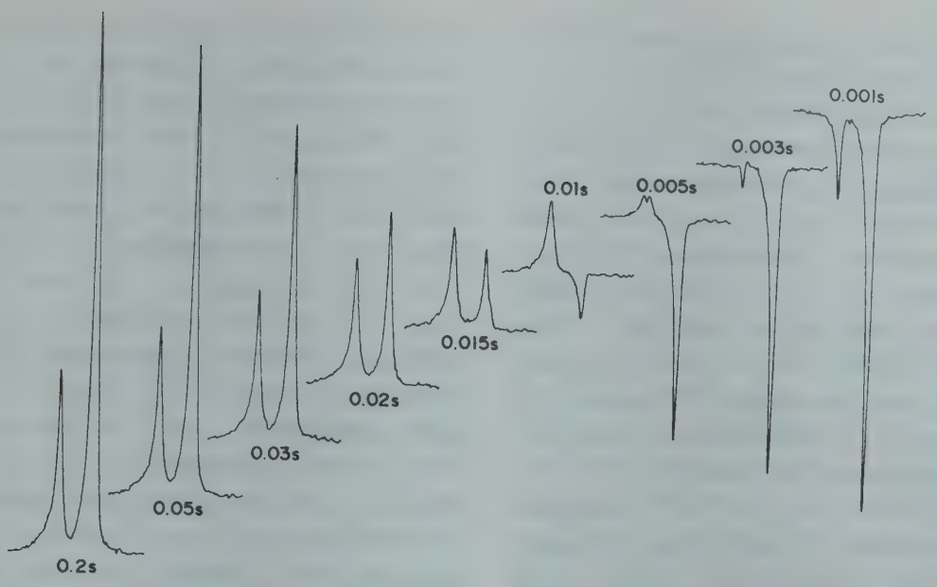

Fig. 4—Partially relaxed inversion-recovery ^{23}Na NMR spectra of *Rana* oocytes in a Ca, Mg-free medium showing evidence for compartmentation of intracellular Na^+ [The larger peak to the right in each trace arises from extracellular $^{23}Na^+$, while the smaller one to the left represents intracellular Na^+. The intracellular $^{23}Na^+$ peak appears composed of at least two components of widely differing widths and spin-lattice relaxation times; e.g. the partially relaxed spectrum at 0.005 sec clearly shows a small inverted negative intracellular $^{23}Na^+$ signal from a compartment superimposed on a predominantly positive peak of other compartments of intracellular Na^+ (ref. 33)]

platelets are rich in Na^+ this NMR-invisible Na^+ does not contribute to the oocyte NMR signal.

Partially relaxed inversion-recovery ^{23}Na FT NMR spectra were obtained to investigate the existence of intracellular compartments with differing magnetic environments and relaxation behaviour within an intact oocyte. The experiments failed to detect the existence of sizeable compartmentation of Na^+ in intact follicles in a normal Ca, Mg-containing Ringer's solution but revealed the existence of two intracellular pools with different longitudinal relaxation behavior in follicles loaded with Na^+ in a Ca, Mg-free medium (Fig. 4). (The possibility that the differently relaxing, superimposed, intracellular Na^+ resonances merely represent the central and outer transitions of the same Na^+ population appears unlikely since the use of 90° sampling pulses in the inversion-recovery sequence should have served to scramble the recovery rates of the narrow and broad transition components). Since yolk platelet Na^+ appears to be NMR-invisible, one of the two observed compartments may be the nucleus which is 400 μm in diameter. However, since this compartment is not detectable in follicles in a normal Ringer's solution, an implication would be that the Na^+ that accumulates in follicle cells during exposure to a Ca, Mg-free Ringer's solution must at least, in part, end-up in the nucleus. In any case, the NMR studies provide evidence for the existence of significant levels of NMR-invisible Na^+ in the amphibian egg and for its release during early development[33].

The role of Na^+ in the mechanism of insulin action in reinitiation of meiotic divisions in follicles and denuded oocytes was also studied[34]. In a normal Ca, Mg-containing Ringer's solution, both NMR-observable and total Na^+ were increased only slightly in insulin-treated denuded oocytes in comparison to controls. However, when follicles were allowed to accumulate Na^+ in a Ca, Mg-free medium containing 1 m*M* EDTA for 1.5 hr, the NMR-visible intracellular Na^+ level increased from 12 to 74 mmols/litre cell water. The follicles lost preloaded Na^+ when returned to Ca, Mg-containing Ringer's solution but the decrease in Na^+ occurred at a slower rate in the presence of 10 μ*M* insulin. About 3 hr after being transferred to a Ca, Mg-containing medium, insulin-treated follicles retained 46 mmols of NMR-visible intracellular Na^+/litre cell water whereas untreated follicles exhibited a significantly lower level of NMR visible Na^+ (33 mmols/litre cell water). Thus, Na^+-loaded oocytes retained a markedly (about 40%) higher level of NMR-visible intracellular Na^+ in insulin-containing medium than in insulin-free controls. In oocytes with low free Na^+ levels, however, only a slight (7%) increase in NMR-visible Na^+ relative to controls was apparent. These observations[34], together with insulin-induced hyperpolarization and decrease in membrane Na^+-conductance[22,29], suggest that insulin stimulates a nonconducting pathway for Na^+ influx in the oocyte plasma membrane. As in the case of rat cardiac myocytes (discussed later)[7], in a Ca, Mg-containing medium, the cytoplasmic level of intracel-

lular free Na^+ in *Rana* oocytes is low and the Na^+-pump may not be saturated with this cation. Any transient increase in internal Na^+ due to increased influx would shift the operating point and would result in enhanced activation of the Na^+-pump. This would tend to return the intracellular Na^+ towards the level found in the absence of insulin. After pre-incubation in a Ca, Mg-free medium, however, the level of intracellular Na^+ is increased and the Na^+ pump is likely to be operating close to its maximal efficiency. Therefore, an insulin-induced increase in influx would result in a markedly higher intracellular Na^+ level.

Part of the increased uptake of Na^+ is apparently due to an increase in fluid phase turnover via endocytosis. About 2% of the total oocyte fluid volume exchanges per hour via endocytosis[22,29]. Since the extracellular medium contains about 110 m*M* Na^+, fluid uptake via endocytosis could account for about 2 mmols/kg/hr Na^+ uptake by the prophase-arrested oocyte, i.e. about one-third of the Na^+ uptake by the prophase oocyte may be via endocytotic vesicles. Insulin increases fluid uptake and turnover by stimulating the endocytotic pathway 2 to 3-fold during the first hour after treatment. This increased endocytosis could be contributing significantly to the insulin-induced increase in NMR-visible Na^+. Insulin also causes an increase in intracellular *p*H as measured by ^{31}P NMR. In *Rana* oocytes, insulin-induced elevation of pH_i was found to be Na^+-dependent indicating that intracellular *p*H may be regulated by Na^+/H^+ exchange[29]. Thus, insulin may act, at least in part, by stimulating the Na^+/H^+ exchange system in the oocyte plasma membrane. The observed increase in NMR-visible Na^+ may be due in part to increased Na^+ uptake in exchange for H^+ as well as increased fluid phase turnover. Insulin stimulation of Na^+/H^+ exchange in the oocyte plasma membrane most likely occurs via a decrease in the activation energy of this system. This would allow Na^+, moving down its free energy gradient into the cell, to provide the energy required to move protons outward, against their free energy gradient, with a resulting increase in intracellular *p*H[60].

(b) Sodium Ions In Blood Cells

(1) *Human erythrocytes*

The concentrations of intra- and extracellular Na^+ of human red blood cells are amenable to study by ^{23}Na NMR via $Dy(PPP_i)_2$. Exposure to the shift reagent does not cause hemolysis, and does not affect the ATP, 2,3-DPG, or free Mg^{2+} levels of human red blood cells and thus has no adverse effect on the energetics of the cell or on the maintenance of ionic gradients[23]. The intensity of the intracellular ^{23}Na resonance is independent of the extracellular concentration of $Dy(PPP_i)_2$, up to at least 5 m*M*, showing that the presence of the reagent does not significantly perturb the concentration or environment of intracellular Na^+ ions. From the spectrum of fresh erythrocytes, an intracellular Na^+ ion concentration of 4.1 mmols/litre cells was estimated[3,23]. This value is significantly (20%) lower than the total concentration of Na^+ in the same red cells as estimated by atomic absorption. The simplest explanation for these results is that the entire pool of intracellular ^{23}Na ions does not contribute to the observed resonance and that the cell makes a part of the intracellular Na^+ somehow invisible to the NMR technique. The resonance of this small, yet measurable, Na^+ ion pool must be experiencing quadrupolar broadening large enough to cause its disappearance.

In the absence of a paramagnetic shift reagent, human red blood cells exhibit only a single ^{23}Na resonance due to overlap of the signals from intra- and extracellular ions. Hemolysis of packed, ATP-rich, human red cells by repeated freeze-thawing caused a $17 \pm 2\%$ increase in the overall ^{23}Na NMR signal[3,36]. This observation indicates that a small NMR-invisible pool of intracellular ^{23}Na ions exists in the human red cell and that ions in this pool become observable upon cell lysis. Using $Dy(PPP_i)_2$ to distinguish between intra- and extracellular ions, the contribution of extracellular Na^+ to the observed signal from well-packed erythrocytes has been estimated to be about 24%. Since the contribution of extracellular Na^+ to the observed signal remains unchanged upon cell lysis, the NMR-invisible pool must represent 0.17/0.76 or about 22% of the total intracellular Na^+ concentration. Essentially all of the Na^+ becomes observable by NMR in the lysed state. A similar (about 20%) increase in the ^{23}Na NMR signal was observed when well-packed fresh red cells were lysed by detergent solubilization of the cellular membranes. In contrast, no NMR-invisible Na^+ was apparent in red blood cells depolarized by treatment with 2.5 or 10 μM gramicidin, as indicated by the absence of any significant increase in the Na^+ signal upon freeze-thawing[36]. These results indicate the existence of a red cell compartment dependent upon the presence of an intact membrane potential that contains a small pool of Na^+ ions experiencing a large quadrupolar interaction. The inability of this Na^+ pool to exchange

rapidly with the free cytosolic Na^+ makes it NMR-invisible. It may be that this pool represents several layers of Na^+ ions associated with negative charges on the cell membrane. The exchange of these ions with free cytosolic Na^+ may be slow (<100/s) in the presence of a negative membrane potential, but is rapid in its absence.

(2.) *Amphiuma red blood cells*

The ^{23}Na NMR technique has been employed to measure Na^+ fluxes during volume regulation in *Amphiuma* red blood cells, which possess a particularly robust electroneutral Na^+:H^+ exchange[42]. The cytotoxicity of the shift reagents was evaluated using the dynamic cell volume regulatory response as a bioassay. The Na^+ shift reagents are known to complex Ca^{2+} [$Dy(PPP_i)_2$ much more so than DyTTHA] and the medium containing these reagents must be titrated to the appropriate [Ca^{2+}] needed to maintain normal cell function. Doing so extends the concentration range beyond which the reagents have cytotoxic effects. At low concentration, the Na^+ shift reagents $Dy(PPP_i)_2$ (<4 m*M*) or DyTTHA (<6 m*M*) do not enter the cells or alter intracellular Na^+, K^+ and Cl^- concentrations, and have no effect on ion transport in *Amphiuma* red blood cells over a 5 hr period when extracellular [Ca^{2+}] is maintained at >0.5 m*M* (ref. 42). At higher reagent concentrations or lower Ca^{2+} concentrations, these cells tend to loose K^+ and gain Na^+ in manner suggestive of membrane damage. It is however clear from this study[42] that despite Ca^{2+} chelation by $Dy(PPP_i)_2$, it is possible to adjust free Ca^{2+} by titrating the reagent with Ca^{2+}. In a solution containing 0.5 m*M* free Ca^{2+}, the shift of Na^+ resonance by 4 m*M* $Dy(PPP_i)_2$ is about 70% as large as that obtained[42] in the absence of any Ca^{2+}. It is interesting that even at free Ca^{2+} levels of 2 mM, which should be sufficient for studies of most Ca^{2+}-dependent processes, $Dy(PPP_i)_2$ provides a shift greater than that provided by other reagents under similar conditions, without any evidence of alterations in complex cellular regulation of membrane ion-transport.

Under conditions where *Amphiuma* red blood cells were allowed to loose Na^+ via a physiological transport pathway, the transported Na^+ appeared to be NMR-visible to the same extent inside or outside the cell. However, in agreement with human erythrocyte studies described above, lysing the cells altered the Na^+ environment so as to increase the total NMR-visible Na^+ by 19%, consistent with the presence of some NMR-invisible Na^+ even in these red blood cells[42].

(3) *Human lymphocytes*

The ^{23}Na NMR technique is also appropriate for the study of living lymphocytes and acceptable spectral signal to noise ratio is easily attainable[3,23]. Because several considerations have led to the hypothesis that an abnormality in the control of intracellular monovalent cations may play a role in the development of some leukemic cells, we measured the NMR-visible Na^+ contents of human normal and leukemic lymphocytes using $Dy(PPP_i)_2$ (ref. 3). Lymphocytes obtained from patients with chronic lymphocytic leukemia (CLL) and normal controls were suspended in their own serum in order to reflect the *in vivo* environment as closely as possible. The ^{23}Na NMR spectra from normal and abnormal (CLL) lymphocytes yielded significantly different NMR-visible intracellular Na^+ ion concentrations (17.5 ± 1.2 mmols/litre cells for normal and 8.7 ± 0.8 mmols/litre for abnormal cells)[3]. These results appear to indicate that NMR-visible Na^+, which is presumed to be predominantly free, is only half the normal level in leukemic lymphocytes. Accordingly, the Na^+ electrochemical gradient across the plasma membrane is two-fold larger in leukemic lymphocytes in comparison to normal lymphocytes. The ability of the ^{23}Na NMR technique to noninvasively monitor the state of intracellular ions in abnormal lymphocytes may be useful as a simple *in vitro* assay for determining the effectiveness of action of cancer chemotherapeutic agents[3].

(c) Intracellular Sodium Ions In Cardiac Myocytes

The maintenance of electrochemical gradients in heart muscle is crucial to the maintenance of resting potential, the development of action potential, and initiation of contraction. Using ^{23}Na NMR via $Dy(PPP_i)_2$ the concentration of Na^+ in cardiac myocytes at rest, as well as the magnitude and reversibility of change in intracellular Na^+ level induced by insulin-deficiency and by removal of extracellular Ca^{2+} have been studied[7]. When Ca^{2+} and insulin are present in the extracellular medium, the intracellular Na^+ level has been measured to be 8.8 ± 1.2 mmols/litre cells[7]. Upon transfer of the myocytes to a Ca^{2+}-free medium a 3-fold increase in the NMR-visible Na^+ to a level of 22.8 ± 2.6 mmols/litre myocytes has been observed. An increase of this magnitude was seen even though the calcium concentration in the extracellular medium was changed only from 300 μM to 10 μM. This increase in intracellular Na^+ was reversed by the addition of 0.3 to 1 m*M*

$CaCl_2$ to the medium. The myocytes thus remained functional in a Ca^{2+}-free medium in the NMR tube[7] and were able to pump their Na^+ down to the characteristic low level when they were transferred again to a Ca^{2+}-containing medium. Insulin-deficiency in the extracellular medium caused only a small (21%) decrease in the NMR-visible intracellular Na^+ to a level of 6.9 ± 0.5 mmols/litre cells in a normal Ca^{2+}-containing physiological medium. In a Ca^{2+}-free, insulin-deficient medium, the NMR-visible Na^+ was increased but to a level (14.6 ± 2.0 mmols/litre cells) markedly (64%) lower than that found in insulin-containing cells (22.8 ± 0.6 mmols/litre cells) under similar conditions. Thus, in a Ca^{2+}-free medium, insulin induced a substantial increase in the NMR-visible cell Na^+. The isolated cardiac myocytes used in this study were functionally intact rectangular cells which contracted repeatedly, synchronously and specifically in response to electrical stimulation in 1 m*M* Ca^{2+} and possessed nearly normal high energy phosphate content. The NMR-measured value (8.8 ± 1.2 mmols/litre cells) of intracellular Na^+ in cardiac myocytes is comparable to a recent measurement of about 8.1 mmols/kg rat myocytes by flame photometry and is similar to values reported by Fossell and Hoefeler for intact perfused hearts[40]; however, it is significantly higher than the < 3 m*M* estimated by Pike *et al.*[41].

The NMR technique allowed measurement of Na^+ loading of isolated adult cardiac myocytes when extracellular Ca^{2+} was removed and demonstrated Na^+ extrusion when extracellular Ca^{2+} was restored. Extrusion of intracellular Na^+ was accompanied by uptake of Ca^{2+} from the extracellular medium and this might occur, in part, via the Na^+/Ca^{2+} exchange system in the sarcolemma. While these effects can also be measured by the usual chemical techniques, the NMR method has the advantage that sequential Na^+ loading and unloading may be demonstrated in the same sample of cells without interference from extracellular sodium. Insulin-deficiency caused only a small decrease (21%) in intracellular Na^+ in Ca^{2+}-containing medium but a marked decrease (36%) in intracellular Na^+ in Ca^{2+}-free medium. These results are consistent with insulin stimulation of Na^+ influx in mammalian cardiac myocytes. In the presence of Ca^{2+}, the level of intracellular Na^+ is low and the Na^+-pump may not be saturated with this cation. Any increase in internal Na^+ by insulin-stimulation of Na^+ influx would shift the operating point resulting in enhanced activity of the Na^+-pump. This would tend to reduce the steady state intracellular Na^+ level towards the value measured in the absence of insulin. In a Ca^{2+}-free medium, however, the increased intracellular Na^+ may saturate the Na^+ site of the Na^+-pump so that it is operating close to V_{max}. Therefore, an increased Na^+ influx causes a more marked increase in the steady state level of this cation. It is interesting to note that increased stimulation of Na^+/K^+ exchange across cell membranes due to increased internal Na^+ would cause depletion of extracellular K^+ and may explain the well known hypokalemic effect of insulin in man.

(d) Sodium Ions In Mammalian Renal Cells

(1) *Rat outer medullary kidney tubules*

The distal nephron in the human kidney is responsible for the fine control of the total body fluid volume and the electrolyte balance, a function regulated partly by adrenal steroids. In defining the regulatory mechanisms operative in the distal tubule, the measurement of the intracellular Na^+ level is of paramount importance, since this level regulates Na^+/K^+-ATPase activity, the final determinant of the amount of Na^+ reabsorbed by the kidney.

Measurements of intracellular Na^+ levels in suspensions of separated tubules from the outer medullary segment of the thick ascending limb of the loop of Henle obtained from rat kidney have been carried[31] out using $Dy(PPP_i)_2$. The intracellular Na^+ level was 37 ± 1 mmols/litre cells water at 22°C and there was a significant decrease in the intracellular Na^+ level measured after 30 min equilibration of the tubular preparation at 37°C. The level measured at 37°C was 23 ± 2 mmols/litre cell water, consistent with a sizeable increase in Na^+/K^+-ATPase activity and a concomitant decrease in intracellular Na^+ level at the higher temperature[31].

The intracellular Na^+ measured at 22°C in the suspension of outer medullary kidney tubules was responsive to defined physiological stimuli. Furosemide, an inhibitor of the $Na^+/K^+/Cl^-$ co-transport system, the major Na^+ transporting system in the thick ascending limb of the loop of Henle, reduced the intracellular Na^+ level from a control value of 35 ± 4 to one of 24 ± 6 mmols/litre cell water. In addition, amiloride (1 m*M*), an inhibitor of the Na^+ channels in medullary collecting tubules (a minor fraction in the tubular preparation used) and the Na^+/H^+ exchange process in segments of the rat thick ascending limb reduced the intracellular level of Na^+ from 37 ± 2 to

23 ± 6 mmols/litre cell water. The Na^+/H^+ exchange mechanism may therefore be an important regulator of intracellular Na^+ levels in the cells of thick ascending limb of the loop of Henle. In contrast, ouabain, a specific Na^+/K^+-ATPase inhibitor, caused a marked rise in the measured intracellular Na^+ to 58 ± 5 from a basal level of 37 ± 2 mmols/litre cell water[31].

In validation of the measurement of the intracellular Na^+ levels, the accessibility of the entire extracellular space to the shift reagent was tested by comparing the extracellular space containing $^{35}Cl^-$ ions with the extracellular space defined by the shift reagent in the same sample of the tubular suspension. The measurement of extracellular space using $^{35}Cl^-$ NMR was based on the expectation that the resonance of intracellular $^{35}Cl^-$ ions may not be detectable due to interactions with intracellular proteins and other components which would be expected to cause a large quadrupolar broadening. Indeed when the extracellular ^{35}Cl signal was broadened beyond detection, by adding the $Zn-HbO_2$ complex, there was no observable ^{35}Cl NMR signal in the tubular suspension. Since $Zn-HbO_2$ would not be expected to penetrate the cell membrane, it was concluded that the intracellular ^{35}Cl signal was NMR-invisible. This invisibility of the intracellular $^{35}Cl^-$ ions meant that the ^{35}Cl NMR signal provided a measure of the extracellular space available to this ion. The extracellular space measured using the $^{35}Cl^-$ ion resonance was, within experimental error, the same as that defined by $Dy(PPP_i)_2$ (ref. 31).

Incubation of outer medullary kidney tubules at room temperature in a medium containing ouabain to inhibit Na^+ efflux and amphotericin B to simultaneously increase Na^+ permeability of the plasma membrane raised the NMR-visible intracellular Na^+ level to 110 ± 10 mmols/litre cell water, a level equal to $82 \pm 7\%$ of that in the incubation medium (135 m*M*). These observations exclude the possibility that nuclear quadrupolar interactions reduce the NMR signal of the free intracellular Na^+ pool by 60%. The somewhat lower estimate of intracellular free Na^+ in comparison to the extracellular Na^+, under conditions which would tend to equilibrate Na^+ across the plasma membrane, could arise from incomplete equilibration of ions among intracellular compartments[31].

(2) *Rat proximal tubules*

Transport of sodium across the proximal tubule cells, as in other transporting epithelia, is regulated by the intracellular Na^+ activity. This in turn facilitates transport of a variety of substances, including HCO_3^-, Cl^-, P_i, carbohydrates, lactate and aminoacids. Thus, precise information regarding the intracellular concentration of Na^+ is essential to the understanding of transport processes across the proximal tubule. Although NMR is noninvasive and permits serial measurements of nonbound intracellular Na^+, its limitations include the requirement for a dense cell suspension and the inability to ascertain the compartmental localization of Na^+. The noninvasiveness and specificity of NMR, however, are decisive advantages over the alternative methods in the study of Na^+ in proximal tubules.

NMR spectroscopy has been used to measure intracellular Na^+ in a suspension of proximal tubules of rat kidney subjected to various maneuvers known to stimulate or inhibit the transport of sodium[35] and thus would appear to offer a useful quantitative approach to the analysis of Na^+ handling by renal epithelial cells. Oxygenation and gentle stirring were required for maintaining tissue viability and no toxic effects of $Dy(PPP_i)_2$ up to concentrations of 5 m*M* were noticeable in a Ca^{2+}-enriched medium. Intracellular Na^+ concentration in these proximal tubules was 34.1 ± 1.8 m*M* at 22°C. Raising the temperature to 37° resulted in a fall in the intracellular Na^+ concentration to 16.3 ± 0.6 m*M*, presumably due to temperature dependence of the Na^+/K^+-ATPase activity. This would increase the extrusion of Na^+ through the basolateral membrane and thus decrease the intracellular Na^+ concentration. Addition of ouabain resulted in a 2-fold increase in Na^+ concentration to 30.9 ± 2.9 m*M*, while in the presence of nystatin, a membrane channel former, there was a 5-fold increase in internal Na^+ (ref. 35).

The basal Na^+ levels in proximal and outer medullary kidney tubules should serve as a basis of reference for further inquiries.

(3) *Sodium in tubules of diabetic rats: Role of glucose*

Renal hypertrophy is a common consequence of diabetes mellitus that precedes and possibly accounts for the increased glomerular filtration rate. Despite the wealth of information regarding the descriptive aspects of the renal hypertrophy of diabetes mellitus, little is known about the cellular mechanisms that result in the enlargement of the kidneys. It has been postulated that the glucose-mediated increase in the intracellular concentration of Na^+ initiates the chain of events leading to the increase in cell size and eventually cell number. At 96 hr after the induction of the diabetes,

there was a 60% increase in the intracellular Na^+ measured by ^{23}Na NMR using $Dy(PPP_i)_2$ compared to control ($P<0.01$) (ref. 6). No further increase in intracellular Na^+ was observed during the subsequent 11 weeks of observation. Ouabain-inhibitable Na^+/K^+-ATPase activity was substantially higher in the renal tubules of diabetic rats, the increase being proportional to that of intracellular Na^+. The rise in glucose concentration from 5 to 25 m*M* resulted in a 52% increase ($P<0.001$) in intracellular Na^+ in proximal tubules of non-diabetic animals comparable to that seen in diabetic animals[6]. Based on these findings, it has been proposed that the rise in intracellular Na^+ observed in the proximal tubules of diabetic rats is due to increased filtered load of glucose that stimulates the entry of glucose and Na^+ into renal cells resulting in an increase in intracellular Na^+. The increase in intracellular Na^+ may stimulate the discharge of Ca^{2+} from intracellular stores into the cytosol and may inhibit the exit of Ca^{2+} through the Na^+/Ca^{2+} antiport. The resulting rise in the concentration of Ca^{2+} has been shown to contribute to the activation of protein kinase C. Experiments with cell cultures have demonstrated that these events result in the rapid expression of a set of proto-oncogenes that code for DNA binding proteins. These proteins by additional mechanisms may prepare the cell for DNA replication[6].

(4) *Na/K—ATPase regulation by steroids*

A possible role of intracellular Na^+ ions in the mechanism of mineralocorticoid and/or glucocorticoid regulation of Na^+/K^+-ATPase activity has been examined[32] by ^{23}Na NMR. Such a role is suggested by the observation that amiloride, a substance known to block Na^+ channels and Na^+/H^+ exchange, markedly reduces the intracellular Na^+ level (by 38%) in segments of the thick ascending limb of the loop of Henle, and inhibited both mineralocorticoid and glucocorticoid Na^+/K^+-ATPase activation[32]. Addition of dexamethasone, a glucocorticoid, to a suspension of rat outer medullary kidney tubule segments results in a significant elevation of the intracellular Na^+ level. The dexamethasone-stimulated Na^+ level was measured to be 46.1 ± 1.2 m*M* (25°C) after 2 hr incubation, while that in the control suspension of tubules, under identical conditions, was 36.9 ± 0.9 m*M*. This effect appeared to be glucocorticoid-specific since aldosterone, a mineralocorticoid, did not change the Na^+ level significantly (38.0 ± 0.4 m*M*). These data implicate glucocorticoids in the regulation of Na^+ ion-transport in the thick ascending limb of the loop of Henle[32]. Elevation of intracellular Na^+ concentration after aldosterone treatment has been observed in mineralocorticoid-sensitive tissue. The observation that glucocorticoids, and mineralocorticoids, appear to elevate Na^+, together with the observation that amiloride both reduces intracellular Na^+ levels and inhibits steroidal Na^+/K^+-ATPase activation, would appear to implicate the intracellular Na^+ level, as a possible mediator, in the steroidal regulation of the Na^+/K^+-ATPase activity. To investigate the possibility that the Na^+ ion was the primary and direct mediator of the steroidal activation of Na^+/K^+-ATPase, the intracellular Na^+ level was elevated artificially to a level of 52 ± 3 m*M* from 26 ± 3 m*M* by superfusing tubule segments in medium containing ouabain at 37°C. Over the time interval required to elicit a maximal steroidal response in the outer medullary tubular preparation (2 hr), no change in Na^+/K^+-ATPase activity was detectable[32]. These results suggested that a change in intracellular Na^+ level was not the primary mediator of either mineralocorticoid or glucocorticoid regulation of Na^+/K^+-ATPase activity in the rat kidney outer medulla. Rather, the data were consistent with some permissive role of Na^+ ions. Superfusion in ouabain-containing medium over longer perods (18 hr), however, did result in an elevation of Na^+/K^+-ATPase activity, an increase markedly larger than that observed after steroidal stimulation[32]. However, intracellular Na^+ levels, which were elevated after 2-4 hr incubations in ouabain-containing medium, were restored to a level not significantly different from control values, after 18-20 hr of treatment. Thus, a chronic elevation in intracellular Na^+ caused an increase in the number of Na^+/K^+-ATPase enzyme sites. The experiments demonstrate a homeostatic mechanism potentially important in any chronic aberration of cellular Na^+ homeostasis[32]. The demonstration of such a response in the suspension of tubular segments responsible for the fine control of total body Na^+ balance, exposes this homeostatic mechanism as one of significant physiological and pathological importance. In essential hypertension smooth muscle cells loose their ability to regulate cellular Na^+ homeostatsis, thus allowing elevation of Na^+, that would normally be restored to basal levels by this homeostatic mechanism.

(e) ^{23}Na NMR And Cancer

Transmembrane ion fluxes and associated changes in intracellular ion concentrations have long been hypothesized as mediators in cell growth. Studies of intracellular concentrations of Na^+ in both neoplastic and nonneoplastic tissue

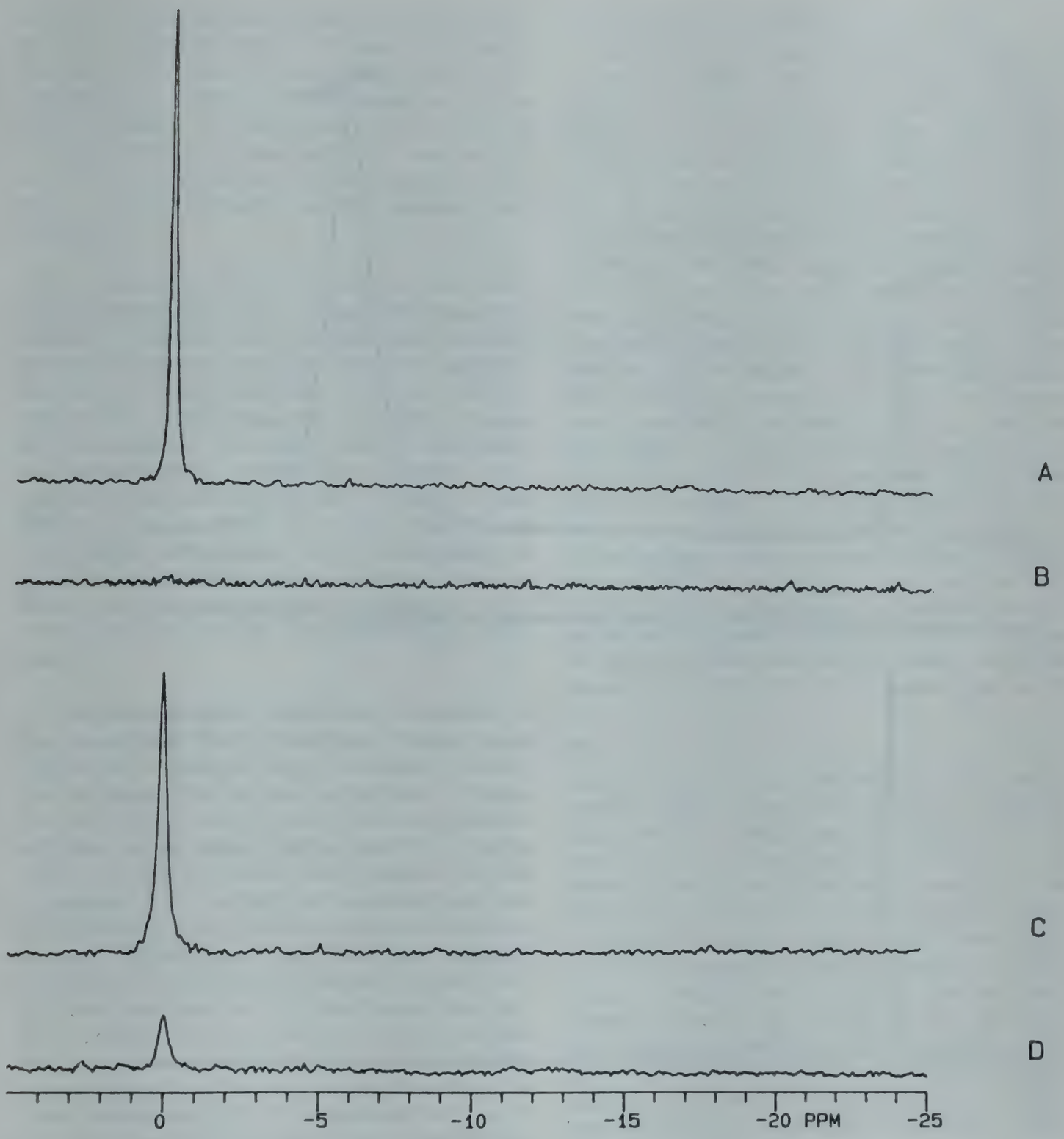

Fig. 5—^{23}Na double quantum NMR spectra of human plasma (A), plasma containing 5 m*M* $Dy(PPP_i)_2^{7-}$ (B), intact blood (C) and intact blood with 5 m*M* $Dy(PPP_i)_2^{7-}$ (D) [The spectra were recorded in the absolute value mode. Each spectrum is the fourier transform of 2048 free induction signals. Other NMR parameters were: acquisition time, 0.1 s; 90° pulse width, 30 μs; sequence recycle time, 0.17 s; double quantum preparation time, 15 ms; evolution time, 20 μs, and Larmor frequency, 132 MHz]

have strongly implicated the Na^+ cation as a mediator in cell growth and proliferation. We have explored the possible involvement in malignancy of intracellular Na^+ in a study of uterine leiomyoma and leiomyosarcoma (the benign and malignant tumors of the smooth muscle) and their nonneoplastic counterpart, myometrium, as well as colonic adenocarcinoma, a malignant tumor, and its nonneoplastic counterpart colonic mucosa[4].

The intracellular Na^+ measured using $Dy(PPP_i)_2$ in benign uterine leiomyomas was 5.1 ± 1.2 mmols/litre tissue. This value is about 3-fold less than the intracellular Na^+ concentration of 14.1 ± 1.2 mmols/litre tissue measured in myomet-

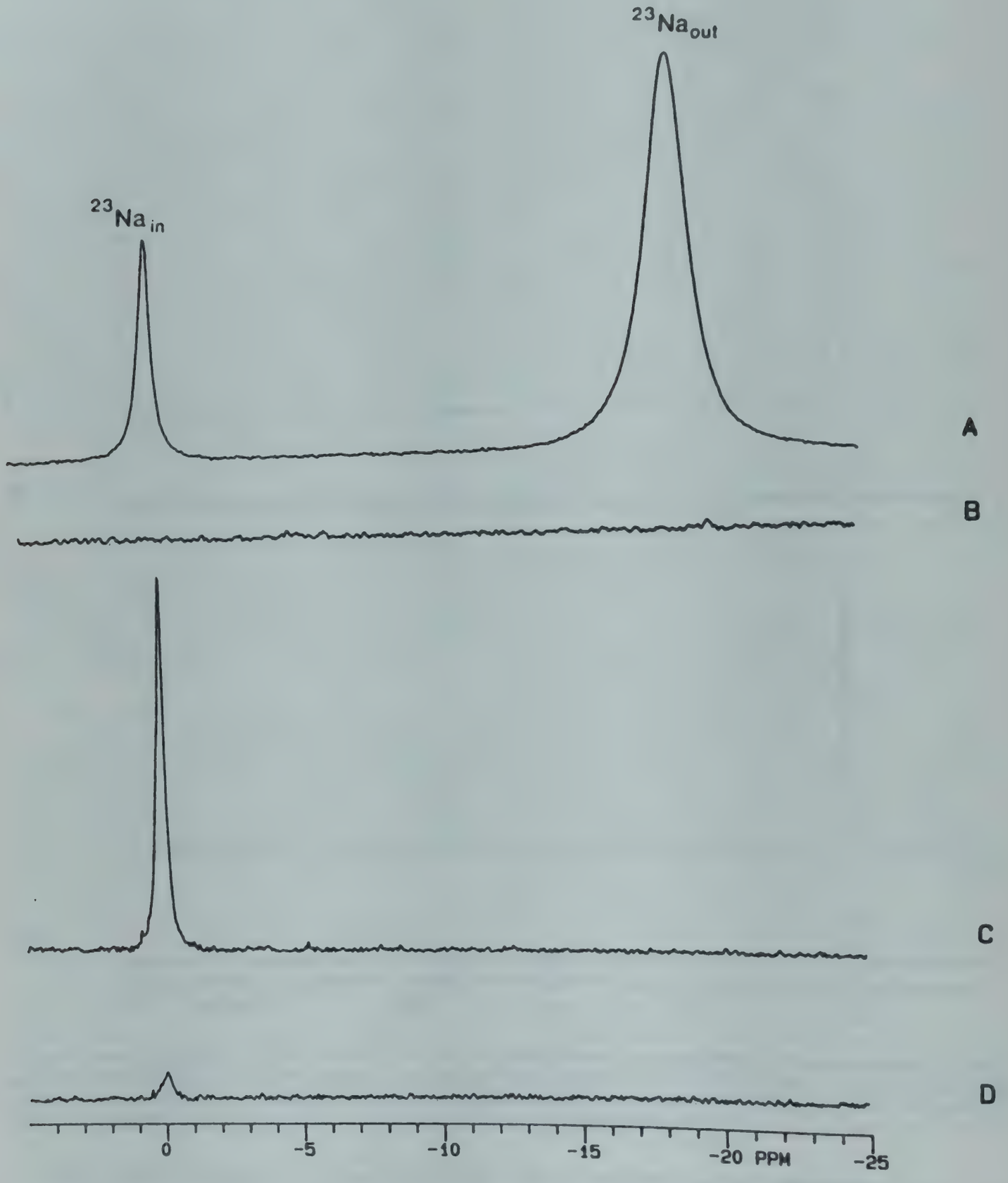

Fig. 6—^{23}Na NMR spectra of human red blood cells washed with Hank's balanced salt solution [Conventional spectrum (A) representing a time-average of 256 transients displayed with a vertical scale reduced by a factor of 10 relative to other spectra, double quantum spectra of Hank's medium (B), red cell suspension (C), and red cell suspension treated with 5 m*M* $Dy(PPP_i)_2$ (D). Double quantum acquisition parameters were the same as in Fig. 5]

rium, the normal smooth muscle layer of the uterus from which the tumor originates. In marked contrast to the sharply lower concentration of intracellular Na^+ observed in leiomyoma, uterine leiomyosarcoma, a rare malignant tumor of smooth muscle, yielded an intracellular Na^+ concentration of 34.6 ± 4.5 mmoles/litre tissue which is an almost 2.5-fold increase over the nonneoplastic counterpart[4].

The intracellulr Na^+ in well-differentiated adenocarcinoma of the colon, a malignant tumor that retains a morphological and functional resemblance to its tissue of origin, was 13.9 ± 1.5 mmoles/litre tissue, about 2-fold higher than the 8.0 ± 1.1 mmoles/litre tissue measured in colonic mucosa, the nonneoplastic counterpart. Poorly differentiated adenocarcinoma, a more highly invasive malignant tumor that deviates further in structure and function from its tissue of origin, displayed an even higher intracellular Na^+ concentration of 21.7 ± 0.6 mmoles/litre tissue, an almost 3-fold increase over the nonneoplastic counterpart and a 1.5-fold increase over the well-differentiated malignancy.

These measurements demonstrated alterations in the intracellular Na^+ in neoplastic human tissue relative to its tissue of origin. In addition, the degree of cellular proliferative activity and/or tumor invasiveness seemed to have a direct correlation with the concentration of intracellular Na^+. As has been observed with colonic and uterine tissue, the progression from normalcy to neoplasia, from benignity to malignancy, and from well-differentiation to poor differentiation were, with one exception, accompanied by increase in the intracellular Na^+. The one exception was the leiomyomas and most of these specimens were taken from peri- or postmenopausal women. Leiomyomas in postmenopausal women tend to regress and, therefore, the lower intracellular Na^+ is consistent with a regressing tissue possessing little or no proliferative activity. The colonic adenomatous polyp, the benign correlate of colonic adenocarcinoma, would provide the proliferative intermediate between normalcy and malignancy. However, such tissue was unobtainable for this study. The data suggest that benignity and malignancy may be distinguishable on the basis of intracellular Na^+ and that ^{23}Na NMR spectroscopy has the potential of becoming a powerful diagnostic tool. That is, once obtained, a measurement of intracellular Na^+ may represent as good a diagnostic and/or prognostic indicator as histopathologic viewing[4].

(f) Double Quantum NMR Of Intra- And Extracellular ^{23}Na In Cells And Tissues

The use of shift reagents to separate intra- and extracellular Na^+ has had much success and is applicable to many biological systems. The one disadvantage to the use of shift reagents lies in the fact that they can be toxic to certain cells and tissues. Because of this possible toxicity, a totally noninvasive NMR approach is preferable in some instances. It has been suggested that double quantum NMR may allow the noninvasive discrimination of different pools of Na^+ *in vivo*[61-63]. For quadrupolar nuclei ($I \geqslant 3/2$) double quantum coherence can be excited by biexponential relaxation[64] which is observed for ^{23}Na when the extreme narrowing condition ($\tau_c \ll 1/\omega_0$) does not hold. When $\tau_c > 1/\omega_0$, the outer transitions ($-3/2 \rightarrow -1/2$ and $1/2 \rightarrow 3/2$) decay more quickly than the inner transition ($-1/2 \rightarrow 1/2$) and the resulting biexponential relaxation can induce violations of the coherence transfer selection rules. The evolution of the spin system under such conditions can be described by representing coherence in terms of irreducible spherical tensor operators[64,65]. Double quantum coherence can be detected using the phase cycled INADEQUATE double quantum filter:

$$90_x - \tau/2 - 180_y - \tau/2 - 90_x - \Delta - 90_x - t\,(\text{acquire})$$

After the first pulse the spin system contains single quantum tensor components of rank 1 which are transformed to single quantum components of rank 3 during τ, the preparation time, due to the effects of biexponential transverse relaxation. The 180_y pulse at the midpoint of the interval τ merely refocuses the chemical shift. The third pulse generates double quantum tensor components of rank 3 which are transformed into single quantum components of rank 3 by the last pulse of the sequence. These components become detectable during the acquisition time t as they evolve into single quantum components of rank 1 as a result of biexponential transverse relaxation. The detected signal is given by Eq. (6)[63]:

$$M_0(3/4)(e^{-\tau/T}2f - e^{-\tau/T}2s)e^{-\Delta/T}dq\cos(2\omega\Delta)$$
$$(e^{-t/T}2f - e^{-t/T}2s)e^{i\omega t} \qquad \ldots (6)$$

where T_{2f} is the T_2 of the outer transitions, T_{2s} is the T_2 of the inner transition, T_{dq} is the relaxation rate of the double quantum transition, ω is the resonance offset, and M_0 is the equilibrium longitudinal magnetization.

It has been suggested that the intracellular Na^+ may be selectively detected with double quantum methods obviating the need for using the shift reagents, such as $Dy(PPP_i)_2$ or DyTTHA to discriminate between intra-

and extracellular Na^+ pools[61]. We have attempted to use the double quantum experiment to detect intracellular Na^+ in human blood in order to test the validity of such an approach[66]. Double quantum spectra of plasma and intact blood are shown in Fig. 5. These were obtained using a 256-step phase cycled INADEQUATE pulse sequence. Preparation (τ) and evolution (Δ) times were optimized to obtain maximum double quantum-filtered signal from the intact blood sample and set at 15 ms and 20 μs, respectively. The double quantum spectrum of plasma alone is shown in Fig. 5A and it is clear that biexponentially relaxing Na^+ present in plasma would contribute significant intensity to the total observed ^{23}Na double quantum signal of the intact blood. The addition of 5 m*M* $Dy(PPP_i)_2$, however, dramatically reduced the plasma double quantum signal as shown in Fig. 5B. We have interpreted this to be due to quenching of the plasma double quantum coherence by paramagnetic interaction of Na^+ with $Dy(PPP_i)_2$ which results in rapid transverse relaxation of ^{23}Na via a non-quadrupolar mechanism. The ^{23}Na double quantum signals of intact blood with and without $Dy(PPP_i)_2$ (5 m*M*) are shown in Figs 5C and 5D, respectively. The dramatic difference in the amplitudes of the filtered signal indicates a dominant contribution from extracellular Na^+ to the observed signal in Fig. 5C (ref. 66).

NMR spectra were also obtained from red blood cells washed with Hank's balanced salt solution with and without $Dy(PPP_i)_2$ (5 m*M*). The chemical shifts of the unshifted and shifted ^{23}Na resonances in a conventional single pulse NMR spectrum are shown in Fig. 6A. Na^+ in the saline medium alone did not give rise to a detectable double quantum signal (Fig. 6B). Figure 6C shows the double quantum spectrum of the washed cell suspension (80% hematocrit). The magnitude of the observed signal is comparable to that from intact blood in Fig. 5C. To determine whether the detected double quantum signal was arising solely from intracellular Na^+, 5 m*M* $Dy(PPP_i)_2$ was added to separate the intra- and extracellular Na^+ double quantum signals. The resulting spectrum is shown in Fig. 6D. A dramatic reduction in the double quantum signal at the unshifted frequency and no signal at the frequency of the shifted extracellular Na^+ were observed, presumably again due to quenching of the signal from extracellular Na^+ by the paramagnetic reagent. The intensity difference between the signals in Figs 6C and 6D suggests a dominant contribution to the double quantum signal from extracellular Na^+ even though the medium alone (without cells) exhibited no double quantum signal. Double quantum coherence from extracellular Na^+ in this case presumably arises from Na^+ interaction with membrane sites on the cell surface which would cause biexponential relaxation. When a paramagnetic reagent is added, the transverse relaxation of extracellular Na^+ is enhanced to the extent that the extracellular double quantum signal is not detectable under our experimental conditions. Double quantum coherence of extracellular Na^+ of a magnitude similar to that observed with 80% red cells was also observed in a suspension containing 40% cells, although in the latter case the interval corresponding to maximal signal was longer[66].

These results demonstrate that the double quantum NMR of cells and tissues allows detection of biexponentially relaxed Na^+. However, it is readily apparent that the detected signal is not solely due to intracellular Na^+ but contains a dominant contribution from extracellular Na^+ which can be quenched by interaction with a paramagnetic relaxation reagent permitting discrimination of contributions from intra- and extracellular Na^+. While the double quantum technique alone cannot be used to quantitate intracellular Na^+ due to significant contributions from the extracellular Na^+, it may be useful in qualitative studies of compartmentation and NMR-invisibility.

(g) ^{23} Na NMR Imaging

Sodium is the second most abundant NMR nucleus in tissue and is primarily present in the extracellular fluid at a concentration of about 145 m*M*. The intracellular Na^+ concentration of 10 to 20 m*M* is maintained by the Na^+/K^+-ATPase pump. Because changes in the physiological state of the cell can alter these relative concentrations ^{23}Na NMR imaging may be useful in studying diseased states. In ^{23}Na imaging studies, image contrast can arise from two general mechanisms: (i) any increase in the extracellular space, i.e., regions of edema, results in an increase in ^{23}Na concentration; and (ii) in the event of cell death the intracellular Na^+ concentration increases dramatically causing the average tissue concentration to increase by as much as an order of magnitude. The biexponential T_2 relaxation behavior of Na^+ provides an additional contrast mechanism. In biological samples the intracellular Na^+ relaxes much more rapidly (T_2 values of about 2 ms) than extracellular Na^+ (T_2 values of about 50 ms).

In vivo imaging of tissue sodium was first performed using animal models and demonstrated the dramatic image contrast expected following stroke and myocardial infarction[67-69]. For these experiments a field strength of 2.7 T was used and data acquisition took up to 4 hr. Since no chemical shift information is available, a conventional three-dimensional fourier imaging sequence was used to typically obtain 32 planes with approximately 2.5 mm resolution. Images of sodium distributions in humans have also been carried out. Hilal *et al.*[70] have obtained an image of the Na^+ distribution

within the head at 1.5 T. Particularly noticeable in these images is the intense signal (observed as a bright area) arising from the high Na^+ concentration within the cerebrospinal fluid, which serves to outline the brain and brainstem. An abnormal Na^+ distribution was observed, appearing as a bright region, in the presence of an arteriovenous malformation of the brain.

Preliminary investigation into the application of shift reagents to separate intra- and extracellular Na^+ in imaging studies have been carried out[71]; however, practical application requires the development of higher field systems as well as a nontoxic shift reagent. The use of ^{23}Na NMR for *in vivo* diagnostic imaging and spectroscopy is thus still limited by the inability to distinguish the intra- from the extracellular Na^+. Although ^{23}Na has a sensitivity of over one order of magnitude less than ^1H, as pointed out elsewhere in the paper, its relaxation times are over two orders of magnitude shorter than those of ^1H. Therefore, with time-averaging, ^{23}Na produces a signal per unit time comparable to that of ^1H. This imaging characteristic, the 100% natural abundance of the isotope, as well as the finding that NMR-visible intracellular $[Na^+]$ is indeed altered in neoplasia and other disease states should provide impetus to refine the technique of ^{23}Na NMR to the point where the intracellular compartment can be observed *in vivo*. The development of a nontoxic, membrane impermeable, paramagnetic shift reagent would permit *in vivo* spectroscopy and chemical shift imaging of the intracellular space. Alternatively, it may be possible to use differences in the relaxation behaviour of the intra- and extracellular Na^+ to obtain an image representing the intracellular Na^+ compartment.

Acknowledgement

The preparation of this article and much of the work described in here were supported, in part, by NIH Grant DK-32030.

References

1 Boynton A L, McKeehan W L & Whitfield J F (eds), *Ions, cell proliferation and cancer* (Academic Press, New York) 1982, pp. 551.
2 Cameron I L, Smith N K R, Pool T B & Sparks R L, *Cancer Res*, **40** (1980) 1493.
3 Gupta R K, Gupta P & Negendank W, in *Ion, cell proliferation, and cancer* (Academic Press, New York) 1982, pp. 1-12.
4 Liebling M S & Gupta R K, *Ann NY Acad Sci*, **508**, (1987) 149.
5 Blaustein M P, *Am J Physiol*, **232** (1977) C165-C175.
6 Kumar A M, Gupta R K & Spitzer A, *Kidney Int*, **33** (1988) 792.
7 Wittenberg B A & Gupta R K, *J biol Chem*, **260** (1985) 2031.
8 Tosteson D C, *J gen Physiol*, **39** (1955) 55
9 Lannigan D A & Knauf P A, *J biol Chem*, **260** (1985) 7322.
10 Cope F W, *Proc natl Acad Sci USA*, **54** (1965) 225.
11 Cope F W, *J gen Physiol*, **50** (1967) 1353.
12 Cope F W, *Biophys J*, **10** (1970) 843.
13 Rotunno C A, Kowalewski V & Cereijido M, *Biochim Biophys Acta*, **135** (1967) 170.
14 Berendsen H J C & Edzes H T, *Ann NY Acad Sci*, **204** (1973) 459.
15 Yeh H J C, Brinley F J & Becker E D, *Biophys J*, **13** (1973) 459.
16 Civan M M & Shporer M, *Biol Magn Reson*, **1** (1978) 1.
17 Gupta R K & Gupta P, *Biophys J*, **37** (1982) 76a.
18 Gupta R K & Gupta P, *J Mag Res*, **47** (1982) 344.
19 Brophy P J, Hayer M K & Riddell F G, *Biochem J*, **210** (1983) 961.
20 Ogino T, den Hollander J A & Shulman R G, *Proc natl Acad Sci USA*, **80** (1983) 5185.
21 Civan M M, Degani H, Margalit Y & Shporer M, *Am J Physiol*, **245** (1983) C313.
22 Morrill G A, Kostellow A B, Weinstein S P & Gupta R K, *Physiol Chem Phys Med NMR*, **15** (1983) 357.
23 Gupta R K, Gupta P & Moore R D, *Ann Rev Biophys Bioeng*, **13** (1984) 221.
24 Pettegrew J W, Woessner D E, Minshew N J & Glonek T, *J Magn Res*, **57** (1984) 185.
25 Pike M M, Fossel E T, Smith T W & Springer C S, *Am J Physiol*, **246** (1984) C528.
26 Sillerud L O & Heyser J W, *Plant Physiol*, **75** (1984) 269.
27 Shinar H & Navon G, *Biophys Chem*, **20** (1984) 275.
28 Gupta R K, Kostellow A B & Morrill G A, in *Magnetic resonance in biology and medicine* (Tata McGraw Hill, New Delhi) 1985, pp. 471-485.
29 Morrill G A, Weinstein S P, Kostellow A B & Gupta R K, *Biochim Biophys Acta*, **844** (1985) 377.
30 Ogino T, Shulman G I, Avison M J, Gullans S R, den Hollander J A & Shulman R G, *Proc natl Acad Sci USA*, **82** (1985) 1099.
31 Rayson B M & Gupta R K, *J biol Chem*, **260** (1985) 7276.
32 Rayson B M & Gupta R K, *J biol Chem*, **260** (1985) 12740.
33 Gupta R K, Kostellow A B & Morrill G A, *J biol Chem*, **260** (1985) 9203.
34 Gupta R K, Kostellow A B & Morrill G A, in *Water and ions in biological systems* (Plenum Press, New York) 1985, pp. 705-714.
35 Kumar A, Spitzer A & Gupta R K, *Kidney Int*, **29** (1986) 747.
36 Petrovich D R & Gupta R K, *Fed Proc*, **44** (1985) 1043.
37 Boulanger Y, Vinay P & Desroches M, *Biophys J*, **47** (1985) 553.
38 Gullans S R, Avison M J, Ogino T, Giebisch G & Shulman R G, *Am J Physiol*, **249** (1985) F160.
39 Ogino T, Shulman G I, Gullans S R, den Hollander J A & Shulman R G, *Proc natl Acad Sci USA*, **82** (1985) 1099.
40 Fossel E T & Hoefeler H, *Magn Res Med*, **3** (1986) 534.
41 Pike M M, Frazer J C, Dedrick D F, Ingwall J S, Allen P D, Springer C S & Smith T W, *Biophys J*, **48** (1985) 159.
42 Anderson S E, Adorante J S & Cala P M, *Am J Physiol*, **254** (1988) C466.
43 Barac-Nieto M, Neiberger R, Spitzer A & Gupta R K, *Biochim, Biophys Acta*, **968** (1988) 359.
44 Castle A M, Macnab R M & Shulman R G, *J biol Chem*, **261** (1986) 3788.
45 Burstein D & Fossell E T, *Am J Physiol*, **252** (1987) H1138.
46 Riddell F G & Hayer M K, *Biochim Biophys Acta*, **817** (1985) 313
47 Cowan B E, Sze D Y, Mai M T & Jardetzky O, *FEBS Lett*, **184** (1985) 130.
48 C S Springer (Jr), *Ann Rev Biophys Biophys Chem*, **16** (1987) 375.
49 R K Gupta in *NMR spectroscopy of cells & organisms* Vol II edited by R K Gupta (CRC Press, Boca Raton, Florida) 1987, pp. 1-32
50 Pike M M & Springer C S, *J Magn Res*, **46** (1982) 348

51 Bryden C C, Reilley C N & Desreux J F, *Anal Chem*, **53** (1981) 1418.
52 Chu S C, Pike M M, Fossel E T, Smith T W, Balschi J A & Springer C S, *J Magn Res*, **56** (1984) 33.
53 Balschi J A, Cirillo V P & Springer C S, *Biophys J*, **38** (1982) 323.
54 Gupta R K & Mildvan A S, *Methods Enzymol*, **54** (1978) 151.
55 Mildvan A S & Gupta R K, *Methods Enzymol*, **49** (1978) 322.
56 Hoffman D & Gupta R K, *J Magn Res*, **70** (1986) 481.
57 Morrill G A, Kostellow A B, Hoffman D & Gupta R K, *Ann NY Acad Sci*, **508** (1987) 531.
58 Morrill G A, Kostellow A B & Murphy J B, *Exp Cell Res*, **66** (1971) 289.
59 Palmer L G, Century T J & Civan M M, *J Memb Biol*, **40** (1978) 25.
60 Moore R D & Gupta R K, *Int J Quant Chem Quant Biol Symp*, **7** (1980) 83.
61 Pekar J, Renshaw P F & Leigh J S (Jr), *J Magn Reson*, **72** (1987) 159.
62 Pekar J & Leigh J S (Jr), *J Magn Reson*, **69** (1986) 582.
63 Rooney W D, Barbara T M & Springer C S (Jr), *J Am chem Soc*, **110** (1988) 674.
64 Jaccard G, Wimperis S & Bodenhausen G, *J chem Phys*, **85** (1986) 6282.
65 Muller N, Bodenhausen G & Ernst R R, *J Magn Reson*, **75** (1987) 297.
66 Jelicks L A & Gupta R K, *J Magn Res*, In press 1989.
67 Hilal S K, Maudsley A A & Simon H E, *Am J Neur Res*, **4** (1983) 245.
68 Maudsley A A & Hilal S K, *Brit Med Bull*, **40** (1984) 165.
69 Ra J B, Hilal S K & Cho Z H, *Magn Reson Med*, **3** (1986) 296.
70 Hilal S K, Maudsley A A & Ra J B, *J Comput Assist Tomogr*, **9** 1-10 (1984).
71 Hilal S K, Fabry M, Segebarth C, Wittekoęk S & Ra J B, in *3rd Annu Meet Soc Magn Reson Med*, New York, August, 1984, pp. 322.

Indian Journal of Chemistry
Vol. 27A, October 1988, pp. 847-850

Papers

Hückel Rule in Annulenes with One Heteroatom

I GUTMAN*†
Division of Physical Chemistry, The University of Trandheim, N-7034 Trondheim-NTH, Norway
and
A K MUKHERJEE
Department of Chemistry, Burdwan Raj College, Burdwan 713104, India

Received 19 *May* 1988; *accepted* 31 *May* 1988

The validity of the Hückel 4m + 2 rule of aromaticity is examined in the case of (4m)-, (4m + 1)-, (4m + 2)- and (4m + 3)-membered annulenes with one heteroatom. Graph-theoretical proof techniques are employed. It has been established that the validity of the Hückel rule depends on the size of the ring and on the values of the heteroatom parameters h and k. Four general rules of modulo 4 type are formulated. These are obtained by examining the sign-change patterns of the coefficients of the characteristic polynomials of the respective molecular graphs.

Rigorous quantum chemical methods for predicting molecular properties require rather involved mathematics and long and tedious computation procedures. As a consequence of this, the connection between the structure of the molceule, under consideration and its predicted properties remains obscure. Furthermore, using these methods it would be rather difficult to establish regulatities valid for entire classes of structurally related molecules. Therefore simple quantum chemical approaches, in spite of their lower accuracy and reliability, remain a matter of choice in contemporary theoretical chemistry. This, in particular, is valid for the Hückel molecular orbital (HMO) theory. For some recent investigations based on the HMO method see references 1-5.

The use of HMO theory for elucidation of dependence of π-electron properties of conjugated molecules on molecular structure is much faciliated by using graph theory. The application of graphs in HMO theory is based on the fact[6,7] that the Hückel-Hamiltonian matrix becomes identical with the adjacency matrix of the molecular graph after choosing the zero energy to be equal to α (= the Coulomb integral of an sp^2-carbon atom) and the energy unit to be equal to β (= the resonance integral between two adjacent sp^2-carbon atoms). An advantage of using the graph theory is that numerous interesting chemical information about the conjugated molecules can be deduced without the actual finding of the HMO eigenvalues and eigenvectors, considering only the characteristic polynomial of the molecular graph[6-8].

†Permanent address: Faculty of Science, University of Kragujevac, P.O. Box 60, YU-34000 Kragujevac, Yugoslavia

The well-known 4m + 2 rule of aromaticity was first given by Hückel[9] and was subsequently investigated by many authors[10-19]. Eventually the rule was extended to polycyclic conjugated hydrocarbons[20,21] as well as to a variety of other chemical phenomena[22-25].

The aim of the present investigation is to test the validity of the Hückel rule in annulenes with one heteroatom. We apply a simple algebraic procedure, based on the Descartes rule of signs. Using the Descartes rule we determine the number of positive zero of the characteristic polynomial $\phi[G(h)], x)$ of the molecular graph G[h] which corresponds to the heteroannulene. Such graph-theoretical techniques have already been employed in the study of the π-electron energy level patterns of conjugated molecules[26,27] and, recently, for verifying the Hückel rule for non-alternant annulenes[19].

The Rules

The Hückel rule states that 4m + 2 π-electron are required for an annulene to have a closed-shell electronic configuration, in the sense that all bonding energy levels are completely occupied and all antibonding and nonbonding levels are empty. Regarding the validity of this rule for annulenes containing a single heteroatom, the following four general rules are deduced. It is assumed (as usual in HMO theory[28]) that the Coulomb integral of the heteroatom X is equal $\alpha_X = \alpha + h\beta$. At this point we consider the case when the carbon-heteroatom resonance integral is equal to the carbon-carbon resonance integral (= β).

Let n be the size of the cycle, i.e. the numbr of

conjugated atoms in the heteroannulene considered. Let further m denote a positive integer.

A1. When $n = 4m + 2$, then the Hückel rule is valid irrespective of the value of the parameter h.

A2. When $n = 4m + 1$, then the Hückel rule is valid if $h > -2$ and is violated if $h < -2$.

A3. When $n = 4m + 3$, then the Hückel rule is violated if $h \geqq 2$ and is valid otherwise.

A4. When $n = 4m$, then the Hückel rule is valid for $h > 0$ and is violated for $h < 0$.

Proof of the Rules

Denote by G[h] the molecular graph of the monocyclic conjugated compound with just one heteroatom X. As usual[7], the cycle with n vertices and the path with $n + 1$ vertices will be denoted by C_n and P_{n-1}, respectivley. Note that C_n is the molecular graph of the [n] annulene (without heteroatoms), whereas P_{n-1} represents the conjugated system obtained by deletion of the heteroatom.

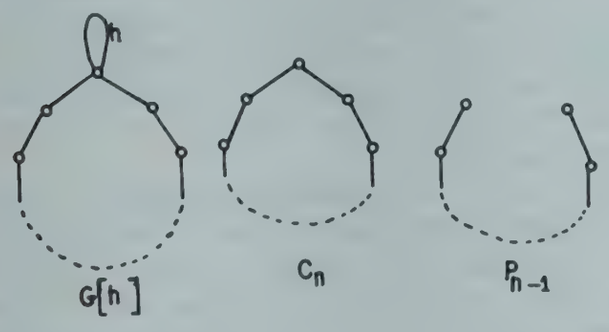

The characteristic polynomial of G[h] will be denoted by $\phi(G[h], x)$ and written in the form

$$\phi(G[h], x) = \sum_{j=1}^{n} a_j x^{n-j} \qquad \ldots (1)$$

According to the Descartes rule the number of positive roots of the equation $\phi(G[h], x) = 0$ is equal to the number of sign-changes in the sequence $a_0, a_1, a_2, \ldots, a_n$ of the coefficients of $\phi(G[h], x)$. On the other hand[6-7] each positive root of $\phi(G[h], x) = 0$ corresponds to a bonding π-electron HMO energy level. Hence by examining the signs of the coefficients of $\phi(G[h], x)$ we can conclude about the number of bonding MOs in the corresponding π-electron system.

The characteristic polynomial lof G[h] satisfies the relation[7] (2),

$$\phi(G[h], x) = \phi(C_n, x) - h\,\phi(P_{n-1}, x) \qquad \ldots (2)$$

Explicit combinatorial expressions for the characteristic polynomials of C_n and P_{n-1} are known[7,29], viz. Eqs (3) and (4)

$$\phi(C_n, x) = -2 + \sum_{j=0}^{[n/2]} (-1)^j \frac{n}{n-j} \binom{n-j}{j} x^{n-2j} \qquad \ldots (3)$$

$$\phi(P_{n-1}, x) = \sum_{j=0}^{[(n-1)/2]} (-1)^j \binom{n-i-j}{j} x^{n-1-2j} \qquad \ldots (4)$$

where [x] stands for the greatest integer smaller than or eqial to x.

Substituting Eq. (3) and (4) back into Eq. (2) and taking into account (1), one obtains expressions (5a-d)

$$a_{2j} = (-1)^j \frac{n}{n-j} \binom{n-j}{j} \qquad j = 0,1,2,\ldots;\ 2j < n \quad (5a)$$

$$a_{2j+1} = -h(-1)^j \binom{n-1-j}{j}$$

$$j = 0,1,2,\ldots, \qquad 2j + 1 < n \qquad (5b)$$

$$a_n = 2(-1)^{n/2} - 2 \qquad \text{if n is even} \qquad (5c)$$

$$a_n = -h(-1)^{(n-1)/2} - 2 \qquad \text{if n is odd.} \qquad (5d)$$

Proof of A1

From the expressions (5) it follows that for $h > 0$ the sign-arrangement of the coefficients of $\phi(G[h], x)$, is of the form

$$+ - - + + - \ldots + - -$$

Since there are $4m + 3$ coefficients of the polynomial $\phi(G[h], x)$there will be $2m + 1$ sign-inversions and conseuqently the number of bonding HMOs is also $2m + 1$. A total of $2(2m + 1) = 4m + 2$ electrons is required to fill these energy levels and thus the closed-shell configuration is achieved by means of $4m + 2$ electrons. The Hückel rule holds.

When $h < 0$ the following sign-arrangement is found:

$$+ + - - + + \ldots + + -$$

implying again $2m + 1$ sign-inversions, i.e. $2m + 1$ positive zeros of $\phi(G[h], x)$.

The completes the proof of Rule A1.

Proof of A2

In this case the sign of the last coefficient of $\phi(G[h], x)$, namely of a_n on h. From Eq. (5d) it is seen that because of

$$(-1)^{(n-1)/2} = (-1)^{2m} = +1$$

a_n is negative if h is greater than -2 and a_n is positive if h is less than -2. If $h > 0$ then we have

the following sign-arrangement of the coefficients of $\phi(G[h], x)$:

$+ - - + + - \ldots . - + + -$

Here $\phi(G[h], x)$ possesses $4m+2$ coefficients and so we have $2m+1$ sign-changes, $2m+1$ bonding MOs and $4m+2$ π-electron needed to achieve a closed-shell configuration. Thus the Hückel rule holds.

If $-2<h<0$, then the sign-arrangement is of form

$+ + - - + + - - \ldots . - - + -$

The signs of a_n and a_{n-1} are opposite and there are again $2m+1$ sign-changes. This means that the Hückel rule holds.

If $h<-2$ the sign-arrangement is

$+ + - - + + - - \ldots . - - + +$

Now the signs of a_n and a_{n-1} are the same and only $2m$ sign-changes occur. This means that only $4m$ π-electron will be needed to completely occupy the $2m$ bonding MOs. The Hückel rule is violated.

This proves the Rule A2.

Proofs of A3 and A4

In this cases the proofs are completely analogous and will not be reproduced here.

A Generalization

If we consider the perturbation of both the Coulomb and the resonance integrals due to the introduction of the heteroatom X, namely, $\alpha_x = \alpha + h\beta$, $\beta_{CX} = k\beta$, then the molecular graph of the heteroannulene takes the form G[h,k]:

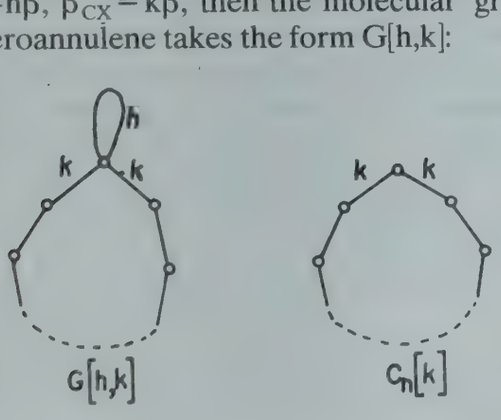

and in analogy to formula (2) we have

$$\phi(G[h,k], x) = \phi(C_n[k], x) - h\phi(P_{n-1}, x).$$

By applying a graph-theoretical technique develop by Aihara[30], which in fact is a modified version of the Sachs theorem[7,8] it can be shown that the characteristic polynomial of $C_n[k]$ is of the form (6)

$$\phi(C_n[k], x) = x^n - (\nu_2 + \lambda_2 k^2)x^{n-2} + (\nu_4 + \lambda_4 k^2)x^{n-4} - (\nu_6 + \lambda_6 k^3)x^{n-6} + \ldots\ldots a_n[k] \quad \ldots (6)$$

where ν_{2i} = number of subgraphs of $C_n[k]$, composed of i copies of K_2, each K_2 having unit edge weight, and λ_{2i} = number of subgraphs of $C_n[k]$, composed of i copies of K_2, one K_2 with edge weight k.

Recall that K_2 is the graph possessing two vertices joined by an edge.

The last term in Eq. (6), denoted by $a_n[k]$, is the term independent of x. It can be obtained by Aihara's method as follows.

For even, n two sets of disjoint K_2s are possible, each with one weighted edge. A further contribution to $a_n[k]$ comes from the cycle with n vertices, whose weight is k_2. If n is odd, then only the cycle contributes to $a_n[k]$. Direct calculation then gives[30]

for $n = 4m+2$; $a_n[k] = 2[(-1)^{2m+1}2^0k^2] + (-1)^1 2^1 k^2 = -4k^2$

for $n = 4m+1$; $a_n[k] = (-1)^1 2^1 k^2 = -2k^2$

for $n = 4m+3$; $a_n[k] = (-1)^1 2^1 k^2 = -2k^2$

for $n = 4m$; $a_n[k] = 2[(-1)^{2m}2^0k^2] + (-1)^1 2^1 k^2 = 0$.

By comparing Eqs (3) and (6) we find that the corresponding coefficients of $\phi(C_n, x)$ and $\phi(C_n[k], x)$ have identical signs. In particular, $a_n[k]$ differs from a_n only by a factor k^2. Therefore the rules A1 to A4 must retain their forms when the perturbation of the resonance integral is included, the only change being in the ranges of h. The modified rules can be formulated as follows:

B1. When $n = 4m+2$, then the Hückel rule is valid irrespective of the values of the parameters h and k.

B2. When $n = 4m+1$, then the Hückel rule is valid if $h > -2k^2$ and is violated if $h < -2k^2$.

B3. When $n = 4m+3$, then the Hückel rule is violated if $h \geqq 2k^2$ and is valid otherwise.

B4. When $n = 4m$, then the Hückel rule is valid for $h > 0$ and is violated for $h < 0$, irrespective of the value of the parameter k.

Conclusions

From Streitwieser's list[28] of HMO heteroatom parameters we find that the only case of $h < -2k^2$ occurs with boron ($h_B = -1$, $k_{CB} = 0.7$). Thus the Rule B_2 suggests that a fivemembered heterocyclic radical with boron contributing one π-electron will be unstable since one electron will occupy an antibonding MO. It such a radical is prepared at all, then it is most likely that the odd electron will reside on a sp^2-hybrid orbital of boron, giving a stable 4π-electron ring conjugated through a vacant p-orbital of B, violating thus the Hückel rule.

As $h_{N:} = 1.5$ and $k_{CN} = 1$, we find $h > 2k^2$ and so by Rule B2 pyrrole should be aromatic. An example of $h > 2k^2$ is found with oxygen contributing two π-electrons ($h_O = 2k_{CO} = 0.8$). Thus by Rule B2, furan is stable and obeys the Hückel rule. By Rule B3, a 7-membered heterocycle with oxygen contributing two π-electron will be relatively stable, disobeying the $4m + 2$ rule.

It should be pointed out here that the presence of requisite number of π-electron does not always imply aromaticity. For larger values of m the predictions based on HMO theory may fail. Thus Dewar and Gleicher[31] have shown, using a variant of SCF MO method, that $(4m + 2)$-annulenes are aromatic up to $m = 5$ and are non-aromatic for $m > 5$. This latter conclusion has been verified by NMR studies[32]. The graph-theoretical analysis outlined in the present paper does not bring out such limits on the value of m. This, however, may be regarded as a drawback of the HMO model itself and not a fault of the graph-theoretical method.

References

1 Haymet A D J, *Chem Phys Lett*, **122** (1985) 421.
2 Haymet A D J, *J Am chem Soc*, **108** (1986) 319.
3 Aihara J, *Bull chem Soc Japan*, **60** (1987) 3143.
4 Stein S E & Brown R L, *J Am chem Soc*, **109** (1987) 3143.
5 Sakurai K & Nishimoto K, *Chem Phys Lett*, **144** (1988) 353.
6 Graovac A, Gutman I & Trinajstić N, *Topological approach to the chemistry of conjugated molecules* (Springer-Verlag, Berlin) 1977 and the references cited therein.
7 Gutman I & Polansky O E, *Methematical concepts in organic chemistry*, (Springer-Verlag, Berlin) 1986 and the references cited therein.
8 Graovac A, Gutman I, Trinajstic N & Zivkovic T, *Theoret chim Acta*, **26** (1972) 67.
9 Hückel E, *Z Phys*, **76** (1932) 628.
10 Polansky O E, *Monatsh Chem*, **91** (1960) 916.
11 Fukui K, Imamura A, Yonezawa T & Nagata C, *Bull chem Soc Japan*, **33** (1960) 1591.
12 Breslow R & Mohάchi E, *J Am chem Soc*, **85** (1963) 431.
13 Fukui K & Fujimoto H, *Bull chem Soc Japan*, **40** (1967) 2024.
14 Figeys H P, *Tetrahedron Lett*, (1970) 5225.
15 Gutman I, Milun M & Trinajstić N, *Croat chem Acta*, **44** (1972) 207.
16 Gutman I, Milun M & Trinajstić N, *Croat chem Acta*, **49** (1977) 441.
17 Inagaki S & Hirabashi Y, *J Am chem Soc*, **99** (1977) 7418.
18 Klein D J & Trinajstić N, *J Am chem Soc*, **106** (1984) 8050.
19 Mukherjee A K, *Indian J Chem*, **25A** (1986) 574.
20 Gutman I & Trinajstic N, *J chem Phys*, **64** (1976) 4921.
21 Gutman I, *Chem Phys Lett*, **46** (1977) 169.
22 Goldstein M J & Hoffmann R, *J Am chem Soc*, **93** (1971) 6193.
23 Randic M, *J Am chem Soc*, **99** (1977) 444.
24 Plath P J, *Match*, **7** (1979) 229.
25 Gutman I & Polansky O E, *Theoret chim Acta*, **60** (1981) 203.
26 Gutman I & Trinajstić N, *Chem Phys Lett*, **20** (1973) 257.
27 Gutman I, Trinajstić N & Živkovic T, *Tetrahedron*, **29** (1973) 3449.
28 Streitwieser A, *Molecular oribital theory for organic chemists*, (Wiley, New York) 1961.
29 Cvetković D, Doob M & Sachs H, *Spectra of graphs-Theory and application* , (Academic Presss, New York) 1980.
30 Aihara J, *J Am chem Soc*, **98** (1976) 2750.
31 Dewar M J S & Gleicher G J, *J Am chem Soc*, **87** (1965) 685.
32 Haddon R C, Haddon V R & Jackman L M, *Topics curr Chem*, **16** (1971) 103.

Indian Journal of Chemistry
Vol. 27A, October 1988, pp. 851-854

Semiempirical CNDO/S & PPP Calculations on Benzimidazole-2(3*H*)-one & Its Different Prototropic Species

ASHOK K MISHRA
P.G. Department of Chemistry, Sambalpur University, Jyoti Vihar, Sambalpur 768 019
and
SNEH K DOGRA*
Department of Chemistry, Indian Institute of Technology, Kanpur 208 016

Received 25 *September* 1987; *revised and accepted* 14 *January* 1988

Semiempirical MO calculations with CI using PPP and CNDO/S methods, both on enol(I) and keto(II) forms of 2-hydroxybenzimidazole, have been made to correlate the predicted transitions with experimental ones. The origin of the longest wavelength transition is clearly demonstrated to be from the benzene ring of form II. The basicity changes on excitation, as predicted from the change in charge densities of the basic centres in the ground and excited states conform to our experimental findings.

2-Hydroxybenzimidazole (BIOH, I) exists mainly in the keto form, i.e. as benzimidazol-2(3*H*)-one (BIOH, II)[1-3], despite the fact that its reaction with $POCl_3$, gives the product arising from the hydroxy form (I)[3]. In the present study, using the semiempirical MO calculations, an attempt has been made to correlate the predicted electronic transitions with experimental transitions and to supplement some of the experimental observations by theory.

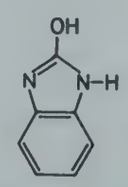

(BIOH I)

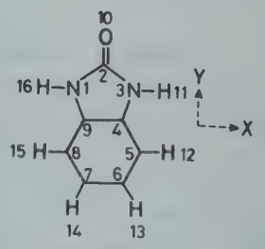

(BIOH II)

Methods of Calculations

Both Pariser-Parr-Pople (PPP)[4,5] and CNDO/S[6] methods were employed to study the ground and excited state structures of the molecule in different prototropic forms. The programs[6] were obtained from QCPE Indiana University, Bloomington, USA. Different parameters required for the calculations were taken from literature[7]. The one-centre two-electron repulsion integrals were calculated by Pariser approximation[8]. Two-centre electron repulsion integrals were calculated by the Nishimato-Mataga method[9]. All the configurations obtained by single electron excitation from the occupied molecular orbitals to the unoccupied molecular orbitals were considered in calculating all configurational interactions.

The closed shell spectroscopic CNDO/S molecular program of DelBene and Jaffe[6], as developed by Ellis *et al.*[10], was used for the study. The excited states were generated from the ground state occupied and virtual orbitals through the application of a configuration interaction procedure amongst the forty lowest singly excited states. The excited state electron densities were calculated using Eq. (1)

$$\rho^*JA = \rho_A^0 + \sum_m^{CI} \sum_\mu^{A} C_{jm}^2 (C_{\mu j}^2 - C_{\mu c}^2) \quad \ldots (1)$$

where in ρ_A^0 is the ground state electron density on atom A and C_{jm} is the coefficient of the m^{th} configuration contributing to the j^{th} state. $C_{\mu j}$ and $C_{\mu i}$ are the orbital coefficients of the final and initial MOs involved in the m^{th} configuration. The characterization of different states was done on the basis of configurational analysis.

The experimental bond lengths and bond angles of the parent benzimidazole were used[11] in the calculations. The atomic centres are numbered as shown in structure (II). The origin of the coordinate system was fixed at the centre of the bridge bond and the axes were labelled as shown. Calculations for the cation and the dication of BIOH by the PPP method could not be done as the empirical parameters for these groups were not available in literature. The present calculations were performed using a Decsystem 10 computer.

Results and Discussion

The experimental and calculated transition wavelengths of different prototropic forms of BIOH(II) along with oscillator strengths are given in Table 1.

Table 1—Electronic Spectra of Benzimidazol-2(3*H*)-one and Its Prototropic Forms

Experimental			PPP			CNDO/S		
Transition wavelength (nm)	Type	Oscillator strength (f)	Transition wavelength (nm)	Type	Oscillator strength (f)	Transition wavelength (nm)	Type	Oscillator strength (f)
				Form(II)				
291			294	$^1\pi\rightarrow\pi^*$	0.186	292	$^1\pi\rightarrow\pi^*$	0.039
285	$^1\pi\rightarrow\pi^*$	0.125	273	$^1\pi\rightarrow\pi^*$	0.037			
281			238	$^1\pi\rightarrow\pi^*$		247	$^1\pi\rightarrow\pi^*$	0.071
227	$^1\pi\rightarrow\pi^*$	0.161	223	$^1\pi\rightarrow\pi^*$	0.109	213	$^1\pi\rightarrow\pi^*$	0.382
				Cation (protonated at oxygen)				
						292	$^1\pi\rightarrow\pi^*$	0.089
273						265	$^1\pi\rightarrow\pi^*$	0.027
267	$^1\pi\rightarrow\pi^*$	0.141				256	$^1\pi\rightarrow\pi^*$	0.010
261						235	$^1\pi\rightarrow\pi^*$	—
220	$^1\pi\rightarrow\pi^*$	0.261				220	$^1\pi\rightarrow\pi^*$	0.069
				Dication				
279						402	$^1\pi\rightarrow\pi^*$	0.022
271						355	$^1\pi\rightarrow\pi^*$	0.073
266	$^1\pi\rightarrow\pi^*$	0.172				259	$^1\pi\rightarrow\pi^*$	0.049
						235	$^1\pi\rightarrow\pi^*$	0.001
235	$^1\pi\rightarrow\pi^*$	0.207				219	$^1\pi\rightarrow\pi^*$	0.019
				Anion				
285	$^1\pi\rightarrow\pi^*$	0.156	291	$^1\pi\rightarrow\pi^*$	0.142	330	$^1\pi\rightarrow\pi^*$	0.084
						304	$^1\pi\rightarrow\pi^*$	—
			262	$^1\pi\rightarrow\pi^*$	0.390	299	$^1\pi\rightarrow\pi^*$	0.181
						229	$^1\pi\rightarrow\pi^*$	0.088
237	$^1\pi\rightarrow\pi^*$	0.230	226	$^1\pi\rightarrow\pi^*$	1.084	221	$^1\pi\rightarrow\pi^*$	0.413

Although experimental spectral data have been taken in water, the band maxima match the O − O transitions predicted both by PPP and CNDO/S to a reasonable degree of satisfaction; however, the oscillator strengths do not match satisfactorily. The discrepency in the experimental and calculated results for the dication and monoanion is only in the long wavelength region, predicted by CNDO/S method. In the case of monoanion, CNDO/S method predicts an $n\rightarrow\pi^*$ band at 304 nm with zero oscillator strength, in agreement with the experimental results that no $n\rightarrow\pi^*$ transition is observed[12,13]. But the agreement of the other predicted transitions is quite good. Similarly the long wavelength transition of the dication, predicted by CNDO/S is also weak and can be discarded. It can further be seen that all the transitions are of $\pi\rightarrow\pi^*$ nature, as reported earlier in calculations carried on benzimidazole molecule[12].

The contributions of various molecular orbitals involved in the longest wavelength singlet transition and their localization at various atomic centres are listed in Table 2. It can be seen that although all the HOMOs are not rigorously localized on the benzene ring, most of them are almost confined to it, confirming previous work[13] that the long wavelength transition originates from the benzene ring moiety. This is particularly more clear from the CNDO/S calculations carried out on the neutral species, because the first LUMO is nearly localized on the benzene ring. In the case of the monocation and the dication, the first LUMO is completely localized on the imidazole ring, indicating that charge migration should occur from the carbocyclic to the heterocyclic ring. This observation is in agreement with the experimental results[14-16] that charge migration from the benzene ring to the imidazole ring is facilitated by the presence of positive charge either on the tertiary nitrogen atom or on the $\rangle C=OH^+$ group. On the other hand, in the case of monoanion the negative charge present on imidazole nitrogen atom will inhibit this charge migration along the direction mentioned above, as has been observed experimentally[17,18].

The electron densities at different basic centres for the ground and first excited singlet states for different forms of BIOH(II), reported in Table 3, show that electron densities at these basic centres do not change significantly on excitation. Nevertheless the electron densities on the oxygen centre in all the prototropic forms, including neutral, always show a small a decrease on excitation, implying participa-

Table 2—Contribution of Various Molecular Orbitals Involved in Longest Wavelength Singlet Transition and Their Localization

Compound	PPP					CNDO				
	Transition	Configuration	Composition (%)	MO	Localization of orbital	Transition	Configuration	Composition (%)	MO	Localization
2(3*H*)-Benzimidazolone	294	5→8	25	5π	1,3,4,5,6,7,8,9	292	25→26	74	24π	3,4,5,6,7,8
		6→7	36	6π	1,3,4,6,7,9,10		24→26	18	25π	delocalized
		6→9	25	7π*	1,2,3,10,5,6,7,8				26π*	2,5,6,7,8,9
				8π*	4,5,6,7,8,9					
Cation						292	25→26	86	24π	3,4,5,6,7,8
							24→26	11	25π	1,2,3,4,7,6
									26π*	1,2,3,10
Dication						402	25→26	36	24π	1,2,3,4,5,7,8
							24→26	50	25π	4,5,6,7,8,9,1
									26π*	1,2,3
Anion	291	4→7	16	4π	4,6,7,9,2,10	330	25→26	81	25π	4,5,6,7,8,9
		5→8	18	5π	1,3,5,6,7,8				26π*	4,5,6,7,8,9
		6→7	44	6π	1,9,3,10					
		6→8	9	7π*	2,5,6,7,8					
				8π*	4,6,7,8,9,1					

Table 3—Electron Densities at Various Basic Centers of Benzimidazol-2(3*H*)-one and Its Prototropic Forms in Ground and First Excited Singlet State

Atomic centres	Electron density (PPP)		Electron density CNDO/S	
	Ground	Excited	Ground	Excited
		Form II		
N 1	1.746	1.672	5.122	5.087
C 2	1.102	1.130	3.676	3.692
N 3	1.736	1.671	5.115	5.022
O 10	1.278	1.146	6.430	6.325
		Monocation		
N 1			5.055	5.102
C 2			3.594	4.130
N 3			5.025	5.115
O 10			6.114	6.102
		Dication		
N 1			5.029	5.222
C 2			3.744	4.176
N 3			5.055	4.981
O 10			5.665	5.310
		Anion		
N 1	1.691	1.665	5.155	5.139
C 2	0.938	0.967	3.688	3.700
N 3	1.401	1.358	5.423	5.190
O 10	1.815	1.669	6.649	6.416

tion of the lone pair on oxygen atom with ring more via conjugation. The small blue shift observed in absorption and fluorescence spectra of neutral species on increasing the polarity of the solvents can thus be due to the solvent restricting this participation through proton donor interaction. In the case of the monocation, change in the charge density on oxygen is not that large and similar behaviour is observed in the case of amides[19]. On the other hand, the charge density at oxygen in the case of the dication is much less than in any other species. This can be explained by the fact that before second protonation, the geometry of the monocation changes to enol form and the dication is formed by the coordinate linkage of the lone pair of oxygen atom of the $-OH$ group. The decrease in charge density on excitation suggests that $-OH_2^+$ is a stronger acid in the S_1 state, in agreement with the experimental observations[20-22]. The changes in the charge densities at nitrogen centres are also consistent with experimental results[23]. For example, in the case of the neutral species both the nitrogen atoms of BIOH(II) are symmetrical and thus possess similar charges in S_0 and S_1 states. The decrease in charge at the nitrogen centres is consistent with the nature of transition in the neutral molecule, i.e. the long wavelength transition is localised on the benzene ring, the lone pairs on ⟩NH groups perturb this and charge migrates to the homocyclic ring. In the case of the monocation, the charge density increases at each of the nitrogen centres upon excitation. This is again in agreement with the experimental results that charge migration will take place

towards the heterocyclic ring due to the presence of positive charge[15] and these centres become more basic, whereas in the case of the dication, N-1 becomes tertiary and N-3 imino group. Thus the charge density at N-1 of the dication will increase on excitation because of positive charge on it, whereas it will decrease on N-3 because of participation of lone pair of the imino group with the ring. Lastly, in the case of the monocation, the change in electron density at N-3 is more than that at N-1, indicating that ⟩NH group is a weaker base in S_1 state.

It has been observed experimentally that protonation sites in the ground state and the excited state are the same, i.e. no phototautomerism is involved. Comparing the electron densities in the ground and excited states at the respective centres in different prototropic forms, it is seen that the general trend of basicity or acidity is still maintained on excitation, i.e. no particular centre becomes relatively much more basic or acidic on excitation. Thus the trend of protonation or deprotonation observed in the ground state is not changed on excitation.

Further, the CNDO/S method does not distinguish between BIOH(I) protonated at the tertiary nitrogen atom and BIOH(II), protonated at the carbonyl group, since the protonated forms will not vary as far as structure is concerned. Although the trends observed in PPP and CNDO/S are similar, the latter is more general to accomodate different kinds of species, whereas in the case of PPP, the different parameters, e.g. ionization potentials and electron affinities for the ions and certain groups, are not available.

References

1 Mishra A K & Dogra S K, *J Photochem*, **29** (1985) 435.
2 Efros L S & Eistov A V, *J gen Chem USSR*, **37** (1957) 755.
3 Brown D, *J chem Soc* (1958) 1974.
4 Pariser R & Parr R G, *J chem Phys*, **21** (1953) 466, 767.
5 Pople J A, *Trans Faraday Soc*, **49** (1953) 1315.
6 Delbene J & Jaffe H H, *J chem Phys*, **48** (1968) 1807, 4050.
7 Hinze J & Jaffe H H, *J Am chem Soc*, **84** (1962) 540.
8 Parison R, *J chem Phys*, **21** (1953) 568.
9 Matage N & Nishimoto K, *Z phys Chemie*, **13** (1957) 140.
10 Ellis R, Kuchnlenz G & Jaffe H H, *Theoret chim Acta*, **26** (1972) 1842.
11 Preston P N, *Benzimidazoles and congeneric tricyclic compounds*, Part I, edited by P N Preston (Interscience, London) 1981, pp. 61.
12 Kamiya M, *Bull chem Soc Japan*, **43** (1970) 3344.
13 Gorden R D & Yang R F, *Can J Chem*, **48** (1970) 1722.
14 Schulman S G, *Physical methods in heterocyclic chemistry*, Vol. VI, edited by A R Katritzky (Academic Press, London) 1974, pp. 174.
15 Tway P C & Clinelove L J, *J phys Chem*, **86** (1982) 5223, 5227.
16 Krishnamurthy M, Phaniraj P & Dogra S K, *J chem Soc Perkin II* (1986) 1917.
17 Sinha H K & Dogra S K, *J chem Soc Perkin Trans II*, (1987) 1465.
18 Mishra A K & Dogra S K, *J Photochem*, **31** (1985) 333.
19 Paul W L & Schulman S G, *Anal Chem*, **45** (1971) 415.
20 Sinha H K & Dogra S K, *Chem Phys*, **102** (1986) 337.
21 Krishnamurthy M & Dogra S K, *Spectrochim Acta*, **42A** (1986) 793.
22 Sinha H K & Dogra S K, *J Photochem*, **36** (1987) 149.
23 Mishra A K & Dogra S K, *J Photochem*, **23** (1983) 163; *J chem Soc Perkin Trans II*, (1984) 943.

Indian Journal of Chemistry
Vol. 27A, October 1988, pp. 855-857

Dimerization in Binary Gaseous Mixtures: Nonadditive Effects & Argon-Krypton Example

CHRISTOPHER J BIERMANN
Department of Forest Products, Oregon State University, Corvallis, Oregon 97331 (USA)

Received 24 *June* 1987; *revised and accepted* 8 *March* 1988

The interaction of second virial coefficients (B_{mix}) in respect of dimerization in gaseous binary mixtures has been investigated. Because of high equilibrium constants for dimerization of carboxylic acids, data from literature on binary mixtures of formic and acetic acids have been used to test the additive nature of virial coefficients. It is found that the equation commonly used to predict the interaction of virial coefficients predicts a higher than actual B_{mix} except in the degenerate case. For most binary gas mixtures the error is small at low pressures. The heat of dimerization of argon-krypton has been calculated as -623 cal/mol.

The second virial coefficient for a binary mixture of two gases is given by Eq. (1), from Lennard-Jones and Cook[1].

$$B_{mix} = X_A^2 B_{AA} + 2X_A X_B B_{AB} + X_B^2 B_{BB} \quad \ldots(1)$$

The analogous equation in terms of equilibrium constants[2] is given in Eq. (3) after K_{mix} is defined in Eq. (2).

$$K_{mix} = P_{dimers}/(\Sigma P_{monomers})^2 \quad \ldots(2)$$

$$K_{mix} = X_A^2 K_A + X_A X_B K_{AB} + X_B^2 K_B \quad \ldots(3)$$

The coefficient of 2 in the second term on the right hand side of Eq. (1) is because there are two types of mixed dimers possible: A-B and B-A. Since these two types of mixed dimers are indistinguishable, the coefficient disappears in Eq. (3); however, one should keep in mind that the equilibrium constant so obtained reflects two possible products and is apt to be larger than the equilibrium constant for the formation of either of the pure dimers. The enthalpy of dimerization is identical, of course, whether for an individual mixed dimer or for the two mixed dimers considered together.

Results and Discussion

Nonadditive effects

Since there will be competition of the monomers to form mixed and pure dimers, the terms are not strictly additive as implied in Eq. (1) and, therefore, Eq. (3). As the pressure increases, the proportion of each species contained in each type of dimer increases; consequently, the error increases with increasing pressure. Equation (3) will always predict an equal or higher than actual K_{mix}. For example, the term $X_A X_B K_{AB}$ does not consider the amount of monomer "tied up" in each of the pure dimers. In the degenerate case where $K_A = K_B = 1/2\ K_{AB}$, Eqs (2) and (3) yield the same results.

In this paper, a study of this error has been made by calculating the K_{mix} predicted by Eq. (3) which assumes no interaction compared to K_{mix} predicted by Eq. (2). To do this, equilibrium constants as well as the ideal pressures of species A and B were chosen arbiterarily. From this information, K_{mix} was directly obtained from Eq. (3). To determine the expected concentration of the two monomers and three trimers, Eqs (4-8) were iterated in order ten times with the initial pressure of dimers at 0. Ten iterations were more than sufficient for the results shown in Table 1. For larger equilibrium constants or higher pressures, more iterations would be needed. For still higher pressures, iteration of these equations may not converge. After iteration of these equations, K_{mix} was calculated from Eq. (2). The results of this exercise are presented in Table 1.

$$P_A = X_A P_{id} - (2{*}P_{AA} + P_{AB}) \quad \ldots(4)$$

$$P_B = X_B P_{id} - (2{*}P_{BB} + P_{AB}) \quad \ldots(5)$$

Table 1 – Determination of K_{mix} from Equations (2) and (3) for arbitrary parameters.

P_A (atm)	P_B (atm)	K_A (atm^{-1})	K_B (atm^{-1})	K_{AB} (atm^{-1})	K_{mix} Eq. (2)[a]	K_{mix} Eq. (3)[b]	Deviation (%)
1	1	0.01	0.02	0.04	0.01750	0.01712	2.2
2	2				0.01750	0.01684	4.0
1	4				0.02920	0.02825	3.4
4	1				0.01120	0.01111	0.8
0.01	0.01				0.01750	0.017496	0.02
1	1	0.04	0.06	0.08	0.04500	0.04486	0.3
2	2				0.04500	0.04476	0.5
0.5	0.5				0.04500	0.04492	0.2
1	1	0.005	0.06	0.03	0.02375	0.02252	5.5
1	1	0.02	0.02	0.04	0.02000	0.02000	0.00

[a] Assumes no interaction between the second virial coefficients.
[b] Assumes interaction of the second virial coefficients.

$$P_{AA} = K_A P_A^2 \quad \ldots(6)$$

$$P_{BB} = K_B P_B^2 \quad \ldots(7)$$

$$P_{AB} = K_{AB} P_A P_B \quad \ldots(8)$$

If there are large differences in the equilibrium constants, the deviation may be considerable at pressures even of the order of 1 atm. In most cases, the deviation of the two models is within experimental error and may be ignored. Because the two models are very close for the pressures and equilibrium constants encountered for most compounds, it is difficult to show that Eq. (2), based on the iterations of Eqs (4-8), is more accurate than Eq. (3) from data in literature. The carboxylic acids, however, have equilibrium constants for dimerization which are of the order of 100-10,000 times larger than those for most gases. The carboxylic acids have the necessary characteristics to test the validity of the two approaches used to determine overall behaviour of gas mixtures.

Barton and Hsu[3] studied pure formic and acetic acids as well as mixtures of these from 323 to 400 K at various pressures. They determined the equilibrium constants as a function of pressure and extrapolated the equilibrium constant to zero pressure. This was necessary because the dimers tended to form trimers, tetramers, and higher clusters.

Considering the pressure of the dimers was generally many times the pressure of the monomers, the tendency to form higher oligomers was very small. I believe that this is because with most gases when the pressure of dimer is of the order of the pressure of monomer, the pressure of trimers, tetramers, and so forth would be much, much higher relative to those of monomers and tetramers of the carboxylic acids. This is true because the H-bonding between two carboxylic acid molecules is strong; much stronger than the forces available to hold two dimers of a carboxylic acid together in a tetramer. With most substances, the forces holding a dimer together are similar in magnitude to those that hold a monomer to a dimer to form a trimer or the forces that hold two dimers together in a tetramer. A case similar to the carboxylic acids, but much more extreme, is nitrogen gas at room temperature. It is almost completely in the form of dimers at room temperature and pressure but very few tetramers of two nitrogen molecules.

The high equilibrium constants for dimerization of carboxylic acids give rise to a property of this class of compounds not usually observed in other compounds. That is, the enthalpy of vaporization increases with temperature for temperatures near the boiling point and below. Also, the enthalpy of dimerization is larger than the enthalpy of vaporization. For example, the enthalpies of vaporization of acetic acid are -5050 cal/mol (at 293 K), -5610 cal/mol (at 383K), and -5120 cal/mol (at 473 K) (see Ref. 4); the heats of vaporization of acetic acid are also given[5] as -9964 and -9487 cal/mol at the boiling point. The enthalpies of dimerization of formic acid are calculated as -13900 cal/mol by Barton and Hsu[3], as -14110 by Taylor and Bruton,[6] and as -14169 by Buttner and Maurer[7]. The enthalpy of dimerization of acetic acid is given[7] as -15750 cal/mol.

To test the two models with the data presented by Barton and Hsu, only the lowest temperature, 323 K, was considered. At the lowest temperature, the equilibrium constant was least affected, relatively speaking, by pressure. (The maximum change was 4% in the pressure range studied at 323 K.) This is expected since the enthalpy of dimerization is much higher than that for trimerization or tetramerization; hence, the equilibrium constant for dimerization will decrease proportionately faster with increasing temperature than the equilibrium constant for trimerization or tetramerization. Of course, formation of trimers or tetramers will increase the apparent K_{mix} of dimerization. Table 2 gives the results of actual K_{mix} determined experimentally and that predicted from the gas composition and equilibrium constants of acetic and formic acids at zero pressure.

The results in Table 2 show that actual K_{mix} value is consistently smaller than that predicted by Eq. (3); consequently, the second virial coefficient is not strictly additive as implied in Eqs (1) and (3).

Enthalpy of mixed dimerization of argon-krypton

The equilibrium constants for argon and krypton have been determined previously[2] as a function of temperature based on the work of Fender and Halsey[8]. In the latter study, the values of B_{AB} were also determined at various temperatures. Table 2 lists these values which are corrected for adsorption and the third virial coefficient. From these values, the equilib-

Table 2 - Predicted and experimental K_{mix} values for mixtures of formic and acetic acids at 323 K.

Amount formic acid		Pressure	K_{mix} (atm^{-1})	
Wt. %	Mol Fr	(atm)	Actual	Predicted [a]
20	0.2459	0.100	162.50	160.03
		0.076	156.86	160.03
		0.045	153.72	160.03
40	0.4652	0.091	122.24	128.78
		0.064	120.65	128.78
		0.046	121.83	128.78
60	0.6618	0.093	90.21	99.46
		0.047	91.69	99.46
80	0.8392	0.094	65.43	71.96
		0.066	66.54	71.96
		0.048	69.35	71.96

[a] Predicted by Eq. (3)

K_A = 193.25; K_F = 46.16; and K_{AF} = 255.3

Table 3 - Equilibrium constants for the dimerization of argon-krypton.

T(K)	-B cm³/mol	K, atm⁻¹	-ln K	-ln K (LR)[a]	Deviation
108.001	236.16	0.05330	2.932	2.933	-0.001
110.567	224.95	0.04958	3.004	3.000	0.004
113.272	216.14	0.04650	3.068	3.068	0.000
115.315	207.99	0.04396	3.124	3.116	0.008
117.083	206.72	0.04304	3.146	3.158	-0.012
117.357	204.26	0.04242	3.160	3.165	-0.005
119.002	198.42	0.04064	3.203	3.202	0.001
120.780	193.74	0.03910	3.242	3.240	0.002
123.616	186.44	0.03676	3.303	3.300	0.003

[a] ln K determined by linear regression

ln K_{AB} -5.839 + 313.724/K ΔH -623 cal/mol

rium constants and enthalpy of dimerization have been determined according to the method used previously[2]. The results are presented in Table 3.

There is a small error in the B-values determined by Fender and Halsey since they used Eq. (1) to determine B_{AB}. Using the method described in the first part of this paper, one finds that a term of approximately 0.00014 should be subtracted from the equilibrium constant at 108K for a mixture of 0.5 atm of each component. A precise correction factor could not be determined since Fender and Halsey did not give the composition of their gas mixture. In any case, the correction factor is sufficiently small so it may be ignored. The enthalpy of dimerization of −623 cal/mol of argon-krypton compares well with the values of −533 cal/mol for the self-dimerization of argon and −708 cal/mol for the self-dimerization of krypton.

Many equations have been proposed to predict the virial coefficient, B_{AB}, from the virial coefficients of the two pure gas species[9]. These equations are probably better applied to the enthalpies of dimerization for the concerned species. The above suggest taking a simple average (linear combination rule) for compunds of similar polarity.

When determining the equilibrium constant for dimerization of two gas species, one should use the original PVT data, if available. This immediately avoids the need to consider the additive effects of the virial coefficients. The equilibrium constants for the self-dimerization of the two individual species, having been determined previously for the temperature of interest, may be used to calculate the equilibrium constant, K_{AB}, by iteration of Eqs (4-8) except that Eq. (9) is substituted for Eq. (8) since K_{AB} is not yet known:

$$P_{AB} = 1/2(P_{id} - (P_A + P_B + 2P_{AA} + 2P_{BB})) \quad \ldots (9)$$

After the equations are iterated, K_{AB} is solved by its definition: $K_{AB} = P_{AB}/(P_A P_B)$. Ideally, K_{AB} is determined at several pressures and extrapolated to zero pressure so that trimerization and higher order interactions may be ignored.

References

1 Lennard-Jones J E & Cook W R, *Proc roy Soc*, A115 (1927) 334.

2 Biermann C J, *Indian J Chem*, (IC 5424).

3 Barton J R & Hsu C C, *J chem Eng Data*, **14** (1969) 184.

4 Vargafting N B *Tables of thermophysical properties of liquids and gases* (Hemisphere, Washington) 1975.

5 Weast R C Edited, *Handbook of Chemistry and Physics* (CRC: Cleveland) 1977-1978, 58.

6 Taylor M D & Bruton J, *J Am chem Soc*, **74** (1952) 4151.

7 Buttner R & Maurer G, *Ber Bunsenges Phys Chem*, **87** (1983) 877.

8 Fender B E F & Halsey Jr G D, *J chem Phys*, **36** (1962) 1881.

9 Beattie J A & Stockmayer W H in *A treatise in physical chemistry, Vol* 2, *States of matter* edited by H S Taylor & S Glastone (Van Nostrand, New York) 1951; p 339-342.

Indian Journal of Chemistry
Vol. 27A, October 1988, pp. 858-861

Electrochemical Behaviour of *cis*- & *trans*-2,2′-Azopyridines at Solid Electrodes

R N GOYAL
Department of Chemistry, University of Roorkee, Roorkee 247 667

Received 3 *November* 1987; *revised and accepted* 1 *February* 1988

The electrochemical reduction of *cis*- and *trans*-2,2′-azopyridines has been studied over a wide *p*H range. Under cyclic voltammetric conditions both the compounds are reduced in a quasi-reversible (2e, $2H^+$) step to give hydrazopyridine, which is further reduced under controlled potential conditions to 2-aminopyridine as the product of electrode reaction. Based upon linear and cyclic sweep voltammetry, coulometry, IR and NMR spectral studies, and product identification, a reaction mechanism has been proposed to account for the reduction reaction.

The polarographic behaviour of *cis*- and *trans*-isomers of azobenzene has been studied in detail. According to some authors[1] there is practically no difference in the half-wave potential of these isomers, although a few have reported[2] some difference in $E_{1/2}$ values. The behaviour of *cis*- and *trans*-azobenzenes has been reported[3,4] to be strongly dependent on the experimental conditions probably due to adsorption of azo or hydrazobenzene.

In contrast to benzenoid azo compounds, polarographic behaviour of heterocyclic azo compounds, however, has received little attention and practically no information is available on the electrochemical behaviour of 2,2′-azopyridine, widely used as chromogenic agent[5]. Therefore we have presently studied the electrochemical behaviour of *cis*- and *trans*-2,2′-azopyridines at the solid electrodes.

Materials and Methods

Cis- and *trans*-2,2′-azopyridines were prepared in the laboratory and their purity ascertained by UV spectra. Equipments used for linear and cyclic sweep voltammetry, coulometry and spectral studies have been described elsewhere[6]. The pyrolytic graphite electrode (area ~ 2 mm^2) was prepared by the method reported in the literature[7]. The glassy carbon electrode (area ≈ 2.8 mm^2) was obtained from PAR, USA while the platinum electrode (area 1.6 mm^2) was fabricated in the laboratory. All potentials were measured against saturated calomel electrode as the reference electrode.

The number of electrons (n) involved in electroreduction was determined by two methods. In the first method, a conventional large scale electrolysis at controlled potential using pyrolytic graphite plates as working electrode, and cylindrical platinum gauze and SCE as counter and reference electrodes respectively. The value of n was calculated by graphical integration of current-time curve[8]. To complete electrolysis in a few minutes, electrolysis was carried out in a thin layer cell prepared by the method reported in the literature[9] and the value of n was determined by the use of current-time curve.

Product characterization

In order to characterize the major end product formed in the electroreduction of 2,2′-azopyridines, about 8-10 mg were reduced in phosphate buffers of desired *p*H in a three-compartment cell. Progress of electrolysis was monitored by cyclic voltammetry. When the peak I_c completely disappeared, electrolysis was stopped, the solution was lyopholised and residue was dissolved in distilled water (1-2 ml) and passed through a column packed with Sephadex G-10 (Sigma, bead size 40-120 μ) to separate phosphate from the product. The doubly distilled water was used as an eluent and fractions (10 ml each) were collected. The fractions 10-15 were found to contain phosphate and hence were discarded. The fractions 17-23 were pooled, freeze-dried and analysed.

Results

Linear sweep voltammetry of *cis*- and *trans*-2,2′-azopyridines exhibited only one well-defined *p*H-dependent reduction peak at pyrolytic graphite electrode at a sweep rate of 10 mVs^{-1}. In cyclic sweep voltammetry at a scan rate of 100 mVs^{-1} one well-defined reduction peak (I_c) was observed for *cis*- and *trans*-azopyridines, when the sweep was initiated in the negative direction. In the reverse swep an anodic peak (I_a) was also observed which formed a quasi-reversible couple with peak I_c. The plot of E_p versus *p*H was linear and the dependence of E_p on *p*H could be expressed by the relations:

For *trans*-isomer

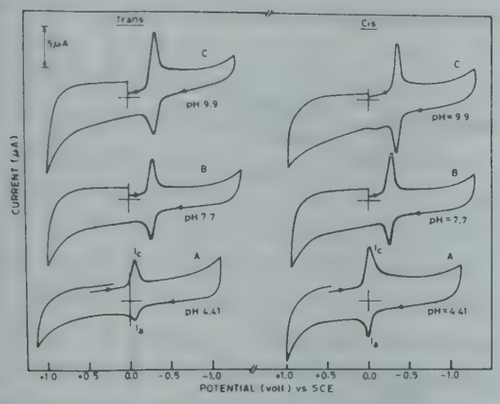

Fig. 1—Typical cyclic voltammograms of *cis*- and *trans*-2,2'-azopyridines in phosphate buffers of different *p*H. Scan rate 100 mVs^{-1}.

E_p = [0.22-0.069 *p*H] versus SCE .. peak I_a
E_p = [0.07 + 0.069 *p*H] versus SCE .. peak I_c
For *cis*-isomer
$-E_p$ = [0.23-0.067 *p*H] versus SCE .. peak I_a
E_p = [0.02-0.060 *p*H] versus SCE .. peak I_c

Peak I_a was clearly observed at a sweep rate > 50 mVs^{-1}. Some typical cyclic voltammograms are presented in Fig. 1. Thus in the entire *p*H range studied, the peak potentials of peak I_a for *cis*-isomer are about 25 mV more positive than those for *trans*-isomer in the acidic *p*H range and practically identical in natural and alkaline *p*H range.

The linear and cyclic sweep voltammetric behaviour at glassy carbon electrode was identical with that of pyrolytic graphite electrode. However, at platinum electrode the reduction and oxidation peaks observed were broad in nature with the peak potentials about 25-50 mV more negative in comparison to pyrolytic graphite electrode. Bascially, however, the voltammetric behaviour was same.

The peak current for peak I_c increased with increase in the concentration of 2,2'-azopyridine upto about 5 m*M*. At concentrations < 5 m*M*, the peak current versus concentration curve was almost linear whereas at concentration > 5 m*M* the peak current values were more or less constant indicating involvement of adsorption in the electrode process. The ratio of anodic[10] to cathodic peak was < 1 confirming quasi-reversible nature of the elctrode reaction which was further supported[11] by the fact that the separation of peak potentials of anodic and cathodic peaks increased with increase in sweep rate in the sweep range of 50-400 mVs^{-1}.

The values of n determined at different *p*H values and potentials in a conventional electrolysis cell (electrolysis took 4 hr for completion) were 4.0 ± 0.2. The value of n determined in a thin layer cell, was found close to 2.0. This clearly pointed out that the products of electroreduction of 2,2'-azopyridines are different under cyclic voltammetric conditions and coulometric conditions.

The progress of electrolysis for *cis*- and *trans*-2,2'azopyridines was monitored at *p*H 3.0, 5.1 and 8.8 by recording cyclic voltammograms at different time intervals. A cyclic voltammogram observed for *trans*-2,2'-azopyridine at *p*H 8.8 before electrolysis is presented in Fig. 2A. After 15 min of electrolysis a new reduction peak II_c appeared after peak I_c (Fig. 2B). With progress of electrolysis peak I_c decreased whereas the peak current for peak II_c increased and reached a maximum (Fig. 2C) after 45 min of electrolysis and a new anodic peak started appearing (peak III_a). Thereafter both the reduction peaks disappeared. The yellow colour of the solution also changed to colourless at the end of electrolysis. Cyclic voltammogram presented in Fig. 2E was recorded after 4 hr of electrolysis and it did not exhibit peaks I_c and II_c when sweep was initiated in negative direction. When the direction of sweep was changed after recording peak III_a, a cathodic peak was observed which formed a quasi-reversible couple with anodic peak observed in subsequent sweep towards positive potentials. The peak potentials of the quasi-reversible couple observed in the exhaustively electrolysed solution were same as those observed for peaks I_c and I_a in compound (I). Thus it is concluded that product of electrolysis of *trans*-2,2'-azopyridine is electroactive in nature and oxidation of the product gives a species, which is reducible and forms a quasi-reversible couple. An exactly identical behaviour was observed with *cis*-2,2'azopyridine. Thus Fig. 2 clearly demonstrates that the product of controlled potential electrolysis is different from the one formed under cyclic voltammetric conditions.

The UV spectral changes during electrolysis of *cis*- and *trans*-2,2'-azopyridines were monitored at *p*H 4.4 and 7.1. As the completely electrolysed solution of *cis*- and *trans*-2,2'-azopyridines exhibited λ_{max} at same wavelengths, it was concluded that the products of electrolysis of both the compounds are the same.

The products of electroreduction at *p*H 4.4 and 7.1 were characterised. The exhaustively electrolysed solution of *cis*- and *trans*-2,2'-azopyridines gave a single spot in TLC with R_f = 0.52 (at both the *p*H) indicating that the products formed at *p*H 4.4 and 7.1 were the same. The lyopholised material obtained from fractions 17 to 23 was analysed by IR and PMR spectra. The colourless proudct obtained from both the azopyridines melted at 59°.

The IR spectrum of the product exhibited bands at 3420, 1600 and 1315 cm^{-1} corresponding to primary amino group. The disappearance of the band at 1560 cm^{-1} (corresponding to azo group) in the product clearly indicated that the reduction had occurred at the azo group of the molecule. The IR

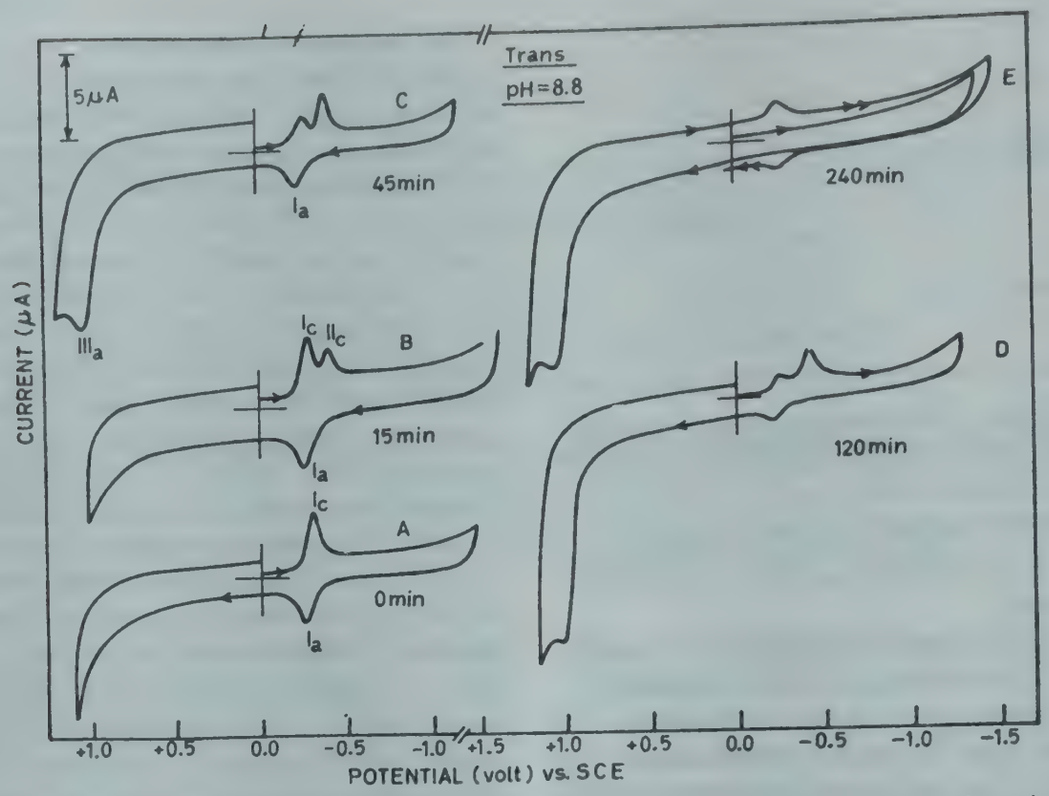

Fig. 2—Cyclic voltammograms at pyrolytic graphite electrode of *trans*-2,2′-azopyridine at *p*H 8.8 before electrolysis (curve A), and after 15 min (curve B), 45 min (curve C), 120 min (curve D) and 240 min (curve E)

spectrum of authentic 2-aminopyridine was superimposable over that of the proudct, thereby confirming the formation of 2-aminopyridine. This was further supported by the PMR spectra. As 2-aminopyridine has been reported as electroactive in nature[12] a comparison of its cyclic voltammetric behaviour was also made with the cyclic voltammograms observed for exhaustively electrolysed solution of *cis*- and *trans*-2,2′-azopyridines. It was interesting to observe that 2-aminopyridine exhibits well-defined anodic wave and a quasi-reversible couple as reported in the literature[12] and the oberved voltammetric behaviour was exactly identical with the cyclic voltammograms observed for exhaustively electrolysed solution of *cis*- and *trans*-2,2′-azopyridnes.

Discussion

The experimental information presented so far clearly indicates that *cis*- and *trans*-2,2′-azopyridines undergo electroreduction involving close to 4 electrons per molecule under coulometric condition and 2.0 ± 0.2 electrons under cyclic voltammetric conditions. As both the azopyridines gave the same product the mechanism as shown in Scheme 1 can be proposed for the electroreduction of these compounds.

The results of electrochemical reduction of *cis*- and *trans*-2,2′-azopyridines differ considerably from those of *cis*- and *trans*-azobenzenes. The (2e, $2H^+$ reduction product of azobenzene is sufficiently stable hence it does not undergo further reduction at d.m.e. or at graphite electrode as reported by Nygard[13] whereas the hydrazo compound formed from *cis*- and *trans*-2,2′-azopyridines is stable only under cyclic voltammetric conditions and undergoes further (2e, $2H^+$) reduction in controlled potential electrolysis to give 2-aminopyridine as the product of electrolysis. This difference in behaviour can be explained on the basis of strongly electron attracting pyridine rings which make hydrazo compound unstable. A four-electron reduction of azobenzene in the presence of heterocyclic rings has been reported in literature[14]. The peak potential of *cis*-isomer is about 25-50 mV less negative in comparison to *trans*-isomer in the entire *p*H range and at all the electrodes used. This difference in behaviour can be explained on the basis of almost planar structure of *trans*-2,2′-azopyridine due to which specific orien-

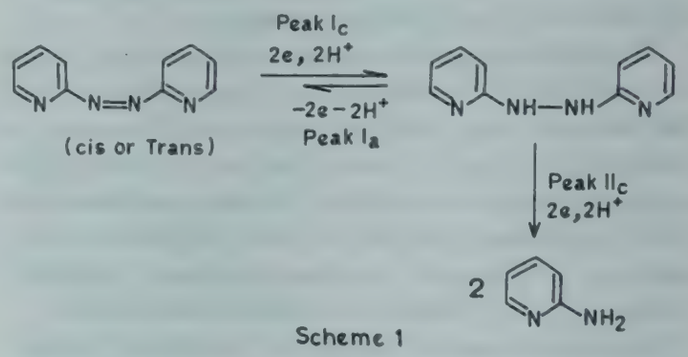

Scheme 1

tation required to reach the surface of electrode is difficult in comparison to that of *cis*-2,2′-azopyridine. As both the pyridine rings are present on one side of azo group in *cis*-isomer its reduction is slightly easier.

The values of peak potentials for *cis*- and *trans*-isomers at pyrolytic graphite and at glassy carbon electrodes are practically identical, probably due to identical nature of the two electrodes. Whereas the broad nature of peak at platinum electrode with slightly more negative values of E_p could be due to the difference in the nature of graphite and platinum electrodes.

Acknowledgement

The author is thankful to M/S Pfizer, USA for the gift of pyrolytic graphite. The financial assistance for this work was provided by the UGC, New Delhi.

References

1 Nygard B, *Arkiv Kemi*, **20** (1963) 163.
2 Chuang L, Fried I & Elving P J, *Analyt Chem*, **37** (1965) 1528.
3 Fieser L F & Fieser M, *Advanced organic chemistry* Reinhold, New York), 1962.
4 Holleck L & Holleck G, in Proc 3rd Int Congress of Polarography, Polaroraphy 1964, Vol 2, London (1966) 825.
5 Shibata H, *Chelates in analytical chemistry*, Vol. 4, edited by H.A. Flaschks and A.J. Barnard (Marcel Dekker, New York), 1972.
6 Goyal R N, Bhushan R & Agarwal A, *J electroanal Chem*, **171** (1984) 281.
7 Goyal R N, Srivastava S K & Agarwal R, *Bull chem Soc Fr*, **4** (1985) 656.
8 Lingane J J, Swain C G & Fields M, *J Am chem Soc*, **65** (1945) 1938.
9 Norvell V E & Mamantov G, *Analyt Chem*, **49** (1977) 1470.
10 Wopschall R H & Shain I, *Analyt Chem*, **39** (1967) 1514.
11 Brown E R & Large R F, in *Physical methods of chemistry*, edited by A. Weissberger and B.W. Rossiter (Wiley Interscience, New York), 1976, 423.
12 Goyal R N & Kumar A, *J electroanal Chem*, **242** (1988) 209.
13 Nygard B, *Arkiv Kemi*, **26** (1966) 167.
14 Florence T M, Johnson D A & Batley G E, *J electroanal Chem*, **50** (1974) 113.

Indian Journal of Chemistry
Vol. 27A, October 1988, pp. 862-867

Effect of Sodium Dodecyl Sulphate on Protonation Equilibrium of (Salicylato)bis(ethylenediamine)cobalt(III): Test of Validity of Pseudo-phase Ion-Exchange Model for SDS Micelles

ANADI C DASH* & RAMESH C NAYAK
Department of Chemistry, Utkal University, Bhubaneswar 751 004

Received 12 *November* 1987; *accepted* 18 *January* 1988

The protonation equilibrium of coordinated salicylate in (salicylato)bis(ethylenediamine)cobalt(III) is strongly favoured in the micellar pseudo-phase of sodium dodecyl sulphate (SDS). *pK* shift of 2 units (relative to water) is observed for $(en)_2CoSalH^{2+}$ due to micellar binding. Our analysis also shows that the potential changes at the bulk-micelle interface contributes to variation in *pK*. The pseudo-phase ion-exchange equilibrium

$$(en)_2CoSal^+_W + Na^+_M \overset{K_R^{Na}}{\rightleftharpoons} (en)_2CoSal^+_M + Na^+_W,$$

holds good with a value of 1.24 ± 0.02 for the forward equilibrium constant, K_R^{Na}, at 30°C which is comparable to the value for the corresponding equilibrium constant for H^+/Na^+ exchange equilibrium for the SDS micelles.

Partitioning of neutral or cationic acids into anionic micellar pseudo-phase of sodium dodecyl sulphate (SDS) enhances their *pK* values[1-4]. Both electrostatic and hydrophobic effects might be responsible for perturbation in their *pK*s. The acids might be positioned in the water-rich Stern layer of the micelles the effective dielectric constant of which is significantly lower (D = 40) than that of the bulk aqueous phase[5]. Hence the electrostatic effect is likely to be a major factor controlling the *pK* of the micelle bound acids. In an earlier study[3] it was observed that the *pK* of the complex acid, bioxalatopentaamminecobalt(III), $(NH_3)_5CoO_2CCO_2H^{2+}$, (*pK* refers to the ionisation of the free carboxylic acid group) bound to the SDS micelles is ~ 1.4 units higher than the same in the aqueous phase. This cobalt(III) substrate has hydrophilic centres and lacks in appreciable hydrophobic interaction with the hydrocarbon chain of SDS. The (salicylato)bis(ethylenediamine)cobalt(III) is a monovalent cation with hydrophobic groups. It possesses a significantly basic site, the coordinated phenoxide. Hence such a substrate offers opportunity to examine the hydrophobic interaction effects, if any, on its protonation equilibrium in the presence of SDS micelles. Besides it was also considered worthwhile to test the applicability of the pseudo-phase ion-exchange model for SDS micelles using the monovalent cation, $(en)_2CoSal^+$.

Materials and Methods

The (salicylato)bis(ethylenediamine)cobalt(III) chloride monohydrate, $[(en)_2CoSal]Cl \cdot H_2O$ was prepared as described by Gillard *et al*[6] and its purity checked by elemental analyses. SDS (GR, E Merck, 99% pure by G C Assay) was used as such and its purity checked by surface tension measurement (c.m.c. = 0.008 mol dm^{-3})[5] by a De Nuoy type surface tensiometer. All other chemicals were of AR grade. Solutions were prepared in doubly distilled conductivity water.

*p*H measurements were made with an Elico digital *p*H meter model LI 120 using a combination electrode model CL 51; the reference Ag/AgCl Cl^- electrode was filled with 2 mol dm^{-3} NaCl. All spectral measurements were made with a Varian-Cary 634S UV-visible spectrophotometer.

Results and Discussion

Micellar binding of (salicylato)bis(ethylenediamine)-cobalt(III) and effect of micelles on its protonation equilibrium

The absorption spectrum of $(en)_2CoSal^+$ (310-390 nm) is little affected by 0.02 mol dm^{-3} $HClO_4$ in the absence of SDS, except that a very weak shoulder appears around 350 nm (curve 3, Fig. 1) which is indicative of partial protonation of the complex[6]. In the presence of 0.1 mol dm^{-3} SDS and 0.02 mol dm^{-3} $HClO_4$, this shoulder is transformed to a well-developed absorption maximum at 352 nm with complete disappearance of the maximum at 330 nm indicating appreciable protonation of the complex (curve 1, Fig. 1). In the presence of 0.1 mol dm^{-3} SDS and absence of $HClO_4$ the absorption spectrum is also modified to a small extent (curves 2

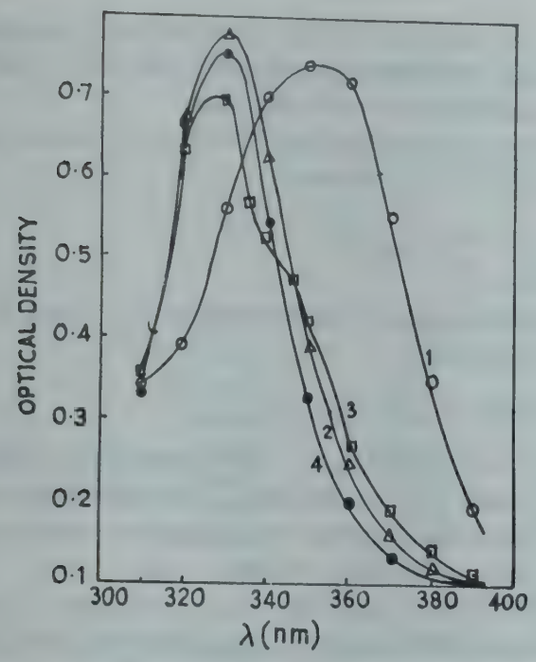

Fig. 1—Effect of varying [SDS] on absorption spectrum of $(en)_2CoSal^+$ at 30°C ($[complex]_T = 3.00 \times 10^{-4}$ mol dm^{-3}; cell path = 1.00 cm. (1) ○-$[SDS]_T = 0.1$, $[HClO_4]_T = 0.02$ mol dm^{-3}, (2) Δ-$[SDS]_T = 0.1$ mol dm^{-3}, $[HClO_4]_T = 0$, (3) ⊡-$[SDS]_T = 0$, $[HClO_4]_T = 0.02$ mol dm^{-3}, (4) ●-$[SDS]_T = [HClO_4]_T = 0$).

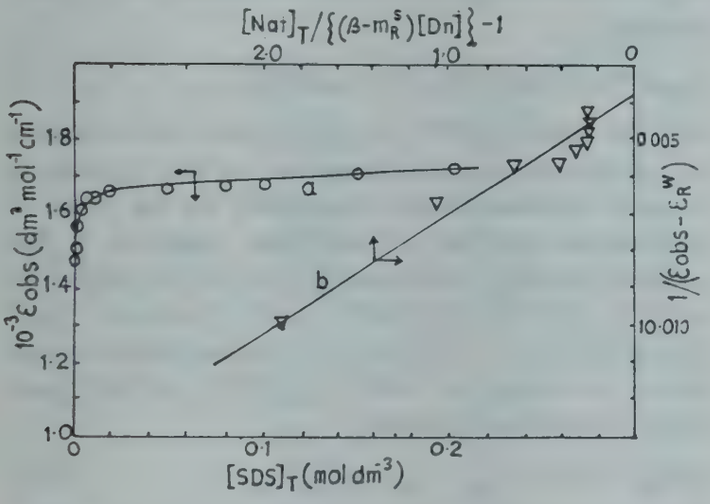

Fig. 2—(a) $10^{-3}\,\varepsilon_{obs}$ dm^3 mol^{-1} cm^{-1} versus $[SDS]_T$ plot at 345 nm showing binding of $(en)_2CoSal^+$ with SDS micelles; (b) $1/(\varepsilon_{obs} - \varepsilon^W_{obs})$ dm^{-3} mol cm versus $[Na^+]_T/\{(\beta - m^s_R)[Dn]\} - 1$ plot at 30°C ($\beta = 0.8$, cmc = 0.001 mol dm^{-3}; $0.002 \leq [SDS]_T \leq 0.2$ mol dm^{-3})

and 4 of Fig. 1) which is indicative of interaction of unprotonated complex ion, $(en)_2CoSal^+$, with the SDS micelles. Similar observations have been made by us earlier for *cis*-$[(en)_2Co(im)X]^+$/SDS (im = N − H deprotonated imidazole; X = NCS^-, N_3^-) system[7,8]. The variation of the observed molar extinction coefficient of the salicylato complex at 345 nm (ε_{obs}) with $[SDS]_T$ (= 0-0.2 mol dm^{-3}) in the absence of added acid is presented in Fig. 2(a). ε_{obs} exhibits a steep increase at $[SDS]_T = 0.001$ mol dm^{-3} and thereafter it increases virtually linearly and slowly with further increase in $[SDS]_T$. This leads us to believe that the complex ion induced micellization of SDS occurs at $[SDS]_T = 0.001$ mol dm^{-3}. Interpretation of the absorbance data is attempted on the basis of the pseudo-phase ion-exchange equilibrium model[9] represented by Eq. (1):

$$R^+_W + Na^+_M \overset{K^{Na}_R}{\rightleftharpoons} R^+_M + Na^+_W \qquad \ldots (1)$$

where $R^+ = (en)_2CoSal^+$, and M and W denote the micellar and aqueous pseudo-phases respectively. Further assuming that

$$(\gamma_{Na^+})_W/(\gamma_{R^+})_W = (\gamma_{Na^+})_M/(\gamma_{R^+})_M$$

where $(\gamma_i)_j$ denote the activity coefficient of the species 'i' in the pseudo-phase 'j', and writing for the dimensionless overall micellar binding parameter (β)

$$\beta = m^s_R + m^s_{Na} = [R^+_M]/[Dn] + [Na^+_M]/[Dn],$$

(where $[Dn] = [SDS]_T - cmc$ and $[R^+_M]$ and $[Na^+_M]$ denote the concentrations of the micelle-bound R^+ and Na^+ respectively), the ion-exchange equilibrium constant is given by Eq. (2)

$$K^{Na}_R = [R^+_M][Na]_W/([Na^+_M])[R^+_W])$$

$$= \frac{m^s_R\{[Na^+]_T - (\beta - m^s_R)[Dn]\}}{(\beta - m^s_R)([R^+]_T - m^s_R[Dn])} \qquad \ldots (2)$$

Equation (2) can be linearized to Eq. (3).

$$[R^+]_T/(m^s_R[Dn]) = 1 + (1/K^{Na}_R)[[Na^+]_T/\{(\beta - m^s_R)[Dn]\} - 1] \qquad \ldots (3)$$

where $[R^+]_T = [complex]_T$ and $[Na^+]_T = [SDS]$; the concentrations are expressed in terms of total solution volume. Writing

$$\varepsilon_{obs}[R^+]_T = \varepsilon^W_R[R^+_W] + \varepsilon^M_R[R^+_M]$$

where ε^j_R denotes the molar extinction coefficient of R^+ ion in the pseudo-phase j (= W,M), we obtain

$$m^s_R = [(\varepsilon_{obs} - \varepsilon^W_R)/(\varepsilon^M_R - \varepsilon^W_R)] \times [R^+]_T/[Dn] \qquad \ldots (4)$$

which when substituted in Eq. (3) yields Eq. (5):

$$(\varepsilon_{obs} - \varepsilon^W_R)^{-1} = (\varepsilon^M_R - \varepsilon^W_R)^{-1} + [K^{Na}_R(\varepsilon^M_R - \varepsilon^M_R)]^{-1} \times X \qquad \ldots (5)$$

where $X = \{[Na^+]_T/(\beta - m^s_R)[Dn]\} - 1$. β is used as an adjustable parameter and its acceptable value is 0.75 ± 0.10 (refs 7, 10). Assuming cmc = 0.001 mol dm^{-3} under the experimental condition as stated earlier, the calculated values of m^s_R ($= [R^+]_T/[Dn]$) for complete micellar binding of the complex ion ranges from 0.07 to 0.0015 for $[SDS]_T = 0.005$-0.2

mol dm^{-3}. Hence as a first approximation it is justifiable to assume $\beta \gg m_R^s$. The least squares best line plots of $(\varepsilon_{obs} - \varepsilon_R^W)^{-1}$ vs $\{[Na^+]_T/(\beta[Dn]) - 1\}$ accordingly yield approximate values of $(\varepsilon_R^M - \varepsilon_R^W)$ and K_R^{Na} for any chosen value of β (= 0.65-0.85). The value of $(\varepsilon_R^M - \varepsilon_R^W)$ enabled us to calculate m_R^s (see Eq. 4) and hence the data were fitted to Eq. (5) by an iterative least squares procedure. The final values of $(\varepsilon_R^M - \varepsilon_R^W)$ and K_R^{Na} are collected in Table 1. Typical plot yielding these parameters are also shown in Fig. 2(b). It is worth noting that K_R^{Na} is insensitive to the chosen value of β and its mean value is taken to be 1.24 ± 0.02 at 30.0 ± 0.1°C. The value of K_R^{Na} is not very much different from the ion-exchange equilibrium constant for H^+/Na^+ exchange with SDS micelle [$K_H^{Na} = 1$ (ref. 11), 2-4 (ref. 10)]. The small difference in the values of K_X^{Na}, however, may be partly reconciled with the fact that $(en)_2CoSal^+$ is a bulkier ion ($r_{R^+} > r_{Na^+} > r_{H^+}$) than Na_{aq}^+ or H_{aq}^+ and the cobalt(III) complex, like Na^+ and H^+, is also positioned in the water-rich Stern layer of the micelle. However, the charge effect on K_R^{Na} is likely to be much smaller than the same on K_H^{Na} from the consideration of the size factor. Hence it is reasonable to think that hydrophobic interaction between the hydrophobic ligand envelop of cobalt(III) and temporarily exposed hydrocarbon chain of the dynamic SDS micelle favours the micellar binding of this complex ion.

Table 2 presents the absorbance data of the complex at 360 nm at varying [SDS] and in the presence of added $HClO_4$. These data clearly reflect the propensity of $(en)_2CoSal^+$ to undergo protonation in the presence of SDS even at low [$HClO_4$] at which it is little protonated in the absence of the surfactant[6]. The site of protonation is the phenoxide oxygen of the chelated salicylate as it is the most basic site in the ion. The protonated complex retains its identity during the course of absorbance measurement as indicated by the fact that the observed spectrum of the complex in acidic medium in the presence and absence of SDS is time-independent. The work of Gillard *et al*[6] and our earlier observations[12] on mercuration of coordinated salicylate of $(en)_2CoSal^+$ in acidic medium also bear this fact.

Table 1—Calculated Parameters of Eq (5)

β	$(\varepsilon_R^M - \varepsilon_R^W)^a$ ($dm^3\ mol^{-1}\ cm^{-1}$)	K_R^{Na}
0.65	304 ± 21	1.26 ± 0.13
0.70	292 ± 19	1.22 ± 0.13
0.75	272 ± 14	1.25 ± 0.11
0.80	258 ± 13	1.25 ± 0.12
0.85	246 ± 11	1.22 ± 0.09
		Av. (1.24 ± 0.02)

[a] 360 nm.

For the protonation equilibrium (6) in the aqueous SDS/$HClO_4$ mixture

$$R^+ + H^+ \overset{K_{ap}}{\rightleftharpoons} RH^{2+} \qquad \ldots (6)$$

the apparent equilibrium constant (K_{ap}) may be defined by Eq. (7)

$$K_{ap} = x/\{(a-x)([H^+]_T - x)\} \qquad \ldots (7)$$

where $x = [RH^{2+}]_T$, $a = [complex]_T = [RH^{2+}]_T + [R^+]_T$ and $[H^+]_T = [HClO_4]$. The absorbance data at 360 nm indicates that the complex is fully protonated at $[HClO_4]_T = 0.05$ mol dm^{-3} and $[SDS]_T = 0.01$-0.1 mol dm^{-3}. ε_R (360 nm) is also insensitive to $[SDS]_T$ in the range 0.005-0.1 mol dm^{-3} and a value of 854 ± 29 $dm^3\ mol^{-1}\ cm^{-1}$ is obtained for ε_R (360 nm). The value of ε_{RH} (360 nm) as obtained from the limiting value of ε_{obs} at $[HClO_4]_T = 0.05$, $0.01 \leqslant [SDS]_T \leqslant 0.1$ mol dm^{-3} is taken to be 2858 ± 21 $dm^3\ mol^{-1}\ cm^{-1}$. Under varying condition of protonation we obtain Eq. (8) assuming

$$\varepsilon_{obs}\, a = \varepsilon_R([R_W^+] + [R_M^+]) + \varepsilon_{RH}[RH_M^{2+}] \qquad \ldots (8)$$

that the species RH^{2+} is partitioned into micellar pseudo-phase and concentration of this species in aqueous pseudo-phase is negligible. As the value of protonation constant of salicylato complex in the aqueous medium in the absence of SDS is quite low {$pK_H^W = 1.0 \pm 0.2$ at 30-40°C, $I = 0.3$ mol dm^{-3} (ref. 12); 1.0 ± 0.3 at 25°C (ref. 6)} the condition stated above is satisfied at $0.002 \leqslant [HClO_4]_T \leqslant 0.02$ mol dm^{-3}. Equation (8) yields

$$[RH_M^{2+}] = x = a(\varepsilon_{obs} - \varepsilon_R)/(\varepsilon_{RH} - \varepsilon_R) \qquad \ldots (9)$$

the concentrations being expressed in terms of total solution volume. The values of log K_{ap} could be calculated by combining Eqs (7) and (9) and using $\varepsilon_R = 854$ $dm^3\ mol^{-1}\ cm^{-1}$ and $\varepsilon_{RH} = 2858$ $dm^3\ mol^{-1}\ cm^{-1}$. Table 2 also presents the calculated values of log K_{ap} and degree of protonation of the complex (see the values of f in Table 2). Representing the protonation equilibrium by Eq. (10)

$$R_W^+ + H_W^+ \overset{K_{ap}^M}{\rightleftharpoons} RH_M^{2+} \qquad \ldots (10)$$

the equilibrium constant (K_{ap}^M) is given by Eq. (11)

$$K_{ap}^M = a_{(RH_M^{2+})}/(a_{(R_W^+)}\, a_{(H_W^+)}) \qquad \ldots (11)$$

where a (i_j) denote the activity of the species 'i' in the pseudo-phase 'j'. We assume $a_{(RH_M^{2+})} = [RH_M^{2+}]$ as no

Table 2—Absorbance, *p*H and Equilibrium Constant Data for Protonation Equilibrium of $(en)_2CoSal^+$ as a Function of $[SDS]_T$ and $[HClO_4]_T$

(λ = 360 nm; $[complex]_T = 3.00 \times 10^{-4}$ mol dm^{-3}; Temp. = 30°C)

$[SDS]_T$ (mol dm^{-3})	ε_{obs} (dm^3 mol^{-1} cm^{-1})	*p*H	*f*	log K_{ap}	log K_{ap}^M	log K_H^M
		$[HClO_4]_T = 0.001$ mol dm^{-3}				
0.00	890	3.18				
0.005	2527	3.59	0.835	3.83	4.31	3.36
0.010	2523	3.61	0.833	3.82	4.32	3.34
0.020	2353	3.62	0.748	3.58	4.18	3.08
0.040	2170	3.95	0.656	3.38	4.26	2.70
0.060	2073	4.06	0.608	3.28	4.29	2.57
0.080	2000	3.75	0.572	3.21	3.92	2.60
0.100	1853	3.78	0.498	3.07	3.82	2.45
		$[HClO_4]_T = 0.002$ mol dm^{-3}				
0.00	822	2.30				
0.005	2603	2.85	0.873	3.60	3.71	4.18
0.010	2567	2.80	0.855	3.52	3.60	4.73
0.020	2466	3.02	0.804	3.37	3.66	3.21
0.040	2367	3.07	0.755	3.24	3.60	2.97
0.060	2300	3.22	0.721	3.16	3.67	2.69
0.080	2150	3.30	0.647	3.00	3.60	2.46
0.100	2090	3.50	0.617	2.95	3.75	2.30
		$[HClO_4]_T = 0.005$ mol dm^{-3}				
0.00	850	2.38				
0.005	2333	2.35	0.738	2.77	2.84	4.25
0.010	2663	2.38	0.903	3.29	3.38	4.26
0.020	2643	2.56	0.893	3.24	3.52	3.15
0.040	2600	2.61	0.871	3.15	3.48	2.94
0.060	2500	2.74	0.821	2.98	3.45	2.57
0.080	2500	2.70	0.821	2.98	3.41	2.62
0.100	2467	2.66	0.805	2.94	3.32	2.64
		$[HClO_4]_T = 0.02$ mol dm^{-3}				
0.00	1050	1.67				
0.020	2747	1.77	0.944	2.94	3.06	3.78
0.040	2723	1.82	0.933	2.85	3.02	3.25
0.060	2733	1.73	0.938	2.88	2.98	4.50
0.080	2800	1.82	0.971	3.23	3.40	3.63
0.100	2797	1.77	0.969	3.21	3.34	4.05

satisfactory theory is at present available to calculate the activity coefficient of RH^{2+} in the micellar pseudo-phase. Our assumption, therefore, amounts to choosing $\gamma_{(RH_M^{2+})}$ = constant so that K_{ap}^M will be shifted by a constant factor. The ionic composition of the aqueous pseudo-phase can be known precisely; and the ionic strength expression,

$$I = 0.5\{cmc + [H_W^+] + [ClO_4^-]_T + (1-\beta)[Dn]\}$$

is used with the initial approximation $a_{(H_W^+)} = [H_W^+]$, cmc = 0.001 mol dm^{-3} and $\beta = 0.8$ to compute the activity coefficient of R_W^+ from the Davies' equation[13]. The calculated values of log K_{ap}^M are also included in Table 2. Further K_{ap} and the protonation equilibrium constant (K_M) of $(en)_2CoSal^+$ in the fully micellar pseudo-phase (given by Eq. 12)

$$K_M = [RH_M^{2+}]/([R_M^+][H_M^+]) \quad \ldots (12)$$

are also interrelated. Writing

$$K_{ap} = \frac{[RH_M^{2+}]}{\{[R_M^+] + [R_W^+]\}\{[H_W^+] + [H_M^+]\}} \quad \ldots (13)$$

we obtain

$$K_{ap} = K_M[(1 + [R_W^+]/[R_M^+])(1 + [H_W^+]/[H_M^+])]^{-1} \quad \ldots (14)$$

The pseudo-phase ion-exchange equilibrium (15) for $[H^+]/Na^+$ exchange,

$$H_W^+ + Na_M^+ \overset{K_H^{Na}}{\rightleftharpoons} H_M^+ + Na_W^+ \quad \ldots (15)$$

in combination with the same for R^+/Na^+ exchange (see Eq 2) yields

$$[R_W^+]/[R_M^+] = (K_H^{Na}/K_R^{Na})[H_W^+]/[H_M^+] \quad \ldots (16)$$

Combining Eqs (16) and (14), and rearranging we obtain

$$K^M = K_{ap}\{1 + (K_H^{Na}/K_R^{Na})[H_W^+]/[H_M^+]\} \times (1 + [H_W^+]/[H_M^+]) \quad \ldots (17)$$

K^M thus calculated is based on

$$[H_M^+] = [H^+]_T - [RH^{2+}] - [H_W^+]$$

and the concentrations are expressed in terms of total solution volume. Micellar volume corrected protonation constant is then given by

$$K_H^M = \bar{V} K^M$$

(see Eq. (12). Using $\bar{V} = 0.16$ dm^3 mol^{-1} (ref. 10), $K_H^{Na} = 1.0$ and $K_R^{Na} = 1.24$, the values of log K_H^M were calculated and these are also presented in Table 2.

It turns out that micellar binding of $(en)_2CoSalH^{2+}$ enhances its pK by 2 units relative to the aqueous phase. Such large effect of the micelles on the protonation equilibrium shift might arise due to various factors such as (i) negative charge of the micelles, (ii) relatively lower polarity of the microenvironment of the complex ion in the Stern layer of the micelles and (iii) presumably hydrophobic interaction between the hydrophobic ligand skeleton of the complex ion and the hydrophobic tail of SDS temporarily exposed to the Stern layer of the micelles. The values of the equilibrium constants (see Table 2) tend to decrease with increase in $[SDS]_T$ and this is particularly important at lower values of $[HClO_4]$ used which might be partly due to Na^+ competition with $(en)_2CoSalH^{2+}$ for micellar binding. The corresponding competition of H^+ with $(en)_2CoSalH^{2+}$ for micellar binding might be also significant at higher $[H^+]_T$. Further the ionic composition of the Stern layer of the micelles does change as $[SDS]_T$ and $[HClO_4]$ are varied. All these factors which are difficult to analyse quantitatively might contribute to the variation of the protonation equilibrium constant with variation of the composition of solution. However, the protonation equilibrium constant, K_{ap}^M (Eq. 11) appears to be more realistic.

Variation of ionic composition of bulk aqueous phase also causes variation in electrical potential difference between micellar pseudo-phase and the bulk aqueous phase ($\Delta\Phi = \Phi_M - \Phi_W$). Variation of $\Delta\Phi$ will also influence the distribution of ions between the aqueous and micellar pseudo-phases which in turn will affect the protonation equilibrium constant. Dorn *et al*[2] have tried to correlate the pK data of indicators measured in aqueous SDS media with the variation of $\Delta\Phi$. Their theory leads to Eq. (18) in our case for K_{ap}^M,

$$\log K_{ap}^M = A - \log\{[Na_W^+]^{0.66} + 2[H_W^+]^{0.69}\} \quad \ldots (18)$$

where A is a constant and it is reasonably assumed that variation of $\Delta\Phi$ depends upon the distribution of Na^+ and H^+ ions. The concentrations of Na_W^+ was computed from the relationship (19)

$$K_H^{Na} \times [H_W^+]/\{[H^+]_T - [H_W^+] - [RH^{2+}]\} = [Na_W^+]/\{[Na^+]_T - [Na_W^+]\} \quad \ldots (19)$$

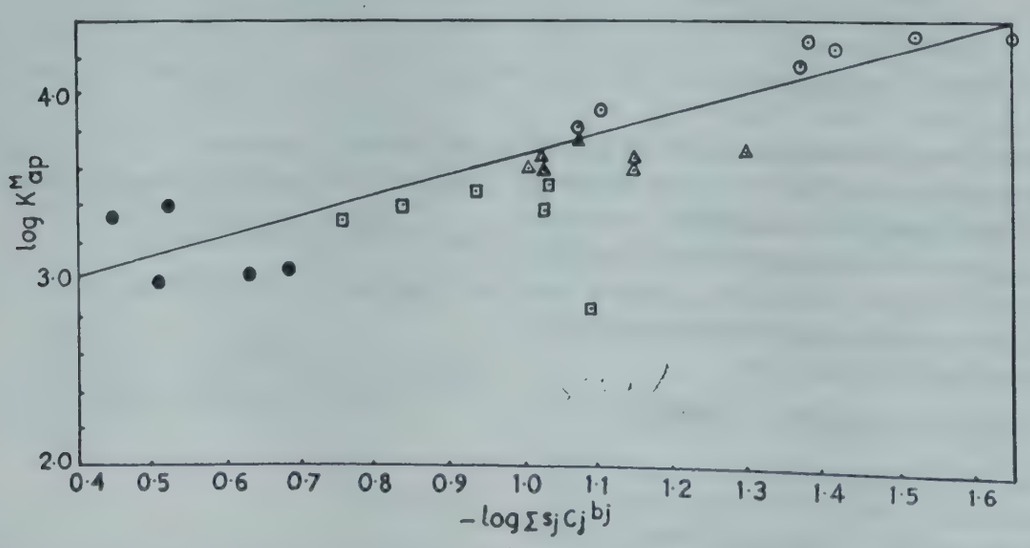

Fig. 3—Log K_{ap}^M as a function of electrical potential difference ($\Delta\phi$) between micellar pseudo-phase and bulk aqueous phase ($\Sigma e_j C_j^{bj} = [Na_W^+]^{0.66} + 2[H_W^+]^{0.69}$ (see ref 2); the data points refer to $[HClO_4]_T = 0.001$ (○), 0.002 (△), 0.005 (□) and 0.02 (●) mol dm^{-3})

valid for Eq. (15) using $K_H^{Na} = 1.0$ and $[Na^+]_T = [SDS]_T$. Log K_{ap}^M data were fitted to Eq. (18). Relevant plot shown in Fig. 3 has a slope of 1.09 in fair agreement with Eq. (18). Thus it is evident that surface potential effects ($\Delta\Phi$) are also important in controlling the protonation equilibrium of the substrate in the presence of SDS micelles.

Acknowledgement

This work is supported by a research grant from the UGC, New Delhi to ACD. RCN is thankful to the Utkal University for the award of a junior research fellowship.

References

1 Fendler E J & Fendler J H, *Adv Phys Org Chem*, **8** (1970) 361.
2 Dorin F, Charbit G & Gaboriaud R, *J Colloid Interface Sci*, **101** (1984) 27.
3 Dash A C & Nayak R C, *Indian J Chem*, **25A** (1986) 234.
4 Dash A C & Nayak R C, *Inorg Chem*, **25** (1986) 2237.
5 Cordes E H & Gitler C, *Progress in bioorganic chemistry*, Vol. I, edited by E T Kaiser & F J Kezdy (Wiley, New York) 1973, pp. 1.
6 Gillard R D, Lyons J R & Mitchell P R, *J chem Soc Dalton Trans*, (1973) 233.
7 Dash A C & Nayak R C, *J chem Soc Faraday Trans I*, **83** (1987) 1307.
8 Dash A C & Nayak R C, *Indian J Chem*, **26A** (1987) 293.
9 Fendler J H, *Ann Rev Phys chem*, **35** (1984) 137 and references cited therein.
10 Garnett C J, Lambie A J, Beck W H & Liler M, *J chem Soc Faraday Trans I*, **79** (1983) 953, 965.
11 Romsted L H in *Surfactants in solutions*, Vol 2, edited by K L Mittal & B Lindman (Plenum, New York) 1984, pp. 1038 [see foot note (a) Table 1 of this reference).
12 Dash AC, Nanda R K & Ray N, *Indian J Chem*, **21A** (1982) 1068.
13 Davies C W, *J chem Soc*, (1938) 2093.

Indian Journal of Chemistry
Vol. 27A, October 1988, pp. 868-872

Cerium(IV) & Manganese (III) Oxidation of Pentaamminecobalt(III) Complexes of Malonic & Methylmalonic Acids

K SUBRAMANI, K R SANKARAN & VANGALUR S SRINIVASAN*
Department of Chemistry, Ramakrishna Mission Vivekananda College, Madras 600 004

Received 6 *August* 1987; *revised and accepted* 7 *March* 1988

Cerium(IV)-induced electron transfer in $(H_3N)_5Co^{III}$-complexes of malonic acids yields nearly quantitative amounts of Co(II), CO_2 and formic acid, suggesting nearly synchronous electron transfer in the binuclear complex formed between Ce(IV) and Co(III) complex. Manganese(III) acetate induced electron transfer in $(H_3N)_5Co^{III}$ complexes of malonic acids gives the mesooxalatocobalt(III) complex. Also the same number of equivalents of manganese(III) is consumed by both unbound and cobalt(III) bound ligands, suggesting the non-participation of cobalt(III) in the Mn(III) acetate reaction with the malonatocobalt(III) complex. The stoichiometry of Ce(IV) reaction with malonatocobalt(III) complex is 5:1 and with unbound ligand, it is 6:1. Such a differential behaviour exhibited by manganese(III) acetate indicates its specificity towards metal-ion bound and unbound ligands.

Cerium(IV) and manganese(III) acetate, both of which, act as one-equivalent oxidants[1,2] and induce electron transfer in pentaamminecobalt(III) complexes of α-hydroxy acids, generating radicals which undergo concerted C—C bond cleavage and reduction at the cobalt(III) centre, producing cobalt(II) and carbonyl compounds. We envisage that both these oxidants may behave in a similar manner towards pentaaminecobalt(III) complexes of malonic and substituted malonic acids. Though both these oxidants are known to generate malonate radical[3-5] during their reaction with malonic acid, the kinetic and stoichiometric data obtained in the present work on Ce(IV) oxidation are different from those of manganese(III) acetate, suggesting the specificity of the latter oxidant towards these ligands, unbound and bound to cobalt(III).

Materials and Methods

The purity of ammonium cerium(IV) nitrate (AR, British Drug House) was checked before use. Manganese(III) acetate dihydrate was prepared and its purity was estimated to be 99%. Malonic and methylmalonic acids (AR, Fluka) were recrystallised twice from methanol-water (1:1 v/v). Diethylmalonic acid was prepared from disodium salt of diethyl malonate and ethyl iodide[6]. The $(H_3N)_5Co^{III}$ complexes of malonic, methylmalonic and diethylmalonic acids were prepared by a modified procedure of Fan[7]. After refluxing Co^{III}-carbonato complex (0.4 g) with ligand (10 mmol) in methanol (20 ml) for 2 hr, $HClO_4$ (3 ml), cooled to 0°C, was added to prevent aquation of complex. The hexaamminedicobalt(III) tris-μ-hydroxo perchlorate, $(H_3N)_3Co(OH)_3Co(H_3N)_3$ $(ClO_4)_3$, [triol], was prepared by the modified procedure of Siebert and coworkers[8,9]. The malonato-bridged dimeric cobalt(III) complex was prepared from triol following our earlier procedure[10]. The identity of all the Co(III) complexes was confirmed by their UV spectra and elemental analyses.

Kinetic measurements

The reactions between cobalt(III) complexes and cerium(IV) were carried out at 30 ± 0.2°C with the [oxidant] in excess. The unreacted [Ce(IV)] was estimated spectrophotometrically at 400 nm. The disappearance of cobalt(III) was followed spectrophotometrically by following the decrease in absorbance at 502 nm [for the monomeric cobalt(III) complex] and at 520 [for the dimeric cobalt(III) complex]. The specific rates calculated from the absorbance measurements in duplicate runs agreed within ± 7%. Similarly rates of manganese(III) acetate oxidation of cobalt(III) bound ligands, were estimated from the decrease in absorbance at 350 nm for the Mn(III), and these reactions were carried out in 76% aq acetic acid with manganese(III) acetate in deficiency. The specific rates calculated from successive half-lives agreed within ± 7% with those obtained from a semilog plot of the changes in absorbance against time.

Stoichiometric studies and product analyses

Cobalt(II) formed in the Ce(IV) reaction with $(H_3N)_5Co^{III}$ complexes of malonic and methylmalonic acids was estimated by diluting the reaction mixture tenfold, after nine half-lives with conc. HCl, allowing evolution of chlorine to cease, and then measuring the absorbance at 692 nm ($\varepsilon = 560$)[11]. While the amount

of cobalt(II) formed was nearly 100% in the cerium(IV) reaction, the amount of cobalt(II) formed in the case of manganese(III) acetate reaction with these complexes is almost negligible.

In the Ce(IV) reaction with these complexes nearly 5 mol of Ce(IV) consumed 1 mol of Co(III) complex, whereas nearly 6 equivalents of Ce(IV) was consumed by the unbound ligands. In manganese(III) acetate reaction with these complexes in nearly 4 mol of Mn(III) consumed 1 mol of Co(III) complex as well as the unbound ligands. Carbon dioxide was estimated by carrying out the reactions with excess oxidant at 40°C for 24 hr. For every mol of Co(III) complex used, nearly 2 mol of CO_2 were formed in Ce(IV) reactions. There was no evolution of CO_2 in manganese(III) acetate reaction. Similar results were obtained in the oxidation of unbound ligands. After nine half-lives the reaction mixtures containing excess of Ce(IV), were neutralised with K_2CO_3 as it precipitated $KClO_4$ and unreacted Ce(IV) as $Ce(CO_3)_2/Ce(OH)_4$. After the *p*H of the filtrate was adjusted to less than 1.0, the product, formic acid, was estimated using standard iodine solution[12] in the case of malonatocobalt(III) complex [under the reaction conditions, the amount of formic acid oxidised by Ce(IV) is negligible] and the percentage yield of formic acid was nearly 90% which was close to the yield of cobalt(II). Nearly the same amount of formic acid was estimated in the Ce(IV) reaction with unbound malonic acid. However, in manganese(III) acetate reaction with Co(III) complex, the IR spectrum of which resembled that of the cobalt(III) complexes of respective ketoacids [mesooxalatocobalt(III) complex in the case of malonatocobalt(III) complex and pyruvatocobalt(III) complex in the case of methyl malonatocobalt(III) complex]. With the unbound ligands, the respective keto acids were obtained as products, which were isolated and fully characterised (co-IR with authentic samples).

Test for free radicals

Mixtures of Ce(IV) and Co(III) complexes of malonic and methylmalonic acids (or of Ce(IV) and unbound ligands) initiated acrylonitrile polymerisation almost instantaneously in nitrogen atmosphere suggesting radical formation whereas neither Ce(IV) nor Co(III) complex initiates such a polymerisation in a comparable time interval. In contrast in manganese(III) acetate reactions with Co(III) complex or unbound ligands the reaction mixtures did not initiate acrylonitrile polymerisation even after 7 days.

Results and Discussion

Table 1 summarises representative kinetic data for the reaction of pentaamminecobalt(III) complex of malonic acid with Ce(IV) and $Mn(OAc)_3$ at 30 ± 0.2°C. Cerium(IV) oxidation exhibits total second order kinetics, first order in each reactant. Similar rate dependence on [Mn(III)] and [Co^{III}] has also been observed when these reactions are carried out in the presence of added Mn(II) of concentration equal to [Mn(III)]. In the absence of added Mn(II), the order in [Mn(III)] is unity, only upto first 25% and deviates from unity beyond that. Hence the rate laws for these reactions are given by Eqs (1) and (2)

Table 1—Kinetic Data for Ce(IV) and Mn(III) Acetate Reaction with Pentaamminecobalt(III) Complex of Malonic Acid[a,c]

10^3[Co^{III}] (mol dm^{-3})	10^2[Ce(IV)] (mol dm^{-3})	[$HClO_4$] (mol dm^{-3})	$10^3 k_1$ (s^{-1})
1.42	4.0	0.48	3.7
2.0	4.0	0.48	3.6
2.0	2.0	0.48	3.6[d]
2.9	4.0	0.48	3.8
5.0	4.0	0.48	3.8
10.0	4.0	0.48	3.8
3.0	3.2	0.48	3.2
3.0	4.8	0.48	4.6
3.0	8.0	0.48	7.8
3.0	4.0	0.12[b]	0.93
3.0	4.0	0.24[b]	0.86
3.0	4.0	0.36[b]	2.8
3.0	4.0	0.48	3.8

	10^4[Mn(III)] (mol dm^{-3})	10^4[Mn(II)] (mol dm^{-3})		$10^4 k_1$ (s^{-1})
4.0	2.8	—	1.83[f]	(1.46)[e]
6.4	2.8	—	2.7	(2.3)
8.0	2.8	—	3.6	(2.7)
4.0	2.8	2.8		1.79
4.0	3.9	3.9		1.82
4.0	5.6	5.6		1.82
4.0	1.12	—	(1.72)[g]	1.78
4.0	2.8	—	(1.83)	1.46
4.0	3.9	—	(1.70)	1.32
4.0	5.6	—	(1.84)	1.08
4.0	2.8	0.70	—	1.04
4.0	2.8	1.40	—	1.00
4.0	2.8	8.0	—	1.00
4.0	2.8	20	—	0.72

[a] Cerium(IV) reactions were carried out 0.48 mol dm^{-3} $HClO_4$ whereas manganese(III) acetate reactions were carried out in 76% aq acetic acid at 30 ± 0.2°C.

[b] Reactions were carried out at constant ionic strength of 0.48 mol dm^{-3} maintained by using $NaClO_4 + HClO_4$ mixture.

[c] Similar kinetic studies were made with cobalt(III) complex of methylmalonic acid dimeric cobalt(III) complex of malonic acid and similar trend in reactivity was observed.

[d] This specific rate was observed in the presence of [Ce(III)] = 1.0×10^{-3} to 1.0×10^{-2} mol dm^{-3}.

[e] These approximate specific rates were obtained in the absence of added Mn(II) acetate from the first 15% of reaction.

[f] These specific rates were obtained in the presence of added Mn(II) acetate.

[g] These were the approximate specific rates obtained in the absence of added Mn(II) from the first 25% of reaction.

$$\text{Rate} = k[Co^{III}][Ce(IV)] \quad \ldots(1)$$
$$\text{Rate} = k[Co^{III}][Mn(III)] \quad \ldots(2)$$

The specific rates for Ce(IV) oxidation of malonatocobalt(III) complex depend nearly on the first power of $[HClO_4]$ within the range, 0.12 to 0.48 mol dm^{-3}, at constant ionic strength. Cerium(IV) is probably present as $CeOH^{3+}$, in these media[13] as the pK_a for $Ce(IV)_{aq}$ is 0.77 (ref. 14). Considering the dimerisation of Ce^{IV} at these $HClO_4$ concentrations[15], the observed first order dependence on $[HClO_4]$ can be traced to the backward shift in the equilibria (3) and (4)

$$Ce(H_2O)^{4+} \rightleftharpoons Ce(OH)^{3+} + H^+ \quad \ldots(3)$$
$$2Ce(OH)^{3+} \rightleftharpoons Ce^{IV} - O - Ce^{IV} + H_2O \quad \ldots(4)$$

with increase in [acid] thereby increasing the concentration of reactive species $Ce(IV)_{aq}$. Cobalt(III) malonato complex will exist mostly in the acid form in the acid concentration used as the pK_a for this complex has been determined as 3.4 (ref. 16). Similar rate dependence on $[HClO_4]$ has been observed in the Ce(IV) oxidation of malonic acid also[3]. Though the addition of Ce(III) does not affect the rate of Ce(IV) reaction, addition of Mn(II) retards the rates of manganese(III) acetate reactions marginally indicating the reversibility of the electron transfer step(5) to some extent in the latter reaction.

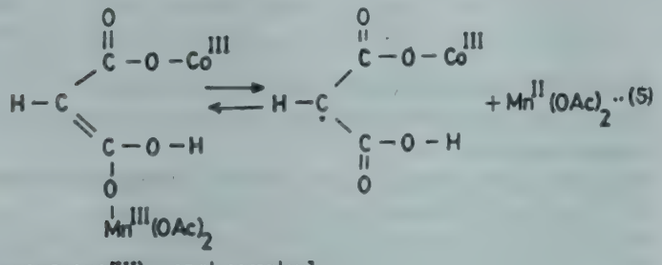

[manganese(III) – enol complex]

As the rate dependence on [Mn(II)] is only marginal, the order in [Mn(II)] may be close to zero. Hence the rate expression for this reaction does not include [Mn(II)]. The absence of such an effect of added Ce(III) in Ce(IV) reaction suggests that the intermediate radical does not oxidise Ce(III) and prefers to undergo facile electron transfer whereas in manganese(III) acetate reactions, possibly, both manganese(III) and manganese(II) compete for the intermediate radical.

The addition of Ce(IV) to malonatocobalt(III) complex is accompanied by a marginal increase in absorbance at 350 nm suggesting a complex formation but its formation constant could not be determined either spectroscopically or kinetically indicating a weak interaction between Ce(IV) and malonatocobalt(III) complex.

Table 2—Comparative Specific Rates of Cerium(IV) and Manganese(III) Acetate Reactions with Pentaamminecobalt(III) Complexes of Malonic and Methylmalonic Acids[a]

$10^3[Co^{III}]$ (mol dm^{-3})	$10^2[Ce(IV)]$ (mol dm^{-3})	$10^2 k_2$ ($dm^3 mol^{-1} s^{-1}$)
L = malonic		
3.0	8.0	9.7
5.0	4.0	9.6
methylmalonic		
2.0	8.0	1.60
5.0	4.0	1.61
$[Co_2^{III}]$ (mol dm^{-3}) malonic		
2.3	8.0	0.035
4.6	2.0	0.031
4.6	6.0	0.032
9.2	8.0	0.033
	$10^4[Mn(III)]$ (mol dm^{-3})	$10^2 k_2$ ($dm^3 mol^{-1} s^{-1}$)
malonic		
4.0	2.3	3.6
8.0	2.8	3.4
methylmalonic		
2.0	2.8	0.81
4.0	2.8	0.91

[a] Cerium(IV) reactions were carried out in 0.48 mol dm^{-3} $HClO_4$ while manganese(III) acetate reactions were carried out in 76% aq acetic acid at 30 ± 0.2°C.

The rates of Ce(IV) reaction with Co(III) complexes of malonic acids are susceptible to electronic influence at the α-carbon. For example, the rate of Ce(IV) induced electron transfer in the methylmalonatocobalt(III) complex is considerably reduced (about 6 times) compared to that of malonato complex (Table 2) due to +I effect of the methyl group at the α-carbon making the α-hydrogen less acidic and probably enol-formation becomes difficult. This is corroboated by the observation that Co(III) complex of dimethylmalonic acid does not react with Ce(IV) as enol formation is not possible in this compoud. It may also be due to destablisation of the precursor complex by the steric effect of methyl group. The dimeric cobalt(III) complex of malonic acid reacts with Ce(IV) at a rate which is about 300 times (Table 2) less than that of the corresponding monomeric Co(III) complex, suggesting pronounced electrostatic influence felt at the seat of attack from the cobalt(III) centres.

The same order of reactivity is observed in the manganese(III) acetate reaction with these cobalt(III) complexes (Table 2).

Cobalt(III) malonato (1.0) < cobalt(III)methylmalonato (0.003)

To account for the quantitative yields of cobalt(II), CO_2, formic acid and consumption of 5 mol of Ce(IV)

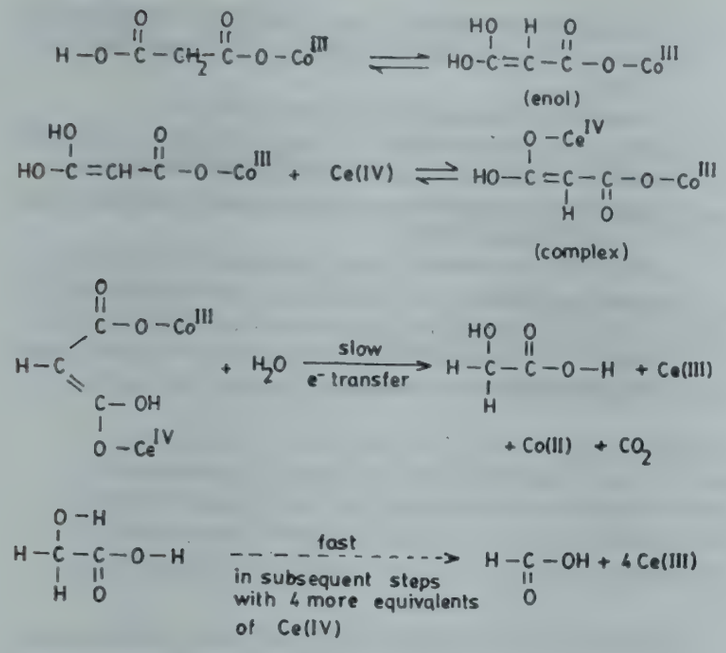

Scheme 1

by 1 mol of Co(III) complex, the mechanism shown in Scheme (1) has been suggested.

The electron transfer, occurring in Ce(IV)-enol complex, with nearly synchronous C—C cleavage and reduction at Co(III) centre, is considered as a slow step. Under identical conditions 1 mol of glycolic acid required 4 mol of Ce(IV) yielding formic acid as one of the products. The reaction between Ce(IV) and glycolic acid is over in the mixing time and hence the rate of this reaction is faster than that of Ce(IV) and malonic acid reaction.

The observed kinetic and stoichiometric data for the manganese(III) acetate reaction with malonatocobalt(III) complex is explained by a mechanism shown in Scheme 2, involving a slow electron transfer in manganese(III)-enol complex in a reversible manner.

The above scheme reasonably accounts for both the kinetic and stoichiometric data.

As nearly 6 equivalents of Ce(IV) are consumed by 1 mol of unbound malonic/methylmalonic acids, yielding nearly 2 mol of CO_2 and 1 mol of formic acid/acetic acid, the mechanism of Ce(IV) oxidation of unbound ligand will be similar to Scheme 1. As the same number of mol of manganese(III) acetate is consumed by both the cobalt(III) bound and unbound ligands, only the ligand portion is attacked by this oxidant without the involvement of Co(III) in the reaction. This may due to the competing reactions of the malonate radical with Mn(II) and Mn(III) and possibly, the rate of Mn(III) acetate reaction with malonato radical is greater than the rate of internal electron transfer involving Co(III). This differential behaviour observed between Ce(IV) and manganese(III) acetate

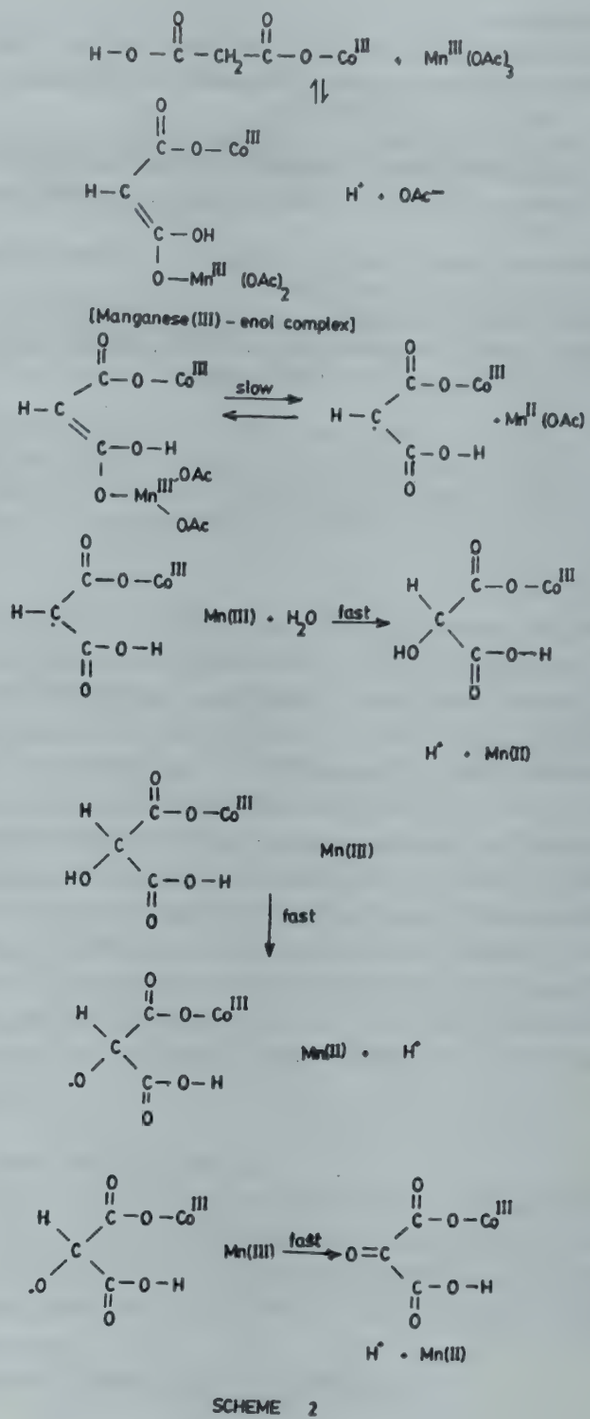

SCHEME 2

towards malonatocobalt(III) complex is absent in their reaction with cobalt(III) complexes of α-hydroxy acids wherein the yield of cobalt(II) is nearly 100% in the both the cases[1,2], evidencing the specificity of the oxidant, manganese(III) acetate, in its reaction with malonatocobalt(III) complexes.

Acknowledgement

One of the authors KS is thankful to the CSIR, New Delhi for awarding senior research fellowship and KRS is thankful to the UGC, New Delhi for awarding junior research fellowship.

References

1 Srinivasan V S & Gould E S, *Inorg Chem*, **20** (1981) 208.
2 Kalidoss P, Shanmugakani C, Sundaram S & Srinivasan V S, *Inorg Chem*, **26** (1987) 968.
3 Amjad Z & McAuley A, *J chem Soc Dalton*, (1977) 304.
4 Tischler F & Marrow J I, *Inorg Chem*, **22** (1983) 2286.
5 Morette A & Waters W A, *Bul Soc chim France* (1954) 956, 3193.
6 Vogel A I, *A text book of practical organic chemistry* (Longman, London) (1980) p 906.
7 Fan F -R F & Gould E S, *Inorg Chem*, **13** (1974) 2639.
8 Srinivasan V S, Singh A N, Wieghardt K, Rajasekar N & Gould E S, *Inorg Chem*, **21** (1982) 2531.
9 a. Linhard M & Siebert H, *Z Anorg Allg Chem*, **364** (1969) 24.
b. Siebert H & Tremmel G, *Z Anorg Allg Chem*, **390** (1972) 292.
c. Sibert H, *Z Anorg Allg Chem*, **441** (1978) 47.
10 Subramani K & Srinivasan V S, *Inorg Chem*, **24** (1985) 235.
11 Gould E S & Taube H, *J Am chem Soc*, **86** (1964) 2318.
12 Vogel A I, *A text book of quantitative inorganic analysis* (Longman, London) (1978).
13 a. French J E & Taube H, *J Am chem Soc*, **91** (1969) 6951.
14 Amjad Z & McAuley A, *J chem Soc* (*Dalton*) (1974) 2521.
15 *a. Heidt L J & Smith M E J Am chem Soc*, **70** (1948) 2476.
b. King E L & Pandow M L, *J Am chem Soc*, **74** (1952) 1966.
16 Svatos G & Taube H, *J Am chem Soc*, **83** (1961) 4172.

Indian Journal of Chemistry
Vol. 27A, October 1988, pp. 873-875

Kinetics & Mechanism of Ru(III) Catalyzed Oxidation of Olefins by N-Methylmorpholine N-Oxide

G CAROLING, J RAJARAM & J C KURIACOSE*
Department of Chemistry, Indian Institute of Technology, Madras 600 036

Received 14 *December* 1987; *revised and accepted* 18 *February* 1988

Epoxidation of cyclohexene, 1-octene and styrene by N-methylmorpholine N-oxide in the presence of catalytic amounts of $RuCl_3$ shows first order dependence each in N-oxide and the catalyst. The order in cyclohexene and 1-octene is variable being zero at high concentrations and one at low concentrations. In the case of styrene the order is fractional at all concentrations. The active oxidant is $Ru^V = O$ species resulting from the oxidation of $RuCl_3$ by NMO. On the basis of experimental observations a reaction mechanism is proposed.

In an earlier paper from our laboratory it has been reported[1] that N-methylmorpholine-N-oxide (NMO) acts as a source of oxygen in oxidising secondary alcohols to ketones in the presence of Ru(III) chloride in DMF as solvent. Since the alkenes may form complexes with the catalyst, a change in the kinetics and mechanism can be expected. This paper deals with the epoxidation of cyclohexene, 1-octene and styrene byN-methylmorpholine-N-oxide in the presence of catalytic amounts of $RuCl_3$ in DMF as solvent.

Materials and Methods

N-methylmorpholine-N-oxide (Fluka) was used as such. Solutions of $RuCl_3$ in DMF were standardised as reported in the literature[2]. Cyclohexene and 1-octene were freed from peroxides, distilled and then used. Styrene was distilled under reduced pressure and its purity was checked by VPC and NMR. DMF was purified as reported in literature[3]. All kinetic runs were carried out under nitrogen atmosphere at $35 \pm 0.1°C$. Aliquots of the reaction mixture were withdrawn at regular intervals of time and analysed for NMO content by titanometric procedure[4]. At low [cyclohexene] and [1-octene], the reaction was followed by estimating the amount of the olefinic compound by iodometric titration.

Results and Discussion

Cyclohexene, 1-octene and styrene are oxidized by N-methylmorpholine-N-oxide in the presence of catalytic amounts of $RuCl_3$ to the corresponding epoxides. The formation of epoxides was confirmed by IR spectral studies and also by comparing the GLC retention times, using an FFAP column, with those of the authentic samples. There is no significant oxidation of the olefin by NMO in the absence of the catalyst. The stoichiometry of the reaction between the substrate and NMO in the presence of the catalyst is 1:1. The reaction in the presence of large excess of olefin shows first order dependence each in N-oxide and catalyst. The order in substrate varies from one at low [substrate] (< 0.01 mol dm^{-3}) to zero at high [substrate] (> 1.0 mol dm^{-3}). Addition of acrylamide to the reaction mixture does not affect the reaction rate. In the case of styrene the order in substrate is fractional even at [substrate] of 2.5 mol dm^{-3} (Table 1). Electronic spectral measurements indicate the absence of complex formation between the catalyst and the substrate. These reactions are not inhibited by N-methylmorpholine (reduction product of NMO) precluding any prior equilibrium step involving N-methylmorpholine.

Mechanism and rate law

The absence of polymerization of acrylamide rules out the possibility of the reaction proceeding by a free radical mechanism. There being no evidence for complex formation the mechanism, shown in Scheme 1 is proposed.

Scheme 1 leads to rate expression (1)

$$\text{Initial rate} = \frac{k_1 k_2 [S][\text{Ru(III)}]_i[\text{NMO}]}{k_{-1} + k_2 [S]} \qquad \ldots (1)$$

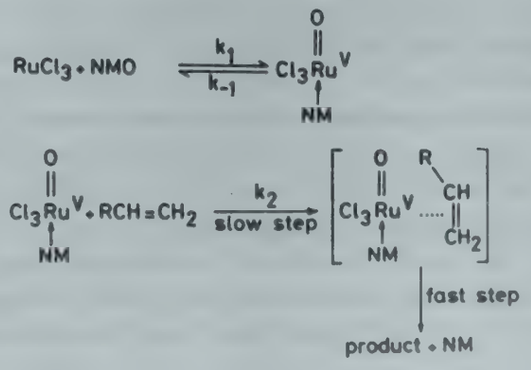

Scheme -1

Table 1—Determination of Orders with Respect to Reactants at High [Substrate]

[Temp. = 35 ± 0.1°C; solvent = DMF]

Substrate	10^2[NMO] (mol dm^{-3})	[S] (mol dm^{-3})	10^4[$RuCl_3$] (mol dm^{-3})	$10^3k'$ (min^{-1})	k_1(dm^{3}mol^{-1}min^{-1}))
Cyclohexene	21.00	2.0	8.0	9.05	11.31
	16.90	2.0	8.0	9.21	11.51
	13.00	2.0	8.0	9.45	11.81
	8.16	2.0	8.0	9.11	11.39
	9.60	2.5	8.0	9.05	11.31
	9.60	2.0	8.0	9.10	11.38
	9.60	1.5	8.0	9.27	11.58
	9.60	1.0	8.0	9.21	11.51
	9.60	1.0	6.0	6.74	11.23
	9.60	1.0	3.0	3.38	11.26
					k_1(mean) = 11.43 ± 0.13
1-Octene	10.00	1.0	4.0	3.34	8.35
	7.32	1.0	4.0	3.34	8.35
	3.20	1.0	4.0	3.32	8.30
	4.70	1.5	4.0	3.34	8.35
	4.70	1.0	4.0	3.45	8.63
	4.70	0.7	4.0	3.39	8.48
	4.70	0.5	4.0	3.47	8.68
	10.00	1.0	8.0	6.78	8.30
	10.00	1.0	6.0	4.98	8.48
					k_1(mean) = 8.43 ± 0.048
Styrene	21.00	2.5	6.0	20.12	
	15.30	2.5	6.0	21.80	
	9.20	2.5	6.0	23.00	
	9.20	1.0	8.0	17.20	
	9.20	1.0	6.0	13.70	
	9.20	1.0	4.0	8.60	
	9.20	1.0	2.0	4.64	
	9.20	2.0	6.0	18.76	
	9.20	1.5	6.0	16.85	

k' = Pseudo-first order rate constant ([S] ≫ [NMO]).
k_1 = Overall second order rate constant (= k'/(Ru(III)])

where the subscript i, indicates initial concentration. Equation (1) can be rearranged as

$$\frac{1}{\text{initial rate}} = \frac{k_{-1}}{k_1 k_2\,[S][Ru(III)]_i[NMO]} + \frac{1}{k_1[Ru(III)_i[NMO]} \qquad \ldots (2)$$

A plot of 1/rate versus 1/[substrate] is linear at low [substrate] and fixed [Ru(III)]$_i$ and [NMO] (Fig. 1). The values of k_1 and k_{-1}/k_2 evaluated from the intercept and slope respectively of this plot are given in Table 2. The values of k_1 determined experimentally from measurements under zero order conditions of the substrate are also given in Table 2. In the case of styrene, for reasons indicated earlier, the value of k_1 could not be experimentally evaluated. At high [substrate], $k_{-1}/k_2 \ll$ [S] and hence the order in the substrate is zero. At low [substrate] (< 0.01 mol dm^{-3}) $k_{-1}/k_2 \gg$ [S] and so the reaction is first order in substrate.

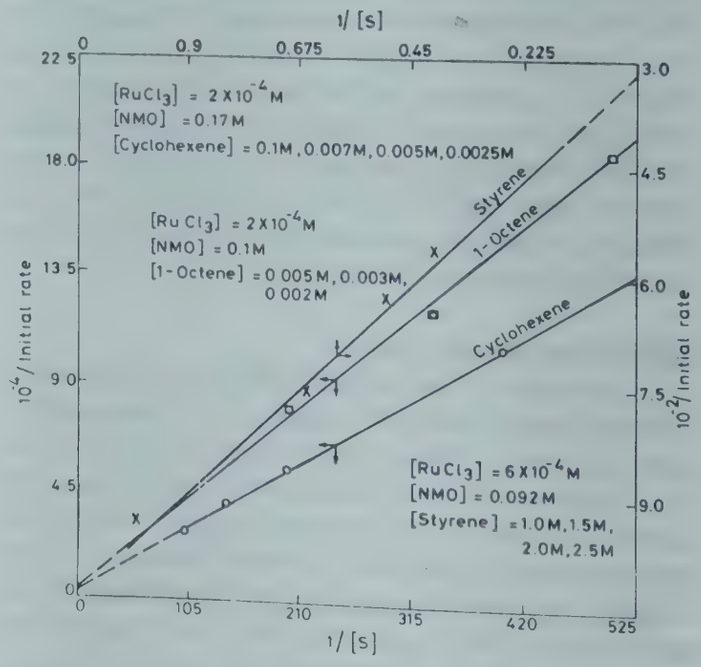

Fig. 1—Double reciprocal plot verifying the rate expression

Table 2—Evaluation of k_1 and k_{-1}/k_2 from Double Reciprocal Plot

Substrate	k_1 ($dm^3mol^{-1}min^{-1}$)		k_{-1}/k_2 ($mol\ dm^{-3}$)
	From pseudo-first order plot	From double reciprocal plot	
Cyclohexene	11.43 ± 0.13	11.36	0.109
1-Octene	8.43 ± 0.048	8.30	0.053
Styrene	—	—	2.085

Table 3—Comparison of Initial Rates of Various Substrates at Low [Substrate]

[NMO] = 0.2 mol dm^{-3}; [S] = 0.01 mol dm^{-3}; [$RuCl_3$] = 2.0×10^{-4} mol dm^{-3}; solvent = DMF; temp. = 35 ± 0.1°C

Substrate	10^5 Initial rate ($mol\ dm^{-3}min^{-1}$)	Relative rate
Cyclohexene	3.63	1.0
Cycloheptene	5.44	1.5
Cyclooctene	4.35	1.2
1-Hexene	2.42	1.0
1-Heptene	2.36	0.97
1-Octene	2.25	0.93

Due to the higher value of k_{-1}/k_2 for styrene even at the highest [styrene]used (2.5 mol dm^{-3}), k_{-1}/k_2 and [S] are comparable, accounting for the order remaining fractional at the highest [styrene].

The order of reactivities of the substrates in the low concentration region where the order in substrate is unity is cycloheptene > cyclooctene > cyclohexene (Table 3). This can be explained in terms of the rate of formation of the epoxide and also the product stability. Cyclohexene which exists in the half-chair conformation experiences considerable steric interactions caused by the axial hydrogens. Hence the $Ru^V=O$ species cannot easily appraoch the substrate. In the case of cycloheptene the hydrogens are in pseudo axial and pseudo equatorial positions. Hence the $Ru^V=O$ species can transfer its oxygen atom with less steric effect. Cycloheptene falls in the intermediate category. Moreover, cyclohexene oxide once formed exists still in the half-chair conformation which is highly strained whereas cycloheptene and cyclooctene oxides take up the more stable conformations[5].

Ru(III)/NMO system oxidizes only the terminal alkenes and not the internal alkenes like *trans*-hept-2-ene and *cis*- and *trans*-stilbenes. The presence of electron withdrawing chlorine atom in the vicinity of the double bond causes a lowering in the activity of allyl chloride and 3-chloro-1-butene towards epoxidation. Thus the epoxidation reaction is governed by both steric and polar factors. The products formed in the epoxidation of allyl chloride and 3-chloro-1-butene are the corresponding epichlorohydrins. The rates of oxidation of terminal alkenes (Table 3) do not show changes with increase in chain length that warrant an explanation. $RuCl_3$/NMO system does not oxidize carbon-carbon triple bonds as they are more resistant to electrophilic attack.

$RuCl_3$/NMO system gives rise to the $Ru^V=O$ species which is the active oxidant for the oxidation of a variety of nucleophilic substrates. Tetraphenylporphyrin salts of manganese and iron also give rise to such oxo species in the presence of oxidants like iodosobenzene and *p*-cyano-N, N-dimethylaniline N-oxide[6]. In order to compare $RuCl_3$/NMO system with $ClMn^{III}TPP$/NMO and $ClFe^{III}TPP$/NMO systems, tetraphenylporphyrin salts of manganese and iron were prepared as reported in the literature[7] and characterized by UV and IR. Using alkenes as substrates reactions were carried out with these tetraphenylporphyrin salts as catalysts in the presence of NMO. The formation of $Mn^V=O$ and $Fe^V=O$ species on the addition of NMO to $ClMn^{III}TPP$ and $ClFe^{III}TPP$ was characterised by spectral methods[8,9]. However these species do not react with alkenes but with the deoxygenated product of NMO, viz. N-methylmorpholine (NM) to give formaldehyde and morpholine as the products.

Conclusions

The $RuCl_3$/NMO system is efficient in the epoxidation of a variety of terminal alkenes. Internal alkenes are not epoxidized. Epoxidation reaction is governed by both steric and polar factors. The active oxidant is the $Ru^V=O$ species resulting from the oxidation of $RuCl_3$ by NMO.

Acknowledgement

One of the authors (GC) is thankful to the CSIR, New Delhi for financial assistance.

References

1 Vijayasri K, Rajaram J & Kuriacose J C, *J Mol Catal*, **39** (1987) 203.
2 Horiuchi Y & Ichiyyo O, *Chem Abstr*, **72** (1970) 50624.
3 Faulkner L R & Bard A J, *J Am chem Soc*, **90** (1968) 6284.
4 Caroling G, Rajaram J & Kuriacose J C, *Curr Sci*, **55** (1986) 1132.
5 Eliel E L, *Stereochemistry of carbon compounds*, (McGraw-Hill, New York), 1962, 271.
6 Powell M F, Pai E F & Bruice T C, *J Am chem Soc*, **106** (1984) 3277.
7 Adler A D, Longe F R, Kampas F & Kim J, *J inorg nucl Chem*, **32** (1970) 2443.
8 Willner I, Otvos J W & Calvin M, *Chem Commun*, (1980) 964.
9 Nee M W & Bruice T C, *J Am chem Soc*, **104** (1982) 6123.

Indian Journal of Chemistry
Vol. 27A, October 1988, pp. 876-879

Kinetics of Oxidation of Alcohols, Diols & α-Hydroxy Acids by Os(VIII) in Aqueous Alkaline Medium: Evidence in Support of Hydride Ion Abstraction Mechanism

P VEERA SOMAIAH, K BAL REDDY, B SETHURAM & T NAVANEETH RAO*

Department of Chemistry, Osmania University, Hyderabad 500 007

Received 7 *December* 1987; *revised* 14 *January* 1988; *accepted* 8 *February* 1988

Kinetics of oxidation of alcohols, diols and α-hydroxy acids by OsO_4 in aqueous alkaline medium have been studied spectrocolorimetrically at 400 nm. The order in [substrate] and [oxidant] is found to be unity each. Increase in $[OH^-]$ increases the rate and the order in $[OH^-]$ is <1.0. No evidence for complex formation has been observed in all these reactions. The products of oxidation are identified as the corresponding carbonyl compounds. A mechanism involving hydride ion abstraction by the oxidant in a slow step is proposed.

Recently we have reported[1] the oxidation of propan-2-ol by OsO_4 and also Os(VIII)-catalysed oxidation of propan-2-ol by different one- and two-equivalent oxidants. It was shown that the rate of oxidation by Os(VIII) is more or less same as Os(VIII) catalysed oxidation. The mechanism proposed involved hydride ion abstraction from α-carbon by Os(VIII) in the slow step. However, it was thought that a structure-reactivity correlation study might help in finding out whether hydride ion transfer occurs in the oxidation of hydroxy compounds or not. The title investigation deals with this.

Materials and Methods

All the chemicals used were of AR grade and wherever necessary purified by the usual methods. All aqueous solutions were prepared in triply distilled water. Allyl alcohol was purified by refluxing it with 2,4-DNP for 4-5 hr followed by distillation. Stock solution of Os(VIII) was prepared by dissolving osmic acid (Johnson-Matthey) in KOH (0.5 mol dm^{-3}) and standardised iodometrically. α-Hydroxy acids were neutralised by standard KOH before use.

The reactions were carried out under pseudo-first order conditions ([hydroxy compound] ≫ [Os (VIII)]) at the desired temperature maintained with an accuracy of ±0.1°C. The course of the reaction was studied by estimating unreacted Os(VIII) spectrocolorimetrically at 400 nm at regular time intervals using a Carl-Zeiss spectrocolorimeter.

Products and stoichiometry

Oxidation products in the case of alcohols were identified as the corresponding carbonyl compounds and confirmed by preparing their 2,4-DNP derivatives. Allyl alcohol afforded glycerol as revealed by spot test[2]. Diols afforded the corresponding glyoxals identified by their characteristic spot tests[2]. α-Hydroxy acids were oxidised to the corresponding keto acids[2].

Stoichiometric studies revealed that one mol of Os(VIII) was consumed for every mol of alcohol or hydroxy acid and 2 mol of Os(VIII) for every mol of diol.

Results and Discussion

Under pseudo-first order conditions ([substrate] ≫ [Os(VIII)] the plots of log (absorbance) versus time were linear for all the substrates (a typical plot for the ethanol-Os(VIII) reaction is given in Fig. 1A) indicating first order in [Os(VIII)]. Pseudo-first order rate constants (k') were evaluated from the slopes of such plots. The plot of log k' versus log [substrate] was linear with a slope of 1.0 indicating that the order in [substrate] was also unity (Figs 1B, 1C and 1D). The k' values increased with increase in $[OH^-]$ and the order in $[OH^-]$ was fractional for all the substrates (Table 1). No polymerisation was observed when acrylamide was added to the reaction mixture under nitrogen atmosphere indicating absence of a free radical pathway. Added salts like KNO_3 and $NaClO_4$ had negligible effect on the rate of oxidation. No reaction was observed between Os(VIII) and tertiary butanol.

In alkaline solutions OsO_4 is known to exist in two forms, viz. $OsO_4(OH)H_2O^-$ and $OsO_4(OH)_2^{2-}$ (ref. 3). While the former exists even at low $[OH^-]$ the latter is possible only at high $[OH^-]$ as per equilibrium (1)

Table 1—Effect of $[OH^-]$ in Oxidation of Hydroxy Compounds by Os(VIII)

[a] Os(VIII)-2-propanol reaction
[2-propanol] = 1.00×10^{-2} mol dm^{-3}; [Os(VIII)] = 3.16×10^{-4} mol dm^{-3}; temp = 304.3 K
[b] Os(VIII)-1,2-propane diol reaction
[1,2-propane diol] = 1.00×10^{-2} mol dm^{-3}; [Os(VIII) = 3.16×10^{-4} mol dm^{-3}; temp = 305 K
[c] Os(VIII)-glycollic acid reaction
[glycollic acid] = 4.0×10^{-3} mol dm^{-3}; [Os(VIII)] = 3.16×10^{-4} mol dm^{-3}; temp = 305 K

a		b		c	
$[OH^-] \times 10^2$ (mol dm^{-3})	$k' \times 10^4$ (s^{-3})	$[OH^-] \times 10^2$ (mol dm^{-3})	$k' \times 10^4$ (s^{-1})	$[OH^-] \times 10^2$ (mol dm^{-3})	$k' \times 10^4$ (s^{-1})
5.00	6.73	5.00	16.7	5.00	4.78
10.0	9.14	10.0	19.1	11.4	5.12
20.0	11.1	20.0	21.2	21.0	5.84
30.0	13.4	30.0	26.2	37.0	5.90
		40.0	34.8	69.8	6.40

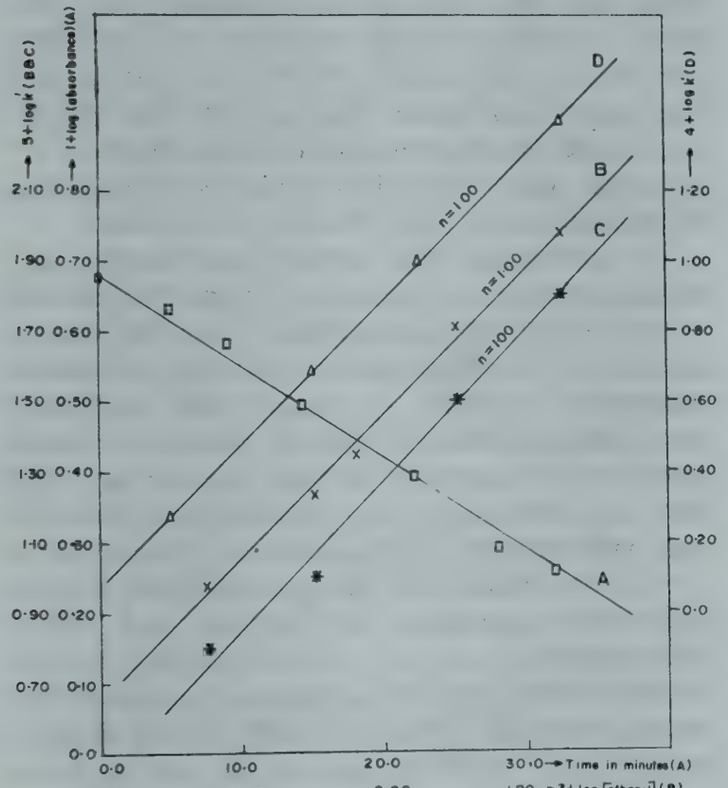

Fig. 1—(A) Plot of 1 + log absorbance versus time in minutes ([ethanol] = 1.00×10^{-2} mol dm^{-3}; [Os(VIII)] = 3.16×10^{-4} mol dm^{-3}; temp = 305 K; $[OH^-] = 5.00 \times 10^{-2}$ mol dm^{-3}).
(B) Plot of 3 + log [ethanol] versus 5 + log k'
(C) Plot of 3 + log [ethanediol] versus 5 + log k'
(D) Plot of 3 + log [glycollic acid] versus 4 + log k' ([Os(VIII)] = 3.16×10^{-4} mol dm^{-3}; $[OH^-] = 5.00 \times 10^{-2}$ mol dm^{-3}; temp = 305 K)

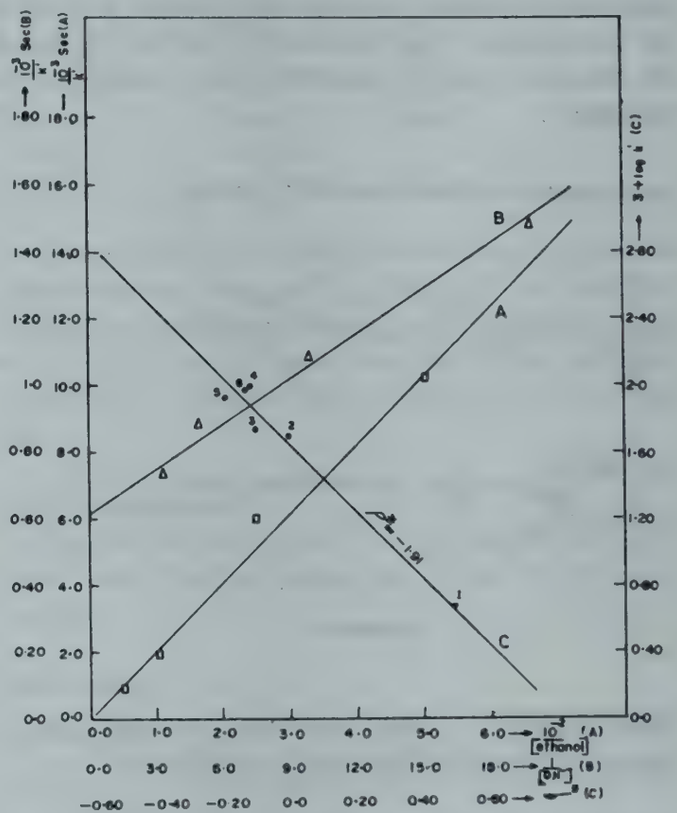

Fig. 2—(A) Plot of 1/[ethanol] versus $1/k'$ ([Os(VIII)] = 3.16×10^{-4} mol dm^{-3}; $[OH^-] = 5.00 \times 10^{-2}$ mol dm^{-3}; temp = 305 K).
(B) Plot of $1/[OH^-]$ versus $1/k'$ ([2-propanol] = 1.00×10^{-2} mol dm^{-3}; [Os(VIII)] = 3.16×10^{-4} mol dm^{-3}; temp = 304.3 K).
(C) Plot of σ^* versus 3 + log k'' ($[OH^-] = 5.00 \times 10^{-2}$ mol dm^{-3}; temp = 305 K (1) methanol (2) ethanol (3) *n*-propanol (4) *n*-butanol (5) Iso-butanol (6) *n*-pentanol).

$$OsO_4(OH)H_2O^- + OH^- \underset{}{\overset{K_1}{\rightleftharpoons}} OsO_4(OH)_2^{2-} + H_2O \quad \ldots (1)$$

The equilibrium (1) envisages an increase in rate with increase in $[OH^-]$ if $OsO_4(OH)_2^{2-}$ is the reactive form of OsO_4. This in fact was observed in the present study suggesting that $OsO_4(OH)_2^{2-}$ is the reactive species under the experimental conditions. The plot of $1/k'$ versus 1/[substrate] was linear passing through the origin (Fig. 2A) indicating absence of complex formation between substrate and OsO_4 prior to oxidation. This was also confirmed by the fact that there was no shift in the λ_{max} of OsO_4 when the substrate was added. All

the above mentioned results suggest that Os(VIII) reacts with the substrate in the slow step to give the products either directly or via formation of a highly unstable complex.

Earlier we have reported a mechanism involving the hydride ion abstraction by OsO_4 in the oxidation of propan-2-ol by OsO_4 in aqueous alkaline medium[1]. If this were to be true the electron-releasing substituents at α-carbon should increase the rate of oxidation while electron-withdrawing substituents should retard it. The order of reactivities with respect to alcohols (methanol < chloroethanol < ethanol < *n*-propanol < propan-2-ol < isobutanol < *n*-pentanol < *n*-butanol < allyl alcohol < benzyl alcohol) supports the above contention. This coupled with the fact that there was no reaction with *t*-butanol supports the hydride ion transfer mechanism. The mechanism for the oxidation of alcohols could therefore be written as in Scheme 1.

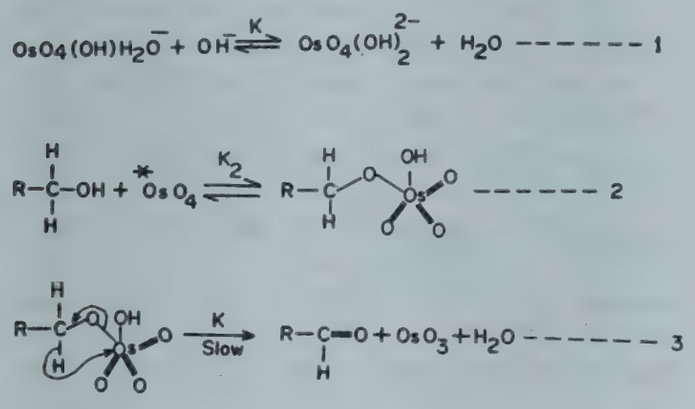

Scheme—1

($[OsO_4(OH)_2]^{2-}$ is written as $*OsO_4$ for simplicity). Rate law (4) can be derived from Scheme 1.

$$\frac{-d \ln [Os(VIII)]}{dt} = k' = \frac{kK_1K_2[\text{alcohol}][OH^-]}{1 + K_1[OH^-]} \quad \ldots (4)$$

Taking reciprocals of Eq. (4) we get

$$\frac{1}{k'} = \frac{1}{kK_1K_2[\text{alcohol}][OH^-]} + \frac{1}{kK_2[\text{alcohol}]} \quad \ldots (5)$$

which satisfactorily explains all the observed kinetic results. According to above rate law the plot of $1/k'$ versus $1/[OH^-]$ should be linear with an intercept. This was found to be the case (Fig. 2B) supporting the proposed mechanism. From the slope and intercept values of the above plot the value of K_1 was found to be 19.6 dm^3 mol^{-1} which is in good agreement with the literature value[4] (22 ± 3 dm^3 mol^{-1} at 25°C). The high rate of oxidation of benzyl alcohol could be due to resonance stabilization of positive charge produced in the transient intermediate resulting by the loss of hydrogen as hydride ion[5]. The rate of oxidation of allyl alcohol is very high compared to the corresponding saturated alcohol, viz., *n*-propanol. Incidentally the product of oxidation of allyl alcohol was identified as glycerol. This may be attributed to specificity of OsO_4 in attacking the double bond in preference to OH^- of allyl alcohol as OsO_4 is known to be a good hydroxylating agent. Under identical conditions ($[Os(VIII)] = 3.16 \times 10^{-4}$ mol dm^{-3}; $[OH^-] = 5.0 \times 10^{-2}$ mol dm^{-3}; temp = 303 K) the rate of oxidation of glycerol by OsO_4 (0.38 dm^3 mol^{-1}) was very much less than that of allyl alcohl (3.23 dm^3 mol^{-1}). Taft's plot (log k'' versus σ^*) is linear ($r = 0.983$) with a slope of $\rho^* = -1.91$ (Fig. 2C). The negative ρ^*-value also supports the hydride ion transfer mechanism. Such a large negative ρ^*-value was also observed by earlier workers during the oxidation of alcohols by different oxidants[6].

To substantiate the hydride ion transfer mechanism proposed, oxidation of a series of 1,2-diols by Os(VIII) was also carried out. The kinetic features of 1,2-diol oxidation are same as those of monohydric alcohols. It is now well established that during oxidation of diols by different oxidants formation of a complex between the diol and oxidant is a prerequisite and the products of oxidation, viz., carbonyl compounds are formed via a C – C bond fission. In the present study a clear first order dependence each in [diol] and $[OsO_4]$ and constancy in the λ_{max} of OsO_4 in the presence of diol clearly indicates absence of complex formation. Also the product of oxidation was identified as the corresponding glyoxal. In view of this a probable mechanism involving C – H bond fission in the slow step and loss of hydrogen as hydride ion is proposed (Scheme 2).

According to Scheme 2 the order of reactivity of different diols should be 1,2-ethanediol < 1,2-propanediol < 1,2-butanediol < 1,2-pentanediol < 1,2-hexanediol. This in fact was observed in the present study supporting the hydride ion abstraction mechanism.

The oxidation of α-hydroxy acids by different one- and two-equivalent oxidants is known to proceed either by C – H bond cleavage to give keto acids or C – C bond cleavage to give CO_2 and corresponding carbonyl compounds[7]. In the present study the products were identified as corresponding keto acids indicating C – H bond fission. The hydroxy acids studied are glycollic, lactic and

Table 2—Second Order Rate Constants and Activation Parameters for Oxidation of Hydroxy Compounds by Os(VIII) in Alkaline Medium

$[Os(VIII)] = 3.16 \times 10^{-4}$ mol dm^{-3}; $[OH^-] = 5.00 \times 10^{-2}$ mol dm^{-3}; temp = 305 K

Substrate	$k'' \times 10^3$ (dm^3 mol^{-1} s^{-1})	E_{exp} (kJ mol^{-1})	$\Delta H^{\ddagger}$ (kJ mol^{-1})	$\Delta G^{\ddagger}$ (kJ mol^{-1})	$\Delta S^{\ddagger}$ (JK^{-1} mol^{-1})
Methanol	4.85	79.8	77.3	88.3	−36.1
Ethanol	51.2	63.8	61.3	82.4	−69.0
Chloroethanol	15.3	51.8	48.5	85.3	−120.8
n-propanol	54.8	68.4	65.8	82.1	−53.4
2-propanol	69.8	63.7	61.2	81.5	−66.7
n-butanol	102.3	76.6	74.0	80.6	−21.3
Isobutanol	83.4	63.8	61.3	81.2	−64.2
n-pentanol	95.9	76.8	74.2	80.7	−21.3
Allyl alcohol	3227	—	—	67.4	—
Benzyl alcohol	16100	—	—	63.5	—
1,2-Ethane diol	32.0	63.8	61.3	83.5	−72.8
1,2-Propane diol	167	73.7	71.1	79.3	−26.8
1,2-Butane diol	349	50.4	47.9	77.5	−97.0
1,2-Pentane diol	383	58.0	55.5	77.2	−71.2
1,2-Hexane diol	548	59.8	57.3	76.3	−62.3
Glycollic acid	119	56.3	53.8	80.0	−86.0
Lactic acid	205	52.3	49.8	78.8	−95.0
Mandelic acid	1279	—	—	74.2	—

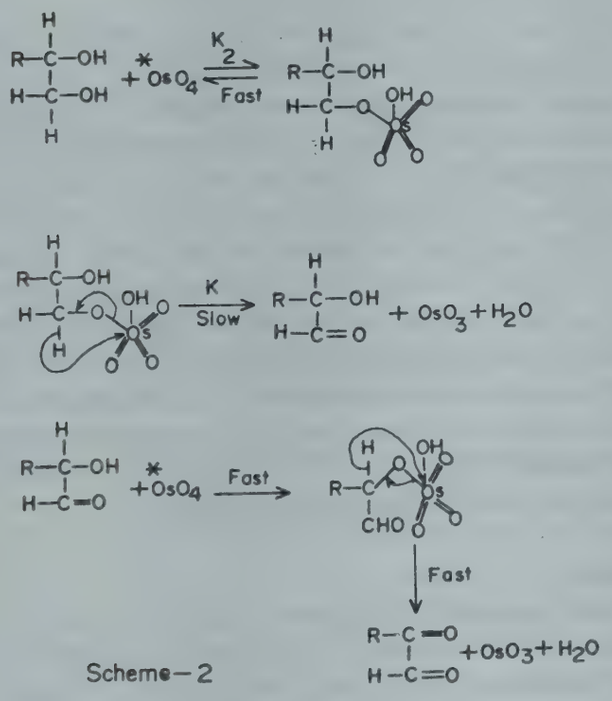

Scheme—2

mandelic and the order of reactivities is glycollic < lactic < mandelic acid. In this study also higher rate of oxidation of lactic acid in comparison to glycollic acid indicates that the electron releasing groups at α-carbon increases the rate of oxidation and vice versa. However, the higher rate of mandelic acid in comparison to lactic acid could be due to the resonance stabilization of the positive charge produced in the transient intermediate as in the case of benzyl alcohol.

The activation parameters calculated for all the substrates are recorded in Table 2. The negative $\Delta S^{\ddagger}$ value indicates formation of transition state with high degree of solvation due to the increased polarity as a result of loss of hydrogen as hybride ion.

Acknowledgement

One of the authors (P V S) is thankful to CSIR, New Delhi for the award of senior research fellowship.

References

1 Veera Somaiah P, Bal Reddy K, Sethuram B & Navaneeth Rao T, *Indian J Chem*, **26A** (1987) 402.

2 Feigl F, *Spot tests in organic analysis* (Elsevier) (1960) 416, 441, 484.

3 Sauerbaum R D & Sandell E B, *J Am chem Soc*, **75** (1953) 4170; Griffith W P, *Quart Rev*, **19** (1965) 254; Couon F A & Wilkinson G, *Advanced inorganic Chemistry* (Wiley Eastern, New Delhi) 1966, p. 153.

4 Latika Butt, Prem Dutt Sharma & Gupta Y K, *Indian J Chem*, **23A** (1984) 560.

5 Bal Reddy K, Sethuram B & Navaneeth Rao T, *Bull Soc Chim Belg*, **90** (1981) 1017.

6 Radhakrishnamurthy P S & Sarangi L D, *Indian J Chem*, **20A** (1981) 301; Mukherji J & Banerji K K, *Indian J Chem*, **20A** (1981) 394; Seema Kothari, Anupama Agarwal & Banerji K K, *Indian J Chem*, **25A** (1986) 722.

7 Levesly P & Waters W A, *J chem Soc*, **217** (1955); Banerji K K, *J chem res*, (5) (1978) 193, (1978) (M) 2561; Bishnoi M L, Negi S C & Banerji K K, *Indian J Chem*, **25A** (1986) 664.

Indian Journal of Chemistry
Vol. 27A, October 1988, pp. 880-882

Kinetics & Mechanism of Oxidation of Unsaturated Alcohols by Chloramine-T in Sulphuric Acid Medium

H M K NAIDU, S N KATGERI & D S MAHADEVAPPA*
Department of Studies in Chemistry, University of Mysore, Manasagangotri, Mysore 570 006, India

Received 7 *December* 1987; *revised and accepted* 12 *February* 1988

The kinetics of oxidation of allyl, crotyl and cinnamic alcohols by chloramine-T (CAT) in H_2SO_4 leads to a simple rate law, $k[CAT][H^+]^{-1}$ at 40°C. Added sulphate ions catalyze the reaction. An order dependence of -0.3 on the gross $[H_2SO_4]$ is noticed, indicating a mixed order kinetics with simultaneous catalysis by H^+ and SO_4^{2-} ions. Ionic strength and added reaction product (*p*-toluenesulphonamide) have no effect on the rate. A suitable mechanism is proposed.

During our investigation[1] on the oxidation of organic compounds by chloramine-T (CAT) in the presence of H_2SO_4, simultaneous catalysis by H^+ and SO_4^{2-} ions was observed. The title work was undertaken with a view to finding out whether similar catalysis occurs in the oxidation of conjugated alcohols, namely, allyl, crotyl and cinnamyl alcohols by the N-haloamine in sulphuric acid medium.

Materials and Methods

The unsaturated alcohols (BDH) were purified by distillation and their purity was checked. Doubly distilled water was used to prepare stock solutions of allyl and crotyl alcohols while ethanol was used as a solvent for cinnamyl alcohol. Chloramine-T (CAT, E. Merck) was purified and its aqueous solution was standardised by iodometry. All other chemicals used were of AR grade.

Kinetic studies

Requisite amounts of alcohol, H_2SO_4, $NaClO_4$ (to maintain ionic strength at 1.0 mol dm^{-3}) and water (to maintain total volume constant for all runs and to make ethanol content 30% (v/v) in the case of cinnamyl alcohol) were thermostated at 40°C. A measured amount of CAT solution, also thermostated at 40°C, was added rapidly to the mixture and the progress of the reaction was followed by the iodometric estimation of unconsumed CAT in a measured aliquot of the reaction mixture withdrawn at regular time intervals. The pseudo-first order constant (k') was calculated from the plot of log[CAT] versus time and was reproducible within ± 5%.

Stoichiometry

Investigations using varying amounts of alcohol and CAT, mixed in the presence of H_2SO_4 (0.02 to 2.0 mol dm^{-1}) at 40°C and the reaction mixture kept for 24 hr showed that one mol of unsaturated alcohol consumed one mol of CAT in accordance with Eq. (1).

$$TsNCl^- + RCH=CHCH_2OH + H^+ + H_2O \rightarrow TsNH_2 + RCH(Cl)CH(OH)CH_2OH \quad \ldots (1)$$

where R = −H for allyl, $-CH_3$ for crotyl, $-C_2H_5$ for cinnamyl and Ts = *p*-$CH_3C_6H_4SO_2$.

Paper chromatography was employed to identify the reaction product *p*-toluenesulphonamide ($MeC_6H_4SO_2NH_2$). Benzyl alcohol saturated with water was used as the solvent with 0.5% vanillin in 1% HCl solution in ethanol as the spray reagent ($R_f = 0.905$). To identify the chlorohydrin formed, the reaction mixture in the case of allyl alcohol was extracted with ether, the ethereal layer separated and the solvent was evaporated. The IR spectrum of residue was similar to that of the substrate, except for the absence of $\nu C=C$ at 1650 cm^{-1} indicating saturation of C=C bond in the product.

Results

With [substrate] in large excess, plots of log [CAT] versus time at different [CAT] are linear indicating first order dependence in $[CAT]_0$ (Table 1). Values of k' are found to be independent of $[alcohol]_0$ indicating zero order in [alcohol]. The rate decreases with increase in $[H_2SO_4]$ (Table 2) and plots of log k' versus log $[H_2SO_4]$ are linear with slopes around -0.3. Addition of SO_4^{2-} ions in the form of Na_2SO_4 at constant $[H_2SO_4]$, (0.5 mol dm^{-3}) increases the rate (Table 2) and plots of log k' versus log $[SO_4^{2-}]$ are linear with slopes ~ 0.6. However, variation of $[H^+]$ at constant $[SO_4^{2-}]$ (kept at 0.5 mol dm^{-3}), indicated an inverse first order dependence in $[H^+]$ in all the cases (Table 3) as shown by the constancy of $k'[H^+]$ values and also by plots of log k' versus log $[H^+]$, which had unit negative slopes. Addition of bisulph-

ate ion ($NaHSO_4$) retards the reaction slightly. However, the rate is not affected by increasing the ionic strength (I) from 1.0 mol dm^{-3} to 2.0 mol dm^{-3} or by the addition of the reaction product, *p*-toluenesulphonamide to the reaction mixture.

The rate decreases with increase in the dielectric constant (by increasing EtOH content in reaction medium) and a plot of log k' versus $1/D$ is linear with a negative slope in all the three cases. The thermodynamic parameters have been evaluated and are listed in Table 4.

Table 1—Effect of Concentration of Reactants on Reaction Rates

$[H_2SO_4] = 0.05$ mol dm^{-3} for allyl and crotyl alcohols and 0.01 mol dm^{-3} for cinnamyl alcohol: $I = 1.0$ mol dm^{-3}; temp. = 40 ± 0.1°C

10^3 [CAT]$_0$ (mol dm^{-3})	10^2 [alcohol] (mol dm^{-3})	$10^4 k'$ (s^{-1})		
		Allyl alcohol	Crotyl alcohol	Cinnamyl alcohol
1.0	5.0	2.83	3.49	0.89
2.0	5.0	2.79	3.47	0.89
3.0	5.0	2.75	3.43	0.88
4.0	5.0	2.75	3.43	0.88
5.0	5.0	2.76	3.41	0.88
5.0	2.5	2.71	3.45	0.82
5.0	10.0	2.76	3.45	0.86
5.0	15.0	2.79	3.48	0.88
5.0	30.0	2.79	3.50	0.85
5.0*	5.0	2.78	3.54	0.83
5.0†	5.0	2.73	3.31	0.80

*With $I = 2.0$ mol dm^{-3}
†In the presence of excess of *p*-toluenesulphonamide

Discussion

It is interesting to note that an unusual rate law (2) has been observed in

$$-\frac{d[CAT]}{dt} = k[CAT][H^+]^{-1} \quad \ldots (2)$$

Chloramine-T is a strong electrolyte and in the acidified solutions, the possible oxidizing species are dichloramine-T ($TsNCl_2$), protonated CAT (TsNHCl) and HOCl (refs 2-4). Recently Narayanan and Rao[5] have shown that under fairly high acidic conditions ($pH < 2$) TsNHCl can be further protonated to give $(TsNH_2Cl)^+$.

Table 2—Effect of Varying $[H_2SO_4]$ and $[SO_4^{2-}]$ on Rate of Oxidation

$[CAT]_0 = 0.005$ mol dm^{-3}; $[substrate]_0 = 0.05$ mol dm^{-1}; $I = 1.0$ mol dm^{-3}

10^3 $[H_2SO_4]$ or $[SO_4^{2-}]$ (mol dm^{-3})[a]	$10^4 k'$ (s^{-1})[b]					
	Allyl alcohol		Crotyl alcohol		Cinnamyl alcohol	
5.0 (2.0)*	2.76	(2.76)	3.41	(3.41)	0.88	(0.88)
10.0 (2.5)*	2.43	(4.19)	3.02	(4.93)	0.83	(1.01)
20.0 (5.0)*	1.97	(6.19)	2.33	(7.81)	0.66	(1.66)
30.0 (7.5)*	1.81	(7.98)	2.08	(10.27)	0.60	(2.09)
40.0 (10.0)*	1.68	(9.37)	1.98	(11.81)	0.56	(2.46)
50.0 —	—	(11.00)	—	(14.20)	—	—

[a] Starred values of concentration refer to cinnamyl alcohol
[b] Values in parentheses refer to concentrations of $[SO_4^{2-}]$ at $[H_2SO_4] = 0.05$ mol dm^{-3} for allyl and crotyl alcohols and $[H_2SO_4] = 0.01$ mol dm^{-3} for cinnamyl alcohol.

Table 3—Effect of Concentration of Hydrogen ions on Reaction at Constant [Sulphate]

$[CAT]_0 = 0.005$ mol dm^{-3}; $[substrate]_0 = 0.05$ mol dm^{-3}; $I = 1.0$ mol dm^{-3}; temp. = 40 ± 0.1°C
$[SO_4^{2-}] = 0.05$ mol dm^{-3} for allyl and crotyl alcohols and 0.01 mol dm^{-3} for cinnamyl alcohol.

10^2 $[H^+]$ (mol dm^{-3})	Allyl alcohol		Crotyl alcohol		Cinnamyl alcohol	
	$10^4 k'$ (s^{-1})	$k'[H^+]\,10^5$	$10^4 k'$ (s^{-1})	$k'[H^+]\,10^5$	$10^4 k'$ (s^{-1})	$k'[H^+]\,10^5$
10.0 (2.0)	11.00	11.0	14.20	14.20	2.46	0.49
20.0 (2.5)	5.58	11.16	7.08	14.06	1.95	0.49
30.0 (5.0)	3.68	11.04	4.74	14.22	0.96	0.48
40.0 (7.5)	2.80	11.20	3.57	14.28	0.63	0.48
50.0 (10.0)	2.19	10.95	2.86	14.20	0.49	0.49

Table 4—Thermodynamic Parameters for Oxidation of Unsaturated Alcohols by Chloramine-T in Sulphuric Acid Medium

Parameters	Allyl alcohol	Crotyl alcohol	Cinnamyl alcohol
E_a (kJ mol^{-1})	53.10	54.63	54.72
$\Delta H^{\ddagger}$ (kJ mol^{-1})	53.98 ± 0.02	52.00 ± 0.02	52.08 ± 0.01
A (mol dm^{-3} s^{-1})	$1.99 \pm 0.01 \times 10^4$	$4.13 \pm 0.01 \times 10^4$	$7.6 \pm 0.02 \times 10^3$
$\Delta S^{\ddagger}$ (JK^{-1} mol^{-1})	− 166.30 ± 0.03	− 160.30 ± 0.01	− 174.6 ± 0.02
$\Delta G^{\ddagger}$ (kJ mol^{-1})	106.0 ± 0.01	102.3 ± 0.01	106.7 ± 0.01

If $TsNCl_2$ were to be the active species, then the rate law predicts a second order dependence in $[CAT]_0$ which is contrary to experimental observations. It is likely that HOCl is involved as the active species and the oxidation of conjugated alcohols occurs in a fast step by the saturation of double bond. Scheme 1 could account for the experimental observations:

$$(TsNH_2Cl)^+ \underset{\text{fast}}{\overset{K_1}{\rightleftharpoons}} TsNHCl + H^+ \quad \ldots (i)$$

$$TsNHCl + H_2O \xrightarrow[\text{slow}]{k_2} TsNH_2 + HOCl \quad \ldots (ii)$$

$$HOCl + \text{alcohol} \xrightarrow[\text{fast}]{k_3} \text{Products} \quad \ldots (iii)$$

Scheme 1

From Scheme 1, rate law (3) could be derived as

$$-\frac{d[CAT]}{dt} = \frac{k_2K_1[CAT][H_2O]}{K_1 + [H^+]} \quad \ldots (3)$$

Protonation constant of RNHCl has been measured by Narayanan and Rao[5] by a radiotracer technique and a value of 103 $dm^3\ mol^{-1}$ has been reported. Although the protonation constant could be lower[6], in the present case it leads to a value of 9.7×10^{-3} for K_1. Hence, the inequality $K_1 < [H^+]$, can be justified and rate law (3) can be modified to Eq. (4).

$$-\frac{d[CAT]}{dt} = k_2K_1[CAT]_t[H^+]^{-1} \quad \ldots (4)$$

Rate law (4) is in agreement with experimental results ($k_2' = k_2[H_2O]$). The proposed mechanism is supported by the moderate values of E_a and the fairly high negative $\Delta S^{\ddagger}$. Further, the constancy of $\Delta G^{\ddagger}$ values indicate that an identical mechanism is operative in the oxidation of allyl, crotyl and cinnamyl alcohols by CAT. The solvent effect supports the involvement of two dipoles in the rate-limiting step. The catalytic influence of sulphate ions can be rationalised by Scheme 2:

$$(TsNH_2Cl)^+ \underset{\text{fast}}{\overset{K_1}{\rightleftharpoons}} TsNHCl + H^+ \quad \ldots (i)$$

$$TsNHCl + SO_4^{2-} \underset{\text{fast}}{\overset{K_4}{\rightleftharpoons}} \underset{(X)}{TsNHCl \ldots -SO_4^{2-}} \quad \ldots (ii)$$

$$X + H_2O \xrightarrow[\text{slow}]{k_5} HOCl + TsNH_2 + SO_4^{2-} \quad \ldots (iii)$$

$$HOCl + \text{alcohol} \xrightarrow[\text{fast}]{k_6} \text{Products} \quad \ldots (iv)$$

Scheme 2

Scheme 2 leads to rate law (5):

$$-\frac{d[CAT]}{dt} = \frac{k_5K_1K_4[CAT]_t[SO_4^{2-}][H_2O]}{K_1 + [H^+] + K_1K_4[SO_4^{2-}]} \quad \ldots (5)$$

Since K_1 is small, i.e. $K_1 < [H^+]$ or $K_1K_4[SO_4^{2-}]$, rate law (5) can be transformed into Eqs (6) and (7)

$$-\frac{d[CAT]}{dt} = \frac{k_5K_1K_4[CAT]_t[SO_4^{2-}][H_2O]}{[H^+] + K_1K_4[SO_4^{2-}]} \quad \ldots (6)$$

$$\frac{1}{k} = \frac{[H^+]}{k_5K_1K_4[SO_4^{2-}][H_2O]} + \frac{1}{k_5[H_2O]} \quad \ldots (7)$$

A double reciprocal plot of k' versus $[SO_4^{2-}]$ is linear ($r > 0.9887$) and from the slope and intercept, K_4 values ($dm^3\ mol^{-1}$) have been calculated to be 53.0, 49.0 and 52.1 and 10^5 k_5 values ($dm^3\ mol^{-1}\ s^{-1}$) as 2.38, 3.07 and 1.10 for allyl, crotyl and cinnamyl alcohols respectively. In these calculations $K_1 = 9.7 \times 10^{-3}$ and $[H_2O] = 55.56$.

The decrease in rate by the addition of bisulphate ion is due to a mass law effect on the dissociation of H_2SO_4.

Acknowledgement

One of the authors (SNK) is grateful to the UGC, New Delhi for the award of a fellowship under the Faculty Improvement Programme.

References

1 Yamuna B, Naidu H M K & Mahadevappa D S, *Indian J Chem*, (In Press).
2 Pryde B G & Soper F G, *J chem Soc*, (1931) 1514.
3 Bishop E & Jennings V J, *Talanta*, **1** (1958) 197.
4 Morris J C, Salazar J A & Wineman M A, *J Am chem Soc*, **70** (1948) 2036.
5 Narayanan S S & Rao V R S, *Radiochim Acta*, **32** (1983) 211.
6 Gupta Y K (Private communication).

Indian Journal of Chemistry
Vol. 27A, October 1988, pp. 883-885

Kinetics of Chromium(VI) Oxidation of DMSO in Aqueous Acetic Acid

(Miss) S KAMPLI, S T NANDIBEWOOR & J R RAJU*
Department of Chemistry, Karnatak University, Dharwad 580 003
Received 30 *July* 1987; *revised* 27 *January* 1988; *accepted* 27 *February* 1988

Oxidation of DMSO by Cr(VI) in aqueous acetic acid in the presence of 1.4 mol dm^{-3} perchloric acid is first order each in [Cr(VI)] and [DMSO] and second order in $[H^+]$. Intervention of Cr(IV) and free radicals is shown in experiments in the presence of added Mn(II) and added acrylamide respectively. Added chloride ions inhibit the oxidation. A mechanism in agreement with experimental data has been proposed.

The kinetics and mechanism of oxidation of dimethyl sulphoxide (DMSO) by a variety of oxidants has been studied earlier[1-7]. However, details of oxidation of DMSO by Cr(VI) are not available. The oxidation of DMSO by Cr(VI) is slow in aqueous medium but facile and amenable to kinetic investigations in aq acetic acid. Herein we present the results of the title investigation.

Materials and Methods

DMSO (Baker, AR) was distilled over calcium hydride under reduced pressure[7]. Stock solutions of Cr(VI) were prepared by dissolving potassium dichromate (BDH, AR) in doubly distilled water. All other chemicals used were of reagent grade. Purified acetic acid was used.

Kinetic runs were followed under pseudo-first order conditions ([DMSO] ≫ [oxidant]) at constant temperature (± 0.05°). The reaction was initiated by the addition of Cr(VI) solution containing required amounts of $HClO_4$ and $NaClO_4$ (to maintain acidity and ionic strength) to DMSO solution. The reaction was followed upto 95% by measuring the absorbance of the unreacted Cr(VI) in solution at 360 nm as a function of time using matched quartz cells and a Bausch and Lomb Spectronic 2000 spectrophotometer. Chromium(VI) obeys Beer's law at 360 nm in the [Cr(VI)] range of 5.0×10^{-4} to 2.25×10^{-3} mol dm^{-3} with $\varepsilon = 914$ (± 1.5%). Rate constants were reproducible within ± 3%.

Results

The reaction products were found to be Cr(III) and dimethyl sulphone. The latter was isolated and identified by spot test, m.p. 108° (lit. m.p. 109°).

At fixed [DMSO] (0.10 mol dm^{-3}), [perchloric acid] (1.4 mol dm^{-3}), ionic strength (2.0 mol dm^{-3}) and temp. (26.5°C), the order in Cr(VI) in the concentration range of 2.0×10^{-4} to 1.2×10^{-3} mol dm^{-3} was unity, the log [Cr(VI)] versus time plots being linear over 90% of reaction. The pseudo-first order rate constants slightly decreased with increase in [Cr(VI)], presumably because of the monomer-dimer equilibrium of the latter[8], the monomer being more active. The monomer concentrations were calculated using the reported dimerisation constant of 98 in water because of nonavailability of reliable data in 50% aqueous acetic acid medium in which the extent of dimerisation may be expected to be higher. When such calculated concentrations of monomer ($HCrO_4^-$) were used to calculate the rate constant, k_{corr} ($= k$[Cr(VI)]/$[HCrO_4^-]$), the latter showed better agreement. The order in DMSO in the concentration range of 2.0×10^{-2} to 24×10^{-2} mol dm^{-3} was one under the same conditions as above at fixed [Cr(VI)] of 1.0×10^{-3} mol dm^{-3} (Table 1). The order in $[H^+]$ under similar conditions was two in $[HClO_4]$ range of 0.20 to 1.98 mol dm^{-3}.

There was no significant effect of initial presence of Cr(III) (0 to 1.0×10^{-2} mol dm^{-3}) on the rate constant of the reaction. Under the conditions mentioned above at [Cr(VI)] = 1.0×10^{-3} mol dm^{-3}, $10^3 k$ increased from 0.62 to 3.7 s^{-1} when % HOAc in the solvent was increased from 40 to 60% v/v. The log k versus 1/D plot was linear with positive slope.

In the presence of added manganese(II) sulphate, the values of $k \times 10^3$ decreased by one-half from 1.4 to 0.7 s^{-1} as 10^4[Mn(II)] increased from 0 to 1.0 mol dm^{-3} and remained constant with further increase in Mn(II). These results parallel those found in the case of the Cr(VI) oxidation of propane-2-ol in aqueous acetic acid[9]. Under the conditions employed in the present case, the appearance of a brown colour indicates the formation of manganese dioxide, which, however, could not be quantitatively estimated owing to extremely low concentration. When the reaction was carried out in 50% aq. acetic acid under the conditions: [Cr(VI)] = 1.0×10^{-2}; [DMSO] = 0.60; $[H^+]$ = 1.0 and [Mn(II)] = 5.0×10^{-3} mol dm^{-3} where reasonable amounts of manganese dioxide was

Table 1—Effect of Varying [Cr(VI)] and [DMSO] in Chromium(VI)-DMSO Reaction in 50% Aqueous Acetic Acid

$[H^+] = 1.40$ mol dm^{-3}; $\mu = 2.0$ mol dm^{-3}; temp. 26.5°C

$[Cr(VI)] \times 10^3$ (mol dm^{-3})	$[HCrO_4^-] \times 10^3$ (mol dm^{-3})	$k \times 10^3$ (s^{-1})	$k_{corr} \times 10^3$ (s^{-1})	$[DMSO] \times 10^2$ (mol dm^{-3})	$k \times 10^3$ (s^{-1})	$k \times 10^3$[DMSO] (mol^{-1}dm^{3}s^{-1})
[DMSO] = 0.10 mol dm^{-3}				[Cr(VI)] = 1.0×10^{-3} mol dm^{-3}		
				2.0	0.25	0.13
				6.0	0.70	0.12
0.20	0.19	1.5	1.6	8.0	1.0	0.13
0.50	0.43	1.6	1.9	10.0	1.4	0.14
0.80	0.64	1.5	1.9	14.0	2.3	0.16
1.0	0.77	1.4	1.8	20.0	3.1	0.17
1.2	0.89	1.4	1.9	20.0	3.6	0.18
				24.0	4.4	0.18

formed after allowing the reaction for about 14 hr, the Mn(IV) was identifiable by sodium bismuthate test[10].

At pH = 2, the reaction between Cr(VI) and iodide ions was very slow while Cr(V)-iodide reaction was fast[11]. Hence, addition of potassium iodide to the reaction at pH = 2.0 to test for Cr(V) as has been attempted elsewhere[11] did not yield iodine to any significant extent presumably because the reaction leading to Cr(V) formation, namely, the first oxidation step of DMSO by Cr(VI), did not occur to any significant proportion. Hence, this approach was not persued further.

When the reaction mixture containing acrylamide was kept over 24 hr and diluted with methanol, no precipitate appeared at higher $[HClO_4]$ (~ 1.4 mol dm^{-3}); however precipitate appeared at lower $[HClO_4]$ (~ 0.4 mol dm^{-3}) showing polymerisation. In the presence of added chloride ions, the Cr(VI) oxidation of DMSO was retarded probably due to formation[12] of $ClCrO_3^-$.

Discussion

Oxidation of DMSO by Cr(VI) in aqueous acetic acid is fourth order, first order each in [oxidant] and [substrate] and second order in $[H^+]$ as shown by Eq. (1). Chromium(III) and dimethyl sulphone are the only products formed and the reaction is not affected by initial addition of

$$-d[Cr(VI)]/dt = k[Cr(VI)][DMSO][H^+]^2 \quad \ldots(1)$$

products. Chromium(VI) oxidation of DMSO is non-complementary involving a three-equivalent oxidant and a two-equivalent reductant and may occur by the intervention of reactive Cr(IV) and Cr(V) species as well as free radicals. The intervention of Cr(IV) is evidenced by the progressive decrease in rate constant in the presence of increasing amounts of added Mn(II), the decrease reaching a limit of about one-half of the rate constant found in the absence of Mn(II). Such results have also been obtained in the case of Cr(VI) oxidation of propan-2-ol in aqueous acetic acid[9]. In the present case, intervention of Cr(V) has been ruled out because the tests in this regard are inconclusive. Nevertheless, the species may be involved in too low quantities to be detected or that the species is more reactive with the substrate as the latter elementary reaction is a complementary one. Evidence for free radical participation has also been found and hence the results may be accommodated by the mechanism shown in Scheme 1 where the protonation of the substrate may be expected in view of the fact that DMSO is a strong hydrogen acceptor and it may be an H-bonded H^+ like DMSO...$H-OH_2^+$ which is involved in protonation. This is followed by interaction with $HCrO_4^-$ leading to a substrate − Cr(VI) complex which, with acid, gives rise to one mol of sulphone and Cr(IV). Chromium(IV) oxidises a second molecule of DMSO in a one-equivalent step to give a free radical such as $(CH_3)_2.\dot{S}O_2$. Alkyl sulphonyl radicals such as $C_2H_5\dot{S}O_2$ ($g = 2.0049$) have been detected[13].

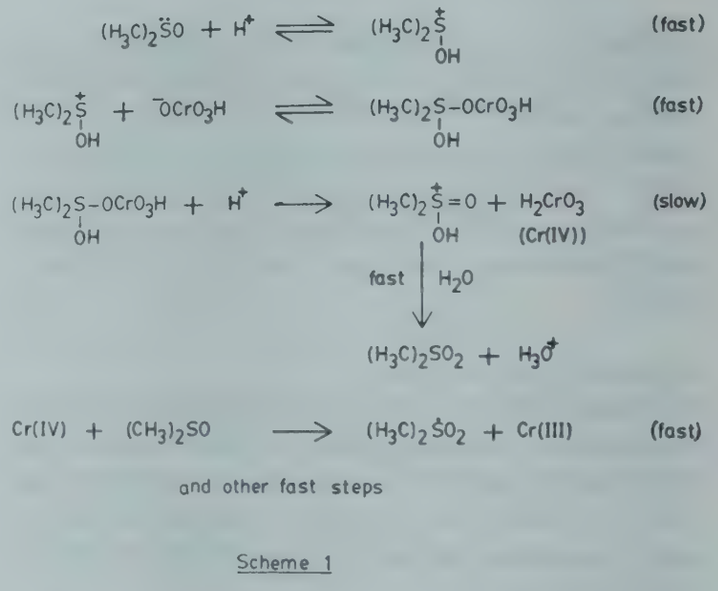

Scheme 1

Scheme 1 accounts for the data obtained and, in particular, for the second order in $[H^+]$. The two prior equilibria are expected to have very low equilibrium constants so that an almost integral order of two in

acidity results. The effect of polarity of the solvent on the reaction implies that the interaction between the reactants is attractive. The effect of added chloride ions on the reaction is due to the conversion of acid chromate ion ($HCrO_4^-$) into chrlorochromate ($ClCrO_3^-$) which has been shown to be a less potent oxidant[12] than the acid chromate ion.

References

1 Radhakrishnamurti P S & Padhi S C, *Curr Sci (India)*, **46** (1977) 517; **43** (1974) 715.

2 Pandey S M, Sharma J, Prakash O & Mushran S P, *Indian J chem*, **20A** (1981) 1021.

3 Mahadevappa D S, Mangegowda M B, Ananda S & Rangappa K S, *Indian J Chem*, **23A** (1984) 325.

4 Radhakrishnamurti P S & Sahu N S, *Indian J Chem*, **20A** (1981) 269.

5 Sambasiva R A & Narayana R J, *Indian J Chem*, **20A** (1981) 60.

6 Rangaswamy & Yathirajan H S, *Curr Sci (India)*, **50** (1981) 757.

7 Pratihari H K, Roy A K & Nayak P L, *J Indian chem Soc*, **53** (1976) 4.

8 Tong J Y & King E L, *J Am chem Soc*, **75** (1953) 6180.

9 Watanabe W & Westheimer F H, *J chem Phys*, **17** (1949) 61.

10 Hillebrand W E & Lundell G E F, *Applied inorganic analysis* (John Wiley, New York), 1929, p 346.

11 Krumpolc M & Rocek J, *J Am chem Soc*, **99** (1977) 137.

12 Cohen M & Westheimer F H, *J Am chem Soc*, **74** (1952) 4387.

13 Gilbert B C, Norman R C & Sealy R C, *J chem Soc Perkin II* (1975) 308.

Indian Journal of Chemistry
Vol. 27A, October 1988, pp. 886-888

Complexes of Copper(II) & Cobalt(II) with Ligands Derived from the Reactions of 1,2-Diphenyl-1-hydroxyiminoethane-2-one with 1,2-Diaminoethane & 1,3-Diaminopropane

H C RAI* & RAMESH KUMAR
Department of Chemistry, L S College, Muzaffarpur 842 001
S N VIDYARTHI
Department of Chemistry, Jadgam College, Chapra
and
BALMIKI SINGH
Department of Chemistry, Bihar University, Mazaffarpur 842 001

Received 25 *August* 1987; *revised and accepted* 8 *February* 1988

A number of complexes of the types $ML^{1,2}$ [M = Co(II), Cu(II)], $Co(H_2L^{1-2})X_2$ [X = Cl^-, Br^-, I^-, NO_3^-, ClO_4^-] and $Cu_2L^{1-2}X_2$ (X = Cl^-, Br^-, ClO_4^-, NO_3^-) where H_2L^1 = bis-(1,2-diphenyl-1-hydroxyimino-2-ethylidine)-1,2-diaminoethane and H_2L^2 = bis-(1,2-diphenyl-1-hydroxyimino-2-ethylidine)-1,3-diaminopropane have been synthesized and characterized on the basis of their elemental analyses, magnetic moment, infrared, electronic and ESR spectral data.

Metal complexes with oximes and imine-oximes have received much attention during recent years[1-7] as the bis complexes with copper(II), nickel(II) and cobalt(II) and tris complexes with iron(II), iron(III) and cobalt(III) have been found to be excellent ligands capable of coordinating further through unused oxygen donor atoms to give homo and hetero polynuclear encapsulation and macrocyclic metal complexes.

In continuation of earlier work in the field[5], we report here isolation and characterization of eleven complexes each of bis-(1,2-diphenyl-1-hydroxyimino-2-ethylidine)-1,2-diaminoethane and bis-(1, 2-diphenyl-1-hydroxyimino-2-ethylidine)-1, 3-diaminopropane (hereafter referred to as H_2L^1 and H_2L^2) with different metal ions.

Materials and Methods

All the chemicals used were BDH reagents except 1,3-diaminopropane which was of Loba make.

Preparation of the complexes

The complexes with both the ligands were prepared under similar experimental conditions. A representative procedure for each category is described.

CuL^1: 1,2-Diphenyl-1-hydroxyiminoethane-2-one (2.25 g, 0.01 mol) was taken in absolute ethanol and gently warmed. To this solution, cupric acetate monohydrate (1.00 g, 0.005 mol) was added when colour of the solution turned grey. An ethanolic solution of 1,2-diaminoethane (0.3 g, 0.005 mol) was added to it with constant shaking and the mixture was heated on a water-bath. A greyish green precipitate formed slowly on standing. It was filtered, washed with ethanol and ether.

$Cu_2L^1X_2$ ($X = Cl^-$, Br^-, ClO_4^- or NO_3^-): To a suspension of bis-(1,2-diphenyl-1-hydroxyimino-2-ethylidine)-1,2-diaminoethane copper(II) (2.92 g, 0.005 mol) in absolute ethanol, a hot ethanolic solution of cupric chloride dihydrate (0.85 g, 0.005 mol) was added with constant stirring. A clear green coloured solution so obtained was refluxed for half an hour. A dark green crystalline solid was obtained when the solution was allowed to stand overnight. It was filtered, washed with small quantities of ethanol and ether and dried *in vacuo*.

$Co(H_2L^2)Cl_2$: To an ethanolic solution of cobalt(II) chloride hexahydrate (2.38 g, 0.01 mol), a hot ethanolic solution of 1,2-diphenyl-1-hydroxyiminoethane-2-one (2.25 g, 0.01 mol) was added followed by the addition of an ethanolic solution of 1,3-diaminopropane (0.37 g, 0.005 mol) with vigorous shaking. The light violet crystals which separated on standing were filtered, washed with ethanol and ether and dried *in vacuo*.

The compounds were analysed by the standard procedure[8]. Magnetic moments were determined by Gouy method using $Hg[Co(NCS)_4]$ as the calibrant. The analytical data and colour are recorded in Table 1. Relevant bands in electronic spectra and the magnetic moments (μ_{eff}) values at room temperature are recorded in Table 2.

Table 1—Analytical Data and Colours of Complexes

Compound	Colour	Found (Calc.), % Metal	N	Halogen
CuL^1	Green	11.76 (11.86)	10.50 (10.45)	
CoL^1	Dark brown	11.21 (11.09)	10.52 (10.54)	
$Cu_2L^1Cl_2$	Green	19.20 (18.96)	8.52 (8.35)	10.46 (10.58)
$Cu_2L^1Br_2$	Greyish green	16.94 (16.74)	7.27 (7.37)	21.00 (21.05)
$Cu_2L^1(NO_3)_2$	Green	18.86 (17.57)	11.51 (11.61)	
$Cu_2L^1(ClO_4)_2$	Greyish green	16.09 (15.92)	6.97 (7.01)	
$Co(H_2L^1)Cl_2$	Light violet	9.75 (9.75)	9.31 (9.27)	11.75 (11.74)
$Co(H_2L^1)Br_2$	Pink	8.75 (8.50)	8.00 (8.08)	23.15 (23.06)
$Co(H_2L^1)I_2$	Blue	7.57 (7.49)	7.02 (7.11)	32.17 (32.26)
$Co(H_2L^1)(NO_3)_2$	Red	9.05 (8.97)	12.51 (12.78)	
$Co(H_2L^1)(ClO_4)_2$	Red	8.29 (8.05)	7.58 (7.68)	
CuL^2	Yellowish green	11.41 (11.54)	10.30 (10.18)	
CoL^2	Dark brown	11.62 (10.82)	13.04 (10.27)	
$Cu_2L^2Cl_2$	Yellowish green	18.99 (18.56)	8.59 (8.18)	10.12 (10.38)
$Cu_2L^2Br_2$	Brownish green	16.60 (16.01)		23.01 (22.69)
$Cu_2L^2(NO_3)_2$	Green	16.99 (16.77)	10.90 (11.09)	
$Cu_2L^2(ClO_4)_2$	Deep green	15.26 (15.64)	6.60 (6.89)	
$Co(H_2L^2)Cl_2$	Light violet	9.42 (9.55)	9.21 (9.06)	11.35 (11.48)
$Co(H_2L^2)Br_2$	Pink	8.42 (8.11)	7.78 (7.70)	24.62 (24.75)
$Co(H_2L^2)I_2$	Blue	7.28 (7.18)	6.92 (6.82)	31.56 (30.93)
$Co(H_2L^2)(NO_3)_2$	Red	9.22 (8.83)	12.52 (12.15)	
$Co(H_2L^2)(ClO_4)_2$	Pink	7.58 (7.90)	7.92 (7.50)	

Table 2—Electronic Spectral Bands (cm^{-1}) and Magnetic Moment Values of Co(II) and Cu(II) Complexes

Co(II) complexes	$^4T_{1g}(P) \leftarrow {}^4T_{1g}(F)$	$\mu_{eff.}$ (B.M.)
$Co(H_2L^1)Cl_2$	16,800	5.10
$Co(H_2L^1)Br_2$	16,700	5.15
$Co(H_2L^1)I_2$	16,100	5.00
$Co(H_2L^1)(NO_3)_2$	17,300	5.20
$Co(H_2L^1)(ClO_4)_2$	17,500	5.15
$Co(H_2L^2)Cl_2$	16,000	5.10
$Co(H_2L^2)Br_2$	16,100	5.14
$Co(H_2L^2)I_2$	15,200	5.20
$Co(H_2L^2)(NO_3)_2$	16,100	5.16
$Co(H_2L^2)(ClO_4)_2$	15,800	5.20
	$^2B_{1g} \leftarrow {}^2A_{1g}$	
CoL^1	21,000	2.00
CoL^2	21,000	2.00

Cu(II) complexes	Chromophore CuO_2X_2	CuN_4	
CuL^1	—	14,000	1.10
CuL^2	—	14,000	1.12
$Cu_2L^1Cl_2$	12,500	17,100	1.85
$Cu_2L^1Br_2$	12,300	17,300	1.80
$Cu_2L^1(NO_3)_2$	12,700	17,200	1.80
$Cu_2L^1(ClO_4)_2$	12,400	17,400	1.85
$Cu_2L^2Cl_2$	12,300	17,000	1.80
$Cu_2L^2Br_2$	12,000	17,500	1.90
$Cu_2L^2(NO_3)_2$	12,700	17,400	1.75
$Cu_2L^2(ClO_4)_2$	12,500	17,000	1.80

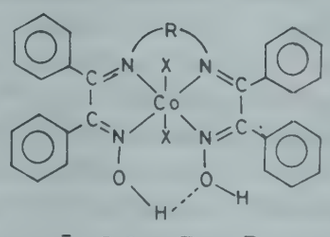

X = Cl^-, Br^-, I^-, NO_3^-, ClO_4^-

R = as in structure-2

STRUCTURE-1

Results and Discussion

The complexes of the type, $Co(H_2L^{1-2})X_2$ show a strong IR band centered at 3400 cm^{-1} assignable to νOH mode of the N−O−H groups (intramolecularly hydrogen bonded) indicating neutral form of the ligands in these complexes. A medium intensity band at 1700 cm^{-1} is observed for $Co(H_2L^{1-2})X_2$ complexes (structure 1), but it is absent in the spectra of the complexes of the types ML^{1-2} and $Cu_2L^{1-2}X_2$ indicating the band to be due to N−O−H deformation[1-4]. The azomethine and oxime C=N group stretching vibrations appearing at 1635 and 1450 cm^{-1} in the spectrum of the ligand H_2L^1 and at 1630 and 1475 cm^{-1} in that of the ligand H_2L^2 respectively are most perturbed on complexation ($\Delta\nu$ = 10-20 cm^{-1}). The IR bands due to phenyl ring systems of the ligand found at 1590, 1570, 1500 and 1442 cm^{-1} are almost unaffected in the metal complexes.

For ML^{1-2} complexes, the high frequency νC−N bands are shifted to a lower frequency region and the low frequency νC−N bands suffer a blue-shift which can be attributed to the variation in electronic environment due to coordination with metal ions (structure 2).

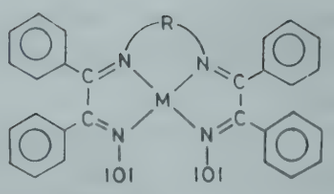

R = -$(CH_2)_2$-, $(CH_2)_3$-

M = Cu(II), Co(II)

STRUCTURE-2

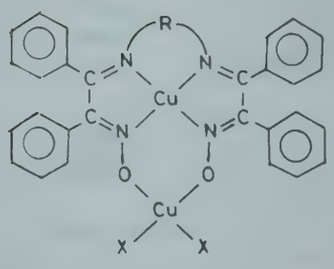

X = Cl^-, Br^-, NO_3^-, ClO_4^-

R = as in structure-1

STRUCTURE-3

For $Cu_2L^{1-2}X_2$ (X = Cl^-, Br^-) complexes, one band is observed in low frequency region (450-200 cm^{-1}), viz., at 420 cm^{-1} for Cu_2LCl_2 and at 318 cm^{-1} for $Cu_2L^{1-2}Br_2$ which could be assigned to terminal νCu − X mode. Three distinct IR bands appear in the region 1100-900 cm^{-1} for the ligands and the complexes; the middle one of these is assigned to νN − O. In both the ligands, this band appears at 1010 cm^{-1} and is shifted to the region 1120-1090 cm^{-1} in the complexes $Co(H_2L^{1-2})X_2$ and ML^{1-2}. For the complexes $Cu_2L^{1-2}X_2$, this band occur at a lower frequency (1040-1000 cm^{-1}) in comparison to that in the spectra of the complexes ML^{1-2}. The lowering most probably arise[5] due to the formation of new links between the copper(II) inner complexes CuL^{1-2} and copper(II) salts CuX_2 as shown in structure 3.

Magnetic moment and electronic spectra

The binuclear $Cu_2L^{1-2}X_2$ complexes show μ_{eff} values of 1.7 to 1.9 B.M. per copper atom, having the ground term ^2D. The electronic spectra of the complexes have been studied in the ligand field region 10,000-25,000 cm^{-1} (Table 2). The spectra of Cu(II) complexes show two broad bands in the regions 10,500-13,000 and 17,000-19,500 cm^{-1}. It would be reasonable to say that the high frequency band arises from the chromophore CuN_4 in D_{4h} symmetry and the low frequency band originates from the chromophore CuO_2X_2 under a lower symmetry such as C_2.

The ESR spectra of the binuclear Cu(II) complexes recorded at RSIC, IIT, Madras show one line and the anisotropy of the *g*-tensors is well resolved. The $g_\perp$ and $g_\parallel$ values are 2.256 and 2.039 respectively at room temperature. These values closely agree with those of the binuclear copper(II) complexes reported earlier[9].

A single broad band centered at 14,000 cm^{-1} is observed for the complexes CuL^{1-2} having the CuN_4 geometry. The broad band which shows considerable structure, represents two or three superimposed absorptions. The band is comparable, both in position and width, with those of the earlier reported planar copper(II) complexes and leads us to beleive that both the inner complexes of copper(II) are essentially square-planar.

$Co(H_2L^{1-2})X_2$ complexes have $\mu_{eff.}$ values in the range 4.9-5.2 B.M. and exhibit a multiplet band structure in the region 16,000 to 19,000 cm^{-1}. The band width, spreading over 3,000 cm^{-1}, suggests an octahedral environment around cobalt(II) ion in these complexes. The cobalt(II) inner complexes are of low-spin type possessing magnetic moments of ~ 2.0 B.M. The spectra show a broad band at 20,000-22,000 cm^{-1} with some amount of structure which manifests that cobalt(II) ion is placed in a square-planar ligand field. However, high intensities of these bands arise probably due to charge-transfer transition.

Acknowledgement

The authors express their gratitude to the UGC, New Delhi for the award of a Teacher Fellowship to one of them (Ramesh Kumar), to CDRI, Lucknow for infrared spectra and analytical data and to RSIC, IIT, Madras for ESR spectra.

References

1 King R B, *Progr inorg Chem*, **15** (1972) 287.
2 Mahapatra B K & Sahoo B, *Indian J Chem*, **24A** (1985) 653.
3 Chakrabarti J & Sahoo B, *Indian J Chem*, **21A** (1982) 48.
4 West B O in *New pathways in inorganic Chemistry*, Edited by E A V Ebsworth, A G Maddock and A G Sharpe, (Cambridge University Press, London) 1968, 303.
5 Rai H C, Chakrabarti J & Sahoo B, *Indian J Chem*, **18A** (1979) 242.
6 Rai H C, Jena A K & Sahoo B, *Inorg chim Acta*, **35** (1979) 29.
7 Sahoo Bhagirathi, Chakrabarti J & Sahoo B, *Indian J Chem*, **23A** (1984) 209.
8 Vogel A I, *A text book of quantitative inorganic analysis* (Longmans, London), 1961, pp 258, 389, 391, 479, 574.
9 Doedens R J, *Progr inorg Chem*, **21** (1976) 209.

Indian Journal of Chemistry
Vol. 27A, October 1988, pp. 889-892

Determination of Dissociation Constants of Salicylidene-2-aminobenzothiazole & *p*-Hydroxybenzylidene-2-aminobenzothiazole in Different Surfactant Systems

(Miss) P K MISHRA, B K MISHRA & G B BEHERA*
Centre of Studies in Surface Sciences and Technology,
Department of Chemistry, Sambalpur University, Jyoti Vihar 768019

Received 27 *July* 1987; *revised and accepted* 8 *January* 1988

The critical micellar concentrations of a number of nonionic surfactants have been determined by dye incorporation method. The *pK* of salicylidene-2-aminobenzothiazole and *p*-hydroxybenzylidene-2-aminobenzothiazole have been determined in different surfactant systems. The shift of *pK* has been attributed to a difference of surface charge of the micelle. The sensitivity of both the schiff bases as indicator, has been discussed.

Hartley and Roe[1] have observed shift in *pK* values of compounds in the presence of micelles and attributed this shift to changes in local interfacial proton activity at the surface of the charged micelles. The change in *pK* values of compounds solubilized in ionic micelles has been attributed by Mukherjee and Banerjee[2] to the electrical potential (Ψ) at the surface. The *pK* values of a few schiff bases have been determined and the trend in *pK* values have been explained considering the difference in polarity of the medium[3] and the charge of the micelle[4].

In the present paper we have determined the critical micellar concentration (CMC) of Tween-20, Tween-40, Tween-60, Tween-80, Brij-35, Brij-98 and Myrj-52s by dye incorporation method at 25°C. The *pK* values of schiff bases salicylidene-2-aminobenzothiazole (2-BAB-2) and *p*-hydroxybenzylidene-2-aminobenzothiazole (4-BAB-2) have been determined in the absence and presence of ionic surfactants, cetyltrimethylammonium bromide (CTAB), sodium lauryl sulphate (NaLS), in the above nonionic surfactants and T-X-100 in dioxane-water mixture (10:90, v/v) at 25°C.

Materials and Methods

CTAB and NaLS (BDH samples) were purified by the literature method[5]. Triton-X-100 (BDH) and all other nonionic surfactants (Sigma, USA) were used as such. Dioxane[6] was purified before use. Methanol (E. Merck, AR) was used as such.

The buffer solution was a mixture of two solutions: solution A and solution B. Solution A consisted of citric acid (6.403 g), boric acid (3.45 g), *N*-phosphoric acid (19 ml), *N* sodium hydroxide (343 ml) and the mixture was diluted to 1000 ml. Solution B consisted of 0.1 *N* HCl. Different volumes of solutions A and B when mixed cover the *p*H range of 3-13. An Elico-model LI-120 digital *p*H meter was used for *p*H measurement. The instrument was standardised with standard phthalate (*p*H 4.0), phosphate (*p*H 6.85) and borate (*p*H 9.18) buffers. All the reagents (E. Merck AR) used for buffer preparation were used without further purification. All solutions were prepared in triply distilled water and were used within seven days of their preparation. Solutions of dye 4-styrylpyridiniumcetyl bromide, **1** (in methanol) and schiff base (in dioxane) were prepared just before use.

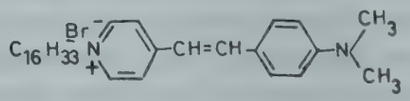

1

The dye (**1**) was obtained by heating γ-picoline and cetyl bromide in a sealed tube at 110°C in an oil-bath for 5 hr. The resulting 4-methylpyridiniumcetyl bromide was refluxed with *p*-N, N-dimethylaminobenzaldehyde and a few drops of piperidine for 8-10 hr[7]. The solid obtained was washed with ether and recrystallized from methanol to obtain pure **1**, m.p. 216°C; yield 75%; IR(KBr): 1600-1575; MS: m/e 529 (M^+), 449 (M − Br) (Found: C, 68.9; H, 9.1. $C_{31}H_{49}N_2Br$ requires C, 70.3; H, 9.2%).

The schiff base salicylidene-2-aminobenzothiazole (2-BAB-2, **2a**) was obtained by refluxing equimolar quantities of 2-aminobenzothiazole and salicyladehyde in a minimum amount of ethyl alcohol containing a few drops of piperidine for 3 hr. The schiff base **2a** thus obtained was recrys-

tallized thrice from ethanol, m.p. 142°C; yield 60%; IR(KBr) 1610, 1570, 3430; (Found C, 66.5; H, 4.0. $C_{14}H_{10}N_2OS$ requires C, 66.1% H, 3.9%). N-(*p*-Hydroxy)benzylidene-2-aminobenzothiazole (4-BAB-2, **2b**) was prepared by the same method. The reflux time was only 30 min, m.p. 206°C; yield 50%; IR(KBr) 1600, 1585, 3410 (Found C, 65.1; H, 3.6. $C_{14}H_{10}N_2OS$ requires C, 66.1; H, 3.9%).

The measurement of critical micellar concentration was monitored spectrophotometrically using a Beckmann model-35 UV spectrophotometer at a fixed dye concentration = 10^{-5} mol dm^{-3} temp. = 25°C and varying concentrations of surfactants in 4% methanol. The solutions were equilibrated for 30 min at the desired temperature. The absorbance values were measured at the λ_{max} of the dye in the corresponding surfactant solution.

A break in the plot of absorbance versus [surfactant] indicated the micelle formation and the intersection point in each case was taken as the CMC of the surfactant. The values are given in Table 1.

Prior to measuring CMC of nonionic surfactants with dye (**1**), some of the surfactants (CTAB, NaLS and Triton-X-100) of known CMC were used to check if the dye (**1**) can be used for this purpose. The results (Table 1) showed that the dye (**1**) could be used for measuring the CMCs.

The *pK* values were measured spectrophotometrically at 25°C at a fixed concentration of the schiff base (5×10^{-5}) mol dm^{-3} in the absence and presence of surfactant in 10% dioxane-water (v/v) mixture (Fig. 1). It was observed that the neutralization process led to a bathochromic shift by about 68 to 85 nm for **2a** and 53 to 69 for **2b**. The band remained sharp both in acidic and alkaline region but remained broad within a narrow *p*H range because of simultaneous existence of both acid and its salt. Since the two break points at lower *p*H (pH_1) and at higher *p*H (pH_2) in the plot of λ_{max} versus *p*H correspond to the existence of 100% acid and 100% salt (anion) respectively neutralization has occurred to an extent of 50% at a $pH = (pH_1 + pH_2)$. Hence this mid *p*H value was taken as the *pK* for the ionisation of the phenol.

Table 1 – Critical Micellar Concentration of Various Nonionic Surfactants in Methanol-Water mixture (4:96 v/v) at 25°C.

Surfactant	CMC, g cm^{-3}	Surfactant	CMC, g dm^{-3}
Tween-20	0.0130	Tween-80	0.1300
Tween-40	0.0150	Myrj-52s	0.0150
Tween-60	0.0115	Brij-35	0.0300
CTAB	8.9×10^{-4}	Brij-98	0.0110
	(9.0×10^{-4})[11]	NaLS	8.1×10^{-3}
Triton-X-100	0.5 vol%		(8.1×10^{-3})[11]
	(0.54 vol%)[11]		

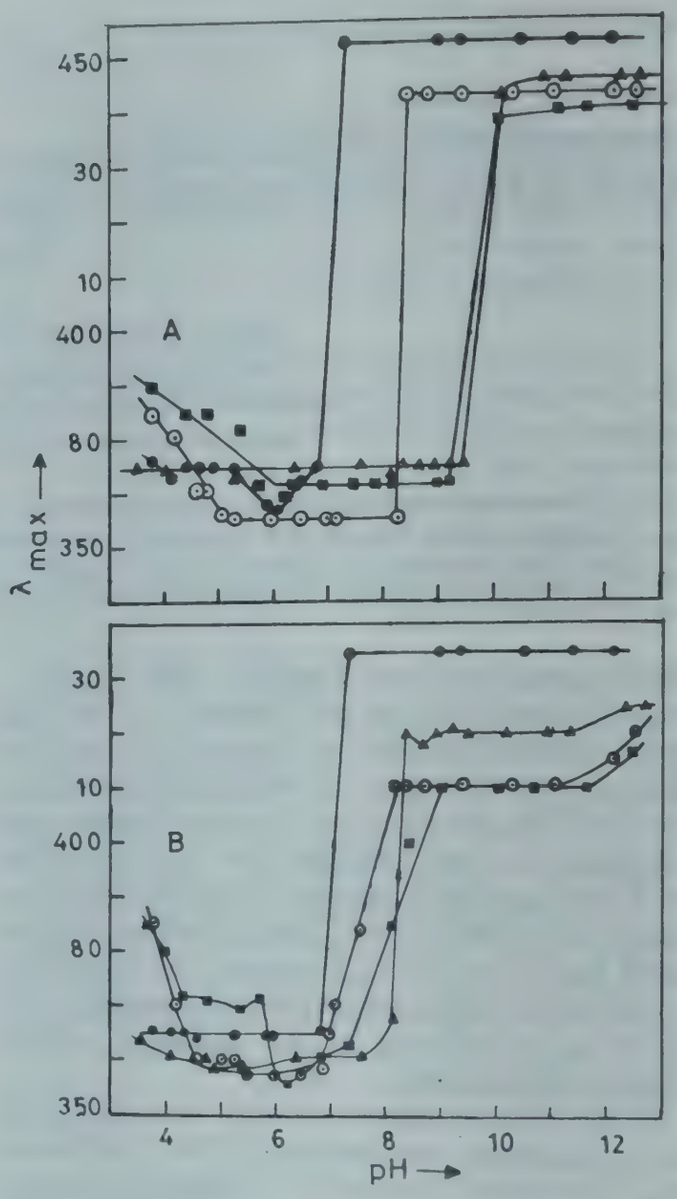

Fig. 1 – Plot of λ_{max} versus *p*H of 2-BAB-2(A) and 4-BAB-2(B) in different surfactant systems and in 10% dioxane-water (v/v). (○ – 10% dioxane-water, ● – CTAB, ■ – NALS, ▲ – T-X-100).

Results and Discussion

The protonation and ionisation of the schiff base is shown in Scheme 1.

Two *pK* values are expected for the schiff bases. The plot of λ_{max} versus *p*H is therefore expected to have three distinct regions relating to species **2, 3** and **4** (Scheme 1). The curve relating to **3** is, however, not obtained because of the requirement of high acidity, in which the schiff base is hydrolysed fast. Experimentally it was not possible to record λ_{max} at low *p*H values. So pK_2 va-

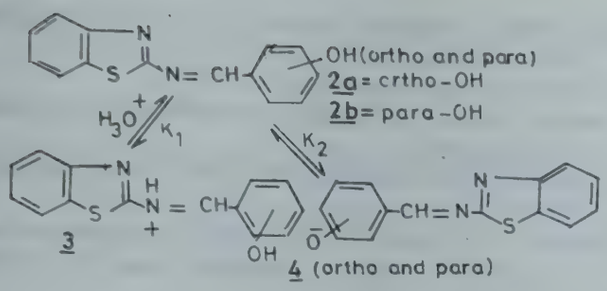

SCHEME 1

lues are only obtained and reported in Table 2. It is observed that the schiff base **2a** shows a sharp change in λ_{max} for slight variance in *p*H in comparison to **2b**. Therefore **2a** is expected to serve as a much better indicator ($\Delta pH = \pm 0.2$).

In evaluating the pK_2 values of the bases, the type of surfactants chosen are: (a) cationic surfactant, CTAB; (b) anionic surfactant, NaLS; and (c) nonionic surfactant having difference in ethylene oxide unit and different hydrophobic chains (Tween-series, Brij-series, Myrj-52s and Triton-X-100).

Change in pK values in charged micelle

The *pK* values of the schiff bases **2a** and **2b** are affected in the presence of micelles. The pK_2 values of 2-BAB-2 (**2a**) is 0.7 units greater than that of 4-BAB-2 (**2b**), which is due to the intramolecular H-bonding in the former.

The pK_2 values of **2a** and **2b** are the same in CTAB but less than the values in water. Menger's model[8] suggests the presence of hydrophobic pocket and charged region on a micellar surface. We have[9] calculated that the hydrophobic pocket is approximately 9% of the total surface in CTAB. The schiff base (**2a**) can anchor on such a surface such that the oxygen and nitrogen are around positively charged region and the aromatic groups can be on hydrophobic pocket. This model would decrease the possibility of intramolecular H-bond formation and hence the difference in *pK* values vanishes. The conjugate base is strongly attracted to the surface which provides the driving force for ionisation to occur. Therefore the values are same in CTAB but less than those in water. This model has received support from the *pK* values in NaLS which is negatively charged micelle. The *pK* values increase to the extent of their decrease in CTAB (1.3 units for 2-BAB-2 and 0.6 units for 4-BAB-2).

Table 2 – pK_2 values of Schiff Bases 2-BAB-2 (**2a**) and 4-BAB-2 (**2b**) in Different Surfactant Systems at 25°C.

Surfactant	[Surfactant]	pK_2	
		2-BAB-2	4-BAB-2
No surfactant	–	8.30	7.60
CTAB	1×10^{-3} mol dm^{-3}	7.10	7.10
NaLS	1×10^{-2} mol dm^{-3}	9.60	8.20
Triton-X-100	0.6 Vol %	9.80	8.20
Tween-20	0.02 g dm^{-3}	8.55	7.75
Tween-40	0.02 g dm^{-3}	8.66	7.60
Tween-60	0.02 g dm^{-3}	9.12	7.85
Tween-80	0.20 g dm^{-3}	9.02	7.85
Brij-35	0.04 g dm^{-3}	9.30	7.80
Brij-98	0.02 g dm^{-3}	8.67	7.85
Myrj-52s	0.02 g dm^{-3}	8.72	7.80

Change in pK values in nonionic micelles

The nonionic surfactants provide a negative surface. In the presence of Triton-X-100, the pK_2 values of both the schiff bases (**2a** and **2b**) are greater than those in the absence of surfactants and are almost equal to the pK_2 values in presence of NaLS. This suggests that the Triton-X-100 micelle perhaps provides the same extent of polarity for the location of schiff base as the negatively charged micelle, NaLS. Fernadez and Fromherz[10] have also made similar observations in the measurement of electrical potential and polarity of NaLS and Triton-X-100 micelles using lipoid *p*H indicators as probes. It is interesting to see that the pK_2 values in the Tween-series having the same polyoxyethylene units are influenced by the length of hydrocarbon chain. According to Menger's model, hydrocarbon chain provides the hydrophobic pocket on the surface. By decreasing the hydrocarbon chain length, the extent of hydrophobic surface decreases and consequently the schiff base cannot be positioned at the surface and therefore pK_2 values approaches the value in water. This is also evident with Tween-80, which contains a C-18 chain with a double bond. The presence of double bond also decreases the hydrophobicity of the surface. It is also observed that an increase in the size of ethylene oxide groups decreases the pK_2 values which can also be due to decrease in hydrophobicity of the surface. Thus it is found that 2-BAB-2 (**2a**) is more sensitive to small changes in *p*H and the nature of surface than 4-BAB-2 (**2b**). This may be due to the presence of intramolecular H-bonding.

Acknowledgement

The authors thank the UGC, New Delhi for financial assistance.

References

1 Hartley G S & Roe J W, *Trans Faraday Soc*, **36** (1940) 101.

2 Mukherjee P & Banerjee K, *J phys Chem*, **68** (1964) 3567.

3 Masoud M S & Elzawawy F M, *Indian J Chem*, **23A** (1984) 149.

4 Beheme M T A, Fullington J G, Noel R & Cordes E H, *J Am chem Soc*, **87** (1965) 266.

5 Duynstee E F & Grunwald E, *J Am chem Soc*, **81** (1959) 4540.

6 Eigenberger E, *J prakt Chem*, **130** (1931) 75.

7 Mukherjee K, Mishra S, Panda C S, Behera G B & Raout M K, *J Indian chem Soc*, **47** (1970) 323.

8 Menger F M, *Acc chem Res*, **12** (1979) 111.

9 Misra P, Panda L N, Mishra B K & Behera G B, *Indian J Chem*, in press.

10 Fernadez M S & Fromherz P, *J Phys Chem*, **81** (1977) 1755.

11 Fendler E J & Fendler J H, *Catalysis in micellar and macromolecular system*, (Academic Press, New York) 1975.

Indian Journal of Chemistry
Vol. 27A, October 1988, pp. 893-897

Synthesis, Characterisation & Dissociation Constants of 1-(3-Aryl-5-hydroxy-4-isoxazolylazo)-4-sulphonic Acid & Its Derivatives

CH NAGARJUN RAO, K C RAJANNA, Y UMA DEVI & P K SAIPRAKASH*
Department of Chemistry, Nizam College (Osmania University), Hyderabad 500 001

Received 10 *June* 1987; *revised* 21 *October* 1987; *accepted* 3 *February* 1988

1-(3-Aryl-5-hydroxy-4-isoxazolylazo)-4-sulphonic acid (PHI-4S) and its derivatives (methyl, methoxy and bromo) have been prepared and characterised on the basis of elemental analysis, IR and NMR spectroscopic studies. Dissociation constants of the ligands have been found to decrease with increase in temperature and ionic strength of the solution. Ion-size parameter (a_0) is evaluated from modified Debye-Huckel equation and found to be 5.10 and 4.90 Å in 30% aqueous methanol and aqueous media respectively. A linear relationship of pK_a versus $1/D$ and/or mol fraction (n_x) has been recorded while the plots of pK_a versus volume (%), weight (%) are non-linear. The order of dissociation constants is BrPHI-4S < PHI-4S < MePHI-4S < MeOPHI-4S. Isoequilibrium temperature (β) value is far below the experimental temperature (290-315 K) indicating the importance of entropy factors in controlling the dissociation equilibria.

A number of isoxazole derivatives have been found to be potential antibacterial, antitubercular, antifungal and/or antiviral reagents. Isoxazoles, having the arylazo group at position-4, have been reported to possess antidiabetic and fungicidal activity. The biological activity of such ligands, is known to be enhanced on complex formation with metals[1-6]. The azo dye derivatives of sulphonic acids containing pyridine moiety have gained much prominence as analytical reagents in complexometric titrations[7-10]. A perusal of literature reveals that synthesis, characterisation and dissociation constant studies pertaining to 1-(3-aryl-5-hydroxy-4-isoxazolylazo)-4-sulphonic acids (PHI-4S) are scanty. This prompted us to synthesise a variety of PHI-4S compounds and study their dissociation constants by potentiometric and spectrophotometric methods.

Materials and Methods

All the chemicals used were BDH or E Merck reagents. Methanol was further purified according to literature procedures[11]. The *p*H corrections for aquo-organic solvents were applied by the method of Van Uitert and Haas[12].

Synthesis of PHI-4S compounds

The ligands under investigation are azodye derivatives of isoxazolones. These were synthesized by diazotising sulphanilic acid[4,13-15] and subsequently coupling the diazotised product with 3-aryl-5-isoxazolone. 3-aryl-5-isoxazolone exists in ketoenol equilibrium and acts as a phenol type compound readily undergoing electrophilic substitution reaction with diazonium ion at 4-position. 3-aryl-5-isoxazolone (0.05 mol) was dissolved in 20%KOH solution and the solution added to a suspension of diazotised sulphanilic acid with vigorous stirring at 5°C. The mixture was allowed to stand for 10 min. A yellow coloured dye stuff separated as a crystalline paste. The product was filtered and repeatedly recrystallized from methanol to get an analytically pure sample.

Determination of dissociation constants

Potentiometric and spectrophotometric methods were used to evaluate the dissociation constants of ligands[16,17]. The potentiometric method used was Calvin-Bjerrum technique as adopted by Irving and Rossotti[17]. The ligands were titrated potentiometrically against standard alkali in an inert (nitrogen) atmosphere. From the titration curves the average number of protons associated with the ligand ($\bar{n}_H$) was calculated. From the $\bar{n}_H - p$H relationship, dissociation constants were evaluated at $\bar{n}_H = 0.5$. Concordant results were obtained by point-wise calculation and linear plots. These values were further confirmed by Albert's spectrophotometric method[16] according to the relationship,

$$pK_a = p\mathrm{H} + \log (d_I - d)/(d - d_M)$$

where d_I, d_M and d indicate the optical densities of ionised, molecular and observed optical density at analytical wavelength (405 nm) respectively.

These studies were carried out as a function of ionic strength (μ), temperature and dielectric constant (D). The pK_a values are reproducible within the limits of ± 0.05 units.

Results and Discussion

The PHI-4S compounds have been characterised

Table 1—Analytical Data of the Azo Dye Derivatives of Isoxazolones

Compound (Mol. formula)	Yield (%) (Colour)	Found (Calc.) %			PMR (DMSO-d_6) δ (PPM)
		C	H	N	
PHI-4S ($C_{15}H_{11}N_3O_5S$)	72 (Pale yellow)	51.41 (52.17)	3.82 (3.21)	12.48 (17.17)	12.19 (−OH, in heterocyclic ring); 8.00-6.80 (two sets of Ar-H in ring A); 8.04-7.88, 6.93, 6.33 (2Ar-H *ortho* to $-SO_3Na$, d-*ortho* to −N=N− in ring B).
MePHI-4S ($C_{16}H_{13}N_3O_5S$)	60 (yellow)	52.82 (53.48)	3.71 (3.65)	11.75 (11.69)	12.19, C−OH, in heterocyclc ring); 8.04-6.80, 3.30(s) (two sets of Ar-H, R-H in ring A), 8.04-7.88, 6.93, 6.33 (2Ar-H *ortho* to $-SO_3Na$, d-*ortho* to −N=N in ring B)
MeOPHI-4S ($C_{16}H_{13}N_3O_6S$)	65 (yellow)	50.96 (51.20)	3.42 (3.49)	11.44 (11.20)	12.19 (−OH in heterocyclic ring); 8.00-6.80, 3.08 (two sets of Ar-H, R-H in ring A), 7.28-7.18, 6.93, 6.33 (2Ar-H *ortho* to $-SO_3Na$, d-*ortho* to −N=N− in ring B).
BrPHI-4S ($C_{15}H_{10}N_3O_5SBr$)	54 (yellow)	41.68 (42.47)	2.32 (2.38)	10.08 (9.91)	12.19 (w, −OH, in heterocyclic ring); 6.97-6.88 (two sets of Ar-H in ring A); 8.04-7.88, 6.93, 6.33 (2Ar-H *ortho* to $-SO_3Na$, d-*ortho* to −N=N− in ring B).

by elemental analysis (Table 1), IR and NMR spectroscopic studies. Melting points of all the compounds have been determined in open capillaries and are uncorrected. These compounds have been observed to be high melting (> 300°C). Purity of the compounds has been checked by TLC.

Infrared spectra of the compounds have been recorded on a "Shimadzu" spectrophotometer using KBr petlets. The IR spectra of PHI-4S show two peaks at 3400 and 1720 cm^{-1} assignable to νOH and νC=O frequencies. The existence of νO−H band at such low frequency and its broad nature can be attributed to the strong intramolecular hydrogen bonding[18,19]. Observation of both νC=O and νOH modes indicates that keto-enol tautomerism exists in these compounds. Similar observations have been made in other isoxazolone derivatives[20]. The νN=N vibration of azo compounds is IR-forbidden but ν_{as}N=N occurs near 1429 cm^{-1}. Isoxazolone shows the corresponding band at 1420 cm^{-1} which is weak due to non-polar nature of the bond.

The four peaks observed around 1600, 1580, 1500 and 1450 cm^{-1} may be assigned to aromatic C=N and C=C stretching modes. The bands near 745 and 860 cm^{-1} may be associated with heterocyclic "ring breathing" modes.

NMR spectra of sodium salts of PHI-4S were recorded on FT NMR model-FX-90 Q using DMSO-d_6 as the solvent and TMS as the internal standard. The data are incorporated in Table 1. A doublet around 6.33 and 6.93 δ may be due to protons of the aromatic ring (B), situated at *ortho* positions to azo group (N=N). The other two protons of ring B, which are *ortho* to sulphonic group (SO_3Na^+) appear downfield at 7.18, 7.28 δ (2H) due to the effect of increased electronegativity of sulphonic group. In the case of methyl derivative, the two protons, adjacent to sulphonic group, have been observed at 7.88 and 8.04 δ. Peaks observed around 6.8 to 8.0 δ may be assigned to aromatic protons of ring A.

A singlet peak appearing around 12.19 δ accounts for a proton corresponding to OH group, though it is generally expected at 10.0 δ. Such a downfield shift may probably indicate that the proton is involved in intramolecular hydrogen bonding. Similar absorptions have been found for other compounds except the bromo derivative. The spectrum of the bromo derivative shows weak signals which may be due to presence of two electronegative groups attached to the two phenyl rings (A and B).

In the ligand (PHI-4S), no aliphatic proton has been observed. However, in the case of methyl and methoxy ($-OCH_3$) derivatives a singlet was observed at 3.30 and 3.08 δ respectively. On the basis of foregoing discussion the structure of the compounds could be given as shown in (I).

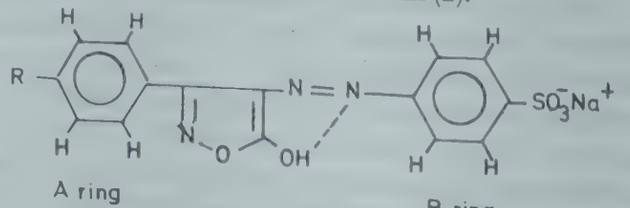

Where R=H, Br, CH_3 or CH_3O

(I)

Dissociation constants (K_a) of PHI-4S compounds

The ligands are monobasic acids. The ligand titration curve falls below the acid titration curve indicating the liberation of a proton. From the acid and ligand titration curves, $\bar{n}_H$ values have been calculated which are in the range of 0.30 to 0.96 for PHI-4S, 0.20 to 0.97 for MePHI-4S 0.28 to 0.96 for MePHI-4S and 0.20 to 0.92 for BrPHI-4S. From the proton-ligand formation curves ($\bar{n}_H$ versus pH), dissociation constants were evaluated at $\bar{n}_H = 0.5$ (Table 2). These were found to be in concordance with the values obtained from linear plots ($\log [\bar{n}_H/(1-\bar{n}_H)]$) as a function of pH, pointwise calculations and Albert's spectrophotometric method[16]. The degree of formation for unprotonated (α_L) and protonated (α_{HL}) species of the ligand has been calculated[17] and the two species are found to be present in equal amounts at a pH equal to pK_a.

Effect of ionic strength (μ) on pK_a

The pK_a values of PHI-4S ligands are found to decrease on increasing ionic strength (μ) of the system (Table 3). The data obtained are cast into the modified Debye-Huckel relationship[21-23],

$$pK_a = pK_a^0 - (A\Delta Z^2\ \mu^{1/2}/1 + Ba_0\ \mu^{1/2})$$

where Z is the valency of the species. For uni-univalent electrolytes, a_0 is assumed as 4 Å. The Debye-Huckel constants A and B have been calculated according to the expressions cited in literature[24]. The values for A and B are found to be 0.625 and 3.44×10^7 respectively for 30% aqueous methanol. For aqueous system, the values of A and B are reported as 1.846 and 5.05×10^7. The plots of pK_a versus $\mu^{1/2}/(1 + Ba_0\mu^{1/2})$ are in accordance with the above equation. But the slope values ($m = A\Delta Z^2$) do not seem to agree with the expected values. The expected ΔZ^2 values are $+1.0$ and -1.0 for monobasic acids and monoacidic bases respectively. The deviation in the observed $A\Delta Z^2$ values from theoretical values may be attributed to the discrepancy in the value of theoretical a_0. In order to gain the correct a_0 value, the plots of pK_a as a function of $\mu^{1/2}/(1 + Ba_0\mu^{1/2})$ have been tested by hit and trial method, using the value of a_0 in the range 3.0 to 6.0 Å. The effect has been found to be fruitful when $a_0 = 5.10$ Å and 4.90 Å in 30% aqueous methanol and aqueous system respectively for all the ligands studied (Table 3). Accordingly, the observed values of most accurate slopes ($A\Delta Z^2$), a_0 values and intercepts have been compiled in Table 3 for MeOPHI-4S as a typical case.

Table 2—Computation of Dissociation Constants by Various Methods

{[Acid] = 2.50×10^{-3} mol dm^{-3}; [T_L] = 2.50×10^{-3} mol dm^{-3}; μ = 0.05 mol dm^{-3}; Temp. = 293 K}

Ligand	Point-wise calculation	Half integral	Linear plots	Albert's spectrophotometric
		(*A*) *Aqueous system*		
MeOPHI-4S	7.68	7.70	7.69	7.67
MePHI-4S	7.35	7.36	7.36	7.35
PHI-4S	7.08	7.08	7.08	7.06
BrPHI-4S	6.55	6.56	6.56	6.54
		(*B*) 40% *Aqueous methanol system*		
MeOPHI-4S	8.16	8.19	8.18	8.16
MePHI-4S	7.85	7.87	7.86	7.85
PHI-4S	7.58	7.59	7.58	7.56
BrPHI-4S	7.16	7.16	7.16	7.15

Table 3—Calculated and Observed Data of Ionic Strength (μ) Effect on PK_a of MeOPHi-4S

{[T_L] = 2.50×10^{-3} mol dm^{-3}; Temp. = 293 K}

Property	Aqueous methanol system		Aqueous system	
	Calc. (a_0 = 5.10 A)	Obs. (a_0 = 4.00 A)	Calc. (a_0 = 4.90 A)	Obs. (a_0 = 4.00 A)
Slope ($A\Delta Z^2$)	0.650	0.590	1.850	1.620
Intercept (pK_{a_0})	8.085	8.160	7.950	7.930
ΔZ^2	1.000	0.943	1.000	0.876

Effect of solvent on the dissociation of PHI-4S compounds

The pK_a values are found to increase in solvents of low dielectric constant (D) (Table 2). The values of D for various proportions of aqueous methanol have been obtained from the data compiled by Akerlof[25]. Though the plots of pK_a versus volume (%) and weight (%) of methanol are nonlinear, it is interesting to note that the plots of pK_a against mol fraction (n_x) and $1/D$ are linear with regression coefficient (γ) 0.985. These are consistent with the relationship proposed by Irving and Rossotti[26], with the intercept equal to pK_a (W) (dissociation constant in aqueous medium). Further, the plot of ΔpK_a versus $(1/D_s - 1/D_w)$ has been found to be linear according to Born's relationship.

$$\Delta pK_a = \frac{e^2}{2.303\ r_0 kT}(1/D_s - 1/D_w)$$

where ΔpK_a = difference in the pK_a values in aqueous methanol and water, e = charge on the electron, k = Boltzmann constant, T = temperature, r_0 = mean radius of anion, D_s = dielectric constant of aqueous

Table 4—Dissociation Constants and Thermodynamic Parameters of Substituted PHI-4S Ligands (RPHI-4S)

$\{[T_L] = 2.50 \times 10^{-3}$ mol dm^{-3}; $\mu = 0.05$ mol dm$^{-3}\}$

Compound	pK_a		$-\Delta H$	$-\Delta G$	ΔS
	293 K	313 K	kJ mol^{-1}		JK^{-1} mol^{-1}
			(A) Aqueous medium		
MeOPHI-4S	7.69	7.27	36.9	43.1	−21.2
Me.PHI-4S	7.36	7.06	26.4	41.3	−50.9
PHI-4S	7.08	6.53	48.2	39.8	28.7
Br.PHI-4S	6.56	6.12	38.7	36.8	6.5
			(B) 40% Aqueous methanol medium		
Me.OPHI-4S	8.18	7.68	43.9	45.9	−6.83
Me.PHI-4S	7.86	7.41	39.6	44.1	−15.4
PHI-4S	7.58	6.96	54.5	42.6	40.6
Br.PHI-4S	7.16	6.23	81.6	40.2	141.3

*Error limits for (i) ΔH & $\Delta G = \pm 2.0$ kJ mol^{-1}
(ii) $\Delta S = \pm 5$ JK^{-1} mol^{-1}
(iii) $pK_a = \pm 0.05$ units.

methanol, D_w = dielectric constant of water. From the slopes of these plots, values of mean radius (r_0) of the ion has been calculated (7.67 Å for PHI-4S, MePHI-4S and MeOPHI-4S and 8.87 Å for BrPHI-4S respectively).

Effect of substituents and temperature on the dissociation of PHI-4S compounds

In the present investigation, the pK_a values of the ligands have been found to be in the order: MeO-PHI-4S > MePHI > PHI-4S > BrPHI-4S at all temperatures and in all the dielectric media indicating that the dissociation is more favourable with the electron releasing substituents (Table 2). This also indicates the importance of high electron density in facilitating the dissociation of PHI-4S compounds.

The pK_a values are found to decrease with an increase in temperature. The thermodynamic parameters (Table 4) calculated for dissociation of PHI-4S ligands reveal that the entropy factor is either positive or negative. For electron releasing groups is has been found to be negative. However, ΔH is positive in all the cases. This trend indicates that the equilibrium is more endothermic in aqueous methanol medium. The negative entropy of methoxy and methyl substituted compounds can be explained in terms of the following equilibria

$$HL + SH \rightleftharpoons SH_2^+ + L^-$$

$$\Delta S = (\Delta S_{SH_2} + \Delta S_{L^-}) - (\Delta S_{HL} + \Delta S_{SH}) + \Delta S(\text{Sol-Sol-int})$$

$$\Delta S = (\Delta S_{SH_2} - \Delta S_{SH}) + (\Delta S_L - \Delta S_{HL}) + \Delta S(\text{Sol-Sol-int})$$

$$\Delta S = x + y + \Delta S\,(\text{Sol-Sol-int})$$

In the above equation the first term is negative since SH_2^+ ion is highly solvated resulting in the decrease in entropy with respect to SH. Similarly, the second term is also negative leading to overall negative values. ΔS (Sol-Sol-int) will depend on the mol fraction of the organic component and its ability to stabilise or destabilise the structure of water. Similar observations were made earlier on the dissociation constant studies of acetic acid, 1-hydroxy-2-nitroso-4-sulphonic acid[28], 2-hydroxy-1-napthoic acid and *o*-pyrocatechuic acid[29].

In order to know to nature of equilibrium[30], the thermodynamic data and dissociation constant data have been cast into Leffler's[31] and Exner's plots[32]. A linear plot of ΔH as a function of ΔS (Leffler's plot) indicates the iso-equilibrium temperature (β) to be 260 K. By and large a similar value (253 K) has been obtained by the Linear plot of pK_a at 293 K versus pK_a at 313 K. Though the β values differ by 10 K from one method to the other, both the values fall far below the experimental temperature range (293 − 313 K) indicating that the equilibrium is controlled by entropy factors.

Acknowledgement

The authors thank Prof T Navaneeth Rao, Vice-Chancellor, Osmania University, Hyderabad for constant encouragement. One of them (Ch Nagar-

jun Rao) thanks the UGC, New Delhi for the award of a junior research fellowship.

References

1 Quilico A, *The chemistry of heterocyclic compounds*, Vol 17 (Wiley Interscience, New York) 1962.
2 Barnes R P, *Heterocyclic compounds*, Vol 5, Chapter 7, edited by R C Elderfield (Wiley, New York) 1952.
3 Kochetkov N K & Sokolev S D, *Advances in heterocyclic chemistry*, Vol 2, edited by A R Katrizsky (Academic Press, New York) 1963.
4 Uma Devi Y, *Synthesis, spectral characteristics of isoxazoles and their derivatives*, Ph.D. Thesis, Osmania University, 1975.
5 Lambein F, Van Parijs R, Schamp N & Vandendriessche L, *Biochem Biophys Res Comm*, **37** (1969) 375.
6 Fax H M, Geoghan M J, Silk J A & Summers L A, *Anna Appl Biol*, **52** (1963) 33.
7 Mehta Y L, Garg B S & Mohan Katyal, *Anal chim Acta*, **86** (1976) 323.
8 Gupta J P, Mehta Y L, Garg B S & Singh R P, *Indian J Chem*, **14A** (1977) 256.
9 Garg H G & Singh R P, *J mednl Chem*, **13** (1970) 1250.
10 Garg S K, Mukharjee S, Garg B S & Singh R P, *J Indian chem Soc*, **59** (1982) 1038.
11 Vogel A I, *A text book of practical organic chemistry* (Longmans, London) 1978, 269.
12 Van Uitert L G & Haas C G, *J Am chem Soc*, **75** (1953) 451.
13 Claisen L & Zedel W, *Berdt chem Ges*, **24** (1891) 142.
14 Posner T & Schreiber G, *Berdt chem Ges*, **37** (1924) 1127.
15 Knorr L & Reuter B, *Berdt chem Ges*, **27** (1894) 1174.
16 Albert A, *Biochem J*, **47** (1950) 531; **50** (1952) 690.
17 Irving H M & Rossotti H S, *J chem Soc*, (1953) 3397.
18 Freedman H H, *J Am chem Soc*, **83** (1961) 2900.
19 Kazitsyana L A & Mischanko M, *Dekl Akad Nauk SSSR*, **150** (1963) 555.
20 Angyal C L & Le Fevre R J W, *J chem Soc*, (1953) 2180.
21 Rossotti F J C & Rossotti H S, *The determination of stability constants* (McGraw Hill, New York) 1961.
22 Debye P & Huckel E, *Phys Z*, **24** (1923) 185.
23 Shelke D N & Jahagirdar D V, *J Indian chem Soc*, **55** (1978) 545.
24 Robinson R A & Stokes R H, *Electrolytic solutions* (Butterworths, London) 1959, 2301, 355.
25 Akerlef G & Short O A, *J Am chem Soc*, **58** (1936) 124.
26 Irving H & Rossotti H S, *Acta chem scand*, **10** (1956) 72.
27 Born M, *Z Physik*, **1** (1920) 45.
28 Lingaiah P & Sundaram E V, *Indian J Chem*, **10** (1972) 670.
29 Pant A N, Soni R & Gupta S L, *Indian J Chem*, **10** (1972) 109.
30 Hammett L P, *Physical organic chemistry* (McGraw Hill, New York), 1940, 186.
31 Leffler J, *J org Chem*, **20** (1955) 1202.
32 Exner O, *Colln Czech chem Commun*, **37** (1972) 1425.

Indian Journal of Chemistry
Vol. 27A, October 1988, pp. 898-901

Notes

Viscosity B-Coefficients of Tetraalkylammonium Bromides in Dimethyl Sulphoxide-Water Mixtures

SUSANTA DAS & DILIP KUMAR HAZRA*
Department of Chemistry, North Bengal University, Darjeeling 734430

Received 5 *May* 1987; *revised* 29 *December* 1987; *accepted* 18 *January* 1988

The relative viscosities of solutions of tetraalkylammonium bromides, R_4NBr (where $R = CH_3-$, C_2H_5-, C_3H_7- and C_4H_9-) have been measured in dimethyl sulphoxide (DMSO) + water mixtures (20, 40, 60, 80 and 100 wt % of DMSO) at 25, 35 and 45°C. The results have been analysed using the Jones-Dole equation and *B*-coefficients have been calculated. The $\Delta\mu_2^{\theta\ddagger}$, $\Delta H_2^{\theta\ddagger}$ and $T\Delta S_2^{\theta\ddagger}$ values of the salts have been determined using the transition state treatment and the temperature coefficient measurements. The ionic *B*-values have been calculated using the reference electrolyte Bu_4NBPh_4. The results have been discussed in terms of structural changes of the solvent.

Viscometry is one of the important tools for the determination of ion-solvent interactions which are the controlling forces in dilute solutions where ion-ion interactions are absent[1]. The variations of solvational properties are reflected in the viscosity *B*-coefficients of ions.

The present communication deals with the determination of viscosity *B*-coefficient of tetraalkylammonium bromides in dimethyl sulphoxide (DMSO)- water mixtures containing 20, 40, 60, 80 and 100 wt% of DMSO at 25°, 35° and 45°C.

The purification of DMSO (Baker analyzed reagent) and of tetraalkylammonium bromides (Fluka, puriss) together with the solvent properties have been described presiously[2]. The various compositions of DMSO + water mixtures employed in the study were prepared by weight with an accuracy of ± 0.2%.

The concentrations of the salts were generally varied from 0.01 *m* to 0.01 *m*, which were prepared by weight dilution of the stock solution (~ 0.2*m*). The conversion of molality into molarity was done using the density values. The kinetic viscosities were measured at the desired temperature (accuracy ±0.01°C) using a suspended Ubbelohde-type viscometer. The densities were measured using an Ostwald-Sprengal type Pycknometer. The details of the experimental procedure employed have been described in our previous paper[2]. The electrical conductivities were measured with a Pye-Unicam conductivity meter (PW 9509) at 2000Hz.

The relative viscosities of the electrolytes at various compositions of DMSO + water mixtures have been analysed by well known Jones-Dole equation[3] (Eq. 1).

$$(\eta/\eta_0 - 1)/\sqrt{C} = A + B\sqrt{C} \qquad \ldots (1)$$

The plots of $(\eta/\eta_0 - 1)/\sqrt{C}$ against $\sqrt{C}$ are linear and the experimental *A*-values at 25, 35 and 45°C, calculated using the least squares method, have been, in general, found to be positive. However, the experimental *A*-values are different from the theoretical *A*-values, as observed in other solvents[4,5]. The *A*-values were calculated theoretically at 25°C from the physical properties of the solvent and the limiting ionic equivalent conductances using Falkenhagen and Vernon[6] equation.

Table 1 contains the theoretically calculated and experimentally determined *A*-coefficient values. Dielectric constant data were not available at high temperatures but the *A*-values will not be significantly different from those at 25°C (ref. 7) and are used at three temmperatures of measurement.

The *B*-coefficients at various temperatures using the least squares method, are presented in Table 2.

The $\Delta\mu_2^{\theta\ddagger}$, the contribution per mol of solute to the free energy of activation for viscous flow of the solution, has been determined using Eq. (2), as suggested by Feakins *et al.*[8]

$$B = \frac{\bar{v}_1^0 - \bar{v}_2^0}{1000} + \frac{\bar{v}_2^0}{1000}\left(\frac{\Delta\mu_2^{\theta\ddagger} - \Delta\mu_1^{\theta\ddagger}}{RT}\right) \qquad \ldots (2)$$

where $\bar{v}_1^0$ and $\bar{v}_2^0$ are the partial molar volumes of the solvent and solute respectively.

$\Delta\mu_1^{\theta\ddagger}$, the free energy of activation per mol of the pure solvent is given by Eq. (3)

$$\Delta\mu_1^{\theta\ddagger} = \Delta G_1^{\theta\ddagger} = RT \ln\left(\frac{\eta_1 \bar{v}_1^0}{hN}\right) \qquad \ldots (3)$$

For the mixed solvents, each solvent mixture is treated as a pure solvent and the molar volume is a mean value,defined as

$$\bar{v}_1^0 = (X_1M_1 + X_2M_2)/\rho_1 \qquad \ldots (4)$$

where X_1, M_1 and X_2, M_2 are mol fractions and molecular weights of water and DMSO respectively, and ρ_1 is the density of the solvent mixture.

Table 1—Theoretical and Experimental *A*-Coefficients at 25°C in Different DMSO-Water Mixtures

Salt	*A*-Coefficients ($dm^{3/2}mol^{-1/2}$) in DMSO-water mixtures containing DMSO (wt%)				
	20	40	60	80	100
Me_4NBr	0.0056 (0.0141)	0.0055 (0.0189)	0.0067 (0.0499)	0.0082 (0.0283)	0.0104 (0.0149)
Et_4NBr	0.0064 (0.0050)	0.0069 (−0.0022)	0.0067 (0.0689)	0.0084 (0.0310)	0.0108 (0.0194)
Pr_4NBr	0.0071 (0.0145)	0.0082 (0.0204)	0.0079 (0.0533)	0.0088 (0.0321)	0.0121 (0.0117)
Bu_4NBr	0.0078 (0.0265)	0.0088 (0.0306)	0.0094 (0.0930)	0.0091 (0.0381)	0.0148 (0.0110)

Values in the parentheses are experimental *A*-Coefficients

Table 2—Viscosity *b*-Coefficients[a] ($dm^3\ mol^{-1}$) in DMSO-Water Mixtures at 25°(1), 35°(2) and 45°(3)

Salt	0%[b]	20%	40%	60%	80%	100%
Me_4NBr	(1) 0.083	0.111	0.281	0.256	0.508	0.719
	(2) 0.09	0.108	0.269	0.204	0.404	0.666
	(3) 0.10	0.072	0.210	0.154	0.342	0.609
Et_4NBr	(1) 0.34	0.641	0.462	0.286	0.609	0.771
	(2) 0.32	0.601	0.365	0.242	0.460	0.703
	(3) 0.30	0.568	0.329	0.210	0.363	0.682
Pr_4NBr	(1) 0.82	0.771	0.665	0.439	0.675	0.865
	(2) 0.73	0.630	0.601	0.292	0.559	0.829
	(3) 0.64	0.591	0.550	0.317	0.399	0.714
Bu_4NBr	(1) 1.24	1.140	0.999	0.689	0.730	0.902[c]
	(2) 1.067	1.012	0.886	0.470	0.652	0.842
	(3) 0.990	0.983	0.752	0.356	0.502	0.782

[a]The correlation coefficient was always greater than 0.98 and the maximum uncertainty in *B*-coefficient value was ±0.006; [b]Ref. 4; [c]Ref. 23.

The activation parameters for viscous flow for the electrolytes are given in Table 3.

It can be seen from Table 1 that *A*-coefficients decrease in the order $Me_4N^+ < Et_4N^+ < Pr_4N^+ < Bu_4N^+$. Further the ionic *A*-values increase with the increase in DMSO content in the solvent mixture though the change is not significant in solvent mixture containing lower percentage of DMSO.

The *B*-values (Table 2), in general, are high and positive. The *B*-values of tetraalkylammonium salts in DMSO increase in a regular fashion as the size of the tetraalkylammonium ion increases. However, variations in the *B*-values for different electrolytes have been observed in mixed solvents due to ion-solvent interactions of different magnitude. For example, in the case of Me_4NBr, *B*-value increases upto 40 wt% but deceases to give a minimum at 60 wt%. Similar trend is exhibited by Et_4N^+. For Pr_4N^+ and Bu_4N^+, *B*-values decrease continuously to give a minimum at 60 wt%. The result must be due to decrease in hydrophobic interactions and consequent structural changes occurring in solution. The *B*-coefficient values at higher temperatures follow the same pattern.

The changes in $\Delta\mu_2^{\theta\ddagger}$ follow the same pattern as the *B*-values. However, $\Delta H_2^{\theta\ddagger}$ and $T\Delta S_2^{\theta\ddagger}$ increase from Me_4N^+ to Pr_4N^+ salts but decrease in the case of Bu_4N^+ salts. The minimum values in entropy and enthalpy of activation of viscous flow generally lie in DMSO-water mixtures containing 60 wt % DMSO.

The dB/dT value of tetrametylammonium bromide in water is positive and characteristic of structure breakers[9,10]. The bromide generally causes structure breaking of the solvent. Me_4N^+ is also known to be a structure breaker in water[11]. However, the dB/dT of the salts are negative in DMSO + H_2O mixture and pure DMSO indicating the structure making properties of these salts in DMSO + H_2O mixtures and DMSO. The dB/dT values for most of the salts pass through a minimum in solvent mixture containing 60 wt% of DMSO.

The ionic *B*-values were calculated by Eq. (5) using Bu_4NBPh_4 as the 'reference electrolyte'[12-15]

$$\frac{B_{Ph_4B^-}}{B_{Bu_4N^+}} = \frac{r^3_{Ph_4B^-}}{r^3_{Bu_4N^+}} = \left(\frac{5.35}{5.00}\right)^3 \quad \ldots (5)$$

The ionic *B*-coefficients for the tetraalkyl ions increase continuously from Me_4N^+ to Bu_4N^+ in DMSO and DMSO + H_2O mixtures. The addition

Table 3—$\Delta\mu_2^{\theta\ddagger}$(kJ mol^{-1})(2), $\Delta H_2^{\theta\ddagger}$(kJ mol^{-1})(1), $T\Delta S_2^{\theta\ddagger}$(kJ mol^{-1})(3) of Tetraalkylammonium Bromides in DMSO-Water Mixtures at 25°C

Salt		20%	40%	60%	80%	100%
Me_4NBr	(1)	34.76	49.99	40.10	47.06	40.37
	(2)	88.85	143.22	150.66	232.56	
	(3)	53.64	92.38	110.26	184.76	
Et_4NBr	(1)	104.53	72.47	52.12	56.21	43.81
	(2)	140.28	230.26	193.30	309.66	
	(3)	35.76	157.94	140.06	253.30	
Pr_4NBr	(1)	145.61	109.95	65.38	67.74	49.88
	(2)	649.38	371.15	178.02	350.82	
	(3)	503.62	262.24	113.24	286.08	
Bu_4NBr	(1)	178.89	138.73	90.23	70.34	53.8
	(2)	321.63	290.56	435.23	292.95	
	(3)	143.04	151.98	345.68	223.50	

Table 4—Ionic Radii ($R_\pm$) Calculated by Einstein's Equation and Relative Solvation of Ions at 25°C

Ion	r_c/Å	$R_\pm$ (Å)				n_s				r_{corr} (Å)			
		20%	40%	60%	80%	20%	40%	60%	80%	20%	40%	60%	80%
Me_4N^+	3.47	3.42	2.96	2.55	3.70	−9.9	−1.6	−3.0	0.5	1.4	1.5	1.4	2.0
Et_4N^+	4.00	3.61	3.71	3.06	4.05	−2.0	−1.3	2.9	0.4	1.9	2.5	1.5	2.1
Pr_4N^+	4.52	4.09	4.56	3.45	4.26	−2.9	0.2	−4.2	−0.8	2.5	3.4	2.1	2.5
Bu_4N^+	4.94	5.01	5.22	4.28	4.37	0.6	2.2	−3.4	−2.2	2.8	4.3	2.9	2.7
Br^-	1.95	3.80	2.52	3.13	3.19	5.7	0.8	1.9	2.5	1.3	1.2	1.7	1.5
BPh_4^-	4.94	5.37	5.59	4.58	4.67	4.1	5.4	−1.9	−1.1	3.0	4.6	3.1	2.9

of DMSO to water causes the B_{ion} values to decrease. However, the B_{ion} values then increase and pass through a minimum at ~60 wt% of DMSO ($X_2 \simeq 0.30$).

The dB/dT values of Me_4N^+, Et_4N^+ and Pr_4N^+ ions are negative (structure making) except at 60 wt% DMSO where positive values are observed (structure breaking). dB/dT value of Bu_4N^+ is always negative though the value appears to be minimum in solvent mixture containing 60 wt% of DMSO.

An analysis of $B_\pm$ coefficients can be made on the basis of Einstein's equation[16].

$$B_\pm = 2.5 \frac{4\pi}{3} \frac{R_\pm^3 N}{1000} \quad \ldots (6)$$

where $R_\pm$ is the radius of the ion assumed as a rigid sphere moving in a continuum and 2.5 is the shape factor for a sphere. The number n_s solvent molecules bound to the ion in the primary solvation sphere can be calculated by combining the Jones-Dole equation with Einstein's[17]

$$B_\pm = \frac{2.5}{1000}(V_i + n_s V_s) \quad \ldots (7)$$

where V_i represents the bare ion molar volume and is related to the crystallographic radius r_c of the ion and V_s is the solvent molar volume. The values of $R_\pm$ and n_s are given in Table 4. The values may be compared with the corrected stokes radii obtained from conductance studies (unpublished data from the authors' laboratory). For cations, R_+ and r_c values agree fairly well, showing that these ions are scarcely solvated in DMSO and DMSO-water mixtures and behave as spherical entities. On the other hand it is difficult to explain the high n_s as well as R_- values for Br^- ion, because they are generally believed to be unsolvated in this class of solvants[18].

Viscometric results have also been analysed using Eq. (4)[8]. It is seen that in mixed solvents, $\Delta H_2^{\theta\ddagger}$ and $T\Delta S_2^{\theta\ddagger}$ are positive for all the salts studied and are several times larger than those of the binary mixtures. This suggests that attainment of transition state for viscous flow is accompanied by breaking and distortion of intermolecular bonds. It may be noted that $\Delta\mu_2^{\theta\ddagger}$ is highly positive for all ions (except for Me_4N^+ ion at 20 wt% of DMSO), thus the formation of a transition state is made less favourable by the presence of these ions. The $\Delta\mu_2^{\theta\ddagger}$ value for the Br^- ion is lower than those for the cations and this shows that cations interact with the DMSO-water mixtures more strongly than do the anions. On the other hand, the value of BPh_4^- ion is much higher than that of

Bu_4N^+ ion in spite of the fact that they are almost isostructural and BPh_4^- is unlikely to be highly solvated owing to its low charge density. It may be of interest that analogous result to that observed in DMSO and DMSO-water mixture has been found in other solvents also[18,19].

The reason for the observed changes in the viscosity *B*-values in the region of 60-80 wt% DMSO may be attributed to structural changes and changed ion-solvent interactions in this region[20,21].

One of the authors (SD) thanks the UGC, New Delhi for the award of a research fellowship.

References

1 Krumgalz B S, *J chem Soc Faraday Trans* 1, **76** (1980) 1275.

2 Das S, Hazra D K & Lahiri S C, *Z phys Chem (Frankfurt)*, **138** (1983) 185.

3 Jones G & Dole M, *J Am chem Soc*, **51** (1929) 2950.

5 Yao N P & Bennion D N, *J phys Chem*, **75**(1971) 1727.

6 Falkenhagen H & Vernon E L, *Phys Z*, **33** (1932) 140; *Phil Mag*, **14** (1932) 537; Harned H S & Owen B B, *The physical chemistry of electrolytic solutions*, 3rd Edn (Reinhold, New York) 1958, p 240.

7 Bickerell R T M, Lawrence K G & Feakins D, *J chem Soc Faraday Trans* 1, **76** (1980) 637.

8 Feakins D, Freemantle D J & Lawrence K G, *J chem Soc Faraday Trans* 1, **70** (1974) 795.

9 Kaminsky M, *Disc Faraday Soc*, **24** (1957) 171.

10 Padova J, *Structure and transport processes in water and aqueous solutions*, edited by R A Horne (Wiley-Interscience, New York) 1971, Chapter 4, p 153.

11 Yang-Wen W, in ref 10, Chapter 15, p 639.

12 Tuan D F & Fuoss R M, *J phys Chem*, **67** (1963) 1343.

13 Gill D S & Sharma A N, *J chem Soc Faraday Trans* 1, **78** (1982) 475.

14 Gill D S & Sekhri M B, *J chem soc Faraday Trans* 1, **78** (1982) 119.

15 Gill D S, *Electochim Acta*, **24** (1979) 701.

16 Einstein A, *Ann phys*, **19** (1906) 289.

17 Feakins D & Lawrence K G, *J chem Soc A*, (1966) 212.

18 Sacco A, Petrella G, Monica M D & Castagnolo M, *J chem Soc Faraday Trans* 1, **73** (1977) 1936.

19 Lawrence K G & Sacco A, *J chem Soc Faraday Trans* 1, **79** (1983) 615.

20 Safford G J, Schaffer P C, Leung P S, Deobbler G F, Brady G W & Lyden E F X, *J chem Phys*, **50** (1969) 2140.

21 Dack M R J, *Chem Soc Rev (London)*, **4** (1975) 211.

Indian Journal of Chemistry
Vol. 27A, October 1988, pp. 902-904

Suppression of Formation of Silicon Tetrachloride during Preparation of Silicon from Trichlorosilane†

M K DONGARE*, I S MULLA & A P B SINHA

Physical Chemistry Division, National Chemical Laboratory
Pune 411 008

Received 3 *December* 1987; *revised and accepted* 12 *February* 1988

The suppression of formation of silicon tetrachloride ($SiCl_4$), an unwanted by product, during the chemical vapour deposition of silicon by hydrogenation of trichlorosilane ($SiHCl_3$) in a Siemen's type reactor is possible by the control of the feed composition.

Currently, major proportion of high purity silicon is produced by Siemen's procedure involving chemical vapour deposition (CVD) from trichlorosilane $SiHCl_3$(TCS) onto hot silicon filaments in a bell jar type of reactor[1]. In this process only 30-35% of TCS is converted into silicon, 30-35% remains unreacted and the remaining gets converted into silicon tetrachloride $SiCl_4$ (STC)[2].

The formation of STC poses a big problem in the effluent disposal and since it is very pure it can not be treated as waste product. The recycling of STC which accounts for 40% of TCS feed is an important consideration in the overall economics of the silicon process. This can be done by converting STC into TCS by hydrogenation or by suppressing the formation of STC during the process by adjusting the feed composition.

While hydrogenation of STC to TCS has been studied by many groups[3–7], not much information is available on the suppression of STC formation. We have carried out extensive investigations on the suppression of STC formation in a Siemen's reactor, and the results are presented in this note.

Trichlorosilane(TCS) was prepared in the laboratory by reaction of Mg-silicon and dry HCl gas in a fluidised bed reactor. During the reaction, some amount of $SiCl_4$ was also formed.

A mixture of purified TCS, STC and H_2 in a desired ratio was passed through a laboratory type two-rod reactor made up of quartz bell jar (height, 60cm; diam, 100 mm) in which two silicon slim rods of 50 cm height were electrically heated at 1050°C. The STC:TCS ratio was controlled by controlling the temperature of STC and TCS bubbler and the rate of H_2 passing through the bubbler. Furthermore the feed rate of the gases was kept in such a way that the residence time of these gases in the reactor was adequate to let the system reach equilibrium. The effluent gases were condensed in the cold traps cooled at liquid nitrogen temperature and were subjected to gas chromatographic analysis after diluting with pure and chilled CCl_4. Silicon rods were weighed after completion of the reaction to know the amount of silicon deposited.

Thermodynamics and kinetics of hydrogenation of chlorosilanes has been studied extensively[8]. Thermodynamically, the species present at temperatures between 700 and 1300°C with significant partial pressure are $SiCl_4$, $SiHCl_3$, SiH_2Cl_2, SiH_3Cl, $SiCl_2$, HCl and H_2. Furthermore, the final equilibrium state of Si-H-Cl system is independent of original distribution of atoms among the species as long as the initial atomic ratios are same. Therefore, the Cl/H ratio in the feed, which remains constant for a reaction is used to define the gas phase composition of the Si-H-Cl system, and the Si/Cl ratio is used to represent the change in composition of the gas phase due to either depositing or etching of silicon during the chemical vapour deposition of silicon.

The Si-H-Cl equilibrium system[8] is illustrated in Fig. 1, which show the variation of the final silicon content of the gas phase (Si/Cl) with initial chlorosilane concentration (Cl/H) at various temperatures. However, when the effluent gaseous mixture is cooled down to room temperature or below, redistribution occurs amongst the silicon-containing spe-

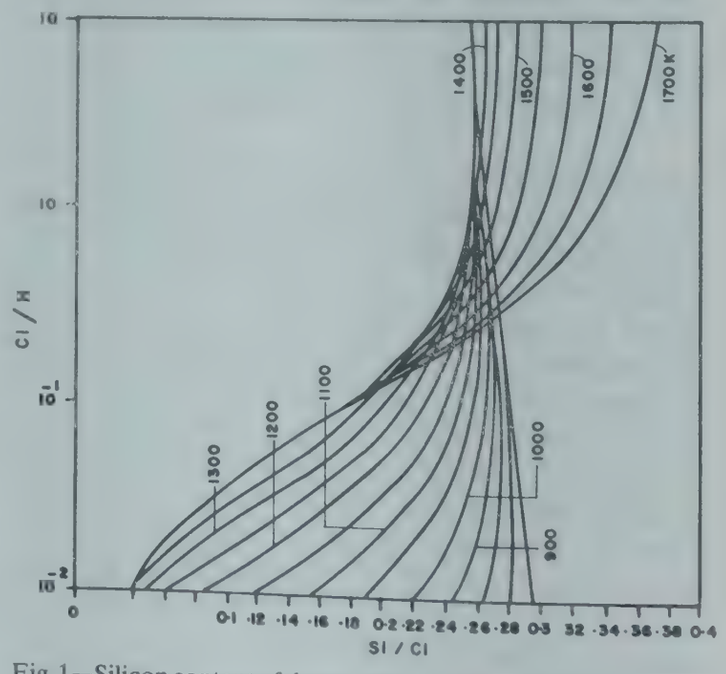

Fig. 1—Silicon content of the gas phase as a function of Cl/H ratio, at 1 atmosphere total pressure for 50° temperature increment (L.P. Hunt and Sirtil[8])

†NCL Communication No.4347

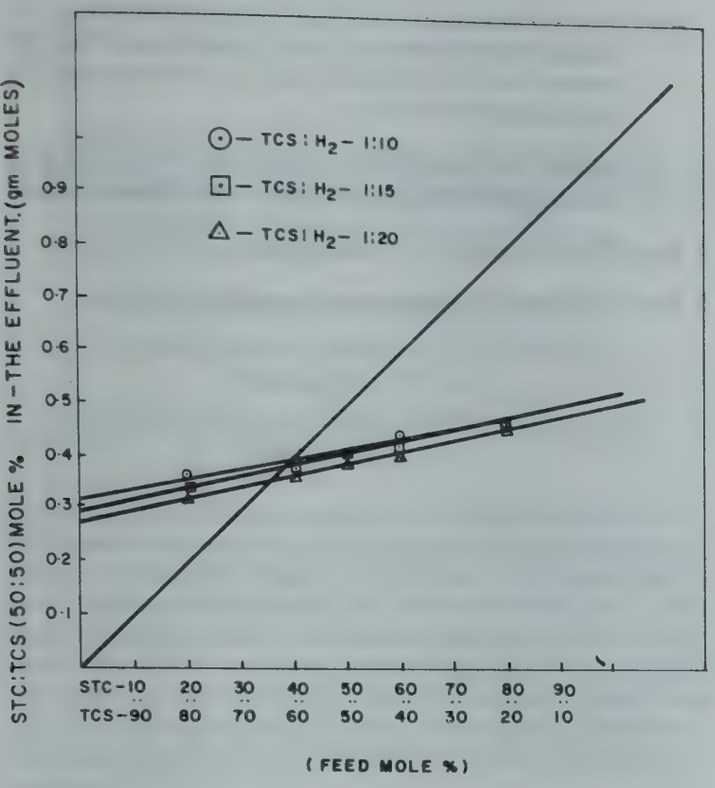

Fig. 2—(STC:TCS) mol % in the feed and effluent

Table 1—STC:TCS Composition to be fed for Various TCS:H_2 Ratios and for Various Temperatures

TCS:H_2 ratio	Temp (K)	STC:TCS ratio
1:10	1250	42:58
	1300	40:60
	1350	38:62
1:15	1250	40:60
	1300	38:62
	1350	35:65
1:20	1250	38:62
	1300	36:64
	1350	32:68

cies and the predominant ones found are only $SiCl_4$ and $SiHCl_3$ with less than 2% of SiH_2Cl_2. Furthermore, it is experimentally found that STC and TCS reach equilibrium with each other when present in the ratio in the vicinity of 1:1.

Equilibrium concentration of STC was calculated for various STC:TCS ratios using thermodynamic data. Cl/H ratio was calculated for various STC:TCS and TCS:H_2 ratios, and Si/Cl equilibrium values were calculated for different Cl/H ratios. The concentration of STC in equilibrium was calculated from the Si/Cl value for a particular Cl/H ratio, considering STC:TCS ratio of 1:1. The concentration of STC in the feed and in the effluent (equilibrium STC) were plotted for various TCS:H_2 ratios. It is observed that upto a certain concentration of STC in the feed, formation of STC in the effluent is observed, while for higher concentration of STC in the feed no formation

Table 2—Analytical Data of CVD Experiments by Cofeeding of STC with TCS

[Temp. = 1050°C; feed rate, 100 ml/hr.]

Parameter	Expt. 1	Expt. 2	Expt. 3	Expt. 4	Expt. 5
Feed					
STC (g)	229	287	387	391	287
TCS (g)	148	192	227	227	191
(STC:TCS mol %)	34:66	35:65	32:68	32:68	35:65
TCS:H_2 mol	1:10	1:10	1:10	1:10	1:9
Si yield (%) based on TCS	21%	26%	22%	21%	26%
Effluent					
STC (g)	108.5	197.5	251	290	169
TCS (g)	108.5	168.5	232	193	197
STC:TCS ratio	1:1	1:1.17	1:1.08	1:1.5	1:1.17

of STC is observed. At higher concentration of STC some amount of STC is in fact converted into Si and $SiHCl_3$. Thus there exists a composition of the feed where no additional formation of STC occurs. It may be noted that at this feed composition the overall efficiency of the reaction goes down if measured in terms Si (deposit)/STC + TCS (fed). However, the conversion efficiency in terms of TCS, i.e. Si(deposit)/TCS(fed) remains constant (35%) for all STC to TCS ratios. The particular ratio of STC:TCS where there is no formation and reduction of STC during the reaction, is calculated from the Fig. 2 where the curve (A) represents the equal concentrations of STC in the feed and the effluent. The point of intersection of this line with the other curves represents the concentration of STC to be fed alongwith TCS, so that the STC formation can be completely suppressed. The STC:TCS compositions to be fed, for TCS:H_2 ratio and for different temperatures are given in Table 1.

It is observed that based on thermodynamic calculations STC:TCS composition lies in the vicinity of 35:65% ± 5% for the various TCS:H_2 ratios and temperatures.

These conclusions are indeed borne out by the results of the experiments carried out. A summary of the results is given in Table 2. It may be seen that STC:TCS ratio in the effluent is in the range of 1:1, a fact which has been used in the above calculations and varies marginally when the composition of STC:TCS fed is changed. This is presumably because of formation of small amount of lower chlorosilanes. It is observed that the desired STC:TCS ratio is again in the vicinity of 35:65 ± 5% which agrees with the thermodynamically calculated results.

References

1 Yaws C L & Miller J W Jr, *Solid State Tech*, (1979) 63.

2 Rodgers M A & Tempe Ariz, *US Patent* 3,933,985, Jan 20, (1976).

3 Union Carbide Corporation, Final Report, DOE/JPL Contract No 954, 334, p 210, DOE Technical Information Centre, Springfield VA (1979).

4 Mui J P, Solar Electronics, Massachussetts Institute of Technology Final Report DOE/JPL Contract No 955 382 DOE Technical Information Centre, Springfield VA (1981).

5 McCornic J, Plahuthik F, Arvidson A, Sawyer D & Sharp K, Hemlock Semiconductor Corpn. Final Report DOE/JPL contract No. 955 533 DOE Technical Information Centre, Springfield VA (1982).

6 Neurgaonkar V G, Sinha A P B, Srivastava P R, Phadnis S B, & Pires J A 281/DEL/86, 25, 3, 86 (1986) [Indian Patent]

7 Ingle W M & Peffley M S, *J electrochem Soc*, (1985) 1236.

8 Hunt L P & Sirtl E, *J electrochem Soc*, **119** (1972) 1741.

Indian Journal of Chemistry
Vol. 27A, October 1988, pp. 905-906

Kinetics of Acid & Base Hydrolyses of *CIS*-(Formato/Acetato-(methylamine)bis-(ethylenediamine)cobalt(III) Ions

G C PRADHAN, R K NANDA* & A C DASH

Department of Chemistry, Utkal University, Bhubaneswar 751004

Received 7 *December* 1987; *revised and accepted* 1 *February* 1988

The aquation of the title complexes is strongly catalysed by H^+. The aquation occurs via spontaneous and H^+-catalysed paths. The base hydrolyses of both the complexes obey overall second order kinetics in the range of $[OH^-] = 0.05$-0.35 mol dm^{-3}. The formato complex reacts ~ 8 times faster than the acetato analogue under comparable conditions, which is fully consistent with the dissociative mode of activation of amido conjugate base involving Co – O bond heterolysis. High positive values of $\Delta S^{\neq}$ for the base hydrolysis path support the SN_1CB mechanism for the base hydrolysis.

Earlier we have reported on the kinetics of acid and base hydrolyses of *cis*-(oxalato)(amine)bis-(ethylenediamine)cobalt(III)[1]. As an extension, herein we report the results of investigations on the kinetics of acid and base hydrolyses of two new complexes *cis*-$[(en)_2Co(CH_3NH_2) \cdot O_2CR]^{2+}$, (R = H, CH_3).

cis-(Formato)(methylamine)bis(ethylenediamine)-cobalt(III) nitrate *cis*-$[(en)_2Co(CH_3NH_2)(HCO_2)] \times (NO_3)_2$, was prepared starting from *cis*-(chloro)(methylamine)bis(ethylenediamine) cobalt(III) chloride, which was prepared as described in the literature[2,3]. The crude product was recrystallised from HCl and then converted into the dinitrate by recrystallising from HNO_3; *cis*-$[(en)_2Co(CH_3NH_2)OH_2](NO_3)_3$ was generated by reaction with calculated amount of $AgNO_3$ solution. The solution of aquo complex was treated with lithium formate/formic acid buffer ($pH \simeq 4$) (ten times excess over the aquo complex) and heated at 60°-70°C for several hours and concentrated to a small bulk. On cooling in an ice bath the desired formato complex was obtained as red crystals, which were filtered, washed with ice-cold ethanol followed by diethyl ether. The product was recrystallised from HNO_3 and finally from water to yield the pure product (Found: C, 19.02; H, 4.9; N, 25.6; Co, 15.4. Reqd: C, 19.0; H, 4.8; N, 25.8; Co, 15.6%).

cis-(acetato)(methylamine)bis(ethylenediamine)-cobalt(III)perchlorate, *cis*-$[(en)_2Co(CH_3NH_2)(O_2CCH_3)](ClO_4)_2$, was prepared adopting a similar procedure as above using lithium acetate/acetic acid buffer. But the complex was isolated as perchlorate salt by adding ice-cold 60% perchloric acid to the ice-cold concentrated slurry. The crude product was recrystallised from $HClO_4$ and finally from water to obtain the pure product (Found: C, 16.6; H, 5.2; N, 14.7; Co, 12.4. Reqd: C, 17.9; H, 5.2; N, 14.9; Co, 12.6%).

All the chemicals used were of AR grade and all solutions were prepared in doubly distilled water. The kinetics of acid and base hydrolyses were followed spectrophotometrically at 500 nm by the batch sample technique as described earlier[1]. An UV-visible spectrophotometer (Elico) was used to measure the absorbance. The pseudo-first order rate constants were calculated from the gradients of the plot of $\log (A_t - A_\infty)$ versus time. The (carboxylato)(methylamine)bis(ethylenediamine)cobalt(III) cations display two ligand field bands at 490 and 350 nm corresponding to $^1T_{1g} \leftarrow {}^1A_{1g}$ and $^1T_{2g} \leftarrow {}^1A_{1g}$ transitions [λ_{max}(nm)(ε_{max}, dm^{3}mol^{-1}cm^{-1}):493(114), 348(79) (formato complex), and 492(130), 350(116) (acetato complex)]. Based on the method of preparation and their UV-visible spectral data we presume that the complexes have been isolated as the *cis*-isomers.

The rate data are collected in Tables 1 and 2. The rate of aquation of both the complexes is strongly catalysed by H^+ ion and the pseudo-first order rate constants fit Eq. (1) satisfactorily.

$$k_{obs} = k_0 + k_H[H^+] \qquad \ldots(1)$$

where k_0 and k_H denote the rate constants for the spontaneous aquation and acid-catalysed aquation respectively as represented by Eqs (2) and (3).

$$[(en)_2Co(NH_2CH_3)O_2CR]^{2+} \xrightarrow[H_2O]{k_0} [(en)_2Co(NH_2CH_3)(OH_2)]^{3+} + RCO_2 \qquad \ldots(2)$$

$$[(en)_2Co(NH_2CH_3)O_2CR]^{2+} + H^+ \xrightarrow[H_2O]{k_H} [(en)_2Co(NH_2CH_3)OH_2]^{3+} + RCO_2H \qquad \ldots(3)$$

Values of k_0 and k_H were obtained by fitting the pseudo-first order rate constants at different $[H^+]$ to Eq. (1) by a least squares computer programme adopted to an IBM 1130 computer. It may be noted that strong acid catalysis for both the complexes precludes evaluation of k_0 more precisely. The acetato complex undergoes acid-catalysed aquation faster than the formato complex. This is attributed to the higher proton affinity of the coordinated acetate group as compared to that of formate. The activation parameters for k_H path (see Table 3) are comparable with similar data

Table 1—Rate Data for Acid Hydrolysis of *cis*-$[(en)_2Co(NH_2CH_3)O_2CR]^{2+}$ (R = H, CH_3):
(I = 1.0; $[complex]_T$ = 0.003 mol dm^{-3})

$[HClO_4]_T$ mol dm^{-3}	$10^4 k_{obs}(s^{-1})$[a]			
	60°	65°	70°	75°.0 ± 0.1°C
0.05	0.13(0.15)	0.22(0.30)	0.22(0.63)	0.34(0.86)
0.20	0.38(0.50)	0.45(0.85)	0.90(1.65)	1.38(2.12)
0.40	0.65(0.90)	0.91(1.60)	1.69(2.96)	2.54(3.60)
0.60	0.92(1.24)	1.24(2.35)	2.67(4.26)	3.93(5.25)
0.80	1.22(1.65)	1.73(3.05)	3.62(5.62)	5.17(7.01)
1.0	1.54(2.06)	2.08(3.80)	4.58(6.87)	6.73(8.57)
$10^4 k_0(s^{-1})$	0.06 ± 0.01(0.08 ± 0.02)	0.09 ± 0.03(0.12 ± 0.01)	−0.05 ± 0.05(0.32 ± 0.02)	−0.02 ± 0.08(0.44 ± 0.05)
$10^4 k_H$ ($dm^3 s^{-1} mol^{-1}$)	1.46 ± 0.02(1.98 ± 0.03)	1.99 ± 0.05(3.68 ± 0.02)	4.59 ± 0.08(6.58 ± 0.03)	6.62 ± 0.13(8.12 ± 0.09)

[a] Values in parentheses are for acetato complex.

Table 2—Rate Data for Base Hydrolysis of *cis*-$[(en)_2Co(NH_2CH_3) . O_2CR]^{2+}$ (R = H, CH_3)
(I = 0.5 mol dm^{-3}; $[complex]_T$ = 0.003 mol dm^{-3})

$[OH^-]_T$ (mol dm^{-3})	$10^4 k_{obs}$, (s^{-1})[a]				
	5°	10°	15°	20°	25.0 ± 0.2°C
0.05	0.54	1.27	2.99	8.02(0.83 ± 0.1)	(1.29 ± 0.01)
0.10	0.93	1.93	6.43	16.19(1.65 ± 0.4)	(2.62 ± 0.03)
0.20	1.85	4.14(0.38)	12.86(1.52 ± 0.05)	26.01(3.23 ± 0.33)	(6.01 ± 0.29)
0.25		(0.72)	(1.64 ± 0.05)		
0.30	2.70	6.49(0.61)	20.86(1.85 ± 0.64)	42.4(5.16 ± 0.52)	(9,95 ± 0.9)
0.35		(1.07)	(2.37 ± 0.33)		
$10^4 k_{oH}$ ($dm^3 mol^{-1} s^{-1}$)	9.61 ± 0.86	21.78 ± 1.7(2.5 ± 0.6)	64.48 ± 3.9(6.8 ± 0.6)	166.33 ± 6.20(16.6 ± 0.4)	(28.7 ± 3.5)

[a] Values in parenthesis are for acetato complex.

Table 3—Activation Parameters for Acid and Base Hydrolyses of *cis*-$[(en)_2Co(NH_2CH_3)O_2CR]^{3+}$ (R = H, CH_3)

	R = H		R = CH_3	
	$\Delta H^{\neq}$ (kJ mol^{-1})	$\Delta S^{\neq}$ ($JK^{-1}mol^{-1}$)	$\Delta H^{\neq}$ (kJ mol^{-1})	$\Delta S^{\neq}$ ($JK^{-1}mol^{-1}$)
k_H-path	101 ± 13	−18 ± 40	90 ± 12	−45 ± 36
k_{OH}-path	129 ± 3	+160 ± 12	116 ± 19	+97 ± 67

for other carboxylatopentaaminecobalt(III) complexes[4].

The base hydrolysis reaction obeys second order kinetics and the pseudo-first order rate constants are given by Eq. (4)

$$k_{obs} = k_{OH}[OH^-] \quad \ldots(4)$$

from which the second order rate constants were calculated. These are collected at various temperatures in Table 2.

It is worth noting that the formato complex undergoes base hydrolysis ≃ 8 times faster than the corresponding acetato complex. In the light of SN_1CB mechanism, the observed rate difference reflects that formate as a leaving group is better than the acetate group. The values of activation entropies are substantially positive, and activation enthalpies are also resonably high. These are comparable to the available activation parameter data for carboxylatopentaamminecobalt(III) complexes for which a mechanism involving heterolysis of Co − O bond has been suggested. Thus the observed leaving group effect and the activation parameter data reveal that the base hydrolysis of the complexes under investigation involves SN_1CB mechanism , in which Co − O heterolysis is the rate-limiting step.

The authors are grateful to the authorities of CDRI Lucknow for the C, H and N analytical data.

References

1 Dash A C & Nanda R K, *J inorg nucl chem*, **36** (1974) 2071.

2 Bailar J C & Clapp L B, *J Am chem Soc*, **67** (1945) 171.

3 House D A, *J chem Edn*, **53** (1976) 125.

4 House D A, *Coord Chem Rev*, **23** (1977) 223.

Indian Journal of Chemistry
Vol. 27A, October 1988, pp. 907-908

Heterolysis of *o*-(α-Hydroxyalkyl)-4-cyanophenyl Nitrite: Simultaneous Polar & Steric Effects

V JAGANNADHAM*† & S STEENKEN
Max-Planck-Institut Fuer Strahlenchemie, D-4330 Muelheim, West Germany

Received 9 *October* 1987; *accepted* 8 *February* 1988

The heterolysis rates of the adducts [4-$CNC_6H_4N(\dot{O})OCH(OH)R_D$], produced pulse-radiolytically in aqueous solution from 4-nitrobenzonitrile (4-NBN) and substituted (R_D) α-hydroxyalkyl radicals have been measured spectrophotometrically following the build-up kinetics of radical anion, $CNC_6H_4NO_2^{\cdot-}$ (λ_{max} 330 nm). Taft linear polar energy relationship is applicable for only non-branched R_D's ($r = 0.988$) while branched R_D's deviate much from linearity. The reason for this is discussed in terms of Pavelich-Taft four-parameter equation assuming that both polar and steric interactions are operative on rates of heterolysis.

Nitro aromatics, which are used as radiation-sensitizers[1], have been often reduced by the radicals derived from alcohols[1a,2] and molecules of biological importance[1b,c,d]. It has been shown that the redox process of α-hydroxyalkyl radicals and nitro aromatics proceeds by an addition/elimination mechanism[1a,2]. In our earlier work[1a] it was shown that Taft linear polar energy relationship could be successfully applied to non-branched alkyl groups. In the present note are presented results on the successful application of Pavelich-Taft four-parameter equation[3] on heterolysis rates for the title radical.

All the compounds used were commercially available and used as such. All the experimental details have been described elsewhere[1a].

The reactions of RĊHOH with nitrobenzenes were studied using *in situ* radiolysis spectroscopic method. RĊHOH radicals were produced by H-abstraction from the corresponding alcohols by OH radicals generated by irradiation of N_2O-saturated aqueous solutions containing 0.1 to 2 mol dm^{-3} alcohol. The reactions of RĊHOH with 4-nitrobenzonitrile (4-NBN) took place via an intermediate adduct[1a] (the title compound) formed bimolecularly (k_R) which decomposed unimolecularly (k_s, s^{-1}) to give final products, i.e. $4\text{-}CNC_6H_4NO_2^{\cdot-}$, RCHO and H^+. It was shown[1a] by time-resolved spectroscopic technique that the adduct [4-$CNC_6H_4N(O)OCH(OH)R_D$] absorbed at 310 nm and $4\text{-}CNC_6H_4NO^{\cdot-}$ absorbed at 330 nm. The k_R values were found to be more or less same with all the alcohols studied within experimental error. Whereas the k_s values for non-branched R_D's followed the Taft relationship[1a] and the branched R_D's deviated much from linearity (Fig. 1, plot of log k_s versus σ*, —open circles). However, Pavelich-Taft equation[3] was found to be applicable to the rate data. Using the method of solving the simultaneous equations[4] the kinetic results for all the nine alcohols studied presently could be fitted well into Eq. (1)[4] with $\rho^* = -6.37 \pm 0.375$, $\delta = 0.65 \pm 0.033$ and log $k_0 = 4.08 \pm 0.088$ (standard deviation for entire correlation was ± 0.120).

$$\log k = \rho^* \sigma^* + \delta E_s + \log k_0 \qquad \ldots(1)$$

In Eq. (1) k and k_0 are the heterolysis rate constants of the adducts with substituted alkyl groups, i.e. different R_D's and for $R_D = CH_3$ respectively. σ* and E_s are the polar and steric substituent constants and ρ* and δ are reaction constants for the same two effects respectively.

The plot of log k versus σ* was non-linear (Fig. 1, $r = 0.92$). Hence, the value of (log $k - \delta E_s$) were plotted against σ* which gave a good linear plot (Fig. 1, $r = 0.985$), showing the presence of both polar and steric effects on the heterolysis of the adducts (k_s). The four-parameter equation (Eq. 1) was successfully applied earlier in some condensation reactions[5] and in chromic acid oxidations[6].

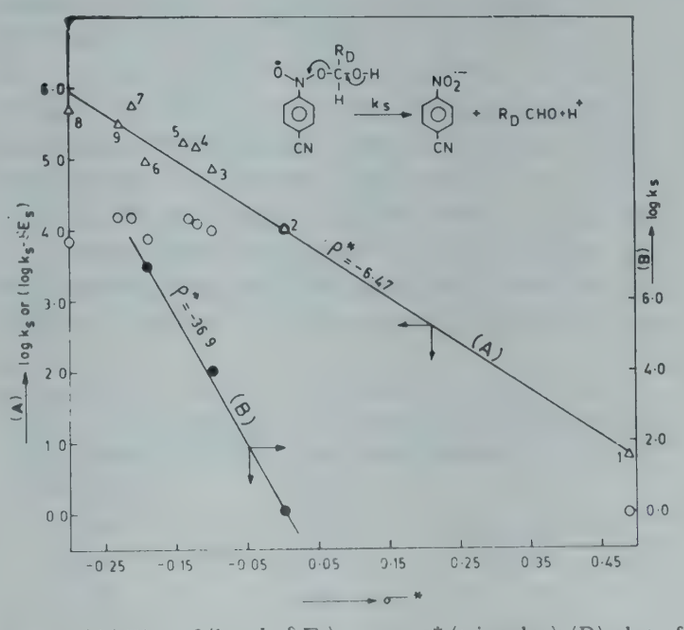

Fig. 1—(A) Plot of (log k_s-δE_s) versus σ* (triangles); (B) plot of log k_s versus σ* (closed circles)

†Department of Chemistry, Nizam College (Osmania Universty), Hyderabad 500 001.

Table 1—Effect of Substitutents (R_D) on Rate Constants[a] (k_s) for Heterolysis of 4-$CNC_6H_4N(\dot{O})OCH(OH)R_D$

Sl No.	R_D	k_s (s^{-1})	σ*(b)	E_s[b]	log k_s	log $k_s - \delta E_s$
1	H	1.00×10^0	0.49	−1.24	0.00	0.810
2	CH_3	1.00×10^4	0.00	0.00	4.00	4.00
3	C_2H_5	1.00×10^4	−0.10	−1.31	4.00	4.85
4	*n*-Pr	1.30×10^4	−0.12	−1.60	4.11	5.15
5	*n*-Bu	1.40×10^4	−0.13	−1.63	4.15	5.21
6	*i*-Pr	7.10×10^3	−0.19	−1.71	3.85	4.96
7	*s*-Bu	1.50×10^4	−0.21	−2.37	4.18	5.72
8	*t*-Bu	7.00×10^3	−0.30	−2.78	3.85	5.66
9	$(Et)_2CH$	1.60×10^4	−0.23	−1.98	4.20	5.49

[a] N_2O-saturated aqueous solutions. [alcohol] = 0.1-1 mol dm^{-3}, [4-NBN] = 1 mmol dm^{-3}, *p*H = 4-5, temp = 293 K.
[b] *σ and E_s values are from: Hansch C & Leo A, *Substituent constants for correlation analysis in chemistry & biology*" (Wiley-Interscience, New York), 1979.

Another important and relevant aspects of the heterolysis of the adducts is that the adduct derived from 4-NBN and CH_2OH decomposes (k_s) at a rate of 1.00 s^{-1}. When one of the H atoms of CH_2OH is replaced by a CH_3 group, e.g. $CH_3\dot{C}HOH$ the k_s value is 1.00×10^4 s^{-1} and when $CH_3\dot{C}HOH$ is changed to $(CH_3)_2\dot{C}OH$ then k_s value[1a] is 1.00×10^7 s^{-1}. This indicates that the change of substitutent at carbon alpha to OH in alcohol radical moiety of the adduct changes the heterolysis rate constant derastically. This is clear from the Taft ρ*-value for the decomposition of the adducts $4\text{-}CNC_6H_4N(\dot{O})OC(OH)R_1R_2$ (where $R_1 = R_2 = H$, $R_1 = H$, $R_2 = CH_3$ and $R_1 = R_2 = CH_3$), which was found to be -36.9 ± 2.25 ($r = 0.999$, Fig. 1). This is not the case with adducts of 4-NBN and other alcohol radicals where the ρ* is only -6.37 ± 0.375. This may be due to the fact that the change in the substituent is only due to R_D and the hydrogen alpha to OH is not changed in the adduct (Table 1).

V J is thankful to Max-Planck-Institut for their hospitality.

References

1 (a) Jagannadham V & Steenken S, *J Am chem Soc*, **106** (1984) 6542; and references cited therein.
(b) Jagannadham V & Steenken S, *J Am chem Soc*, (1987) (In press).
(c) Jagannadham V & Steenken, *J Phys Chem* (in press), 1987.
(d) Steenken S & Jagannadham V, *J Am chem Soc*, **107** (1985) 6818.

2 McMillan M & Norman R O C, *J chem Soc B* (1968) 590.

3 Pavelich W A & Taft (Jr) R W, *J Am chem Soc*, **79** (1957) 4935.

4 For solving the simultaneous equations see the appendix at the end of ref. 3.

5 Jagannadham V, Sethuram B & Naveneeth Rao T, *Curr Sci*, **46** (1977) 704.

6 Reddy P M, Jagannadham V, Sethuram B & Navaneeth Rao T, (a) *Z phys Chem*, **127** (1981) 251; (b) *Bull Soc Chim Belg*, **91** (1982) 707.

Indian Journal of Chemistry
Vol. 27A, October 1988, pp. 909-911

Iodide-induced Debromination of Cinnamic Acid & Substituted Cinnamic Acid Dibromides in 2-Methoxyethanol

K SUBRAMANIAN & I M MATHAI*
Department of Chemistry,
Madras Christian College, Madras 600059

Received 12 *August* 1987; *revised* 23 *December* 1987; *accepted* 20 *January* 1988

The second order rate constants for the iodide-induced debromination of cinnamic acid and substituted cinnamic acid dibromides in 2-methoxyethanol are reported; the reactivities follow the order: p-OCH_3 > o-CH_3 > p-CH_3 > p-NO_2 > p-Cl > m-NO_2 > −H > m-CH_3 > m-OCH_3 > o-Cl. The m-CH_3 and p-Cl derivatives have higher enthalpies and lower negative entropies of activation whereas methoxy substituted derivatives are characterised by lower enthalpies and higher negative entropies of activation than the unsubstituted acid. The free energy of activation is nearly constant.

Iodide-induced dehalogenation of vicinal dibromides has been reviewed by Saunders and Cockerill[1]. Baciocchi *et al.*[2] reported that both electron-attracting p-NO_2 and electron-releasing p-OCH_3 substituents increased the rate of debromination in *meso*-stilbene dibromide. But in the debromination of cinnamic acid dibromides by iodide-ion in 80% aqueous acetic acid, *para*- and *meta*-nitro substituents reduced the rate while p-OCH_3 group increased the rate considerably[3]. Studies on iodide-induced debromination of cinnamic acid dibromides in 2-propanol indicated that the substituents at *meta*- and *para*-positions facilitated the reaction to a small extent; but the electron-attracting and electron-releasing *ortho*-substituents retarded and accelerated the reaction, respectively[4]. These conflicting reports in different systems prompted us to take up the title investigation to understand the effects of structure of the substrates and the nature of the solvent on debromination kinetics.

2-Methoxyethanol (BDH), a protic solvent was rendered anhydrous and distilled before use. Sodium iodide (E. Merck) was dried at 150°C for 12 hr and stored in a desiccator. Cinnamic acid (BDH) was recrystallised before use while substituted cinnamic acids were prepared from the corresponding substituted benzaldehydes by Knoevenagel reaction. The dibromides were prepared by the addition of bromine to cinnamic acids in chloroform, purified by crystallisation and the purity checked (PMR, elemental analyses and melting points). The dibromides were of the *erythro* type, as revealed by their PMR spectra.

The dibromides (0.004 mol) were mixed with sodium iodide (0.04 mol) in 2-methoxyethanol at 323 K. The reaction mixture was kept for one week in dark coloured reaction bottle and the iodine liberated was titrated against sodium thiosulphate. The extent of debromination as revealed by the liberated iodine value, was found to be 95.1 ± 1.5%. Further under the experimental conditions iodine was not consumed by the solvent; also solvolysis of the cinnamic acid dibromides and addition of iodine to the unsaturated acids were not observed. Cinnamic acid, and p-nitro- and p-methoxy-cinnamic acids were the reaction products in the debromination of corresponding acid dibromides.

The kinetics of the reaction was followed titrimetrically. A stoichiometry of 1:3 (substrate: iodide ion) was established and hence in all kinetic runs, five-fold excess of iodide ions was used. The overall reaction may be represented by Eq. (1).

$$R-CHBr-CHBr-COOH + 3I^- \rightarrow R-CH=CH-COOH + I_3^- + 2Br^- \quad \ldots (1)$$

The second order rate constants varied only within the experimental error (± 3%). The reaction was found to be first order each in the reactant (Table 1). The specific rate constants and activation parameters are presented in Table 2. The observed order of reactions, viz. p-OCH_3 > o-CH_3 > p-CH_3 > p-NO_2 > p-Cl > m-NO_2 > −H > m-CH_3 > m-OCH_3 > o-Cl can be explained by hyperconjugation, inductive and mesomeric effects. The presence of groups like o-CH_3 and p-CH_3 stabilises the developing double bond in the transition state by hyperconjugative effect, whereas the electron-releasing p-OCH_3 and p-Cl stabilises the incipient double bond through conjugation. The

Table 1 – Debromination of Cinnamic Acid Dibromide by Sodium Iodide in 2-Methoxyethanol at 308K.

10^3 [substrate] (mol dm^{-3})	10^2 [NaI] (mol dm^{-3})	10^3 k_2 (mol^{-1} dm^3 s^{-1})
6.59	6.61	1.16
6.59	8.34	1.18
5.27	5.29	1.15
3.84	5.29	1.16

Table 2 – Specific Rate Constants and Activation Parameters of the Systems Investigated
(X – C_6H_4 – CHBr – CHBr – COOH)

X	$10^4\ k_2$ (dm^{3}mol^{-1}s^{-1})				$\Delta H^{\neq}$ (kJ mol^{-1})	$\Delta S^{\neq}$ (JK^{-1} mol^{-1})	$\Delta G^{\neq}$ (kJ mol^{-1})
	303K	308K	313K	318K			
H	7.65	11.6	18.8	29.9	70.3	−73.4	92.8
o-Cl	4.72	7.38	12.2	17.5	67.9	−84.7	94.0
p-Cl	8.37	15.1	20.8	34.9	70.8	−69.5	92.1
o-CH_3	18.5	26.5	40.2	55.0	56.2	−112	90.7
m-CH_3	6.13	9.68	15.9	25.6	73.6	−63.9	93.3
p-CH_3	13.0	19.2	29.0	42.4	60.5	−101	91.6
m-NO_2	7.51	12.5	16.4	25.8	60.8	−104	92.6
p-NO_2	10.5	17.2	23.9	37.7	63.7	−91.3	91.8
m-OCH_3	5.81	9.37	11.5	17.2	52.6	−133	93.4
p-OCH_3	26.2	39.8	52.6	75.2	52.3	−122	89.7

mesomeric effect of *p*-NO_2 group enhances the stability of the transition state. The *m*-CH_3 and *m*-OCH_3 groups influence the rate nearly to the same extent at 308K. Further, in the case of $-NO_2$, $-OCH_3$ and $-CH_3$ substituted dibromo acids, *para* compounds react faster than the *meta* ones. In these cases mesomeric effect seems to be the controlling factor for the stabilisation of the incipient double bond in the transition state.

As compared to the parent acid, the $\Delta H^{\neq}$ values are lower for *o*-CH_3, *p*-CH_3 and *p*-OCH_3 substituted acids. This is due to conjugative stabilisation in the transition state and due to the ease of cleavage of the C – Br bond. The low $\Delta H^{\neq}$ value in the case of *p*-nitro-cinnamic acid dibromide may be due to conjugative stabilisation alone. The influence of *m*-OCH_3, *m*-NO_2 and *o*-Cl substituents on $\Delta H^{\neq}$ cannot be explained satisfactorily.

The variation of $\Delta S^{\neq}$ values can be explained by considering the solvation of the substrate and transition state. The iodide ion and the substrates are solvated in protic solvent via H-bond. Partial desolvation of I^- and substrate has to occur to form the transition state. The substituents alter the polarisation of the C_β – Br bond to different extents and in turn affect the solvation of the transition state. In the *anti*-elimination, the transition state is planar and hence the formation of C = C and the cleavage of C_β – Br bond occur in a concerted manner. The electron-releasing substituents like *o*-CH_3, *p*-CH_3 and *p*-OCH_3 help in cleaving the C_β – Br bond to an extent comparatively larger than that in the parent dibromide and thus increase the electron density on the β-bromine. As a result, solvation of the transition state by H-bonding in these substituted dibromides occurs to a larger extent and makes the entropy of activation more negative than the parent

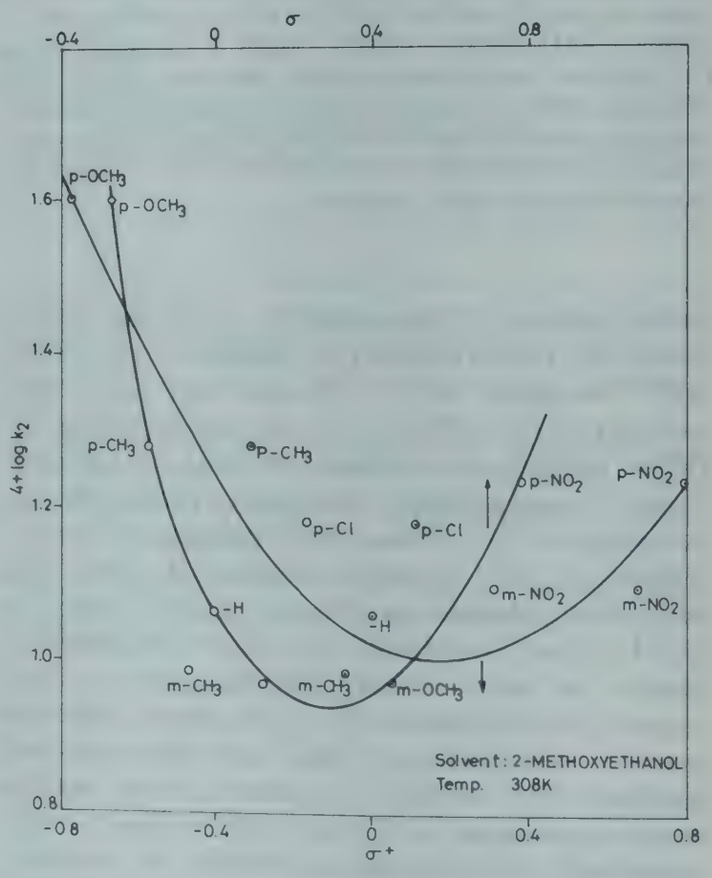

dibromide. The opposite effect will be seen due to the presence of electron-attracting substituents. However, the observed entropy of activation in the case of *m*-OCH_3 substituted acid, cannot be explained satisfactorily.

The variation of $\Delta G^{\neq}$ values with the substituents is not much ($\Delta G^{\neq} = 92.2 \pm 1.02$ kJ mol^{-1}). This is due to the fact that factors responsible for lower $\Delta H^{\neq}$ and more negative $\Delta S^{\neq}$ values are operating in opposite direction, thus rendering $\Delta G^{\neq}$ values almost constant and consequently the variation in rate is not significant. The plot of

$\Delta H^{\neq}$ versus $\Delta S^{\neq}$ is linear ($r=0.988$), indicating the operation of the same mechanism in all the substrates. The plot of $\log_{10} k_2$ (308 K) versus σ or σ^+ is not linear and a curve with a minimum is obtained (Fig. 1). Similar Hammett curve was obtained by Nasielski *et al.*[5]. This behaviour can be due to the high polarisability of the transition state.

The second order kinetics and formation of *anti*-debromination product, in the debromination of dibromides studied, indicate the possibility of E2-elimination reaction. In the reaction, the attack of iodide ion can take place at either α- or β-Br. Since the carboxyl group is more electron-attracting than phenyl group, α-bromine becomes more electrophilic than β-bromine and hence the attack of I^- at α-bromine. This is consistent with the departure of Br^- from $C_\beta - Br$. One can envision a "spectrum" of transition states, ranging from the "El-like" (I) in which $C_\beta - Br$ bond is appreciably stretched, through the synchronous E2 (II) in

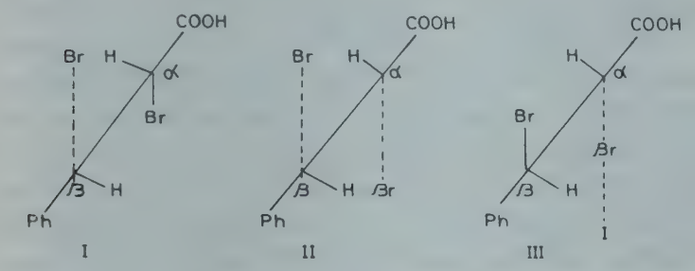

which both the carbon-halogen bonds are stretched to about the same extent, and finally to the "EICB-like" (III) in which only the $C_\alpha - Br$ bond is appreciably stretched. The type III possesses carbanion character at the α-carbon and should be stabilised by electron-attracting substituents. The experimental results show that electron-attracting groups such as $m-OCH_3$ decrease while electron-releasing groups enhance the reaction rate. Hence the transition state (III) is less favourable in the reaction studied. The increase in reactivities of p-NO_2 and m-NO_2 substituted cinnamic acid dibromides as compared to unsubstituted dibromo acid cannot be due to the operation of EICB-like mechanism, since the groups are far away from the α-carbon. The nitro group stabilises the incipient double bond in the transition state to a greater extent compared to that in the unsubstituted cinnamic acid dibromide by mesomeric effect. Hence in the case of p-NO_2, m-NO_2 and other substituted cinnamic acid dibromides, the reaction proceeds by the transition state which lies between "El-like" (I) and E2 (II).

The financial assistance from the UGC, New Delhi is gratefully acknowledged.

References

1 Saunders Jr W H & Cockerill A F, *Mechanism of elimination reactions* (John Wiley, New York) 1973, 332.

2 Baciocchi E & Schiroli, *J Chem Soc*, (1969) 554.

3 Ibne Rasa K M, Ahmed Ashfag & Amir Ud Din, *J Sci Res* (Lahore) **3** (1968) 1.

4 Philip V J, Ph.D. Thesis, University of Madras, India (1979).

5 Nasielski J & Guietle-Limbourg V, *Bull Soc Chim Belges*, **81** (1972) 351.

Indian Journal of Chemistry
Vol. 27A, October 1988, pp. 912-913

Organotin(IV) Complexes of Arylazopyridines

A K KUMAR & T K CHATTOPADHYAY*
Department of Chemistry, University of North Bengal, Darjeeling 734 430
and
E RIVAROLA
Institute of General Chemistry, University of Palermo, Italy

Received 29 *September* 1987;
revised and accepted 29 *February* 1988

A few mono- and di-organotin(IV) complexes of the ligand 4-(2-pyridylazo)-N,N-dimethylaniline have been prepared and characterised by elemental analysis, infrared, ^{119}Sn Mössbauer and electronic spectral studies. All the compounds have 1:1 stoichiometry and distorted octahedral structures in the solid state.

Transition metal complexes of 2-(arylazo)pyridines have recently been reported[1]. Transition metal and organotin complexes of 2,2′-azopyridine and related molecules have also been investigated[2-4]. However, organotin complexes of arylazopyridines have not been reported. As part of a research programme on the study of organotin complexes of pyridylazo derivatives we present in this note synthesis and characterisation of some mono- and di-organotin(IV) complexes of 4-(2-pyridylazo)-N,N-dimethylaniline.

The ligand 4-(2-pyridylazo)-N,N-dimethylaniline(L) was an Aldrich reagent and was used as such.

The organotin derivatives were prepared in about 90% yields by mixing equimolar benzene solutions of the reactants with stirring, at room temperature and by filtering off the resulting intensely coloured solids. Recrystallisation from benzene and petroleum ether (60-80) afforded coloured crystalline products.

A Pye Unicam SP3-300S IR spectrophotometer was used to record the IR spectra of the complexes in nujol in the region 4000-200 cm^{-1}. Electronic spectra were recorded on a Shimadzu model UV-240 spectrophotometer. ^{119}Sn Mössbauer spectra were recorded at liquid nitrogen temperature at the Institute of General Chemistry, University of Palermo, Italy; the apparatus and techniques were the same as reported earlier[4].

The analytical data of the organotin adducts along with their melting points are summarized in Table 1. In the IR spectrum of the ligand, the $\nu(N=N)$ mode is assigned at 1560 cm^{-1} by comparing the spectrum of the ligand (L) with that of 2-phenylazopyridine[1]. In the adducts, $\nu(N=N)$ is lowered by ~30 cm^{-1} indicating coordination by the azo group[1]. Pyridine breathing mode in L is identified at 989 cm^{-1} which is raised to ~1000 cm^{-1} in the complexes indicating coordination by the pyridine N-atom[5]. It is difficult to assign unambiguously vibrations due to $\nu(Sn-Cl)$ and $\nu(Sn-C)$ modes because of the presence of ligand bands in the 600-200 cm^{-1} region. However, a broad doublet appearing below 350 cm^{-1} for all the adducts, which is lowered by ~100 cm^{-1} on going from the organotin halides to the organotin derivatives of the ligand, is tentatively assigned to $\nu(Sn-Cl)$ mode. On the other hand, both ν_s and $\nu_{as}(Sn-C)$ modes remain, as expected[6], rather unaltered in the complexes relative to their positions in the organotin components. Occurrence of both ν_s and $\nu_{as}(Sn-C)$ in $R_2SnCl_2.L$ suggests that the SnC_2 group is not perfectly linear[6].

^{119}Sn Mössbauer spectral data of the complexes are collected in Table 2. The isomer shift (IS) values are typical of quadrivalent tin in inorganic and organometallic compounds and confirm the presence of six-coordinated tin in each species[4]. The values decrease with the progressive substitution of electronegative chlorine indicating a decrease in *s*-electron density at the tin atom for the $RSnCl_3.L$ adducts as compared to the $R_2SnCl_2.L$ compounds. The decrease further indicates lesser covalency of the $Sn-C$ bonding in $RSnCl_3.L$ in consequence of a poorer overlap between the sigma bond of the ligand and the sp^3d^2 hybrid orbital of the metal atom. The spectra show the characteristic doublet structures associated with molecules having a symmetry lower than O_h or T_d with one or more $Sn-C$ bonds. The full width at half maximum values generally lie around 0.9 $mm\,sec^{-1}$ and are characteristic of a single tin site. The magnitudes of the quadrupole

Table 1—Analytical Data of the Complexes

Compound (m.p., °C)	Found (Calc), %			
	C	H	N	Sn
$PhSnCl_3.L$ (200)	45.42 (43.11)	4.01 (3.59)	9.36 (10.59)	—
$BuSnCl_3.L$ (179)	39.35 (40.12)	4.44 (4.52)	10.21 (11.01)	24.31 (23.34)
$Ph_2SnCl_2.L$ (209)	53.81 (52.62)	3.91 (3.51)	9.08 (9.82)	21.15 (20.82)
$Me_2SnCl_2.L$ (186)	40.85 (40.36)	5.05 (4.48)	11.85 (12.56)	—

Table 2—Mössbauer & Electronic Spectral Data of the Complexes

Compound	I.S. ($mm\,sec^{-1}$)	Q.S. ($mm\,sec^{-1}$)	$\Gamma \pm$ ($mm\,sec^{-1}$)	λ_{max}, nm($\varepsilon \times 10^{-4}$)	
				Benzene	Methanol
L	—	—	—	418 (3.04)	435 (2.97)
$SnCl_4$.L	—	—	—	418 (sh), 600 (3.00)	435, 540
$PbSnCl_3$.L	0.89	1.60	1.08	420 (sh), 575 (2.95)	435, 540
$BuSnCl_3$.L	1.04	1.77	0.79	420 (0.67), 565 (2.54)	430 (sh), 540
Ph_2SnCl_2.L	1.32	3.47	0.87	418 (2.30), 555 (sh)	435, 540
$MeSnCl_2$.L	1.42	3.79	0.87	418 (2.75), 555 (sh)	435, 540

splitting (QS) for $RSnCl_3$.L are also consistent with six-coordinated structures but in the absence of XRD study, it is impossible to discriminate between $Sn-Cl_3$ facial or meridional arrangements. The QS parameters of R_2SnCl_2.L adducts are also typical of octahedral geometry. The values, twice as large as that observed for the mono-organotin(IV) compounds, are indicative of *trans*-octahedral configuraton[4] of the two organic groups although the $C-Sn-C$ bond angle is distorted from perfect linearity as demonstrated by IR frequencies.

Electronic spectral data of the organotin compounds in the visible region also support these structural propositions (Table 2). The longest wavelength transition of the azo group in the ligand is red-shifted in the complexes indicating $N \rightarrow Sn$ coordination by the azo group[7,8].

The strength of the $N \rightarrow Sn$ dative bond should be proportional to the lewis acidity of R_nSnCl_{4-n}. This fact is reflected in the spectral data as the intensity of the longest wavelength band of the complexes decrease markedly on going from $SnCl_4$.L to R_2SnCl_2.L. In methanol, as concentration of this polar solvent is increased, the $N \rightarrow Sn$ bonds gradually break down with consequent solvation at tin[8] ultimately producing the free ligand.

The IR, Mössbauer and electronic spectral data are, therefore, consistent with distorted octahedral structures for all the complexes in the solid state with 1:1 stoichiometry.

One of the authors (AKK) is grateful to the UGC, New Delhi, for financial assistance. The authors thank the Director, CDRI, Lucknow for the analytical data.

References

1 Datta D & Chakravorty A, *Inorg Chem*, **22** (1983) 1085.
2 Baldwin D A, Lever A B P & Parish R V, *Inorg Chem*, **8** (1969) 107.
3 Beadle P J, Grazeskowiak, Goldstein M & Goodgame D M L, *J chem Soc* (*A*), 1970, 305.
4 Rivarola E, Silverstri A, Alonzo G & Barbieri R, *Inorg chim Acta*, **99** (1986) 87.
5 Srivastava T N & Srivastava P C, *J Indian chem Soc*, **LIII** (1976) 365.
6 Poller R C, *The chemistry of organotin compounds* (Logos Press Ltd, London), 1970.
7 Suzuki H, *Electronic absorption spectra and geometry of organic molecules* (Academic Press, New York), 1967, Chap. 23.
8 Majee B & Banerjee S, *J organometal Chem*, **140** (1977) 151.

Indian Journal of Chemistry
Vol. 27A, October 1988, pp. 914-915

Chelated Complexes of Chlorophenoxides of Titanium(IV) with Acetoacetanilide

SUBHASH C CHAUDHRY* & (Ms) JATINDRA GUPTA
Department of Chemistry, Himachal Pradesh University, Summer Hill, Shimla 171 005

Received 23 *November* 1987; *revised and accepted* 7 *March* 1988

Compounds of compositions $Ti(OC_6H_4Cl)_2$.2acan, $TiCl(OC_6H_4Cl)$.2acan, $Ti(OC_6H_4Cl)_3$.acan, $TiCl(OC_6H_4Cl)_2$.acan and $TiCl_2(OC_6H_4Cl)$.acan have been isolated by reacting monochloro-, dichloro- and trichlorotitanium(IV) chlorophenoxides with acetoacetanilide (acanH).

In a recent communication[1], we have reported the synthesis of chlorophenoxy derivatives of titanium(IV) of the composition $Ti(OC_6H_4Cl)_nCl_{4-n}$ where n = 1-4 and proposed dimeric structures bridging through chlorophenoxy groups. In continuation of this work, we now report the reactions of these derivatives of titanium(IV) with acetoacetanilide (acanH) which is well known to form stable chelates with metal chlorides[2,3] and chloroalkoxides[4].

Acetoacetanilide (BDH) was recrystallised from aqueous methanol and the sample having m.p. 85° was used for the reactions. Chlorophenoxy derivatives of titanium(IV) were prepared by the method reported earlier[1] using *o*-chlorophenol and titanium(IV) chloride.

Compounds of compositions $Ti(OC_6H_4Cl)_3$.acan; $TiCl(OC_6H_4Cl)_2$acan; $Ti(OC_6H_4Cl)_2$.2acan; $TiCl_2(OC_6H_4Cl)$.acan and $TiCl(OC_6H_4Cl)$.2acan (where acanH = acetoacetanilide) were prepared by adding a solution of acetoacetanilide in benzene to suspensions of monochlorodichloro- and trichloro-titanium (IV) chlorophenoxides respectively in calculated molar ratios. The contents were refluxed on a water-bath till evolution of hydrogen chloride gas ceased. The complexes precipitated on cooling or addition of pet. ether were filtered, washed with petroleum ether and finally dried *in vacuo*.

Titanium was estimated as titanium dioxide gravimetrically and chlorine by Volhard's method. Conductance measurements were made with an Elico-conductivity bridge. Molecular weights of the complexes were determined cryoscopically in nitrobenzene using Beckman's method. Infrared spectra of the complexes were recorded in KBr on a double grating Perkin-Elmer spectrophotometer.

The compounds isolated in the present studies are listed in Table 1. Evolution of hydrogen chloride gas, accompanied by a change in colour of the solutions was observed during refluxing of the mixture of components. Therefore, the reactions leading to the formation of the products may be postulated as follows:

$$TiCl_2(OC_6H_4Cl)_2 + acanH \xrightarrow{benzene} TiCl(OC_6H_4Cl)_2.acan + HCl$$

Similar reactions may be proposed in the case of other chlorophenoxides of titanium(IV). Stoichiometric composition of these compounds has been established by elemental analysis. These compounds are high melting reddish to orange coloured solids, moisture-sensitive but stable in dry atmosphere. Most of these compounds are soluble in nitrobenzene, acetonitrile, THF, DMF and chloroform. Molar conductances of 10^{-3} *M* solutions of these compounds in

Table 1—Analytical Data and Principal IR Spectral Bands (cm^{-1}) of Chelates of Chlorophenoxides of Titanium(IV) with Acetoacetanilide

Compound	Colour (m.p.,°C)	Found* (Calc.), %		Mol.Wt in $PhNO_2$	ν(C=O)	νN-H	ν(Ti-O) (Bridging)	ν(Ti-Cl)
		Ti	Cl	Found (Calc.)				
$Ti(OC_6H_4Cl)_3$.acan	Orange (260 d)	8.20 (7.91)	17.91 (17.55)	994 (606.5)	1578	3292	590 (510)	
$TiCl(OC_6H_4Cl)_2$.acan	Reddish (219)	9.61 (9.32)	20.32 (20.69)	1004 (514.5)	1570	3284	598 (520)	350
$Ti(OC_6H_4Cl)_2$.2acan	Reddish (221)	7.38 (7.32)	10.91 (10.83)	— (655)	1580	3290	595 (—)	—
$TiCl_2(OC_6H_4Cl)$.acan	Reddish (250)	11.30 (11.36)	25.53 (25.20)	832 (422.5)	1572	3314	600 (525)	360
$TiCl(OC_6H_4Cl)$.2acan	Reddish (208)	8.90 (8.52)	12.95 (12.61)	554 (563)	1574	3310	605 (—)	365

*Carbon and hydrogen analysis were satisfactory within the limits of experimental error

nitrobenzene are quite low (0.76-3.10 $ohm^{-1}cm^2mol^{-1}$) as compared to those expected for 1:1 electrolytes, which, therefore, suggest that the complexes are non-ionic in character. Molecular weight determinations of some of these compounds cryoscopically where solubility permitted, suggest that compounds of compositions $Ti(OC_6H_4Cl)_2.2acan$ and $TiCl(OC_6H_4Cl).2acan$ are monomers while the compounds of compositions $Ti(OC_6H_4Cl)_3.acan$, $TiCl(OC_6H_4Cl)_2.acan$ and $TiCl_2(OC_6H_4Cl).acan$ are dimers. Apparently, there seems to be a breakdown of dimeric structure of the parent chlorophenoxides of titanium(IV)[1] on chelate formation with acetoacetanilide in the former case.

Acetoacetaniide is known to exist almost entirely in the keto form as evidenced by infrared[5] and substantiated by NMR spectra.

In the IR spectra of these compounds, a significant lowering of the carbonyl stretching frequency and slight upward shift of the band due to NH stretching modes of acetoacetanilide have been observed which suggest the absence of nitrogen coordination and are in line with the earlier reports on the chelates of acetoacetanilide[5]. The strongest band observed in the region 1570-1580 cm^{-1} in these compounds (Table 1) has been assigned predominantly to a carbonyl stretching frequency[6,7]. The trends of the shifts in the amide-I, amide-II and amide-III bands have been found to be in agreement with the earlier reports[8].

Bands at 595 and 605 cm^{-1} in $Ti(OC_6H_4Cl)_2.2acan$ and $TiCl(OC_6H_4Cl)..acan$ respectively have been assigned to terminal ν(Ti-O) modes[9,10]. No band that could be assigned to bridging Ti−O→Ti mode has been observed which, therefore, suggests that dimeric structure of theparent chlorophenoxides of titanium(IV) is ruptured on compound formation followed by the coordination of the ligand. In the case of the compounds of composition $Ti(OC_6H_4Cl)_3.acan$, $TiCl(OC_6H_4Cl)_2.acan$ and $TiCl_2(OC_6H_4Cl).acan$, however, bands due to both terminal ν(Ti-O) and bridging Ti ⟋ O ⟍ Ti have been observed. Bands in the region 350-365 cm^{-1} have been assigned to ν(Ti-Cl) in an octahedral environment[11]. No band that could be assigned to bridging Ti ⟋ Cl ⟍ Ti mode has been observed, thus excluding the possibility of bridging through chlorine. Moreover, since the bands due to ν(Ti-Cl) in $TiCl_2(OC_6H_4Cl).acan$ are comparatively simple and there is no splitting of bands, it is suggested that chlorines in this compound occupy *trans*-positions rather than *cis*. Thus, based upon the limited available data presented here, a dimeric struture (I) for $TiCl_2(OC_6H_4Cl).acan$ is proposed.

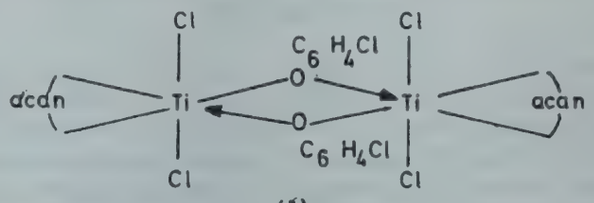

(I)

Similar dimeric structures involving chlorophenoxy bridges may be proposed for $TiCl(OC_6H_4Cl)_2.acan$ and $Ti(OC_6H_4Cl)_3.acan$.

References

1 Chaudhry S C & Gupta J, *Indian J Chem*, **24A** (1985) 150.
2 Dietrich W, Eisinger H K & Latscha H P, *Z Naturforsch*, **B 35** (1980) 17.
3 Syamal A, *J Indian chem Soc*, **45** (1968) 347, 374.
4 Syamal A, Fricks D H, Pantaleo D C, King P G & Johnson R C, *J less-common Metals*, **19** (1969) 141.
5 Seen D N & Umapathy P, *Indian J Chem*, **6** (1968) 516.
6 Bellamy L J, Spicer G C & Strickland J D H, *J chem Soc*, (1952) 4653.
7 Shigorin D N, *Zh fiz Khim*, **27** (1953) 554.
8 Miyazawa T, Shimanouchi T & Mizushima S, *J chem Phys*, **29** (1958) 611.
9 Paul R C, Gupta P K, Gulati M & Chadha S L, *Inorg nucl Chem Lett*, **13** (1977) 665.
10 Paul R C, Sharma P, Gupta P K & Chadha S L, *Inorg chim Acta*, **20** (1976) 7.
11 Malhotra K C, Sharma N & Chaudhry S C, *Trans Met Chem*, **6** (1981) 238.

Indian Journal of Chemistry
Vol. 27A, October 1988, pp. 916-917

New Mixed Ligand Complexes of Ruthenium(II) with β-Diketones & Triphenylphosphine

N JAYAKUMAR & K NATARAJAN*

Department of Chemistry, Bharathiar University, Coimbatore 641 046

Received 11 *November* 1987; *revised and accepted* 15 *February* 1988

Ruthenium(II) mixed ligand complexes of the types $[RuH(CO)(RCOCHCOCF_3)(PPh_3)_2]$ and $[RuCl(CO)(RCOCHCOCF_3)(PPh_3)_2]$ (R = C_6H_5; 3′, 4′-$(OMe)_2C_6H_3$; 4′-BrC_6H_4; 2′-ClC_6H_4; 4′-MeC_6H_4 and 2′-$MeOC_6H_4$) have been synthesised by the reactions of various β-diketones with $[RuH_2(CO)(PPh_3)_3]$ and $[RuHCl(CO)(PPh_3)_3]$ respectively. All the complexes obtained have been characterised on the basis of elemental analyses, IR, magnetic moment and electronic spectral data.

There has been an upsurge of interest in the chemistry of metal β-diketonates owing to their varied applications[1,2] in diverse fields. Though a number of β-diketonato-metal complexes are known[3–5], only a very few β-diketonato complexes of Ru(II) containing triphenylphosphine have been reported[6–9]. In this note, the synthesis and characterisation of a number of new mixed complexes of Ru(II) with β-diketones and triphenylphosphine as the ligands have been described.

All the reagents used were of CP or AR grade. Carbonyldihydrotris(triphenylphosphine)ruthenium(II), carbonyl chlorohydridotris (triphenylphosphine) ruthenium(II) and β-diketones were prepared by the reported literature methods[10,11].

Carbon and hydrogen analyses were carried out at the College Science Instrumentation and Analytical Centre, Virudhunagar, India.

IR spectra of the complexes were recorded with a Perkin-Elmer 597 IR spectrophotometer in the range 4000-300 cm^{-1} using KBr pellets of the samples. Electronic spectra of the complexes in chloroform solution were recorded with a Hitachi Perkin-Elmer model 20/200 spectrophotometer in the range 900-300 nm. Melting points were recorded with a Boetius micro-heating table and are uncorrected.

Preparation of complexes

The β-diketones used are of the type $[R\text{-}CO\text{-}CH_2\text{-}CO\text{-}CF_3]$ (R = C_6H_5; 3′,4′-$(OMe)_2C_6H_3$; 4′-BrC_6H_4; 2′-ClC_6H_4; 4′-MeC_6H_4 and 2′-$(MeO)C_6H_4$).

(i) *Complexes of the type* $[RuH(CO)(RCOCHCOCF_3)(PPh_3)_2]$

To a solution of $[RuH_2(CO)(PPh_3)_3]$ (0.1 g) in benzene (10 ml), the appropriate β-diketone (0.02 to 0.03 g) in ethanol (5 ml) was added (Ru : β-diketone was 1:1). The solution was heated under reflux for 3 hr whereby a yellow solution was obtained. After concentrating the solution to about 3 ml, it was cooled. The separated yellow complex was filtered, recrystallised from methanol and dried *in vacuo*; yield, 66-95%.

(ii) *Complexes of the type* $[RuCl(CO)(RCOCHCOCF_3)(PPh_3)_2]$

These complexes were prepared in a similar manner as described in (i), from $[RuHCl(CO)(PPh_3)_3]$ and the appropriate β-diketones; yield, 40-65%.

The analytical data (Table 1) show that by reacting $[RuH_2(CO)(PPh_3)_3]$ with various β-diketones, one hy-

Table 1—Analytical Data for the New Ru(II) Complexes

Complex	Colour	M.P. (°C)	Found(Calc), %	
			Carbon	Hydrogen
$[RuH(CO)C_6H_5COCHCOCF_3)(PPh_3)_2]$	Yellow	146	65.12(64.90)	4.20(4.28)
$[RuH(CO)(3',4'\text{-}(OMe)_2C_6H_3COCHCOCF_3)(PPh_3)_2]$	Yellow	210	62.9(63.3)	4.48(4.44)
$[RuH(CO)(4'\text{-}BrC_6H_4COCHCOCF_3)(PPh_3)_2]$	Yellow	195	60.00(59.5)	3.74(3.82)
$[RuH(CO)(2'\text{-}ClC_6H_4COCHCOCF_3)(PPh_3)_2]$	Yellow	159-60	62.24(62.42)	3.92(4.01)
$[RuH(CO)(4'\text{-}MeC_6H_4COCHCOCF_3)(PPh_3)_2]$	Yellow	162	64.71(65.23)	3.84(4.45)
$[RuH(CO)(2'\text{-}MeOC_6H_4COCHCOCF_3)(PPh_3)_2]$	Yellow	170	64.42(64.07)	4.70(4.37)
$[RuCl(CO)C_6H_5COCHCOCF_3)(PPh_3)_2]$	Yellow	180	61.8(62.5)	4.39(4.013)
$[RuCl(CO)(3',4'\text{-}(OMe)_2C_6H_3COCHCOCF_3)(PPh_3)_2]$	Yellow	170	61.22(61.03)	4.64(4.18)
$[RuCl(CO)(4'\text{-}BrC_6H_4COCHCOCF_3)(PPh_3)_2]$	Yellow	161-63	57.83(57.42)	3.36(3.59)
$[RuCl(CO)(2'\text{-}ClC_6H_4COCHCOCF_3)(PPh_3)_2]$	Yellow	101-103	60.81(60.14)	3.82(3.76)
$[RuCl(CO)(4'\text{-}MeC_6H_4COCHCOCF_3)(PPh_3)_2]$	Yellow	180	63.10(62.78)	4.48(4.17)
$[RuCl(CO)(2'\text{-}MeOC_6H_4COCHCOCF_3)(PPh_3)_2]$	Yellow	165	62.31(61.7)	4.40(4.10)

dride ion and a molecule of triphenylphosphine are replaced by one molecule of β-diketone to give complexes of the type $[RuH(\beta dk)(CO)(PPh_3)_2]$ ($\beta dk = \beta$-diketone). Similarly, complexes of the type $[RuCl(\beta dk)(CO)(PPh_3)_2]$ are obtained by the reaction of $[RuHCl(CO)(PPh_3)_3]$ with β-diketones.

In the IR spectra of all the β-diketonato complexes two to three sharp bands appeared in the region 1520-1625 cm^{-1}. The positions of these bands are characteristic of the mixed mode of vibrations arising due to the normal coordinate having contributions from $\nu C=O$ and $\nu C=C$ of the coordinated β-diketones[12]. In addition, all these complexes showed a band around 1920-1960 cm^{-1} which can be assigned to the ν_{CO} of the coordinated carbonyl group. The infrared spectra of the complexes of the type $[RuH(\beta dk)(CO)(PPh_3)_2]$ showed a band in the region 2000-2050 cm^{-1} which is due to νRu-H; this band was absent in the compounds of the type $[RuCl(\beta dk)(CO)(PPh_3)_2]$ confirming the substitution of one hydride ligand present in the starting materials.

All the compounds are found to be diamagnetic as expected for t_{2g}^6 ground state of Ru(II) in an octahedral field.

The electronic spectra of the complexes in chloroform showed two bands in the regions 23000-27000 and 29850-33333 cm^{-1}. The lower energy weak band (ε, 500-2500) between 23000 and 27000 cm^{-1} can be tentatively assigned to the *d-d* transition, $^1A_{1g} \rightarrow {}^1T_{1g}$[13]. The relatively higher intensity of the second band (ε, 1900-11065) suggests that it may be due to charge-transfer. Most probably charge-transfer arises due to excitation of an electron from metal t_{2g} level to unfilled molecular orbital derived from the π^* level of the ligands[13].

On the basis of analytical data, IR and electronic spectral studies, the following structures (I—IV) are equally possible for these complexes. In the absence of X-ray single crystal studies, it is not possible to prefer one over the other. Also, in the case of these unsymmetrical β-diketonate complexes there are seven possible isomers.

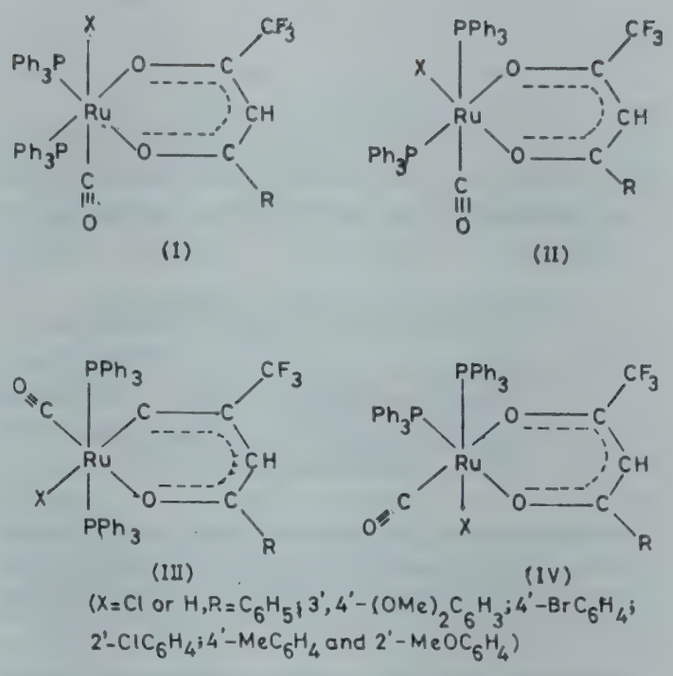

References

1 Hinckley C C, *J Am chem Soc*, **91** (1969) 5160.

2 Weissman S J, *J chem Phys*, **10** (1942) 214.

3 Haszeldine R N, Musgrave W K R, Smith F & Turtan L M, *J chem Soc*, (1951) 609.

4 Joshi Krishna C & Joshi Bidya S, *Indian J Chem*, **24A** (1985) 257.

5 Mehrotra R C, Bohra R & Gaur D P, *Metal β-diketonates and allied derivatives* (Academic Press, New York) 1978.

6 Gilbert J D & Wilkinson G, *J chem Soc*(A), (1969) 1749.

7 Natarajan K, Poddar R K & Agarwala U, *J inorg nucl Chem*, **39** (1977) 431.

8 Natarajan K & Agarwala U, *Inorg nucl Chem Lett*, **14** (1978) 7.

9 Gopinathan S, Pandit S K & Gopinathan C, *Indian J Chem*, **24A** (1985) 615.

10 Ahmad N, Levison J J, Robinson S D & Uttley M F, in *Inorganic syntheses*, Vol 15, edited by G W Parshall (McGraw-Hill, New York) 1974, 48.

11 Das M, *Inorg chim Acta*, **36** (1979) 79.

12 Nakamoto K, *Infrared spectra of inorganic and coordination compounds* (John Wiley, New York) 1964.

13 Lever A B P, *Inorganic electronic spectroscopy*, 2nd Edn (Elsevier, New York) 1984.

Indian Journal of Chemistry
Vol. 27A, October 1988, pp. 918-920

Protolysis Constants (pK_a) of Some Antitubercular Compounds Containing Diaryl Sulphide & Diaryl Sulphone Moieties

P K JADHAV*, P V ARUR, V D BALGI &
(Mrs) USHA P KAMAT

Department of Chemistry, Ismail Yusuf College,
Jogeshwari, Bombay 400 060

Received 18 *August* 1987; *revised and accepted* 29 *February* 1988

Protolysis constants (pK_a) of substituted 2-carboxy-4-nitrodiphenyl sulphides, 2-carboxy-4-nitrodiphenyl sulphones and their reduction products are reported. The influence of the various constituent groups on ionization constants is discussed.

Compounds containing diaryl sulphide and diaryl sulphone moieties are well known antimicrobial agents[1-5]. Antitubercular activity of 2-carboxy-4-aminodiphenyl sulphides, 2-carboxy-4-aminodiphenyl sulphones, and their thioureas have been reported by Arur *et al.*[6,7] However, the ionization constants (pK_a) of these compounds have not been reported yet. The pK_a values of these compounds may be helpful in correlating their established biological activity with their ionic equilibria. This led us to investigate the protolysis constants of the following compounds:

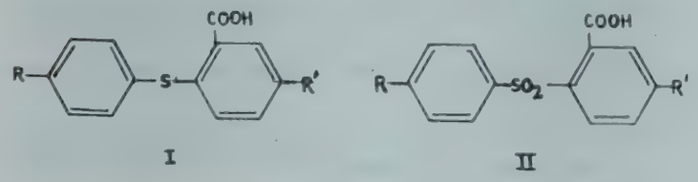

I II

R = H, Cl, CH_3 and OCH_3
R′ = NO_2 and NH_2

All the reagents and chemicals were of GR grade (Merck) or AnalaR grade (BDH). Commercial methanol was purified[8] before use. Compounds I and II were synthesized as per the reported method[6,7].

Potentiometric titrations were carried out in absolute methanol using an ELICO-DIGITAL *p*H Meter LI-120 (accuracy: ± 0.01 units) with a glass-calomel electrode system at 25° ± 0.1°C in dry nitrogen atmosphere saturated with methanol vapours.

A 0.05 *M* methanolic KOH solution served as the basic titrant. Methanolic buffer (*p*H 7.54) solution containing salicylic acid (1.38 g/l) and sodium salicylate (1.6 g/l) was used as the standard reference buffer for the system[9].

Stock solutions (0.01 *M*) of compounds I and II were prepared in methanol and 100 ml of the stock solution was titrated against standard methanolic-KOH solution.

Following ionic equilibria exist when a carboxylic acid (RCOOH) is dissolved in methanol:

$$R\text{-}COOH \rightleftharpoons RCOO^- + H^+ \quad \ldots (1)$$

$$H^+ + CH_3OH \rightleftharpoons CH_3OH_2^+ \quad \ldots (2)$$

$$R\text{-}COOH + CH_3OH \rightleftharpoons RCOO^- + CH_3OH_2^+ \quad \ldots (3)$$

($CH_3OH_2^+$ is the solvated proton analogous to the hydrated proton H_3^+O)

$$K_a = \frac{[CH_3OH_2^+][RCOO^-]}{[RCOOH]} \quad \ldots (4)$$

$$pK_a = p\text{H}^* - \log \frac{[RCOO^-]}{[RCOOH]} \quad \ldots (5)$$

Eq. (6) is the modified form of Eq. (5), expressed in terms of volume of the basic titrant.

$$pK_a = p\text{H}^* - \log \frac{V}{V_e - V} \quad \ldots (6)$$

where V is the volume (ml) of KOH consumed and V_e is the volume (ml) of KOH required at the equivalence point.

The equivalent volume (V_e) was evaluated by Gran's plot method[10,11]. Then, a series of values of $\log (V/V_e - V)$ were calculated and these values were plotted against the corresponding *p*H*. These plots obtained are straight lines with intercepts at $\log (V/V_e - V) = 0$. The *p*H* corresponding to $\log (V/V_e - V) = 0$, is the pK_a of the compound. The pK_a of the compounds evaluated thus are given in Table 1.

Relationship of pK_a values of the carboxylic acids in methanol and in pure water was well established by many investigators[11]. The same expression (Eq. 7) is employed in this investigation to compute the pK_a of the compound in pure water. The values so obtained are presented in Table 1.

$$pK_a(H_2O) = pK_a(MeOH) - 4.80 \quad \ldots (7)$$

The protolysis constants (pK_a) of carboxylic acids largely depend on the partial positive (Δ^+) charge on the carboxyl carbon atom. The electron withdrawing groups in the phenyl ring increase this

charge, while the electron releasing groups exert an opposite effect. Thus, the strength of aromatic carboxylic acids depends upon the electron attracting ability of the substituents and their position in the aromatic ring with respect to COOH group[12].

Table 1—Protolysis Constants (pK_a) of 2-Carboxy-4-nitrodiphenyl Sulphide and Sulphones [$(R)C_6H_4$-X-$C_6H_3(COOH)R'$]

Sr. No.	Substituents			In Methanol at 25°C	In Pure Water at 25°C
	R	-X-	R'	pK_a	pK_a
1	H	S	NO_2	8.02	3.22
2	H	SO_2	NO_2	6.95	2.14
3	Cl	S	NO_2	7.66	2.86
4	Cl	SO_2	NO_2	6.72	1.92
5	CH_3	S	NO_2	7.64	2.84
6	CH_3	SO_2	NO_2	6.86	2.06
7	OCH_3	S	NO_2	7.96	3.16
8	OCH_3	SO_2	NO_2	6.85	2.05
9	H	S	NH_5	8.70	3.90
10	H	SO_2	NH_5	8.10	3.30
11	Cl	S	NH_5	8.72	3.92
12	Cl	SO_2	NH_5	8.02	3.22
13	CH_3	S	NH_5	8.97	4.17
14	CH_3	SO_2	NH_5	8.22	3.42
15	OCH_3	S	NH_5	9.05	4.20
16	OCH_3	SO_2	NH_5	8.41	3.61

$pK_a(H_2O) = pK_a(CH_3OH) - 4.80$

Compounds 1-8 in Table 2 are the derivatives of *m*-nitrobenzoic acid. pK_a values of these compounds are less than pK_a of *m*-nitrobenzoic acid. $\Delta^1 pK_a$ values suggest that both phenylmercapto (C_6H_5S) and phenyl sulphonyl ($C_6H_5SO_2$) groups exert inductive ($-I$) effect. They facilitate the ionization of the carboxyl group; hence, these compounds are stronger acids than the *m*-nitrobenzoic acid.

Compounds 9-16 in Table 2 are the derivatives of *m*-aminobenzoic acid. The pK_a values of these compounds are less than the pK_a of *m*-aminobenzoic acid (4.78). The $\Delta^0 pK_a$ values suggest that both phenylmercapto and phenyl sulphonyl groups, due to their electron withdrawing ability ($-I$ effect), result in the formation of stronger acids.

Table 2 shows that chloro, methyl and methoxy substituents in 2-carboxy-4-nitrodiphenyl sulphide and in 2-carboxy-4-nitrodiphenyl sulphone, lower the pK_a values and tend to strengthen the acids.

In 2-carboxy-4-aminodiphenyl sulphide and in 2-carboxy-4-amino-diphenyl sulphone, presence of methyl and methoxy substituents increases pK_a and consequently weaker acids result. Chloro substitution has very little influence on pK_a in this series of compounds.

The influence of the substituents on pK_a is not to the extent expected (as observed in substituted benzoic acid). These substituents are located in the phe-

Table 2—Influence of Various Substituents and Groups on pK_a of 2-Carboxy-4-nitrodiphenyl Sulphides and Sulphones [(R)-C_6H_4-X-$C_6H_3(COOH)(R')$]

Sr. No.	Substituents			pK_a in H_2O	Influence of substituents/groups				
	R	-X-	R'		$\Delta' pK_a$	ΔpK_a	$\Delta^0 pK_a$	$\Delta'' pK_a$	$\Delta''' pK_a$
1	H	S	NO_2	3.22	0.27	—	—	—	—
2	H	SO_2	NO_2	2.14	1.34	—	—	1.07	—
3	Cl	S	NO_2	2.86	0.63	—	—	—	0.36
4	Cl	SO_2	NO_2	1.92	1.57	—	—	0.94	0.22
5	CH_3	S	NO_2	2.84	0.65	—	—	—	0.38
6	CH_3	SO_2	NO_2	2.06	1.43	—	—	0.78	0.08
7	OCH_3	S	NO_2	3.16	0.33	—	—	—	0.06
8	OCH_3	SO_2	NO_2	2.05	1.44	—	—	1.10	0.09
9	H	S	NH_2	3.90	—	0.68	0.88	—	—
10	H	SO_2	NH_2	3.30	—	1.16	1.48	0.60	—
11	Cl	S	NH_2	3.92	—	1.06	0.86	—	−0.02
12	Cl	SO_2	NH_2	3.22	—	1.30	1.56	0.70	0.08
13	CH_3	S	NH_2	4.17	—	1.33	0.61	—	−0.27
14	CH_3	SO_2	NH_2	3.42	—	1.36	1.36	0.75	−0.12
15	OCH_3	S	NH_2	4.20	—	1.04	0.58	—	−0.30
16	OCH_3	SO_2	NH_2	3.61	—	1.54	1.11	0.59	−0.31

$\Delta' pK_a = 3.49 - pK_a$ (pK_a of *m*-nitrobenzoic acid is 3.49)
ΔpK_a = Influence of reduction on pK_a
$\Delta^0 pK_a = 4.78 - pK_a$ (pK_a of *m*-aminobenzoic acid is 4.78)
$\Delta'' pK_a$ = Influence of oxidation on pK_a
$\Delta''' pK_a$ = Influence of Cl, CH_3 and OCH_3 on pK_a

nyl ring (at 4′-position) which does not contain ionizable carboxyl group, hence, their influence on dissociation of COOH group fades away as the distance of these substituents from the COOH group increases.

pK_a values listed in Table 2 indicate that the oxidation of substituted diphenyl sulphides to the corresponding substituted diphenyl sulphones brings about a decrease in (pK_a) by 0.60 to 1.11 (pK_a) units, depending upon the nature of the substituent in the aromatic ring. This large change is attributed to the strong electron withdrawing ability ($-I$ effect) of sulphonyl (SO_2) moiety and its *ortho* position with respect to ionizable COOH group. Because of these combined effects, the carboxyl group loses proton easily, resulting in stronger acidic character of sulphones in comparison with the corresponding sulphides.

When 2-carboxy-4-nitrodiphenyl sulphide, 2-carboxy-4-nitrodiphenyl sulphone and their 4′-substituted derivatives were reduced to the corresponding amino compounds (Table 2, Sr. No. 1-16), the increase in (pK_a) was about 0.70 to 1.54 (pK_a) units (column ΔpK_a in Table 2), depending upon the type of substituents in the aromatic ring. This is mainly attributed to the electron releasing ability of NH_2 group, which reduces the (Δ^+) charge on the carboxyl carbon and thereby suppresses the ionization of COOH group, consequently the NH_2 group weakens the carboxylic acids.

References

1 Iyengar J R, Bhattacharya S C & Guha P C, *Curr Sci*, **20**(7) (1951) 184.

2 Rist E, *Compt rend Soc Biol*, **130** (1939) 972; 976.

3 Guha P C & Doaiswami K R, *Curr Sci*, **13** (1944) 207.

4 Goghari M H & Parikh A R, *Indian Chem J*, **12** (5) (1978) 17.

5 Burger Alfred, *Medicinal chemistry*, Part I, 3rd Edn (Wiley-Interscience, New York), 1970.

6 Arur P V & Kulkarni S N, *Indian J Chem*, **20(B)** (1981) 150.

7 Arur P V, *Potential antitubercular compounds*, Ph.D. Thesis, Poona University, 1978.

8 Kolthoff I M & Fleving P J, *Treatise on analytical chemistry*, Part I, Vol. II, (Interscience-John Wiley, N.Y.) 1975, 7076.

9 Lange N A & Dean J A, *Handbook of chemistry*, 11th Edn., (McGraw-Hill, N.Y.) 1973, 2-78.

10 Gran G, *Acta chem scand*, **4** (1950) 559; *Analyst*, **77** (1952) 66.

11 Budevsky O, *Foundation of chemical analysis*, (McGraw-Hill, N.Y.), 1979, 140, 339.

12 Finar I L, *Organic chemistry*, Vol I, 6th Edn. (Longmans-Green, London) 1967, 241, 770.

Indian Journal of Chemistry
Vol. 27A, October 1988, pp. 921-922

Extraction of Copper from Sodium Salicylate & Its Spectrophotometric Determination with 4-(2-Pyridylazo)-resorcinol

V M SHINDE
Analytical Laboratory, Department of Chemistry,
The Institute of Science, 15, Madam Cama Road,
Bombay 400 032

Received 24 *July* 1987; *revised and accepted* 21 *January* 1988

A method is described for the extraction and separation of microgram amounts of copper(II) from sodium salicylate solution using mesityl oxide as an extractant. The metal ion is stripped from the organic phase with water and determined photometrically as its 4-(2-pyridylazo)resorcinol complex. The method is applicable to the analysis of synthetic mixtures and pharmaceutical samples.

Copper is associated with iron, aluminium, nickel, manganese, lead, zinc, chromium and molybdenum in industrially important copper-base alloys. It is also found in a number of pharmaceuticals. Separation and quick estimation of copper is thus desired. We report here a method for the extration of microgram amounts of copper with mesityl oxide from sodium salicylate solution (0.1*M*; *p*H 4-4.5). The metal ion is stripped from the organic phase with water and determined photometrically as its 4-(2-pyridylazo)resorcinol complex at 540 nm. The method permits separation of copper from Zn(II), Cd(II), Mn(II), Fe(III), Al(III), Ti(IV), V(V), Cr(VI) and Mo(VI) and has been successfully applied to the analysis of steel, brass, aluminium alloy and pharmaceutical samples.

The stocks solution of copper(II) was prepared by dissolving 0.42 g of copper sulphate pentahydrate (AR grade) in 50 ml of distilled water containing 0.5 ml of conc. sulphuric acid. The solution was standardised[1] and diluted as required for working purpose.

A Philips *p*H-meter (Precision type) and a Zeiss (Jena) spectrophotometer with 1 cm silica cells were used for *p*H and absorbance measurements respectively.

Mesityl oxide used was doubly distilled (b.p. 128°). A 0.1% aqueous solution of 4-(2-pyridylazo)resorcinol (PAR) was used for the estimation of copper[2]. All other chemicals used in this work were of guaranteed reagent grade.

Extraction procedure

An aliquot containing 25 μg of copper was taken and to it was added 400 mg of sodium salicylate (0.1 *M*) and the *p*H was adjusted to 4.0-4.5 in a total volume of 25 ml. Extraction was carried out for 45 sec with 10 ml of undiluted mesityl oxide. The organic phase was collected, copper stripped with two 10-ml portions of water and the metal ion was determined in the combined aqueous phase spectrophotometrically with PAR at 540 nm[2].

The extraction of copper was studied at various *p*H values (3.5-9.0), sodium salicylate concentrations (0.025-0.2*M*) and mesityl oxide concentrations (20-100%, using benzene as the diluent). A single extraction for 45 sec with 10 ml of undiluted mesityl oxide was found to be adequate for quantitative extraction of copper from 0.1*M* salicylate solution of *p*H 4.0-4.5. Beyond *p*H 4.5, the extraction decreased and the distribution ratios were calculated as usual[3].

The log-log plots of distribution ratio vs salicylate concentration (at fixed *p*H and mesityl oxide concentration) or vs mesityl oxide concentration (at fixed *p*H and salicylate concentration) gave a slope of 1.9 indicating molar ratio of 1:2 with respect to both extractant and salicylate. Hence, the probable nature of the extracted species is $Cu(HOC_6H_4\ COO)_2$. 2 Meo where Meo stands for mesityl oxide. 2500 μg each of Ag(I), Mn(II), Hg(II), Pb(II), Cd(II), Ni(II), Ca(II), Sr(II), Ba(II), Cr(III), Sc(III), La(III), Y(III), In(III), Ga(III), Sb(III), Au(III), Al(III), As(III), Th(IV), Ce(IV), Pt(IV), V(V), Cr(VI), U(VI), Mo(VI), thiocyanate, thiourea, ascorbate, perchlorate, Cl^-, Br^-, NO_3^-, PO_4^{3-} and tartrate; 1000 μg each of Be(II), Sn(II), Ir(III), Ti(IV), Os(VIII) and citrate; 500 μg of Fe(III); 200 μg each of Pd(II) and Rh(III) did not interfere in the estimation. However, Co(II), Bi(III) and EDTA interfered severely and must be absent.

Extraction of copper (25 μg) by the recommended procedure facilitates its separation from ions such as Zn(II), Mn(II), Cd(II), Fe(III), Al(III), Ti(IV), V(V), Cr(VI) and Mo(VI) as they do not extract into mesityl oxide. The recoveries were > 99.0% from the binary mixtures.

Synthetic mixtures containing either Mn(2.5 mg), Ni(0.5 mg), Cr(0.5 mg), Mo(1 mg), Fe(200 μg), Cu(25 μg) or Ni(0.5 mg), Fe(200 μg), Zn(2.5 mg), Mn(2.5 mg), Cu(25 μg) or Al(2.5 mg),

Table 1 — Analysis of Standard Samples

Sample/Item	Composition of Alloy	Copper %		Rel. error, %
		Declared	Found	
1 33 d NBS	C, 2.4; Si, 1.63; Mn, 0.63; Ni, 2.38; Cr, 0.32; Mo, 0.48; rest iron (90.3)	1.54	1.52	1.3
2 41 Brass (NML)	Pb, 2.35; Zn, 40.65; Fe, 0.009	56.9	56.4	0.9
3 Aluminium alloy	Ni, 2.12; Mn, 1.7; Fe, 0.031, rest Al	4.0	3.9	1.2
4 Multivite FM capsules (Allenbury, India)	Vitamin A, 5000 IU; Vitamin D_3, 200 IU; Vitamin E, 7.5 mg; Vitamin B_1, 2.5 mg; Vitamin B_2, 2.5 mg; Nicotinamide, 25 mg; Folic acid, 500 mcg; Ferrous fumerate, 25 mg; Calciumdibasic phosphates, 35 mg; Copper sulphate, 0.1 mg; Manganese sulphate, 0.01 mg; Zinc sulphate, 50 mg; Potassium iodide, 0.025 mg; Magnesium oxide, 0.15 mg	0.1 mg	0.1 mg	—

Fe(200 μg), Ni(0.5 mg), Mn(0.5 mg), Cu(25 μg) or Pb(1 mg), Zn(2.5 mg), Cu(25 μg) were analysed by the recommended procedure. The results show that the detection and determination of copper is possible in presence of these metal ions with greater than 99% recovery of copper (Table 1).

The method also permits separation and determination of copper in 33 d cast iron steel (NBS), 41 Brass (NML), aluminium alloy and in multivite FM capsules.

The reproducibility of results was satisfactory and the results were found to be accurate within $\pm 0.5\%$ with a standard deviation of ± 0.004 from the mean. The 95% confidence limit for the mean is 0.0042.

The author thanks CSIR, New Delhi, for financing the project.

References

1 Welcher F J, *The analytical uses of EDTA* (Van Nostrand, New York) 1961, 242.

2 Talaev O A, Akhmedov S A & Akhmedov Kh A, *Zh analit Khim*, **24** (1969) 834.

3 Gawali S B & Shinde V M, *Analyt Chem*, **48** (1976) 63.

THE WEALTH OF INDIA

An Encyclopaedia of Indian Raw Materials and Industrial Products, published in two series :
(i) Raw Materials, and **(ii) Industrial Products.**

RAW MATERIALS

The articles deal with Animal Products, Dyes & Tans, Essential Oils, Fats & Oils, Fibres & Pulps, Foods & Fodders, Drugs, Minerals, Spices & Flavourings, and Timbers and other Forest products. Names in Indian languages, and trade names are provided.

For important crops, their origin, distribution, evolution of cultivated types and methods of cultivation, harvesting and storage are mentioned in detail. Data regarding area and yield and import and export are provided. Regarding minerals, their occurrence and distribution in the country and modes of exploitation and utilization are given. The articles are well illustrated. Adequate literature references are provided.

Eleven volumes of the series covering letters A–Z have been published.

Vol. I : A (Revised) Rs. 300.00; Vol. I (A-B) Rs. 120.00; Vol. II (C) Rs. 143.00; Vol. III (D-E) with index to Vols. I-III Rs. 158.00; Vol. IV (F-G) Rs. 150.00; Vol. IV Suppl. Fish & Fisheries Rs. 84.00; Vol. V (H-K) Rs. 171.00; Vol. VI (L-M) Rs. 135.00; Vol. VI : Suppl. on Livestock including poultry Rs. 153.00; Vol. VII (N-Pe) Rs. 150.00; Vol. VIII (Ph-Re) Rs. 129.00; Vol. IX (Rh-Sc) Rs. 200.00; Vol. X (Sp-W) Rs. 338.00; Vol. XI (X-Z) with Cumulative Index to Vols. I-XI Rs. 223.00.

INDUSTRIAL PRODUCTS

Includes articles giving a comprehensive account of various large, medium and small scale industries. Some of the major industries included are : Acids, Carriages, Diesel Engines, Fertilizers, Insecticides & Pesticides, Iron & Steel, Paints & Varnishes, Petroleum Refining, Pharmaceuticals, Plastics, Ship & Boatbuilding, Rubber, Silk, etc.

The articles include an account of the raw materials and their availability, manufacturing processes, and uses of products, and industrial potentialities. Specifications of raw materials as well as finished products and statistical data regarding production, demand, exports, imports, prices, etc. are provided. The articles are suitably illustrated. References to the sources of information are provided.

Nine volumes of the series covering letters A–Z have been published.

Part I (A-B) Rs. 87.00; Part II (C) Rs. 111.00; Part III (D-E) with Index to Parts I-III Rs. 150.00; Part IV (F-H) Rs. 189.00; Part V (I-L) Rs. 135.00; Part VI (M-Pi) Rs. 42.00; Part VII (Pl-Sh) Rs. 90.00; Part VIII (Sl-Tl) Rs. 99.00; Part IX (To-Z) with Index to Parts I-IX Rs. 120.00.

HINDI EDITION : BHARAT KI SAMPADA—PRAKRITIK PADARTH

Vols. I to VII and two supplements of Wealth of India—Raw Materials series in Hindi already published.

Published Volumes :

Vol. I (अ-औ) Rs. 57.00; Vol. II (क) Rs. 54.00; Vol. III (ख-न) Rs. 54.00; Vol. IV (प) Rs. 125.00; Vol. V (फ-मेरे) Rs. 90.00; Vol. VI (मेल-रू) Rs. 120.00; Vol. VII (रे-वाटा) Rs. 203.00; Vol. VIII (वाय-सीसे) Rs. 300.00.

Supplements :

Fish & Fisheries (Matsya & Matsyaki) Rs. 74.00;
Livestock (Pashudhan aur Kukkut Palan) Rs. 51.00

Vols. IX to XI under publication.

Please contact :

SENIOR SALES AND DISTRIBUTION OFFICER

PUBLICATIONS & INFORMATION DIRECTORATE, CSIR
Hillside Road, New Delhi 110 012

RN 7090/63

CSIR PUBLICATIONS

WEALTH OF INDIA

An encyclopaedia of the economic products and Industrial resources of India issued in two series

RAW MATERIALS SERIES – Contains articles on plant, animal and mineral resources.

	Rs.	$	£
Vol. I(A) (Revised)	300.00	94.00	74.00
Vol. I (A-B)	120.00	60.00	26.00
Vol. II (C)	143.00	66.00	34.00
Vol. III (D-E)	158.00	64.00	40.00
Vol. IV (F-G)	98.00	54.00	24.00
Supplement (Fish & Fisheries)	84.00	32.00	21.00
Vol. V (H-K)	171.00	68.00	42.00
Vol. VI (L-M)	135.00	68.00	30.00
Supplement (Livestock including Poultry)	153.00	68.00	39.00
Vol. VII (N-Pe)	150.00	60.00	38.00
Vol. VIII (Ph-Re)	129.00	64.00	28.00
Vol. IX (Rh-Se)	156.00	70.00	38.00
Vol. X (Sp-W)	338.00	150.00	85.00
Vol. XI (X-Z)	223.00	77.00	44.00

INDUSTRIAL PRODUCTS SERIES – Deals with major, Small-Scale and Cottage Industries

Part I (A-B)	87.00	40.00	22.00
Part II (C)	111.00	48.00	28.00
Part III (D-E)	150.00	67.00	39.00
Part IV (F-H)	189.00	84.00	48.00
Part V (I-L)	135.00	46.00	34.00
Part VI (M-Pi)	42.00	16.00	5.60
Part VII (Pl-Sh)	90.00	36.00	12.00
Part VIII (Si-Ti)	99.00	54.00	20.00
Part IX (To-Z)	120.00	68.00	24.00

BHARAT KI SAMPADA (Hindi Edition of Wealth of India, Raw Materials):

Vol. I (अ-औ)	57.00	32.00	13.00
Vol. II (क)	54.00	30.00	12.00
Vol. III (ख-न)	54.00	30.00	12.00
Vol. IV (प)	125.00	68.00	32.00
Vol. V (फ-मेरे)	90.00	44.00	20.00
Vol. VI (मेल-रू)	120.00	54.00	26.00
Vol. VII (रे-वाटा)	203.00	80.00	50.00
Vol. VIII (वाय-सीसे)	300.00	80.00	50.00
Livestock (Kukkut Palan)	51.00	30.00	12.00
Fish & Fisheries (Matsya aur Matsyaki)	74.00	42.00	10.00
A Dictionary of Generic & Specific Names of Plants & Animals Useful to Man	45.00	22.00	10.00

Please Contact :

SENIOR SALES & DISTRIBUTION OFFICER
PUBLICATIONS & INFORMATION
DIRECTORATE, CSIR
HILLSIDE ROAD, NEW DELHI - 110012

OTHER PUBLICATIONS

	Rs.	$	£
The Useful Plants of India	192.00	64.00	48.00
A Dictionary of the Flowering Plants in India by H. Santapau & A.N. Henry	63.00	28.00	16.00
Glossary of Indian Medicinal plants by R.N. Chopra, S.L. Nayar & I.C. Chopra	93.00	32.00	20.00
Supplement to Glossary of Indian Medicinal Plants by R.N. Chopra, I.C. Chopra & B.S. Verma	51.00	18.00	12.00
The Flora of Delhi by J.K. Maheshwari	42.00	16.00	5.50
Illustrations to the Flora of Delhi by J.K. Maheshwari	105.00	44.00	26.00
Herbaceous Flora of Dehra Dun by C.R. Babu	216.00	120.00	44.00
Gnetum by P. Maheshwari & Vimla Vasil	30.00	12.00	4.00
Marsilea by K.M. Gupta	62.00	27.00	16.00
Aquatic Angiosperms	30.00	12.00	4.00
Indian Fossil Pteridophytes by K.R. Surange	99.00	44.00	25.00
Cedrus by P. Maheshwari & Chhaya Biswas	63.00	28.00	16.00
Proteaceae by C. Venkata Rao	108.00	48.00	27.00
Pinus by P. Maheshwari & R.N. Konar	45.00	22.00	16.00
Loranthaceae by B.M. Johri & S.P. Bhatnagar	83.00	37.00	21.00
Abies & Picea by K.A. Chowdhury	21.00	12.00	4.20
Indian Thysanoptera by T.N. Ananthakrishnan	39.00	16.00	5.20
The Millipede Thyropygus by G. Krishnan	18.00	7.00	2.40
Indian Sardines by R.V. Nair	33.00	14.00	4.40
Drug Addiction with special Reference to India by R.N. Chopra & I.C. Chopra	19.00	7.00	2.40
Diosgenin & other Steroid Drug Precursors by L.V. Asolkar & Y.R. Chandha	54.00	26.00	12.00
Cholera Bacteriophages by Dr. Sachimohan Mukerjee	45.00	20.00	12.00
Cottonseed Chemistry & Technology by K.S. Murti & K.T. Achaya	116.00	64.00	26.00
Corrosion Map of India	27.00		3.60
Rural Development and Technology: A Status Report-cum-Bibliography by PR Bose and V.N. Vashist	150.00	76.00	34.00
Termite Problems in India	14.00	6.00	1.80
Research & Development Management	38.00	20.00	
Proceedings of the Seminar on Primary Communications in Science & Technology in India by R.N. Sharma & S. Seetharama	78.00	35.00	68.00

Packing and Postage Extra

Printed & Published by Shri S.S. Saksena, Editor, Publications & Information Directorate (PID)
Hillside Road, New Delhi 110012, at PID Photocomposition-cum-Printing Unit

Regd No. D(C)-1018